PARTICLE TRANSPORT THEORY WITH ICRH AND ECRH IN TOKAMAKS

A Dissertation

Presented to

The Academic Faculty

by

K. Indireshkumar

In Partial Fulfillment

of the Requirements for the Degree

Doctor of Philosophy

in Nuclear Engineering

Georgia Institute of Technology

October 1992

PARTICLE TRANSPORT THEORY WITH ICRH AND ECRH IN TOKAMAKS

Approved:

W. M. Stacey, Jr., Chairman

D. B. Lancaster

A. V. Larson

J. Mandrekas

C. E. Thomas, Jr.

Date Approved by Chairperson: 10-12-92

ACKNOWLEDGMENTS

I wish to record my sincere thanks to Prof. W. M. Stacey, Jr. for his guidance throughout the course of this investigation. It has been a pleasure working with him and I am grateful for the freedom he accorded me in choosing this topic and the course of investigation. I would like to thank John (Dr. J. Mandrekas) for his help in various forms too numerous to list here - from teaching me the rudiments of supercomputer usage to letting me borrow books from his private library! In particular, I appreciate his friendliness. I wish to express my gratitude to Dr. C. E. Thomas, Jr. for his interest in this work, his helpfulness, and his interest in my progress since I joined the fusion program at Georgia Tech. I would like to thank Dr. A. V. Larson for introducing me to the field of plasmas. I greatly appreciate his helpfulness and his interest in my progress. I am grateful to Dr. D. B. Lancaster for his time and effort as a member of my thesis reading committee. Finally, I acknowledge the DOE grant DE-FG05-87ER52141 responsible for this work.

TABLE OF CONTENTS

	Page
ACKNOWLEDGMENTS	iii
TABLE OF CONTENTS	iv
LIST OF TABLES	viii
LIST OF FIGURES	ix
SUMMARY	xii
CHAPTERS	
I INTRODUCTION	1
II BACKGROUND	5
2.1 ICRH and ECRH	5
2.1.1 General Theory	5
2.1.2 ICRH	10
2.1.3 ECRH	13
2.2 Drift Kinetic Equation	16
2.2.1 Basic Equations	17
2.2.2 Ordering	19
2.2.3 Drift-Kinetic Equation	26
2.3 Collision Operators	28
2.3.1 Fokker-Planck Collision Term	29
2.3.2 Other Collision Operators	30
2.4 Quasilinear Theory	34

III PARTICLE TRANSPORT DURING WAVE HEATING - THEORY . 37
3.1 Electric Fields during Cyclotron Wave Heating in Tokamaks . . . 37
3.1.1 Poloidal Potential Variation During Wave Heating 37
3.1.2 Electric Fields during Wave Momentum Absorption 47
3.2 Effect of Poloidal Potential Variation on Particle Trapping 54
3.2.1 $e\tilde{\Phi}(\theta)/T \sim \mathcal{O}(\epsilon)$ and $e_j\Phi_{in} < e_j\Phi_{out}$ 55
3.2.2 $e\tilde{\Phi}(\theta)/T \sim \mathcal{O}(\epsilon)$ and $e_j\Phi_{in} > e_j\Phi_{out}$ 56
3.3 Particle Transport During Wave Heating 58
3.3.1 Effect of Poloidal Potential Variation on Transport 59
3.3.2 Transport Due to Wave Particle Interactions 65
3.4 Summary and Conclusion 73
IV WAVE HEATING AND TRANSPORT - EXPERIMENTS 75
4.1 ECRH 75
4.1.1 Changes in Electron Density 75
4.1.2 Impurity Transport 76
4.1.3 Other Effects Related to Transport 79
4.2 ICRH 82
4.2.1 Effect on Electron Density 82
4.2.2 Impurity Transport 82
4.2.3 Other Effects Related to Transport 85
4.3 Summary and Conclusion 87
V TRANSPORT IN THE BANANA REGIME 89
5.1 Low collisionality Ordering 89
5.1.1 Untrapped Particle Region 91
5.1.2 Trapped Particles 93
5.2 Solution of Drift Kinetic Equation 96
5.2.1 Calculation of $< u_{j1}(v) >$ and r_{kj} 97

5.3 Calculation of $f_{t\Phi}$ 101
VI PARTICLE TRANSPORT 105
6.1 Expression for Particle Flux 105
6.2 Calculation of Transport Coefficients 107
6.2.1 Response to the Radial Electric Field 107
6.2.2 Particle Flux due to the Gradient Terms 108
6.2.3 Particle Flux due to the Parallel Electric Field 111
6.3 Results and Discussion 113
6.3.1 Electron Transport 115
6.3.2 Ion Transport 122
6.3.3 Ware Pinch Effect 125
6.3.4 Plasma Rotation Velocity 127
6.3.5 Summary and Conclusion 130
VII PLASMA CURRENT 136
7.1 Expression for Plasma Current 136
7.2 Parallel Conductivity 137
7.3 Bootstrap Current 138
7.4 Results and Discussion 140
7.4.1 Neoclassical Conductivity 140
7.4.2 Bootstrap Current 145
7.4.3 Summary and Conclusion 164
VIII SUMMARY AND RECOMMENDATIONS 167
8.1 Summary 167
8.2 Suggestions for Future Work 169
APPENDIX A 171
A.1 Expressions for $d\mu/dt$, dE/dt, and $d\xi/dt$ 171
A.2 Gyro-averaging Procedure 172

A.2.1 Calculation of $\overline{d\mu/dt}$ 172
A.2.2 Calculation of $\overline{d\bar{f}_1/dt}$ 174
APPENDIX B 178
B.1 Boundary Layer Formalism 178
B.2 Calculation of Restoring Coefficients 180
APPENDIX C 182
C.1 Expression for Parallel Velocity Difference 182
C.2 Bootstrap Current Coefficients 185
BIBLIOGRAPHY 188
VITA 193

LIST OF TABLES

2.1 Characteristics of RF-Heating (ICRH and ECRH) Systems. 7

6.1 Effect of Impurity Species on Ion Transport ($X_0 = 1$) 124

7.1 Effect of Impurity Species on Bootstrap Current Enhancement Factor ($X_0 = 1.0$) 154

LIST OF FIGURES

2.1 A Schematic Representation of RF-Heating (ECRH) System. 6

2.2 Guiding Center Coordinates 18

3.1 Particle Trapping During Wave Heating 38

3.2 Potential Asymmetry during Wave Heating 38

3.3 Creation of Dipoles during RF-Heating 49

3.4 Polarization of the Plasma during Wave Heating 52

3.5 Particle Trapping when $e_j\Phi_{in} < e_j\Phi_{out}$ 57

3.6 Particle Trapping when $e_j\Phi_{in} > e_j\Phi_{out}$ 57

3.7 Drift Orbit Modification during RF Heating with $k_\parallel = 0$ 70

3.8 Drift Orbit Modification for Co- and Counter-Flowing ions 70

4.1 Central Electron Temperature, Loop Voltage, and Line-Averaged Electron Density vs Time for 80-kW microwave pulse of 16-ms duration. Data from ISX-B [1]. 77

4.2 Experimental radiances of six iron lines for high density D-He iron dominated (ID) discharges ('fond' refers to background radiation). The central T_e and P_{EC} are also shown. Data from TFR [2]. 77

4.3 Experimental (left) and Simulated (right) Radiances of the High Density Discharges presented in Fig. 4.2. Simulated signals: the solid lines are for $D = 0.4\ m^2.s^{-1}$ and $V = 6.0\ m/s$; the dashed lines are for $D = 0.8\ m^2.s^{-1}$ and $V = 12.0\ m/s$. Data from TFR [2]. 80

4.4 Experimental (left) and Simulated (right) Radiances of the Low Density ID Discharges. Simulated signals: the solid lines are for $D = 0.6\ m^2.s^{-1}$ and $V = 6.0\ m/s$; the dashed lines are for $D = 1.2\ m^2.s^{-1}$ and $V = 12.0\ m/s$ with 1 gyrotron and for $D = 1.8\ m^2.s^{-1}$ and $V = 18.0\ m/s$ with 2 and 3 gyrotrons. Data from TFR [2]. 80

4.5 Typical Behavior of Intermediate Charge States of Injected Scandium. With ECRH, the Decay Time for Sc^{+12} decreases. Data from TEXT [3]. 81

4.6 Typical Discharge on JIPP T-IIU with $P_{RF} = 2$ MW. W_p and $W_e(0)$ are the total stored energy and stored energy density of electrons respectively. Data from JIPP T-IIU [4]. 83

4.7 Time Dependence of the Ti XX signal after Laser Blow-off into Ohmic and Auxiliary Heated Discharges. Data from ASDEX [5]. 86

4.8 Brightness of O VI (1032 Å) emission during ICRH Shot. I_p=343 kA; $\bar{n}_e = 3.0 \times 10^{13}\ cm^{-3}$; $T_e(0) = 700\ eV$. Data from TEXTOR [6]. . . . 86

5.1 Marginally Trapped-Untrapped Orbits 95

6.1 Particle Transport Coefficients as a Function of X_0 (Impurity: Carbon, $Z_{eff} = 3.0$) 118

6.2 Effect of Impurity Content on Transport Enhancement (Impurity: Carbon, $X_0 = 1.0$) 120

6.3 Ware Pinch Enhancement as a Function of X_0 126

6.4 Variation of Ware Pinch Enhancement with Z_{eff} 128

6.5 Comparison of Ware Pinch Enhancement with Chang's Results 129

6.6 Rotation Enhancement Factors as a Function of X_0 (Impurity: Carbon, $Z_{eff} = 3.0$) 131

6.7 Rotation Enhancement Factors as a Function of Z_{eff} (Impurity: Carbon, $X_0 = 1.0$) 132

7.1 Neoclassical Conductivity Reduction as a Function of X_0 146
7.2 Neoclassical Conductivity Reduction as a Function of Z_{eff} 147
7.3 Bootstrap Current Enhancement Factors
(Impurity: Carbon, $Z_{eff} = 3.0$) 150
7.4 Variation of Bootstrap Current Enhancement with Z_{eff} (Impurity:
Carbon, $X_0 = 1.0$) 152
7.5 α_n/α_T v/s X_0 for Bootstrap Current Enhancement ($\Phi_{in} > \Phi_{out}$) . . . 160
7.6 α_n/α_T v/s X_0 for Bootstrap Current Enhancement ($\Phi_{in} < \Phi_{out}$) . . . 161
7.7 Temperature and Density Profiles for a Pellet Injected JET Shot [7] . 163

SUMMARY

Previous theoretical studies have shown that a poloidal potential variation of order ϵ $(= r/R)$, which is likely to be produced during high power electron and ion cyclotron wave heating (ECRH and ICRH), can significantly enhance neoclassical transport in a simple plasma model consisting of one ion species and electrons in the low collisionality regime. The more realistic case of a plasma model with one or more impurity ion species present, in which the effects of a poloidal potential variation are likely to be more significant, has not been investigated previously.

In this thesis, the effects of a poloidal electric field of order ϵ upon particle transport and current in a tokamak plasma with a significant impurity content are studied theoretically. A kinetic theory approach is used to obtain the neoclassical transport coefficients for a large aspect ratio ($\epsilon \ll 1$) tokamak in the low collisionality regime.

Calculations indicate that, in an impure plasma, a poloidal electric field can significantly enhance (by a factor of ~ 3) ion diffusion, while its effect on the electron transport is similar to that obtained in the previous studies for a simple plasma. The magnitude of the ion transport enhancement is found to depend upon the impurity content, impurity species, and the magnitude of the poloidal electric field.

Enhancement of the neoclassical conductivity is found to be similar to that obtained in the previous studies; however, in the presence of a large impurity concentration, results of the present work can sometimes differ from those in the previous studies by $\sim 20\%$. A poloidal electric field causes a significant enhancement (a factor of ~ 2) of the bootstrap current coefficients. However, the nature of density and temperature profiles seem to be important in determining the change in the boot-

strap current. With parabolic profiles and carbon impurity, there is a decrease in the bootstrap current in most cases. The bootstrap current increases only when the potential on the outside is greater than that on the inside of the tokamak (as during ICRH) and the density profile is more peaked than roughly the square root of the temperature profile.

CHAPTER I

INTRODUCTION

Success of controlled fusion in a tokamak requires confining fuel ions, such as deuterium and tritium ions, under conditions which lead to substantial production of thermonuclear power. This requires heating the plasma to temperatures in excess of 10 keV in order to achieve a significant fusion rate. Ohmic heating alone is probably not sufficient to raise the temperature to the desired levels. Two additional methods that are being actively pursued include neutral beam injection heating (NBI) and "radio-frequency" (RF) heating (included in this term are both radio-frequency and microwave heating). Neutral beam heating has been used successfully, but its disadvantages include its size, complexity, and inefficiency at high energies in its present form. RF-heating offers greater flexibility in depositing energy, decouples heating and fueling, and has the potential of being a continuous source of power. Two of the several forms of wave heating methods that are being considered are the ion cyclotron resonance heating (ICRH) and the electron cyclotron resonance heating (ECRH).

With the emergence of RF heating as a dominant technique, it has become increasingly important to understand the effect of wave heating on particle and energy confinement. High power wave heating can significantly affect particle transport. Study of transport, in addition to helping us understand confinement, could lead to novel methods of impurity control, fueling, and burn control.

One aspect of transport that has been studied well over the last few decades is the collisional transport in the presence of the spatially varying magnetic field of a toka-

mak. This theory, known as neoclassical transport, was first developed for a simple plasma consisting of only one ion species and electrons (see the review by Hinton and Hazeltine [8]). Neoclassical transport is generally greater than the classical collisional transport in a uniform magnetic field. Connor [9] and Hirshman et al. [10] extended the neoclassical transport formalism to include the effect of impurities. It turns out that the presence of an impurity, even in small amounts, greatly enhances plasma transport.

The presence of an auxiliary heating mechanism can significantly influence neoclassical transport. Cyclotron wave heating, for example, can cause an increase in the trapping of the resonant particles (ions during ICRH and electrons during ECRH), leading to a poloidally varying potential. The potential variation, $\tilde{\Phi}(\theta)$, has been shown to reach magnitudes of order ϵ, i.e. $e\tilde{\Phi}(\theta)/T \sim \epsilon(= r/R)$ during high power wave heating [11]. Such a potential variation can also be caused by perpendicular and parallel NBI [12].

A poloidally varying potential of order ϵ changes neoclassical transport significantly. Chang [12] and Shurygin and Yushmanov [13] have studied the effect of a poloidal electric field on neoclassical transport in a simple plasma. Chang concludes that a poloidal electric field can cause a significant (a factor of 2 or more) enhancement of the neoclassical transport coefficients. A similar conclusion has also been reached by Shurygin and Yushmanov [13].

The purpose of the present work is to study the effect of a poloidal potential variation of order ϵ upon neoclassical transport in a tokamak plasma with a significant impurity content. We will be primarily concerned with calculation of the particle transport and plasma current in the low collisionality, or banana, regime. In an impure plasma, the presence of a poloidal electric field affects the collisional coupling between the main ions and the impurity ions in addition to affecting the electron-ion collisional coupling. The result of such a modification is an enhancement (or

reduction) of the ion transport as well as plasma current. The thesis is organized as follows.

In Chapter II, we first review briefly the wave heating theory. We then derive a form of the drift-kinetic equation commonly employed in studying neoclassical transport. We end the chapter with a brief consideration of collision operators and the quasilinear theory.

Chapter III is concerned mainly with a review of the theoretical literature on the effect of wave heating on particle transport. We begin by studying the production of electric fields during wave heating. We then examine the effect of a significant poloidal electric field, likely to be produced during wave heating, on particle trapping. The effect of a poloidal electric field on transport is then examined. Finally, we end the chapter with a brief review of wave-induced transport.

In Chapter IV, the experimental literature on the effect of wave heating on transport is reviewed. Our emphasis here is on the experimental literature containing evidence of changes in electron and impurity transport during wave heating. We also consider such related effects as change in the plasma potential and plasma rotation that may have a bearing on particle transport.

We begin solving the drift-kinetic equation in Chapter V. The solution methodology closely parallels the analytical technique used by Connor [9] and Hirshman et al. [14] in the absence of a significant poloidal electric field. The objective of this chapter is to derive a closed set of equations for the so called restoring coefficients [14], which now include the new effects of a poloidal potential variation. We end the chapter by deriving an expression for the neoclassical factor $f_{t\Phi}$ which contains the effect of the poloidal electric field.

In Chapter VI, the restoring coefficients derived in Chapter V are used to obtain expressions for the diffusive electron and ion fluxes as well as the convective Ware pinch effect, which now contain the effect of the poloidal electric field. Numerical

results are presented at the end of the chapter showing the variation of the transport coefficients as a function of the magnitude of the potential variation, impurity content, and impurity species.

In Chapter VII, we consider modifications to the plasma current due to the poloidal electric field in an impure plasma. We obtain expressions for the neoclassical conductivity and bootstrap current coefficients. Numerical results are presented on the variation of the transport coefficients with the potential variation as well as with the impurity concentration. We conclude the chapter with a consideration of the effect of density/temperature profiles on bootstrap current enhancement (reduction).

Finally, in Chapter VIII, we give a brief summary of the important results obtained in this work and a few suggestions for future work in this area.

CHAPTER II

BACKGROUND

The purpose of this chapter is to introduce some background material relevant to the study of wave heating and transport in tokamak plasmas. We will be making use of much of the material in this chapter in the subsequent chapters. We first introduce briefly the fundamentals of ion and electron cyclotron resonance heating (ICRH and ECRH respectively). Much of the material on wave heating discussed here is based on Refs. [15–30]. We then derive a form of the drift kinetic equation commonly employed in transport studies. We also discuss some of the collision operators used for calculating the collisional transport in tokamaks. Finally, we present a brief discussion of the quasilinear operator commonly employed in studying wave heating of fusion plasmas.

2.1 ICRH and ECRH

2.1.1 General Theory

Radiofrequency wave heating transfers energy from a remote source to the plasma by means of electromagnetic waves. It consists mainly of a rf-source, a transmission line, and a launch structure to ' inject ' the wave into the plasma. As an example, an ECRH system is schematically represented in Fig. 2.1. A list of sources, transmission lines and launch structures are shown along with other rf-heating parameters in Table 2.1.

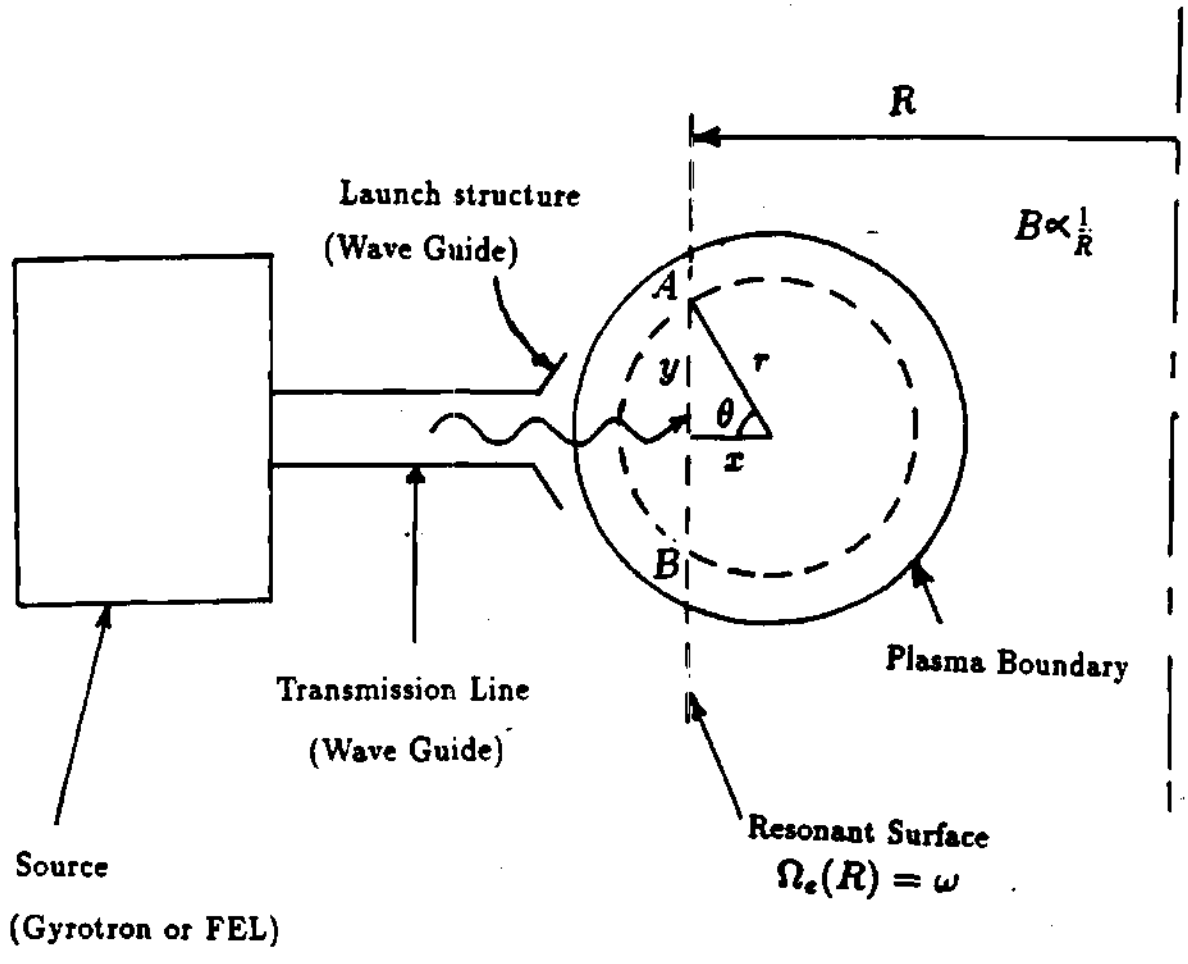

Figure 2.1: A Schematic Representation of RF-Heating (ECRH) System.

Table 2.1: Characteristics of RF-Heating (ICRH and ECRH) Systems.

Nature (type)	Characteristic frequency (f)	Density limit	Direction of incident energy	Energy source	Trans-mission line	Launch Structure	Comments
ICRH (Fast wave)	50-150 MHz	$na^2 \geq \frac{\pi^2 B^2}{\mu_0 m \omega^2}$ with		Tubes (Triode and tetrode)	Coaxial Lines	Coils (ridged wave guides may be possible)	
Minority Heating	f_i	$\omega = \Omega_i$	From inside or outside				
Second harmonic heating	$2f_i$	$\omega = 2\Omega_i$	From inside or outside				
ECRH	> 50 GHz			Gyrotrons FEL(future)	Wave guide	Wave guide or Horn	High power FEL under development
O-mode heating	f_e	$\Pi_e^2 < \Omega_e^2$	From inside or outside				Good spatial deposition control
X-mode heating ($\omega = \Omega_e$)	f_e	$\Pi_e^2 < 2\Omega_e^2$	From inside				Poor spatial deposition control
X-mode heating ($\omega = 2\Omega_e$)	$2f_e$	$\Pi_e^2 < 2\Omega_e^2$	From inside or outside				Good spatial deposition control

Once the wave is coupled to the plasma, it is required to propagate to the localized absorption zone with negligible loss. The requirements of accessibility of the absorption zone, its location and the process of absorption are matters of plasma physics. Fundamental to the understanding of propagation and absorption are the dispersion relations discussed briefly below.

Dispersion relations

Dispersion relations for a plasma determine the relation between the propagation vector $\mathbf{k}$ and the frequency ω for which waves propagate in the plasma. The first step in developing the dispersion relations for a magnetized plasma is to derive an expression for the dielectric tensor $\mathbf{K}$.

We have the electric displacement $\mathbf{D} = \epsilon_0\mathbf{E} + \mathbf{P}$, where $\mathbf{P}$ is the polarization vector, $\mathbf{E}$ is the electric field and ϵ_0 is the vacuum dielectric constant. Assuming a perturbation of the type $exp\, i(\mathbf{k}.\mathbf{r} - \omega t)$, the polarization current $\mathbf{j} = \frac{\partial \mathbf{P}}{\partial t} = -i\omega\mathbf{P}$.

Hence $\mathbf{D} = \epsilon_0\mathbf{E} + \frac{i}{\omega}\mathbf{j} = \epsilon_0\mathbb{K}\cdot\mathbf{E}$, or

$$\mathbf{D} = \epsilon_0\mathbf{E} + \frac{i}{\omega}\sum_k n_k q_k \mathbf{v}_k = \epsilon_0\mathbf{K}\cdot\mathbf{E} \tag{2.1}$$

Using the above relations in the Maxwell's equations

$$\begin{aligned} \nabla\times\mathbf{E} &= -\frac{\partial\mathbf{B}}{\partial t} \\ \nabla\times\mathbf{H} &= \mathbf{j} + \epsilon_0\frac{\partial\mathbf{E}}{\partial t} = \frac{\partial\mathbf{D}}{\partial t} \end{aligned}$$

we get [23],

$$\mathbf{N}\times(\mathbf{N}\times\mathbf{E}) + \mathbf{K}\cdot\mathbf{E} = \mathbf{0}$$

where $\mathbf{N} = \mathbf{k}c/\omega$. Here, c is the speed of light in vacuum. The above equation with the expression for the dielectric tensor gives the dispersion relation.

When the wave propagates through the plasma to the absorption zone, if its phase velocity $v_{ph} \gg v_{th,j}$, where $v_{th,j}$ is the thermal velocity of species j, then the procedure

for developing the dispersion relation is simplified considerably. We can then neglect the thermal velocity of the particles and, in Eq. 2.1, $\mathbf{v}_k$ is obtained using the Lorentz equation [23], giving us the dispersion relation,

$$K_\perp N_\perp^4 - [(K_\perp - N_\parallel^2)(K_\perp + K_\parallel) - K_\chi^2]N_\perp^2 + K_\parallel[(K_\perp - N_\parallel^2)^2 - K_\chi^2] = 0 \qquad (2.2)$$

where $N_\perp = K_\perp c/\omega$; $N_\parallel = K_\parallel c/\omega$ and

$$\begin{aligned} K_\perp &= 1 - \sum_k \frac{\Pi_k^2}{(\omega^2 - \Omega_k^2)} \\ K_\parallel &= 1 - \sum_k \frac{\Pi_k^2}{\omega^2} \\ K_\chi &= -\sum_k \frac{\Pi_k^2 \Omega_k}{(\omega^2 - \Omega_k^2)\omega} \end{aligned}$$

where $\Pi_k^2 = n_k^2 e_k^2/\epsilon_0 m_k$; $\Omega_k = -e_k B_0/m_k$. Here, n_k, m_k, e_k stand for the number density, mass, and charge of species k, and B_0 is the magnetic field. Π_k and Ω_k are the plasma frequency and the cyclotron frequency respectively for the species k.

Normally, in rf-heating experiments, the $N_\parallel$ spectrum is determined by the antenna and ω is determined by the generator. Hence, Eq. 2.2 is an equation for $N_\perp$. Solutions $N_\perp = 0$ and $N_\perp \to \infty$ characterize cold plasma cut-off and resonance respectively. While the cold plasma model is satisfactory for predicting the propagation characteristics and accessibility of the absorption zone, it breaks down close to a resonance. Also, it fails to predict resonances due to finite temperature effects. This is the case, for example, for ordinary wave heating with ECRH, for which the cold plasma model predicts no resonance. To develop the hot plasma dispersion relation, $\mathbf{v}_k$ in Eq. 2.1 is replaced by

$$< \mathbf{v}_k >= \int\int\int \mathbf{v}_k f_{1k} dv_x dv_y dv_z$$

An expression for the perturbed distribution function f_{1k} is obtained from the linearized Vlasov equation. The procedure and the results are rather cumbersome and will not be reproduced here. Detailed derivation of the hot plasma dielectric tensor

appears in Refs. [16, 21, 24]. Power absorbed per unit volume during wave heating is given by

$$P = \sum_k \overline{(\mathbf{j} \cdot \mathbf{E})_k} = \sum_k \overline{(nq < \mathbf{v} > \mathbf{E})_k}$$

where the overbar signifies time average. Using the warm plasma dielectric tensor [16, 21, 24], this expression reduces to

$$P = -\frac{i\epsilon_0\omega}{4}[\mathbf{E} \cdot (\mathbf{K}^* - \mathbf{I}) \cdot \mathbf{E}^* + \mathbf{E}^* \cdot (\mathbf{K} - \mathbf{I}) \cdot \mathbf{E}] \tag{2.3}$$

where $*$ denotes complex conjugate and $\mathbf{I}$ is the unit dyad. Alternatively, power absorbed may be obtained using a single particle picture [22] or the WKB theory may be used to obtain the absorption coefficient as is commonly done in the case of ECRH [17, 25]. Power absorption in specific heating methods is discussed in the following paragraphs.

2.1.2 ICRH

Heating the plasma in tokamaks near the ion cyclotron frequency may be done using the two-ion mode (minority heating and mode conversion), the second harmonic scheme or with the Ion-Bernstein waves (IBW). The two ion mode and the second harmonic schemes employ the fast Alfvén wave. The slow Alfvén wave is not suitable for heating tokamak plasmas because it does not propagate above the cyclotron frequency. (Fast and slow Alfvén waves are low frequency ($\omega \sim \Omega_i$) electromagnetic waves. The fast wave has a larger phase velocity than the slow wave). As typical examples, we will consider two-ion (minority heating) and second harmonic heating. One or both of these schemes are being used in the present generation machines like JET, ASDEX and TFTR.

The dispersion relation for hydromagnetic (fast and slow) waves can be obtained from Eq. 2.2 using the low frequency ($\mid \omega \mid \ll \Omega_e$), high conductivity ($\mid E_z \mid \ll \mid E_x \mid ; \mid E_y \mid$ where E_z is the electric field in the direction of static magnetic field)

approximation. The resulting expression [22] is,

$$N_{\perp,a}^2 = A - N_{\parallel,a}^2 + \frac{A(1-A)}{A - N_{\parallel,a}^2} \tag{2.4}$$

where $N_{\perp,a}$ and $N_{\parallel,a}$ are Alfvén refractive indices defined by

$$N_{\perp,a}^2 = N_{\perp}^2 \left(\frac{B^2}{\mu_0 n_i m_i c^2} \right)$$

$$N_{\parallel,a}^2 = N_{\parallel}^2 \left(\frac{B^2}{\mu_0 n_i m_i c^2} \right)$$

and $A = \frac{\Omega_i^2}{(\Omega_i^2 - \omega^2)}$. The electric field polarization is given by

$$\frac{E^+}{E^-} = \frac{E_x + iE_y}{E_x - iE_y} = \frac{\frac{\Omega_i}{\omega+\Omega_i} - N_{\parallel,a}^2}{\frac{\Omega_i}{\omega-\Omega_i} + N_{\parallel,a}^2} \tag{2.5}$$

The condition for fast wave propagation is obtained [15,22] by setting $k_{\parallel,n} = 2\pi p/2\pi R = p/R$ and $k_{\perp,n} = 2\pi q/2a = \pi q/a$ in Eq. 2.4. Here, $k_{\parallel,n}$ and $k_{\perp,n}$ are the natural parallel and perpendicular wave numbers, p, q are integers, R and a are the major and minor radii of the tokamak. By setting $p = 0$ and $q = 1$, we get the marginal condition for propagation as

$$na^2 \geq \frac{\pi^2 B^2}{\mu_0 m_i \omega^2} = 5.1 \times 10^{17} \left(\frac{\Omega_i}{\omega} \right)^2 \left(\frac{m_i}{m_H} \right) \ m^{-1}$$

Here, m_H is the mass of the hydrogen ion. This equation implies that fast wave propagation requires relatively large and dense devices, especially if $\omega < \Omega_i$.

Minority Heating Scheme

Heating a single ion species plasma at the fundamental ion cyclotron frequency is virtually impossible because the right handed component of the electric field, E^+, is extremely small in magnitude. In fact, if we put $N_{\parallel,a} \simeq 0$ and $\omega = \Omega_i$ in Eq. 2.5, we find $E^+ \simeq 0$. The inclusion of hot plasma effects gives a small but finite value for E^+. Presence of a second ion species even in concentrations as small as $\leq 5\%$ improves the scenario dramatically. If we have a small percentage of hydrogen ions

in a predominantly deuterium plasma, we would find that $E^+/E^- = 1/3$ for $N_{\parallel,a} = 0$ by setting $\omega = \Omega_H$ in Eq. 2.5. This procedure neglects the contribution of hydrogen ions and hot plasma effects. An exact calculation should take these effects into consideration [19,22].

Power absorbed by cyclotron damping may be computed using Eq. 2.3 or using the single particle approach as done by Stix [22]. The result of the second approach is

$$< P >= \frac{n_{i,res}(r)e_i^2 \mid E^+ \mid^2 R}{m_i \Omega_i r \mid \sin\theta \mid} \tag{2.6}$$

where r, R and θ are defined in Fig. 2.1. $< P >$ is the power absorbed per unit volume at the location r. $\mid E^+ \mid$ is obtained from Eq. 2.6 by putting $\Omega = \Omega_{i,minority}$ or, more accurately, from the wave equation using the hot plasma dielectric tensor.

In addition to cyclotron damping, power may be absorbed by the electrons moving along the magnetic field lines via Landau and transit-time damping. Particles which absorb power by these collisionless processes satisfy the resonance condition $\omega - k_\parallel v_\parallel = 0$. Detailed discussion of these phenomena appear in Refs. [16, 21, 22, 24, 28]. These damping mechanisms are active in a plasma with an electron distribution function having a negative slope in the neighborhood of the wave phase velocity. In the case of Landau damping, the force on the particles is qE; for transit-time damping, it is $-\bar{\mu}\nabla B_w$, where $\bar{\mu} = 1/2(mv_\perp^2/B)$ is the magnetic moment and B_w is the wave magnetic field. Both mechanisms are active in fast wave damping, but the two effects are coherent and cross terms have to be included. The power absorbed can be computed using Eq. 2.3. It turns out that the transit-time terms cancel with the cross-terms leaving only the Landau damping term [22]. The result is

$$P = \frac{\omega\beta_e N_\perp^2}{16\sqrt{\pi}} \frac{\omega}{k_\parallel v_{th,e}} \mid E_y \mid^2 \exp - \left(\frac{\omega}{k_\parallel v_{th,e}}\right)^2 \tag{2.7}$$

where $\beta_e = (2\mu_0 n_e T_e)/B^2$ and $v_{th,e}^2 = 2T_e/m_e$, T_e being the electron temperature.

Second Harmonic Heating

Second harmonic heating is a finite Larmor radius effect. Indeed, when $\omega = 2\Omega_i$, the sign of $\mathbf{E}_\perp.\mathbf{V}$ changes twice during one orbit. If the electric field is spatially homogeneous, then the energy gained during one half of gyration is lost during the other half. If the wave has a finite perpendicular wavelength, the cancellation is incomplete and the particle gains energy. Power absorption during second harmonic heating is given by [26],

$$< P >= \frac{n_{i,res}(r)e_i^2 |\ E^+\ |^2 R}{m_i \Omega_i r |\ \sin\theta\ |} \left(\frac{n_\perp^2 v_\perp^2}{c^2}\right) \tag{2.8}$$

Here $n_\perp$ is to be obtained from the dispersion relation and E^+ is obtained from the wave equation using the hot plasma dielectric tensor. If we use Eq. 2.5, we get $E^+ \simeq |\ E_y\ |$.

2.1.3 ECRH

Radiofrequency heating near the electron cyclotron frequency can be done by launching either an ordinary wave with the electric field parallel to the magnetic field (O-mode heating) or an extraordinary wave with the electric field perpendicular to the magnetic field (X-mode heating). One or both of these methods have been used successfully to heat the plasma in several tokamaks like ISX-B, TFR, DOUBLET-III D, and T-10 [31]. ECRH is considerably simpler than all other rf-heating methods in all aspects except for the availability of high power millimeter wave sources. With the anticipated development of free electron lasers or high power gyrotrons, it could become a major heating method.

The cold plasma dispersion relations for the O- and X-modes can be obtained from Eq. 2.2. For propagation perpendicular to the magnetic field, in the high frequency limit ($\omega \simeq \Omega_e \gg \Omega_i$) we obtain, for the O-mode,

$$k_\perp^2 = \frac{\omega^2 - \Pi_e^2}{c^2} \tag{2.9}$$

and, for the X-mode,

$$k_\perp^2 = \frac{[(\Pi_e^2 - \omega^2)^2 - \Omega_e^2\omega^2]}{c^2[\omega^2 - \Pi_e^2 - \Omega_e^2]} \tag{2.10}$$

Power absorption during ECRH can be obtained from Eq. 2.3 or, alternatively, wave damping can be calculated along the ray trajectories using the WKB theory.

Ordinary Wave Heating

An ordinary wave has its electric field parallel to the static magnetic field. From Eq. 2.9, it is clear that the O-mode has no resonance in the cold plasma limit. However, the inclusion of hot plasma effects introduces resonances at the cyclotron harmonics. Physically, this is because the Lorentz force on the electron due to its finite parallel velocity and the wave magnetic field can be split into two components; the left circularly polarized and the right circularly polarized components. It is the right handed component of the force that accelerates the electrons.

From Eq. 2.9, the density limit for the O-mode propagation can be obtained by putting $k_\perp = 0$ (cut-off condition) as

$$\Pi_e^2 < \Omega_e^2 \quad or \quad n_e < \epsilon_0 B^2/m_e$$

Furthermore, the wave can be launched from the outside of the tokamak. Power absorption during O-mode heating has been calculated using Eq. 2.3 by Fidone et al. [29]. In the nonrelativistic limit, power absorbed per unit volume is

$$P = \frac{\epsilon_0\omega}{2\sqrt{\pi}} \frac{X v_{th,e}}{2N_\parallel c} \frac{N_\parallel^2}{N_\parallel^2 + \frac{v_{th,e}^2}{\pi c^2}} \mid E_x \mid^2 \tag{2.11}$$

where $X = \Pi_e^2/\omega^2$. Power absorption increases for $N_\parallel \to 0$.

Alternatively, the absorption coefficient along a ray trajectory can be calculated [17, 28, 30] and the result is

$$A_0 = 1 - T_0$$

where A_0 is the absorption coefficient and T_0 is the transmission coefficient [30].

$$T_0 = \exp(-2\pi\eta_0) \tag{2.12}$$

where

$$\eta_0 = \frac{R\omega\alpha^2}{4c}\frac{[1-\alpha^2]^{1/2}}{[1+N_\parallel^2(1-\alpha^2)]}\frac{T_e}{mc^2}$$

and $\alpha = \Pi_e^2/\omega^2$.

Extraordinary Wave Heating

An extraordinary wave has its electric field perpendicular to the static magnetic field. The electric field polarization calculated using the cold plasma theory is given by

$$E^- = E_x - iE_y = -iE_y\left[\frac{K_\chi - K_\perp}{K_\chi}\right]$$

As $\omega \rightarrow \Omega_e$, $E^- \rightarrow 0$. Hence, there is no electron heating unless we introduce warm plasma effects. Hot plasma theory predicts resonances at the cyclotron harmonics.

The density limit for X-wave heating can be obtained from Eq. 2.10 by putting $k_\perp = 0$. This gives

$$\Pi_e^2 \leq 2\Omega_e^2 \quad or \quad n_e \leq 2\epsilon_0 B^2/m_e$$

Hence, X-mode heating has a higher density limit than O-mode heating. However, X-mode heating at the fundamental frequency can be done only by launching the wave from the inside of the tokamak because the wave encounters a low density cut-off before resonance if launched from the outside. On the other hand, X-mode heating at the second harmonic can be done by launching the wave from the outside. Power absorption at the cyclotron fundamental has been calculated by Fidone et al. [29]. In the nonrelativistic limit, the power absorption per unit volume is

$$P_{(x)} = \frac{\epsilon_0\omega}{\sqrt{\pi}}\left(\frac{N_\parallel v_{th.e}}{Xc}\right)\mid E_y \mid^2 \tag{2.13}$$

From this equation, it is clear that as $N_{\parallel} \to 0$, power absorption becomes negligible. Power absorption can also be written down in terms of an absorption coefficient [30],

$$A_{X1} = 1 - T_{X1} \tag{2.14}$$

where

$$T_{X1} = \exp(-2\pi\eta_{X1})$$
$$\eta_{X1} = \frac{R\omega N_{\parallel}^2}{4c\alpha^2}(2-\alpha^2)^{3/2}(1+\alpha^2)^2\left(\frac{T_e}{mc^2}\right)$$

For the X-mode second harmonic heating, absorption is given by [17]

$$A_{X2} = 1 - T_{X2} \tag{2.15}$$

$$T_{X2} = \exp(-2\pi\eta_{X2})$$
$$\eta_{X2} = \frac{R\omega\alpha^2}{c}\left(\frac{3-2\alpha^2}{3-4\alpha^2}\right)^2\left(\frac{4(1-\alpha^2)^2-1}{3-4\alpha^2}\right)^{1/2}\frac{T_e}{mc^2}$$

2.2 Drift Kinetic Equation

Microscopic description of a thermonuclear plasma centers around the plasma kinetic equation

$$\frac{df}{dt} = C(f) \tag{2.16}$$

where the left hand side is the substantial derivative of the particle distribution function along the particle trajectory and the right hand side is the collision operator. The collision operator $C(f)$ describes scattering of particles of the species under consideration (test particles) due to collisions with particles of the same species as well as other species (field particles). Eq. 2.16 has the form of a conservation equation in the phase space, and it can be derived from the Liouville equation for the many particle distribution function [21, 32].

The plasma kinetic equation is quite complicated and, hence, a simplified form of the kinetic equation, known as the drift-kinetic equation (DKE) is commonly employed in collisional transport studies. The DKE may be thought of as an equation for describing the motion of the guiding centers of the charged particles in the presence of electromagnetic fields and collisional scattering. DKEs for many applications have been derived by several authors [32,8,33,34]. We shall be particularly concerned with a form of the drift-kinetic equation relevant to tokamak transport applications. In the following sections, we will derive the drift-kinetic equation. The derivation follows arguments similar to those found in Refs. [8,33,34].

2.2.1 Basic Equations

We write the left hand side of Eq. 2.16 in terms of the time coordinate t, space coordinates $\mathbf{x}$, and the velocity space variables μ, E, and ξ. Here $\mu = (v_\perp^2/2B)$ is the magnetic moment per unit mass, $E = (v^2/2 + e\Phi/m)$ is the energy of a particle per unit mass, and ξ is the gyrophase of the particle. Referring to Fig. 2.2,

$$\xi = -\tan^{-1}\left(\frac{\mathbf{v}\cdot\hat{e}_2}{\mathbf{v}\cdot\hat{e}_3}\right)$$

With this, Eq. 2.16 can be written as

$$\frac{\partial f}{\partial t} + \mathbf{v}\cdot\nabla f + \frac{\partial f}{\partial \mu}\left(\frac{d\mu}{dt}\right) + \frac{\partial f}{\partial E}\left(\frac{dE}{dt}\right) + \frac{\partial f}{\partial \xi}\left(\frac{d\xi}{dt}\right) = C(f) \qquad (2.17)$$

We note here that an equation similar to 2.17 has been derived rigorously from the Liouville equation by Balescu [32, Vol.1, chap. 2]. Eq. 2.17 forms the starting point in our analysis. We now derive expressions for the time derivatives of μ, E, and ξ. The equation of motion for a charged particle in an electromagnetic field is

$$\frac{d\mathbf{v}}{dt} = \frac{d}{dt}(\mathbf{v}_\perp + \mathbf{v}_\parallel) = \frac{e}{m}(\mathbf{E} + \mathbf{v}\times\mathbf{B}) \qquad (2.18)$$

Referring to Fig. 2.2, we write the following useful expressions

$$\mathbf{v}_\perp = (2\mu B)^{1/2}\hat{n}_\perp = (2\mu B)^{1/2}(\hat{e}_2\cos\xi - \hat{e}_3\sin\xi) \qquad (2.19)$$

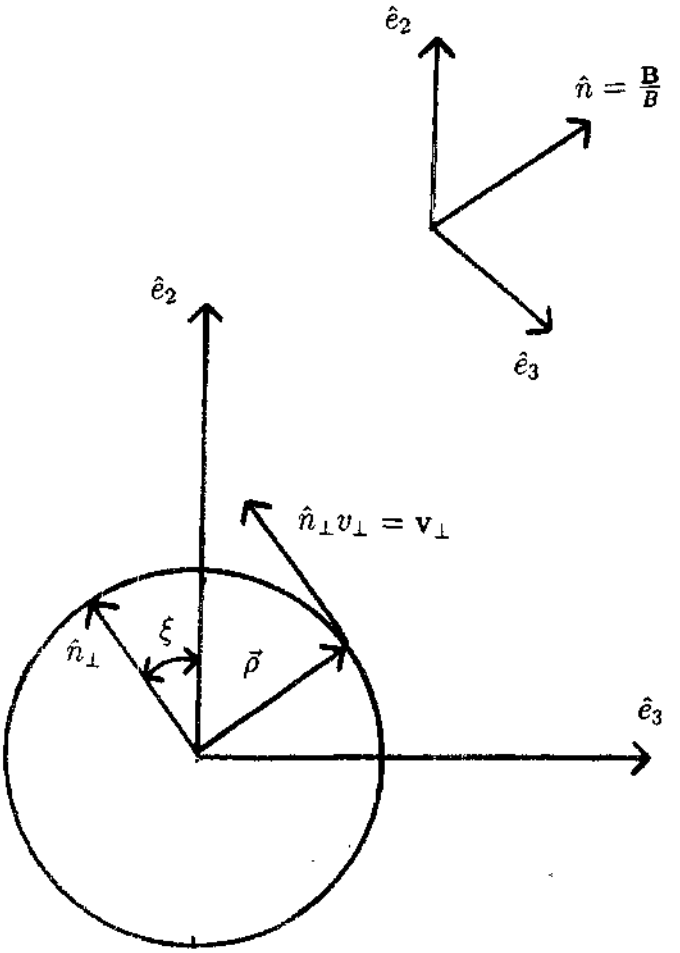

Figure 2.2: Guiding Center Coordinates

Also

$$\hat{\rho} = \hat{n} \times \hat{n}_\perp = \hat{e}_3 \cos\xi + \hat{e}_2 \sin\xi$$

where $\hat{n}$ is the unit vector along the magnetic field line. With the help of these identities, Eq. 2.18 can be written as

$$\frac{d\mathbf{v}_\perp}{dt} + \frac{d\mathbf{v}_\parallel}{dt} = \frac{e}{m}\mathbf{E} - \Omega v_\perp \hat{\rho} \tag{2.20}$$

where $\Omega = eB/m$ is the cyclotron frequency of the charged particle. (In this section, the variables e and m denote the charge and mass of the species j.) By taking the dot product of Eq. 2.20 with $\mathbf{v}_\perp$, $\mathbf{v}$, and $\hat{\rho}$, we obtain the following expressions for the time derivatives of μ, E, and ξ (see Appendix A for details)

$$\frac{d\mu}{dt} = -\frac{\mu}{B}\frac{dB}{dt} - \frac{v_\parallel}{B}\mathbf{v}_\perp \cdot \frac{d\hat{n}}{dt} + \frac{e}{mB}\mathbf{E}\cdot\mathbf{v}_\perp \tag{2.21}$$

$$\frac{dE}{dt} = \frac{e}{m}\left(\frac{\partial\Phi}{\partial t} - \mathbf{v}\cdot\frac{\partial\mathbf{A}}{\partial t}\right) \tag{2.22}$$

$$\frac{d\xi}{dt} = \Omega + \hat{e}_3 \cdot \frac{d\hat{e}_2}{dt} + \frac{v_\parallel}{v_\perp}\hat{\rho}\cdot\frac{d\hat{n}}{dt} - \frac{e}{mv_\perp}\hat{\rho}\cdot\mathbf{E} \tag{2.23}$$

where the electric field is given by $\mathbf{E} = -\nabla\Phi - \frac{\partial\mathbf{A}}{\partial t}$ with $\mathbf{A}$ being the vector potential. Using the expressions 2.21-2.23, Eq. 2.17 can be rewritten as

$$\begin{aligned}\frac{\partial f}{\partial t} + v_\parallel \hat{n}\cdot\nabla f + v_\perp(\hat{e}_2\cos\xi - \hat{e}_3\sin\xi)\cdot\nabla f \\ + \frac{\partial f}{\partial\mu}\left[-\frac{\mu}{B}\frac{dB}{dt} - \frac{v_\parallel}{B}\mathbf{v}_\perp\cdot\frac{d\hat{n}}{dt} + \frac{e}{mB}\mathbf{E}\cdot\mathbf{v}_\perp\right] + \frac{\partial f}{\partial E}\left[\frac{e}{m}\left(\frac{\partial\Phi}{\partial t} - \mathbf{v}\cdot\frac{\partial\mathbf{A}}{\partial t}\right)\right] \\ + \frac{\partial f}{\partial\xi}\left[\Omega + \hat{e}_3\cdot\frac{d\hat{e}_2}{dt} + \frac{v_\parallel}{v_\perp}\hat{\rho}\cdot\frac{d\hat{n}}{dt} - \frac{e}{mv_\perp}\hat{\rho}\cdot\mathbf{E}\right] = C(f)\end{aligned} \tag{2.24}$$

2.2.2 Ordering

Our next task is to introduce certain simplifying assumptions to obtain a set of ordering parameters which can then be used to obtain a hierarchy of equations from Eq. 2.24. It turns out that it is simpler to solve the simplified equations obtained after ordering than it is to solve the original equation (Eq. 2.24).

We note that the choice of the assumptions (or ordering parameters) depends upon the problem we want to solve. In the present case, we are interested in the solution of the kinetic equation for a tokamak plasma in the presence of large poloidal electric fields in the low collisionality regime. It should be pointed out that the neoclassical transport theory depends crucially on the presence of drifts caused by the magnetic field curvature (∇B, curvature, and, in the present case, $\mathbf{E}_\theta \times \mathbf{B}$ drifts). Hence, the version of the drift kinetic equation to be derived would have to explicitly involve these drifts in addition to the collisional scattering phenomena. Our ordering scheme will indeed be influenced by these considerations. We will adopt most of the ordering assumptions of the standard neoclassical theory [8]. We will relax these assumptions only when the present problem requires such changes to be made.

We begin by defining the scale length for changes in such macroscopic parameters as pressure, temperature, etc. by

$$l = \left(\frac{\nabla p}{p}\right)^{-1}$$

where p could be any macroscopic parameter. At this stage, we do not make any assumption regarding the aspect ratio (i.e. R/r) of the device. Hence, l is a fairly general gradient scale length.

We define the transit frequency as

$$\omega = \frac{v_{th}}{l} \tag{2.25}$$

Defining the gyroradius as $\rho = v_{th}/\Omega = (mv_{th}/eB)$, we have the basic ordering assumption as

$$\delta = \frac{\rho}{l} = \frac{\omega}{\Omega} \ll 1 \tag{2.26}$$

(It turns out that the more relevant parameter is $\delta_\theta = (1/l)(mv_{th}/eB_\theta) = (B/B_\theta)\delta$. In a low β plasma, $B \simeq B_\phi \gg B_\theta$. Hence $\delta_\theta \gg \delta$. We shall adopt the stronger constraint $\delta_\theta \ll 1$. We will, however, continue to use the symbol δ to denote δ as well as δ_θ.)

We further assume that the macroscopic quantities like density, temperature, etc. vary slowly. Specifically, we assume, consistent with Hinton and Hazeltine [8], that

$$\frac{\partial}{\partial t} \sim \mathcal{O}(\delta^2 \omega) \tag{2.27}$$

Also, we assume the "drift ordering" [8], i.e.,

$$\frac{E}{B v_{th}} \sim \mathcal{O}(\delta) \tag{2.28}$$

which merely states that the drift velocities (including the bulk rotation velocity) are small compared with the typical thermal velocity. This is expected to be the case for an ohmically heated plasma as well as for a plasma heated by perpendicular NBI and electromagnetic waves.

The effect of ohmically induced electric field $E_\parallel$ is expected to be significant only for the electrons due to their smaller mass. Hinton and Hazeltine [8] use an ordering scheme ("maximal ordering") according to which $E_\parallel \sim \mathcal{O}(\delta_{\theta,e}) E_{run}$ where $E_{run} \sim m_e v_{th,e}/e\tau_e$. Here τ_e is the electron-ion collision frequency given by [8],

$$\tau_e = \frac{3}{16\sqrt{\pi}} \frac{m_e^2 v_{th,e}^3}{Z^2 e^4 n_i \ln \Lambda}$$

In the ion equation, it turns out that $E_\parallel \sim \mathcal{O}(\delta_{\theta,i}^2) E_{run}$ [8]. Hence, $E_\parallel$ is significant only in the electron equation. We, however, retain $E_\parallel$ in the electron as well as ion equation in order to keep the formalism quite general, i.e. we assume, for ordering purposes,

$$E_\parallel \sim \mathcal{O}\left(\delta \frac{m v_{th}}{e\tau}\right) \tag{2.29}$$

We assume initially that $v_\parallel \sim v_\perp \sim \mathcal{O}(v_{th})$ and the transit frequency $\omega \sim \mathcal{O}(\nu)$, where ν is the collision frequency. Later, when we specialize for the banana regime, we will distinguish between the collision and transit frequencies. With the above choice of assumptions and ordering parameters, we order the various terms in Eq 2.24 as follows.

we first note that the operator $\mathbf{v}\cdot\nabla \sim \mathcal{O}(v_{th}/l) \sim \mathcal{O}(\omega)$.

$$\begin{aligned}
\frac{\partial}{\partial t} &\sim \mathcal{O}(\delta^2\omega) \\
v_\parallel \hat{n}\cdot\nabla &\sim \mathcal{O}(\omega) \\
\mathbf{v}_\perp\cdot\nabla &\sim \mathcal{O}(\omega) \\
\frac{\partial}{\partial\mu}\left(\frac{\mu}{B}\frac{\partial B}{\partial t}\right) &\sim \mathcal{O}(\delta^2\omega) \\
\frac{\partial}{\partial\mu}\left(\frac{\mu}{B}\mathbf{v}\cdot\nabla B\right) &\sim \mathcal{O}(\omega) \\
\frac{\partial}{\partial\mu}\left(\frac{v_\parallel}{B}\mathbf{v}_\perp\cdot\frac{\partial\hat{n}}{\partial t}\right) &\sim \mathcal{O}(\delta^2\omega) \\
\frac{\partial}{\partial\mu}\left(\frac{v_\parallel}{B}\mathbf{v}_\perp\cdot(\mathbf{v}\cdot\nabla)\hat{n}\right) &\sim \mathcal{O}(\omega)
\end{aligned}$$

Using the drift ordering assumption, i.e., $(E/B) \sim \mathcal{O}(\delta v_{th})$,

$$\frac{\partial}{\partial\mu}\left(\frac{e}{mB}\mathbf{E}\cdot\mathbf{v}_\perp\right) \sim \mathcal{O}(\delta\Omega)$$

$$\frac{\partial}{\partial E}\left(\frac{e}{m}\frac{\partial\Phi}{\partial t}\right) \sim \mathcal{O}(\delta^2\omega)$$

Using our ordering assumption for $E_\parallel = -(\partial\mathbf{A}/\partial t)$ according to Eq. 2.29,

$$\frac{\partial}{\partial E}\left(\frac{e}{m}\mathbf{v}\cdot\frac{\partial\mathbf{A}}{\partial t}\right) \sim \mathcal{O}(\delta\omega)$$

where we have used $1/\tau = \nu \sim \mathcal{O}(\omega)$.

$$\begin{aligned}
\Omega\frac{\partial}{\partial\xi} &\sim \mathcal{O}(\Omega) \\
\frac{\partial}{\partial\xi}\left(\hat{e}_3\cdot\frac{d\hat{e}_2}{dt}\right) &\sim \mathcal{O}(\omega) \\
\frac{\partial}{\partial\xi}\left(\frac{v_\parallel}{v_\perp}\hat{\rho}\cdot\frac{d\hat{n}}{dt}\right) &\sim \mathcal{O}(\omega) \\
\frac{\partial}{\partial\xi}\left(\frac{e}{mv_\perp}\hat{\rho}\cdot\mathbf{E}\right) &\sim \mathcal{O}(\delta\omega) \\
C(f) &\sim \mathcal{O}(\omega)
\end{aligned}$$

With this, we now expand the distribution function f in terms of the basic ordering parameter δ.

$$f = f_0 + f_1 \tag{2.30}$$

where $f_1 \sim \mathcal{O}(f_0\delta)$. Using the above expression in Eq. 2.24, we can obtain a hierarchy of equations by collecting terms of the same order. To facilitate ordering, we shall divide all terms in Eq. 2.24 by Ω.

Order δ^0

To the lowest order in δ, i.e. δ^0, we have

$$\Omega\frac{\partial f_0}{\partial \xi} = 0 \tag{2.31}$$

This immediately leads to the conclusion that f_0 is independent of the gyrophase. Hence

$$f_0 \neq f_0(\xi)$$

Order δ

To the order δ, we have

$$\begin{aligned} &v_\parallel \hat{n}\cdot\nabla f_0 + v_\perp(\hat{e}_2\cos\xi - \hat{e}_3\sin\xi)\cdot\nabla f_0 \\ &+\frac{\partial f_0}{\partial \mu}\left[-\frac{\mu}{B}\frac{dB}{dt} - \frac{v_\parallel}{B}\mathbf{v}_\perp\cdot\frac{d\hat{n}}{dt} + \frac{e}{mB}\mathbf{E}\cdot\mathbf{v}_\perp\right] + \frac{\partial f_1}{\partial \xi}\Omega = C(f_0) \end{aligned} \tag{2.32}$$

where, in the substantial derivatives, we have retained only the convective part according to our ordering scheme. We have also used the property that f_0 is gyrophase independent in obtaining the above equation.

Gyro-averaging Eq. 2.32, we have

$$v_\parallel \hat{n}\cdot\nabla f_0 + \frac{\partial f_0}{\partial \mu}\left(\overline{\frac{d\mu}{dt}}\right) = C(f_0) \tag{2.33}$$

where $\overline{F}$ is the gyro-average of the quantity F defined by

$$\overline{F} = \frac{1}{2\pi}\int_0^{2\pi} F\, d\xi$$

Also,

$$\overline{\frac{d\mu}{dt}} = \overline{-\frac{\mu}{B}\frac{dB}{dt} - \frac{v_\parallel}{B}\mathbf{v}_\perp \cdot \frac{d\hat{n}}{dt} + \frac{e}{mB}\mathbf{E}\cdot\mathbf{v}_\perp}$$

While gyro-averaging, quantities which do not explicitly depend upon the gyrophase are treated as constants [35]. In the presence of a wave heating mechanism, some quantities like $\mathbf{E}_\perp$ may not be independent of the gyrophase throughout the plasma volume. We, however, treat these quantities as gyrophase independent for the following reasons.

- In many wave heating scenarios, particles of only one species participate in the energy absorption process. For instance, during ECRH only electrons take part in the energy absorption process, while during ICRH, ions are the main participants. (We note that in some instances, electrons can also participate via Landau damping and transit time magnetic pumping). Furthermore, in many wave heating mechanisms, such as ICRH (minority heating), only a small fraction of particles participate in wave heating.

- In most wave heating scenarios, the launched wave has $k_\parallel \neq 0$. This means that only a fraction of the particles satisfying the resonance condition $\omega - k_\parallel v_\parallel = 0$ participate in wave heating. Furthermore, the resonance zone where $\mathbf{E}_\perp$ may not be zero is confined to a thin region across a vertical plane. Hence, for the bulk of the particles over most of the plasma volume, $\mathbf{E}_\perp = 0$ is a good assumption.

Carrying out the gyro-averaging process (see Appendix A), we find that

$$\overline{\frac{d\mu}{dt}} = 0$$

to the order δ. Hence, to the order δ, we have

$$v_\parallel \hat{n}\cdot\nabla f_0 = C(f_0) \tag{2.34}$$

Multiplying Eq. 2.34 by $\ln f_0$ and integrating over the velocity space, we have

$$\int v_{\parallel}\hat{n}\cdot\nabla f_0 \ln f_0 d^3v = \int C(f_0)\ln f_0 d^3v \tag{2.35}$$

Specializing for a tokamak, and using the Jacobian to transform to μ, E, and ξ coordinates, we get

$$\sum_{\sigma}\sigma B\left(\frac{B_\theta}{\tau B}\right)\int\frac{\partial f_0}{\partial\theta}\ln f_0 d\mu dE d\xi = \sum_{\sigma}\sigma B\left(\frac{B_\theta}{\tau B}\right)\frac{\partial}{\partial\theta}\int(f_0\ln f_0 - f_0)d\mu dE d\xi \tag{2.36}$$

where σ is the sign of the parallel velocity ($\sigma = \pm$). Transforming back to the velocity coordinates, we have

$$\mathbf{B}\cdot\nabla\int\frac{v_{\parallel}}{B}(f_0\ln f_0 - f_0)d^3v = \int \ln f_0 C(f_0)d^3v \tag{2.37}$$

Carrying out the flux surface average, i.e., for a tokamak

$$< F >= \int_0^{2\pi}\left(\frac{F}{2\pi}\right)(1+\epsilon\cos\theta)d\theta$$

and noting that $< \mathbf{B}\cdot\nabla F >= 0$, we get

$$\left\langle\int \ln f_0 C(f_0)d^3v\right\rangle = 0 \tag{2.38}$$

Here we note that $C(f_0) = C(f_{j0}) = \sum_k C(f_{j0}, f_{k0})$. If the collision operator $C(f_{j0}, f_{k0})$ satisfies the H-theorem, we know that [36],

$$\int \ln f_0 C(f_0)d^3v \leq 0 \tag{2.39}$$

Thus, in general, Eq. 2.38 can only be satisfied if

$$\int d^3v \ln f_0 C(f_0)d^3v = 0$$

which in turn is satisfied if $C(f_0) = 0$ [8,32]. The solution of this equation is the Maxwellian

$$f_0 = n\left(\frac{m}{2\pi T}\right)^{3/2}\exp\left(-\frac{mv^2}{2T}\right) \tag{2.40}$$

Using this equation in the zeroth order kinetic equation, Eq. 2.34, we have, for a tokamak,

$$\frac{v_\parallel B_\theta}{rB}\frac{\partial f_0}{\partial \theta} = 0$$

Using the expression for f_0, and noting that the energy of a particle is $E^* = (v^2/2) + (e\tilde{\Phi}(\theta)/m)$, where $\tilde{\Phi}(\theta)$ is the poloidally varying component of the potential, we obtain

$$\frac{1}{n}\frac{\partial n}{\partial \theta} = -\frac{e}{T}\frac{\partial \tilde{\Phi}(\theta)}{\partial \theta}$$

or

$$n = < n > \exp\left(-\frac{e\tilde{\Phi}(\theta)}{T(r)}\right) \tag{2.41}$$

Here we assume the temperature to be a function of the flux surface only. Hence

$$f_0 = n_0\left(\frac{m}{2\pi T}\right)^{3/2}\exp\left(-\frac{mE^*}{T}\right) \tag{2.42}$$

where $n_0 = < n >$.

2.2.3 Drift-Kinetic Equation

Letting $f_1 = \overline{f_1} + \tilde{f}_1$, where $\overline{f_1}$ is the gyrophase independent part of f_1 and $\tilde{f}_1$ is the gyrophase dependent part, and noting that f_0 is independent of μ, Eq. 2.32 reduces to

$$v_\perp(\hat{e}_2\cos\xi - \hat{e}_3\sin\xi)\cdot\nabla f_0 = -\frac{\partial \tilde{f}_1}{\partial \xi}\Omega$$

or

$$\tilde{f}_1 = -\frac{v_\perp}{\Omega}(\hat{e}_2\sin\xi + \hat{e}_3\cos\xi)\cdot\nabla f_0 = -\frac{v_\perp}{\Omega}\hat{\rho}\cdot\nabla f_0 \tag{2.43}$$

Order δ^2

To the order δ^2, Eq. 2.24 can be written as

$$v_\parallel\hat{n}\cdot\nabla f_1 + v_\perp(\hat{e}_2\cos\xi - \hat{e}_3\sin\xi)\cdot\nabla f_1 +$$
$$\frac{\partial f_1}{\partial \mu}\left(\frac{d\mu}{dt}\right) + \frac{\partial f_0}{\partial E}\left(\frac{dE}{dt}\right) + \frac{\partial f_2}{\partial \xi}\Omega + \frac{\partial f_1}{\partial \xi}\left(\frac{d\xi}{dt} - \Omega\right) = C(f_1) \tag{2.44}$$

where the derivatives of the velocity space variables are given by Eqs. 2.21-2.23. Using $f_1 = \overline{f_1} + \tilde{f}_1$, we have

$$v_\parallel \hat{n} \cdot \nabla \tilde{f}_1 + v_\perp (\hat{e}_2 \cos\xi - \hat{e}_3 \sin\xi) \cdot \nabla \tilde{f}_1 + \frac{\partial \tilde{f}_1}{\partial \mu}\left(\frac{d\mu}{dt}\right)$$
$$+\frac{\partial f_0}{\partial E}\left(\frac{dE}{dt}\right) + \frac{\partial f_2}{\partial \xi}\Omega + \frac{\partial \tilde{f}_1}{\partial \xi}\left(\frac{d\xi}{dt} - \Omega\right) + v_\parallel \hat{n} \cdot \nabla \overline{f_1}$$
$$+v_\perp (\hat{e}_2 \cos\xi - \hat{e}_3 \sin\xi) \cdot \nabla \overline{f_1} + \frac{\partial \overline{f_1}}{\partial \mu}\left(\frac{d\mu}{dt}\right) = C(f_1) \qquad (2.45)$$

We note that

$$\frac{d\tilde{f}_1}{dt} = \frac{\partial \tilde{f}_1}{\partial t} + \mathbf{v} \cdot \nabla \tilde{f}_1 + \frac{\partial \tilde{f}_1}{\partial \mu}\left(\frac{d\mu}{dt}\right) + \frac{\partial \tilde{f}_1}{\partial E}\left(\frac{dE}{dt}\right) + \frac{\partial \tilde{f}_1}{\partial \xi}\left(\frac{d\xi}{dt}\right)$$

Dropping terms of the order δ^3 and higher, we obtain

$$\frac{d\tilde{f}_1}{dt} = \mathbf{v} \cdot \nabla \tilde{f}_1 + \frac{\partial \tilde{f}_1}{\partial \mu}\left(\frac{d\mu}{dt}\right) + \frac{\partial \tilde{f}_1}{\partial \xi}\Omega + \frac{\partial \tilde{f}_1}{\partial \xi}\left(\frac{d\xi}{dt} - \Omega\right)$$

or

$$\mathbf{v} \cdot \nabla \tilde{f}_1 + \frac{\partial \tilde{f}_1}{\partial \mu}\left(\frac{d\mu}{dt}\right) + \frac{\partial \tilde{f}_1}{\partial \xi}\left(\frac{d\xi}{dt} - \Omega\right) = \frac{d\tilde{f}_1}{dt} - \frac{\partial \tilde{f}_1}{\partial \xi}\Omega$$

Using the above equation in Eq. 2.45,

$$\frac{d\tilde{f}_1}{dt} - \Omega\frac{\partial \tilde{f}_1}{\partial \xi} + \frac{\partial f_0}{\partial E}\left(\frac{dE}{dt}\right) + \frac{\partial f_2}{\partial \xi}\Omega + v_\parallel \hat{n} \cdot \nabla \overline{f_1}$$
$$+v_\perp (\hat{e}_2 \cos\xi - \hat{e}_3 \sin\xi) \cdot \nabla \overline{f_1} + \frac{\partial \overline{f_1}}{\partial \mu}\left(\frac{d\mu}{dt}\right) = C(f_1) \qquad (2.46)$$

Gyro-averaging the above equation, and noting that

$$\overline{\frac{\partial \tilde{f}_1}{\partial \xi}} = \overline{\frac{\partial f_2}{\partial \xi}} = 0$$

due to the single valuedness of the distribution function, we have

$$\overline{\frac{d\tilde{f}_1}{dt}} - \frac{ev_\parallel}{m}\hat{n} \cdot \frac{\partial \mathbf{A}}{\partial t}\frac{\partial f_0}{\partial E} + v_\parallel \hat{n} \cdot \nabla \overline{f_1} = \overline{C(f_1)} \qquad (2.47)$$

where we have used the result $\overline{\frac{d\mu}{dt}} = 0$ to the order δ^2. Now we turn to the evaluation of the first term in the above equation. From Eq. 2.43, we have

$$\tilde{f}_1 = -\frac{v_\perp}{\Omega}\hat{\rho} \cdot \nabla f_0$$

Denoting $v_\perp \hat{\rho}/\Omega = \vec{\rho}$ and $\nabla f_0 = \mathbf{h}$, we write the Eq. 2.47 as

$$-\overline{\frac{d}{dt}(\vec{\rho}\cdot\mathbf{h})} - \frac{ev_\parallel}{m}\hat{n}\cdot\frac{\partial \mathbf{A}}{\partial t}\frac{\partial f_0}{\partial E} + v_\parallel \hat{n}\cdot\nabla\overline{f_1} = C(\overline{f_1}) + \overline{C(\tilde{f}_1)} \tag{2.48}$$

Carrying out the gyro-average of the first term in the above equation (see Appendix A for details), we obtain

$$(\mathbf{v}_D + \breve{v}_\parallel \hat{n})\cdot\nabla f_0 + \frac{e}{m}E_\parallel v_\parallel \frac{\partial f_0}{\partial E} + v_\parallel \hat{n}\cdot\nabla\overline{f_1} = C(\overline{f_1}) + \overline{C(\tilde{f}_1)} \tag{2.49}$$

where $\mathbf{v}_D$ is the perpendicular guiding center drift velocity, given by

$$\mathbf{v}_D = \frac{\mathbf{E}\times\hat{n}}{B} + \frac{\hat{n}}{\Omega}\times[\mu\nabla B + v_\parallel^2(\hat{n}\cdot\nabla)\hat{n}] \tag{2.50}$$

and $\breve{v}_\parallel$ is the parallel guiding center velocity, given by

$$\breve{v}_\parallel = \frac{v_\perp^2}{2\Omega}[\hat{n}\cdot(\nabla\times\hat{n})] \tag{2.51}$$

As all the quantities in the collision operator except for $\tilde{f}_1$ are independent of the gyrophase, $\overline{C(\tilde{f}_1)} = 0$. Noting that $\hat{n}\cdot\nabla f_0 = 0$, we obtain the drift kinetic equation as

$$v_\parallel \hat{n}\cdot\nabla\overline{f_1} + \mathbf{v}_D\cdot\nabla f_0 + \frac{e}{m}E_\parallel v_\parallel\frac{\partial f_0}{\partial E} = C(\overline{f_1}) \tag{2.52}$$

Eq. 2.52 forms the basis of the neoclassical transport theory. Before proceeding with the solution of the drift kinetic equation, we shall examine a few collision operators commonly employed in transport calculations.

2.3 Collision Operators

We have so far not discussed the nature of the collision operator $C(f)$ appearing in the Eq. 2.16. The collision operator is usually the Fokker-Planck operator (FPO) or a simplified version of it. Thus, we begin by discussing the FPO. We shall then discuss simplified versions of the FPO commonly employed in the transport theory.

2.3.1 Fokker-Planck Collision Term

The Fokker Planck collision operator is a very general collision term suitable for describing the evolution of the particle distribution function in a thermonuclear plasma. It can be used when small angle scatterings outnumber large angle scatterings.

If $G(\mathbf{v_0}, \Delta\mathbf{v})d^3v_1$ is the probability that a particle with an initial velocity $\mathbf{v_0}$ gets scattered by $\Delta\mathbf{v} = \mathbf{v_1} - \mathbf{v_0}$ into a volume d^3v_1 around $\mathbf{v_1}$ in unit time, then the rate of change of the distribution function $f_1(\mathbf{v_1})$ at $\mathbf{v_1}$,

$$\left(\frac{\partial f_1(\mathbf{v_1})}{\partial t}\right)_c = -[\textit{particles lost}] + [\textit{particles gained}]$$

or,

$$\left(\frac{\partial f_1(\mathbf{v_1})}{\partial t}\right)_c = -\int f_1(\mathbf{v_1})G(\mathbf{v_1}, \Delta\mathbf{v})d^3(\Delta v) + \int f_1(\mathbf{v_0})G(\mathbf{v_0}, \Delta\mathbf{v})d^3v_0 \qquad (2.53)$$

Using Taylor expansion,

$$\begin{aligned} f_1(\mathbf{v_0})G(\mathbf{v_0}, \Delta\mathbf{v}) &= f_1(\mathbf{v_1})G(\mathbf{v_1}, \Delta\mathbf{v}) + (v_0 - v_1)_i \frac{\partial}{\partial v_{1i}} f_1(\mathbf{v_1})G(\mathbf{v_1}, \Delta\mathbf{v}) \\ &\quad + \frac{1}{2}(v_0 - v_1)_i (v_0 - v_1)_j \frac{\partial}{\partial v_{1i}} \frac{\partial}{\partial v_{1j}} f_1(\mathbf{v_1})G(\mathbf{v_1}, \Delta\mathbf{v}) + \ldots \end{aligned}$$

Putting this in Eq. 2.53,

$$\begin{aligned} \left(\frac{\partial f_1}{\partial t}\right)_c &= -\frac{\partial}{\partial v_i} f_1(\mathbf{v_1}) \int (\Delta v_i)G(\mathbf{v_1}, \Delta\mathbf{v})d^3(\Delta v) + \\ &\quad \frac{1}{2}\frac{\partial}{\partial v_i}\frac{\partial}{\partial v_j} f_1(\mathbf{v_1}) \int (\Delta v_i)(\Delta v_j)G(\mathbf{v_1}, \Delta\mathbf{v})d^3(\Delta v) \\ &\simeq -\frac{\partial}{\partial v_i}[f_1(\mathbf{v_1})\overline{(\Delta v_i)_{v_1}}] + \frac{1}{2}\frac{\partial}{\partial v_i}\frac{\partial}{\partial v_j}[f_1(\mathbf{v_1})\overline{(\Delta v_i)(\Delta v_j)_{v_1}}] \end{aligned}$$

All the higher order terms have been omitted. Here, the Fokker-Planck coefficients defined by

$$\overline{(\Delta v_i)_{v_1}} = \int (\Delta v_i)G(\mathbf{v_1}, \Delta\mathbf{v})d^3(\Delta v)$$

$$\overline{(\Delta v_i)(\Delta v_j)_{v_1}} = \int (\Delta v_i)(\Delta v_j)G(\mathbf{v_1}, \Delta\mathbf{v})d^3(\Delta v)$$

are called the dynamical friction coefficient and the velocity space diffusion tensor respectively. For a thermonuclear plasma, these coefficients can be calculated by considering Coulomb collisions [21], leading to

$$\left(\frac{\partial f}{\partial t}\right)_c = \sum_\alpha \left[-\frac{\partial}{\partial v_i} f_t \frac{\partial h_\alpha}{\partial v_i} + \frac{1}{2}\frac{\partial^2}{\partial v_i \partial v_j}\left(f_t \frac{\partial^2 g_\alpha}{\partial v_i \partial v_j}\right)\right] \Gamma_\alpha \tag{2.54}$$

where f_t is the test particle distribution function and $\Gamma_\alpha = 4\pi n_\alpha q_t^2 q_\alpha^2 \ln\Lambda / m_t^2$. Here $\ln\Lambda$ is the Coulomb logarithm [21]. The summation over α denotes summation over all types of particles in the plasma.

$$g_\alpha(\mathbf{v}) = \int \mathbf{f}_\alpha(\mathbf{v}') \mid \mathbf{v} - \mathbf{v}' \mid \mathbf{dv}'$$

$$h_\alpha(\mathbf{v}) = \frac{m_t}{\mu_\alpha} \int \frac{f_\alpha(\mathbf{v}')}{\mid \mathbf{v} - \mathbf{v}' \mid} d\mathbf{v}'$$

where $\mu_\alpha = m_t m_\alpha/(m_t + m_\alpha)$ and $\mathbf{v}'$ is the field particle velocity. The plasma kinetic equation with the FPO is usually solved numerically. In many cases, simpler forms of the equation are used to obtain analytical solutions. One such form used commonly to describe collisions of electrons with ions or ions with heavier ions is the Lorentz operator. It is obtained by approximating $\mid \mathbf{v} - \mathbf{v}' \mid \simeq \mid \mathbf{v} \mid$ in the formulas for g_α and h_α and by assuming $m_t/m_\alpha \ll 1$. This gives [20],

$$\left(\frac{\partial f}{\partial t}\right)_c = \sum_\alpha \frac{\Gamma_\alpha}{2}\left[\frac{\partial}{\partial \mathbf{v}}.\mathbf{U}(\mathbf{v}).\frac{\partial f_t}{\partial \mathbf{v}}\right] = C_{PAS}(f_t) \tag{2.55}$$

where

$$\mathbf{U}(\mathbf{v}) = U_{ij}(\mathbf{v}) = \frac{\delta_{ij}}{\mid \mathbf{v} \mid} - \frac{v_i v_j}{\mid \mathbf{v} \mid^3}$$

. The above operator, also known as the pitch angle scattering operator, describes the change in the perpendicular velocity of the particle while conserving the total energy of the particle.

2.3.2 Other Collision Operators

The Fokker-Planck operator is quite complicated and, hence, in tokamak transport theory, simpler collision operators are employed. These collision operators are either

constructed using ad hoc procedures or derived rigorously from the FPO. Perhaps the simplest version of the FPO widely used in the transport theory is the Lorentz or the pitch angle scattering operator. As discussed in the previous paragraphs, the pitch angle operator provides an excellent approximation for electrons (or lighter particles) colliding with ions (or heavier particles). In terms of the magnetic moment variable, the linearized version of the pitch angle scattering operator is given by

$$C_{jk}(f_{j1}, f_{k1}) = C_{PAS}(f_{j1}) = \nu_{jk}\frac{q}{B}\frac{\partial}{\partial\mu}(\mu q)\frac{\partial f_{j1}}{\partial\mu} \tag{2.56}$$

where $\mu = v_\perp^2/2B$ is the magnetic moment per unit mass and q is the magnitude of the parallel velocity ($v_\parallel = \sigma q$ with $\sigma = \pm 1$). In Eq. 2.56, the subscript j refers to the lighter species, and the collision frequency ν_{jk} is defined later in this section.

The pitch angle scattering operator alone cannot be used for describing like particle collisions or collisions between particles of similar masses. Early studies in the neoclassical transport theory (Rosenbluth et al. [37], Rutherford [38]) used ad hoc procedures to construct collision operators for like particle collisions. The procedure is to write the linearized collision operator as [37]

$$C(f_{j1}) = C_{PAS}(f_{j1}) + C_{ES}(f_{j1}) + C_{FP}(f_{j1}) \tag{2.57}$$

where C_{ES} is the energy scattering part of the collision operator (describing the change in the energy), and C_{FP} is the field particle response. We have seen that C_{PAS} contains derivatives with respect to μ. C_{ES} contains derivatives with respect to the total energy $w(= v^2/2)$. In the neoclassical theory, change in $v_\parallel$ (pitch angle scattering) is the dominant event. Hence, Rosenbluth et al. [37] assume $\partial f_{j1}/\partial\mu \gg \partial f_{j1}/\partial w$, and hence, retain only the pitch angle scattering part. Thus the collision operator reduces to

$$C(f_{j1}) = C_{PAS}(f_{j1}) + C_{FP}(f_{j1}) \tag{2.58}$$

Here $C_{FP}(f_{j1})$ is modeled as

$$C_{FP}(f_{j1}) = \frac{\nu_{jj} f_{j0} q p}{v_{th,j}^2} \tag{2.59}$$

where f_{j0} is the equilibrium (Maxwellian) distribution function and $v_{th,j}$ is the thermal velocity of the species j ($v_{th,j} = \sqrt{(2T_j/m_j)}$). p is a velocity, to be determined to satisfy the momentum conservation, i.e.

$$\int C(f_{j1}) q d^3v = 0 \tag{2.60}$$

Using Eqs. 2.58 and 2.59 in 2.60, p is found to be [37]

$$p = v_{th,j}^2 \frac{\int d^3v \nu_{jj} q f_{j1}}{\int d^3v \nu_{jj} q^2 f_{j0}} \tag{2.61}$$

Connor [9] modified the operator 2.58 to handle unlike particle collisions as

$$C_{jk}(f_{j1,k1}) = C_{PAS}(f_{j1}) + \nu_{jk}(x_j^2) \frac{q f_{j0}}{v_{th,j}^2} \frac{\int d^3v \nu_{kj} q f_{k1}}{\int d^3v \frac{\nu_{kj} q^2}{v_{th,k}^2} f_{k0}} \tag{2.62}$$

where $x_j^2 = (m_j v^2/2T_j)$. If the collision frequencies ν_{jk} are determined to satisfy the constraint

$$m_j \int d^3v \frac{q^2}{v_{th,j}^2} \nu_{jk} f_{j0} = m_k \int d^3v \frac{q^2}{v_{th,k}^2} \nu_{kj} f_{k0}$$

the operator 2.62 conserves momentum as well as number and energy.

The ad hoc procedures used by Rosenbluth et al. [37], Rutherford [38], and Connor [9], while intuitively appealing, suffer from many disadvantages.

1. The connection between the ad hoc procedures and the exact Fokker-Planck operator is not apparent. This is because the ad hoc operators are not derived rigorously from the exact Fokker-Planck operator.

2. The operators possess only a few of the properties of the exact Fokker-Planck operator. In most instances, the operators are made to satisfy one or more conservation laws by defining collision frequencies (see Connor [9]) or by defining a velocity (see Rosenbluth et al. [37]).

To alleviate these problems, Hirshman et al. [39, 14, 40] derived an approximate collision operator for transport theory applications from the exact Fokker-Planck operator.

The approximate collision operator has the form

$$C_{jk}(f_{j1}, f_{k1}) = \nu_{jk}^D \mathcal{L} f_{j1} + \frac{2v_\parallel r_{kj}}{v_{th,j}^2}\nu_{jk}^S f_{j0} + [\nu_{jk}^D - \nu_{jk}^S]\frac{v_\parallel u_{j1}(v)}{v^2} f_{j0} \tag{2.63}$$

where

$$\nu_{jk}^D = \nu_{jk}\left[\phi\left(\frac{v}{v_{th,k}}\right) - G\left(\frac{v}{v_{th,k}}\right)\right] / \left(\frac{v}{v_{th,j}}\right)^3 \tag{2.64}$$

is the deflection frequency (characterizing pitch angle scattering [39, 41]).

$$\nu_{jk}^S = \frac{2T_{j0}}{T_{k0}}\left(1 + \frac{m_k}{m_j}\right)\nu_{jk} G\left(\frac{v}{v_{th,k}}\right) / \left(\frac{v}{v_{th,j}}\right) \tag{2.65}$$

is the slowing down frequency (characterizing dynamical friction due to the field particles [39, 41]). Here

$$\nu_{jk} = 4\pi n_k e_j^2 e_k^2 \ln\Lambda / [(2T_j)^{3/2} m_j^{1/2}] \tag{2.66}$$

where $e_j = Z_j e$ and $e_k = Z_k e$ are the charge on the species j and k respectively.

$$G(x) = \frac{\phi(x) - x\phi'(x)}{2x^2} \tag{2.67}$$

is the Chandrasekhar function, where $\phi(x) = (2/\sqrt{\pi})\int_0^x exp(-t^2)dt$ is the error function. The pitch angle operator is defined as

$$\mathcal{L} = \frac{v_\parallel}{B}\frac{\partial}{\partial\mu}(\mu v_\parallel)\frac{\partial}{\partial\mu} \tag{2.68}$$

Also,

$$u_{j1}(v) f_{j0} = (3/4\pi)\int v_\parallel f_{j1} d\Omega \tag{2.69}$$

where $d\Omega = 2\pi v^{-1} dv_\parallel = \pi\sum_\sigma (B d\mu/w)(v/|v_\parallel|)$ [14, 40]. The momentum restoring coefficient r_{kj} is defined as

$$r_{kj} = \frac{\int m_k \nu_{kj}^S v_\parallel f_{k1} d^3v}{m_j n_j \{\nu_{jk}^S\}} \tag{2.70}$$

where the integration operator $\{\}$ is defined as

$$\begin{aligned}\{F^{jk}(v)\} &= 2\int\left(\frac{v_\parallel}{v_{th,j}}\right)^2 F^{jk}(v)\frac{f_{j0}}{n_j} d^3v \\ &= \left(\frac{8}{3\sqrt{\pi}}\right)\int_0^\infty x_j^4 exp(-x_j^2) F^{jk}(x_j) dx_j\end{aligned} \tag{2.71}$$

where $F^{jk}(v)$ is an arbitrary function of the velocity v. We note that by setting $\nu_{jk}^D = \nu_{jk}^S$ in Eq. 2.63, we recover operators similar to those given by Eqs. 2.62 and 2.58. Collision frequencies defined by Connor [9] and Rosenbluth et al. [37] are similar to ν_{jk}^D. Thus, the Hirshman-Sigmar operator, in addition to its rigorous derivation, can be looked upon as an extension of earlier collision operators to include the difference between the pitch angle scattering frequency and the slowing down frequency. In many instances, the difference makes a significant contribution to transport calculations. In addition, the collision operator 2.63 possesses most of the desirable properties of the exact Fokker-Planck operator, such as the conservation laws (particle, momentum, and energy), self-adjointness, and the H-theorem [39, 14, 40]. We shall be using the Hirshman-Sigmar operator (Eq. 2.63) in our calculations of the neoclassical transport coefficients.

2.4 Quasilinear Theory

Quasilinear theory, originally developed to study weak plasma turbulence, is widely employed in wave heating applications to describe the collisionless evolution of the distribution function. The theory separates the particle distribution f, the electric field $\mathbf{E}$ and the magnetic field $\mathbf{B}$ into a space independent component f_0, $\mathbf{E_0}$, $\mathbf{B_0}$ and a small, rapidly varying component $f_1, \mathbf{E_1}, \mathbf{B_1}$. The component f_1 is obtained using the linearized Vlasov equation. The linearized solution f_1 is then used in a nonlinear equation describing the time evolution of f_0 to determine f_0. The basic idea behind quasilinear theory is explained below for an electrostatic wave in an unmagnetized plasma. Similar arguments hold for an electromagnetic wave in a magnetized plasma.

Collisionless evolution of the distribution function f_α of a species α in an unmagnetized plasma with an electrostatic disturbance is governed by the Vlasov equation,

$$\frac{\partial f_\alpha}{\partial t} + \mathbf{v}.\frac{\partial f_\alpha}{\partial \mathbf{x}} + \frac{q_\alpha}{m_\alpha}\mathbf{E}.\frac{\partial f_\alpha}{\partial \mathbf{v}} = 0 \tag{2.72}$$

and the Gauss' law

$$\nabla.\mathbf{E} = 4\pi \sum_{\alpha} n_\alpha q_\alpha \int f_\alpha d\mathbf{v}$$

Eq. 2.72 is solved using a perturbation approach.

$$f_\alpha = f_{\alpha 0} + f_{\alpha 1}$$

where $f_{\alpha 0}$ is the spatially averaged part

$$f_{\alpha 0} = \frac{1}{V} \int f_\alpha d\mathbf{x} = < f_\alpha >$$

and $f_{\alpha 1}$ is the rapidly fluctuating part.

$$\mathbf{B_0} = \mathbf{0} \;\; ; \;\; \mathbf{E}_0 = 0 \;\; ; \;\; \mathbf{E} = \mathbf{E_1} \;\; ; \;\; < f_{\alpha 1} >=< E_1 >= 0$$

Under these conditions, an equation for the evolution of $f_{\alpha 0}$ is obtained by spatially averaging Eq. 2.72, leading to

$$\frac{\partial f_{\alpha 0}}{\partial t} = -\frac{q_\alpha}{m_\alpha} \nabla_{\mathbf{v}} . < \mathbf{E_1} f_{\alpha 1} > \tag{2.73}$$

An equation for $f_{\alpha 1}$ is obtained by putting $f_\alpha = f_{\alpha 0} + f_{\alpha 1}$ in Eq. 2.72 and using Eq. 2.73

$$\left(\frac{\partial}{\partial t} + \mathbf{v}.\nabla \right) f_{\alpha 1} = -\frac{q_\alpha}{m_\alpha} \mathbf{E_1}.\nabla_{\mathbf{v}} f_{\alpha 0} - \frac{q_\alpha}{m_\alpha} \nabla_{\mathbf{v}} .(\mathbf{E_1} f_{\alpha 1} - < \mathbf{E_1} f_{\alpha 1} >)$$

Linear solution to $f_{\alpha 1}$ is obtained by neglecting the second order quantities $\mathbf{E_1} f_{\alpha 1}$. Letting

$$f_{\alpha 1}(t) = \frac{1}{(2\pi)^3} \int f_{\alpha \mathbf{k}}(\mathbf{x}, t) d\mathbf{k} \tag{2.74}$$

$$\mathbf{E_1}(t) = \frac{1}{2\pi^3} \int \mathbf{E_k}(\mathbf{x}, t) d\mathbf{k}$$

where

$$f_{\alpha \mathbf{k}} = \overline{f_{\alpha \mathbf{k}}} \exp(i\mathbf{k}.\mathbf{x}) \exp(-i\omega t)$$

$$\mathbf{E_k} = \overline{\mathbf{E_k}} \exp(i\mathbf{k}.\mathbf{x}) \exp(-i\omega t)$$

Using these forms, we find

$$f_{\alpha \mathbf{k}} = -\frac{q_\alpha}{m_\alpha} \frac{\mathbf{E_k}.\nabla_\mathbf{v} f_{\alpha 0}}{i(\mathbf{k}.\mathbf{v} - \omega)} \tag{2.75}$$

Eqs. 2.74 and 2.75, when used in Eq. 2.73, result in the following diffusion equation for $f_{\alpha 0}$

$$\frac{\partial f_{\alpha_0}}{\partial t} = \nabla_\mathbf{v}.D_\mathbf{v}.\nabla_\mathbf{v} f_{\alpha 0}(t) \tag{2.76}$$

where

$$D_\mathbf{v} = (\frac{q_\alpha}{m_\alpha})^2 \frac{1}{V} \int \frac{\mathbf{E_k}.\mathbf{E_{-k}}}{i(\mathbf{k}.\mathbf{v} - \omega)} \frac{\mathbf{kk}}{\mathbf{k^2}} \frac{d\mathbf{k}}{(2\pi)^3}$$

is the quasilinear diffusion coefficient.

For the electromagnetic case, we arrive at a similar equation with a more complicated expression for $D_\mathbf{v}$ [24, 42].

In wave heating applications, the equation for the evolution of f_0 is of the form

$$\frac{\partial f_0}{\partial t} = \nabla_\mathbf{v}.D_\mathbf{v}.\nabla_\mathbf{v} f_0 + (\frac{\partial f_0}{\partial t})_c \tag{2.77}$$

where $(\frac{\partial f_0}{\partial t})_c$ is the collision operator. The above equation describes the situation where particles are gaining energy from the wave (described by the quasilinear operator) as well as losing energy to other particles (described by the collision operator).

CHAPTER III

PARTICLE TRANSPORT DURING WAVE HEATING - THEORY

In this chapter, we review the theoretical literature related to particle transport during wave heating. We begin by examining the production of electric fields during wave heating in tokamaks. We then examine, in section 3.3, the effect of poloidal electric fields on particle transport. Section 3.4 contains a summary and the conclusions of our review.

3.1 Electric Fields during Cyclotron Wave Heating in Tokamaks

Equipped with some of the tools of wave heating and transport theory, we are now in a position to study some of the effects of wave heating. In Section 3.1.1, we study the production of poloidal electric fields during wave heating. We then examine, heuristically, in Section 3.1.2, the production of electric fields during the wave momentum absorption process.

3.1.1 Poloidal Potential Variation During Wave Heating

Production of a significant poloidal potential variation during cyclotron wave heating has been studied by Hsu et al. [11] and Chan et al. [43]. Much of the material

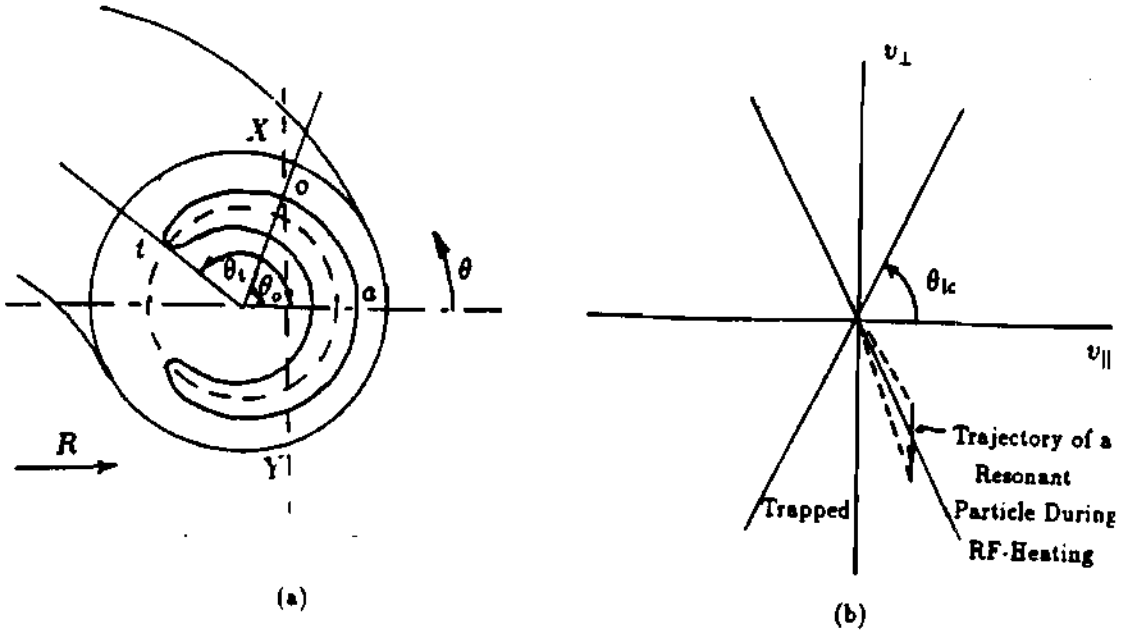

Figure 3.1: Particle Trapping During Wave Heating

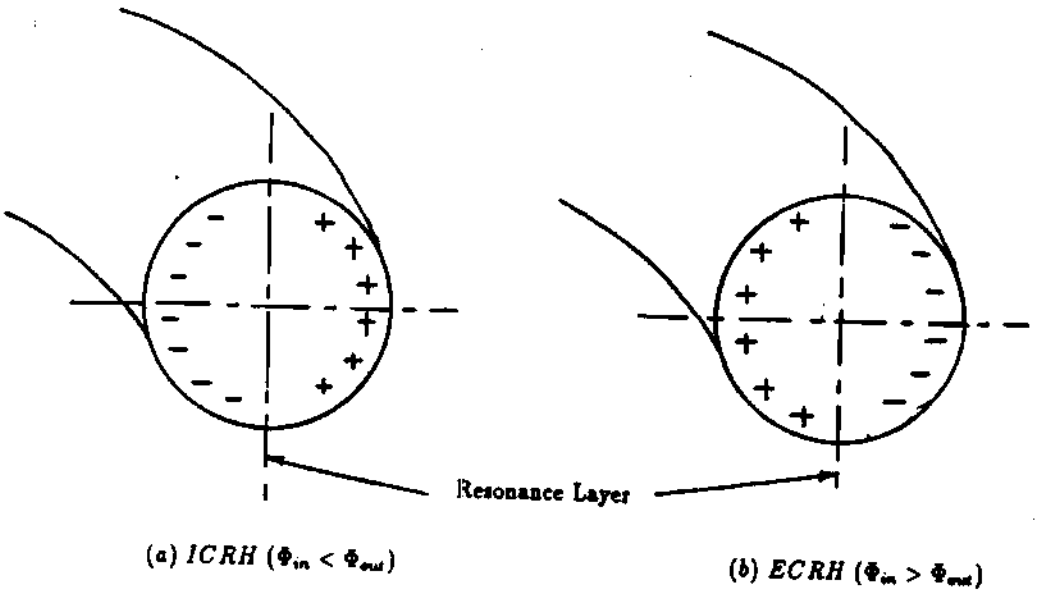

Figure 3.2: Potential Asymmetry during Wave Heating

presented in this section is based on Ref. [11].

Particle Trapping and Resonance Localization

Production of a significant poloidal electric field in tokamaks during cyclotron wave heating is related to the phenomenon of particle trapping inherent in the tokamak geometry. In a tokamak, the magnetic field varies as $1/R$ and, hence, is weaker on the outside of the torus. It is this variation of the field that is responsible for particle trapping. Referring to Fig. 3.1, conservation of energy gives,

$$\left(\frac{mv^2}{2}\right)_o = \left(\frac{mv^2}{2}\right)_t \tag{3.1}$$

where $v^2 = v_\parallel^2 + v_\perp^2$. Also, invariance of the magnetic moment gives

$$\overline{\mu} = \frac{(mv_\perp^2)_o}{2B_o} = \frac{(mv_\perp^2)_t}{2B_t} \tag{3.2}$$

Using Eqs. 3.1 and 3.2,

$$v_{\parallel,t}^2 = v_o^2 \left[1 - \left(\frac{B_t}{B_o}\right)\left(\frac{v_{\perp,o}^2}{v_o^2}\right)\right] \tag{3.3}$$

As $(B_t/B_o) > 1$, for particles with sufficiently small $v_{\parallel,o}$, $v_{\parallel,t}$ can approach zero and the particle can be reflected at t. Indeed, in a tokamak with an inverse aspect ratio ϵ, a fraction of particles, $\sim \sqrt{\epsilon}$, are trapped in the manner described above, and such particles execute a 'banana' shaped orbit as shown in Fig. 3.1(a). Noting that for particles reflected at t, $(mv_\perp^2/2)_t = (mv^2/2)_o$,

$$\left(\frac{v_\perp}{v}\right)_o = \sqrt{\frac{B_o}{B_t}} = \sin\theta_{lc}$$

Particle at o with $(\frac{v_\perp}{v}) > \sqrt{\frac{B_o}{B_t}}$ are reflected at t. θ_{lc} is the loss cone angle shown in Fig. 3.1(b).

Turning to cyclotron heating, we note that the very nature of cyclotron heating is to increase the perpendicular energy of the resonant particles. Assuming that resonance occurs along a vertical plane X-Y in Fig. 3.1(a), Eq. 3.3 holds between points o

and t. From Eq. 3.3, it is clear that everytime a particle crosses the resonance region with an increase in its perpendicular energy, $v_{\parallel,t}^2$ grows smaller. Hence, marginally untrapped particles before wave heating get trapped as $v_{\parallel,t}^2$ approaches zero. The situation is depicted in Fig. 3.1(b), where an untrapped particle is shown crossing into the trapped region during rf-heating. Thus, during cyclotron heating the trapped particle population of the resonant species increases, leading to an increased in-out asymmetry in the electrostatic potential (see Fig. 3.2).

In addition to particle trapping, rf-heating leads to resonance localization ,i.e., banana tips (point t in Fig. 3.1) of trapped particles slowly move toward the resonance layer. This follows easily from the conservation of energy. For a large aspect ratio tokamak with $B(\theta) \simeq B_0(1 - \epsilon\cos\theta)$, we could write, referring to Fig. 3.1,

Before wave heating,

$$\frac{mv_{\parallel,o}^2}{2} + \overline{\mu}B_0(1 - \epsilon\cos\theta_o) = \overline{\mu}B_0(1 - \epsilon\cos\theta_t) \tag{3.4}$$

During wave heating,

$$\frac{mv_{\parallel,o}^2}{2} + \overline{\mu}' B_0(1 - \epsilon\cos\theta_o) = \overline{\mu}' B_0(1 - \epsilon\cos\theta_t') \tag{3.5}$$

where θ_t' is the new position of the banana tip. Subtracting Eq. 3.5 from Eq. 3.4, we have

$$\frac{\cos\theta_o - \cos\theta_t'}{\cos\theta_o - \cos\theta_t} = \frac{\overline{\mu}}{\overline{\mu}'} \tag{3.6}$$

Eq. 3.6 implies that as $\overline{\mu}'$ continues to rise, the banana tip moves closer to the resonance location, i.e. $\theta_t' \rightarrow \theta_o$.

Thus, during cyclotron wave heating, (i) there is an increase in the trapped particle population of the resonant species and (ii) the trapped particles experience resonance localization. The combined effect of these two phenomena gives rise to a poloidal asymmetry in the potential. The magnitude of the potential can be expected to rise until the potential has sufficient strength to expel particles out of the magnetic well.

This means that the potential asymmetry could be of the order of the magnetic well depth, which is of the order $\sim \epsilon (= r/R)$.

Poloidal Potential Variation

Before outlining the formal calculation of the poloidal potential variation, we could get a quick estimate of the order of magnitude of the variation based on energy conservation considerations. Taking $\theta_o = \pi/2$, Eq. 3.4 reads,

$$\frac{m v_{\|,o}^2}{2} + \overline{\mu} B_0 = \overline{\mu} B_0 (1 - \epsilon \cos\theta_t)$$

After resonant heating, taking potential $\Phi(\theta_o) = \Phi(\pi/2) = 0$,

$$\frac{m v_{\|,o}^2}{2} + \overline{\mu}' B_0 = \overline{\mu}' B_0 (1 - \epsilon \cos\theta_t') + e\Phi(\theta_t')$$

Using these equations,

$$\frac{e\Phi(\theta_t')}{\overline{\mu} B_0} \simeq \epsilon \left(\frac{\overline{\mu}'}{\overline{\mu}} \cos\theta_t' - \cos\theta_t \right)$$

To maintain charge neutrality, if we demand $\theta_t' \simeq \theta_t$,

$$\frac{e\Phi(\theta_t)}{\overline{\mu} B_0} \simeq \frac{e\Phi(\theta_t)}{T} \simeq (r/R)(\cos\theta_t) \left(\frac{\Delta\overline{\mu}}{\overline{\mu}} \right)$$

Here, $(\Delta\overline{\mu})/\overline{\mu}$ is roughly the temperature anisotropy $(T_\perp - T_\|)/T_\|$. Rf-heating tries to maintain temperature anisotropy while collisions try to destroy it. Hence, it is conceivable that $(\Delta\overline{\mu}/\overline{\mu}) \sim O(\nu_{rf}/\nu_c)$ where ν_{rf} is the effective rf-heating rate and ν_c is the collision frequency. Hence

$$\frac{e\Phi(\theta_t)}{T} \simeq \epsilon \left(\frac{\nu_{rf}}{\nu_c} \right) \cos\theta_t \tag{3.7}$$

The formal evaluation of potential variation makes use of the drift-kinetic equation

$$\frac{\partial f}{\partial t} + \frac{B_\theta v_\|}{Br} \frac{\partial f}{\partial \theta} + e E_\theta v_\| \frac{B_\theta}{B} \frac{\partial f}{\partial W} = Q_{rf}(f) + C(f)$$

where Q_{rf} and C are quasilinear and Coulomb collision operators and $W = m v_\|^2/2 + \overline{\mu} B$. The equation is linearized in a manner similar to the one used in deriving Eq. 2.52

to yield

$$\frac{\partial f^0}{\partial t} + \frac{v_\parallel}{r}\frac{B_\theta}{B}\frac{\partial f^1}{\partial \theta} + eE_\theta v_\parallel \frac{B_\theta}{B}\frac{\partial f^0}{\partial W} = Q_{rf}(f^0) + C(f^0) \tag{3.8}$$

Here f^1 is of the order $(\nu_c/\omega_B) \ll 1$ where ω_B is the bounce frequency. We are thus restricting ourselves to the low collisionality regime. Bounce average of Eq. 3.8 gives

$$< q^{-1} > \frac{\partial f^0}{\partial t} =< q^{-1} Q_{rf}(f^0) > + < q^{-1} C(f^0) > \tag{3.9}$$

where $q =\mid v_\parallel \mid$. The angular brackets are defined by $< x >= \oint x\, d\theta / \oint d\theta$. Subtracting Eq. 3.9 from 3.8 gives

$$\begin{aligned} \sigma q \Theta \left[\frac{1}{r}\frac{\partial f^1}{\partial \theta} - \frac{e}{r}\frac{\partial \Phi}{\partial \theta}\frac{\partial f^0}{\partial W}\right] &= Q_{rf}(f^0) + C(f^0) - < q^{-1} >^{-1} (< q^{-1} Q_{rf}(f^0) > \\ &\quad + < q^{-1} C(f^0) >) \end{aligned} \tag{3.10}$$

where $\sigma = v_\parallel/q$ and $\Theta = B_\theta/B$. This equation can be integrated over θ, over the velocity space and summed over σ. This eliminates the collision terms, which are independent of the sign of $v_\parallel$. If we restrict ourselves to $k_\parallel \simeq 0$, the quasilinear terms are also independent of the direction of $v_\parallel$ and, hence, vanish. The procedure gives an expression for the first order density perturbation in terms of the zeroth order distribution function.

$$n^1 = \int f^1 d^3v = \sum_\alpha \int\int e\Phi \frac{\partial f^0}{\partial W}\frac{2\pi B d\bar{\mu} dW}{m^2 q} \tag{3.11}$$

Charge neutrality gives, $n_i \simeq n_e$, or

$$n_i^0 + n_i^1 = n_e^0 + n_e^1 \tag{3.12}$$

Restricting attention on ECRH, the ion distribution function can be taken as a Maxwellian to evaluate n_i^0 and n_i^1. This yields $n_i = n_0(1 - e\Phi/T_i)$. In the weak rf limit, i.e. $\nu_{rf}/\nu_c = \delta < 1$, f_e^0 in Eq. 3.11 can be assumed to be a Maxwellian to evaluate n_e^1 to give $n_e^1 = (e\Phi/T_e)n_0$. Eq. 3.12 thus reduces to

$$e\Phi[\frac{1}{T_i} + \frac{1}{T_e}] = 1 - \frac{1}{n_0}\int\int f_e^0 \frac{4\pi B d\bar{\mu} dW}{q m^2} \tag{3.13}$$

f_e^0 is obtained from Eq. 3.9. Equation 3.9 is solved by expanding f^0 and $\frac{\partial}{\partial t}$ in the small expansion parameter δ, i.e.

$$f^0 = f_0^0 + \delta f_1^0 + ...$$

$$\frac{\partial}{\partial t} = \nu_c \left(\frac{\partial}{\partial t_0} + \delta \frac{\partial}{\partial t_1} + ... \right.$$

To the lowest order,

$$< q^{-1} > \frac{\partial f_0^0}{\partial t_0} =< C(f_0^0) q^{-1} >$$

This equation is satisfied by taking f_0^0 to be the Maxwellian

$$f_0^0 = n(t_1) \left[\frac{m}{2\pi T(t_1)} \right]^{3/2} \exp \left[-\frac{W}{T(t_1)} \right]$$

To the next order, setting $\frac{\partial f_1^0}{\partial t_0}$ [11],

$$< q^{-1} > \frac{\partial f_0^0}{\partial t_1} =< q^{-1} Q_{rf}(f_0^0) > + < q^{-1} C(f_1^0) > \tag{3.14}$$

The collision operator is taken to be the Lorentz operator

$$< q^{-1} C f^0 >= \frac{m \nu_{ei} Z_{eff}}{2v^3} \frac{\partial}{\partial \overline{\mu}} < q B^{-1} > \overline{\mu} \frac{\partial f^0}{\partial \overline{\mu}}$$

where $\nu_{ei} = 4\pi n e^4 \ln \Lambda / m^2$ and Z_{eff} is the effective charge on the ions ($Z_{eff} = \sum_{j \neq e} n_j Z_j^2 / n_e$). Also, for ECRH, the rf-frequency $\nu_{rf} = e^2 E_-^2 / 2^{3/2} m_e \Omega_e \epsilon T_e$. The quasilinear operator with the fundamental resonance at the plasma center reduces to

$$< q^{-1} Q_{rf}(f^0) >= \mathcal{L}_0 \frac{e^2 \mid E^- \mid^2 \overline{\mu} B_0 N}{4\pi \Omega_0 \epsilon [2m(W - \overline{\mu} B_0)]^{1/2}} \mathcal{L}_0 f^0$$

where $\mathcal{L}_0 = \frac{\partial}{\partial W} + \frac{\partial}{\partial \overline{\mu}} B_0$, Ω_0 is the cyclotron frequency at the resonance layer and N is the number of passages through the resonance region. Using the above operators, Eq. 3.14 reduces to

$$\left[\frac{n'}{n} + \frac{WT'}{T^2} - \frac{3T'}{2T} \right] f_0^0 \int_0^{\overline{\mu}} < q^{-1} > d\overline{\mu} =$$

$$\left[\frac{T}{W} \right]^{3/2} \overline{\mu} m < q B^{-1} > \frac{\partial f_1^0}{\partial \overline{\mu}}$$

$$+ \int_0^{\overline{\mu}} \frac{m^{1/2} N}{2\pi} \left[\frac{\overline{\mu} B_0}{T} - 1 \right] (W - \overline{\mu} B_0)^{-1/2} f_0^0 d\overline{\mu} \tag{3.15}$$

Here, the prime denotes derivative with respect to t_1. The details of obtaining this equation can be found in Ref. [11]. n'/n and T'/T can be obtained from Eq. 3.14 by multiplying the equation by 1 and W and integrating over the velocity space. Using $f^0 = f_0^0 + \delta f_1^0$, the charge neutrality condition reduces, after performing the $\overline{\mu}$ integration, to

$$e\Phi\left[\frac{1}{T_i}+\frac{1}{T_e}\right] = 1 - \frac{n(t_1)}{n_0} - \frac{\delta}{n_0}\int\int \frac{4\pi B_0 q dW d\overline{\mu}}{m}\left(\frac{1}{B_0}\right)\frac{\partial f_1^0}{\partial \overline{\mu}} \qquad (3.16)$$

$\frac{\partial f_1^0}{\partial \overline{\mu}}$, obtained from Eq. 3.15, can be used in Eq. 3.16 to determine the potential. The integrals are evaluated by Hsu et al. [11] for the trapped particles and passing particles separately to yield

$$\frac{e\Phi_1}{T} = \frac{e\Phi_t}{T} + \frac{e\Phi_p}{T} \qquad (3.17)$$

where

$$\frac{e\Phi_t}{T} \simeq O(\delta\epsilon^{3/2})$$

and

$$\frac{e\Phi_p}{T} = 0.2\delta\epsilon \qquad (3.18)$$

Here Φ_1 is the $\cos\theta$ component of the potential. Φ_t and Φ_p are the trapped and passing particle contributions to the potential. In Eq. 3.7, if we compute the average value of $\cos\theta_t$ for trapped particles, we get $< \cos\theta_t > \sim 0.37$. This would mean

$$\frac{e\Phi(\theta_t)}{T} \simeq 0.37\epsilon\delta$$

from Eq. 3.7, which is quite close to the value in Eq. 3.18.

We note that in the above arguments leading to Eqs. 3.7 and 3.18, we have used $\theta_t \simeq \theta_t'$ or, equivalently, assumed quasineutrality. We have, thereby, treated resonance localization to be weak. During high power rf-heating, resonance localization can be strong, leading to the movement of the banana tips closer to the resonance layer. Under such conditions the magnitude of the potential asymmetry can be larger than that given by Eq. 3.18.

Turning to ICRH, we could expect the procedure carried out above for ECRH to remain the same. The main difference comes from the collision operator, which, for ions, includes the slowing down effect in addition to pitch angle scattering. This may lead to a different numerical coefficient in Eq. 3.18. We note here that for large aspect ratio tokamaks, we may be able to represent the collision term by the pitch angle scattering operator even for ions. Also, if we assume the plasma to contain a relatively large amount of heavy impurities such that $n_I z^2/n_i > 1$, pitch angle scattering between ions and impurities is likely to dominate and we can expect the above calculations to hold good for ICRH. Finally, we note that a calculation of poloidal variation in potential in the collisional regime carried out by Chan et al. [43] yields a value for the potential much smaller than that obtained above.

Before considering the effect of poloidal electric field on transport, we would like to estimate the magnitude of δ in some experiments.

In the case of ECRH, we consider typical DOUBLET III parameters: rf-power $P_{rf} = 1\ MW$, frequency $f = 60\ GHz$, $T_e \sim 2\ keV$, $n_i \sim n_e \sim 2 \times 10^{19}\ m^{-3}$, $R = 1.67\ m$, $a = 0.67\ m$.

Considering resonance along the vertical chord through the center, the power density on the resonant surface is $P = P_{rf}/(2\pi R)(2a) = 71120\ Watts/m^2$. Letting

$$P = \mid \mathbf{S} \mid = \mid \frac{\mathbf{E} \times \mathbf{B}}{\mu_0} \mid \simeq \frac{E_0^2}{2\mu_0 c} \quad ,$$

we obtain $E_0 = 7318\ Volts/m$. Here, E_0 is the amplitude of the wave which is assumed to be of the form $\mathbf{E} = \mathbf{E}_0 \cos\omega t$. Also, we have assumed the phase velocity to be roughly equal to the phase velocity in vacuum (i.e. c).

The right circularly polarized component of the wave is

$$E_- \simeq k_\perp \rho E_0 \simeq (v_{th,e}/c)E_0 = 0.1\ E_0 = 732\ Volts/m$$

For a point at $r = 0.1\ m$, we get,

$$\nu_{rf} = \frac{e^2 E_-^2}{2^{3/2} m_e \Omega_e \epsilon T_e} = 738/s$$

$\nu_c \sim \nu_{ei} = 1/\tau_{ei}$ with

$$\tau_{ei} = 1.09 \times 10^{16} \frac{T_e^{3/2}}{n(m^{-3}) \ln \lambda} \; s \quad (T_e \; in \; keV)$$

Using this, $\nu_{ei} = 9730/s$. Hence

$$\delta = \nu_{rf}/\nu_{ei} \simeq 0.1 < 1$$

Here, we have assumed the injected power to be 1 MW. With an increase in the injected power, we could expect almost a linear increase in ν_{rf} and a decrease in ν_{ei}, due to increased temperature, leading to a larger value of δ. Indeed, for power levels of the order $\sim$ 10-20 MW, we could expect $\delta \sim \mathcal{O}(1)$. Furthermore, the focussing effect likely to be present during cyclotron heating increases the power density, and hence, the poloidal variation in potential can be expected to be higher.

Turning to ICRH, we will consider the parameters relevant to PLT. We assume minority heating at the fundamental frequency in a deuterium-hydrogen plasma. We use $n_D \sim n_e \simeq 3 \times 10^{19} \; m^{-3}$, $T_D = T_H = T_e = 1 \; keV$, $f = 25 \; MHz$, $R = 1.32 \; m$, $a = 0.4 \; m$, $P_{rf} = 500 \; kW$.

We again consider resonance along the vertical chord passing through the center. $\nu_{rf} = < P(r) > /nT$ where $< P(r) >$ is the power absorbed per unit volume on a flux surface at radius r. Using Eq. 2.6, we obtain,

$$\nu_{rf} = \frac{e^2 E_+^2}{m_H \Omega_H \epsilon T_H \mid \sin\theta \mid}$$

Whang et al. [44] obtain a value for $E_+ \simeq 1700 Volts/m$ for the typical PLT parameters. Using this and considering a point at $r = 0.1 \; m$, $\nu_{rf} = 23533/s$.

The relevant collision frequency to be considered during ICRH depends to a large extent on the ion slowing down process. For low to moderate energy ions, ion-ion collisions are important. For high energy tail ions, much of the slowing down is due to the background electrons. Considering ion-ion collisions, $\nu_{ii} = 1/\tau_i$ with

$$\tau_i = 6.60 \times 10^{17} \left(\frac{m_i}{m_H}\right)^{1/2} \frac{T_i^{3/2}}{n \ln \Lambda_i} \; s \quad (n \; in \; m^{-3}; \; T_i \; in \; keV)$$

For PLT,$\nu_{ii} = 813/s$. This gives

$$\delta = \nu_{rf}/\nu_{ii} \simeq 29 \ >> 1$$

In the present case, due to the strong rf-effect in comparison with the weak collisional damping, we could expect a strong anisotropy in the resonant ion distribution function and, hence, strong resonance localization. Thus, a significant contribution to the potential asymmetry could be due to resonance localization.

3.1.2 Electric Fields during Wave Momentum Absorption

During plasma heating using neutral beam injection (NBI) or radio-frequency (RF) waves, considerable momentum (mechanical or electromagnetic) is deposited in the plasma. It has been pointed out by Düchs [45] that during perpendicular NBI, the absorption of momentum could lead to the creation of significant electric fields. Microscopically, the input neutral particle splits giving rise to an electric dipole. While we expect similar electric fields during RF heating, the mechanism responsible for the production of such fields, especially the microscopic mechanism, is not as transparent as it is in the case of NBI. During RF heating, the dipoles have to be created within the plasma during the energy absorption process. Indireshkumar et al. [46] studied the production of electric fields during the wave momentum absorption process using a simple model. The material presented below is based on Ref. [46].

Microscopic Picture

We develop the microscopic model for the case of ICRH with $k_{\|} \simeq 0$. Similar arguments are expected to be valid for ECRH. During ICRH in a tokamak, resonance occurs along a vertical chord. As an ion-electron pair with coinciding guiding centers crosses the resonance region, the ion picks up energy moving to a larger orbit. In the present model, we assume that during such a process, the ion center of gyration is

displaced from the electron guiding center in such a way that the resulting electric field between the particles crossed with the equilibrium magnetic field (i.e. $\mathbf{E} \times \mathbf{B}$) gives rise to field momentum in the same direction as that of the incident wave [see Fig. 3.3]. The ion picks up energy everytime it crosses the resonance layer, but keeps losing energy to non-resonant ions, impurities, and electrons. Thus, absorption of RF energy by the ions gives rise to electric dipoles in a manner similar to that produced by an external electric field in a dielectric. With this picture in mind, we proceed to calculate the electric field production rate.

If $v_{\perp,i}(t)$ is the initial perpendicular velocity of a resonant ion and $v_{\perp,f}(t+\Delta t)$ is its velocity at the end of an interval of time Δt (Δt could be taken as the time for the resonant particle to cross the resonance layer. We assume $\Delta t < \tau_c$, the characteristic collision time) then the separation between the guiding centers of the ion and the electron (see Fig. 3.3) is,

$$x_g = r_f - r_i = \frac{m_i}{Z_i e B}(v_{\perp,f} - v_{\perp,i}) \tag{3.19}$$

Here m_i, $Z_i e$ are the mass and charge of the ion, and B is the magnetic field. If n_{res} is the density of resonant ions, then the energy absorbed per unit volume in time Δt is,

$$P \cdot \Delta t = \frac{1}{2} m_i (v_{\perp,f}^2 - v_{\perp,i}^2) n_{res} \tag{3.20}$$

If $v_{\perp,f} - v_{\perp,i} \ll v_{\perp,i}$, we could write

$$P \cdot \Delta t \simeq \frac{1}{2} m_i (v_{\perp,f} - v_{\perp,i}).2 v_{\perp,i} n_{res}$$

or

$$(v_{\perp,f} - v_{\perp,i}) = \frac{P \cdot \Delta t}{m_i n_{res} v_{\perp,i}} \tag{3.21}$$

Using 3.21 in 3.19 and putting $v_{\perp,i} \simeq v_{th,i}$ (ion thermal velocity), we get

$$x_g = \frac{P \cdot \Delta t}{Z_i e B v_{th,i} n_{res}} \tag{3.22}$$

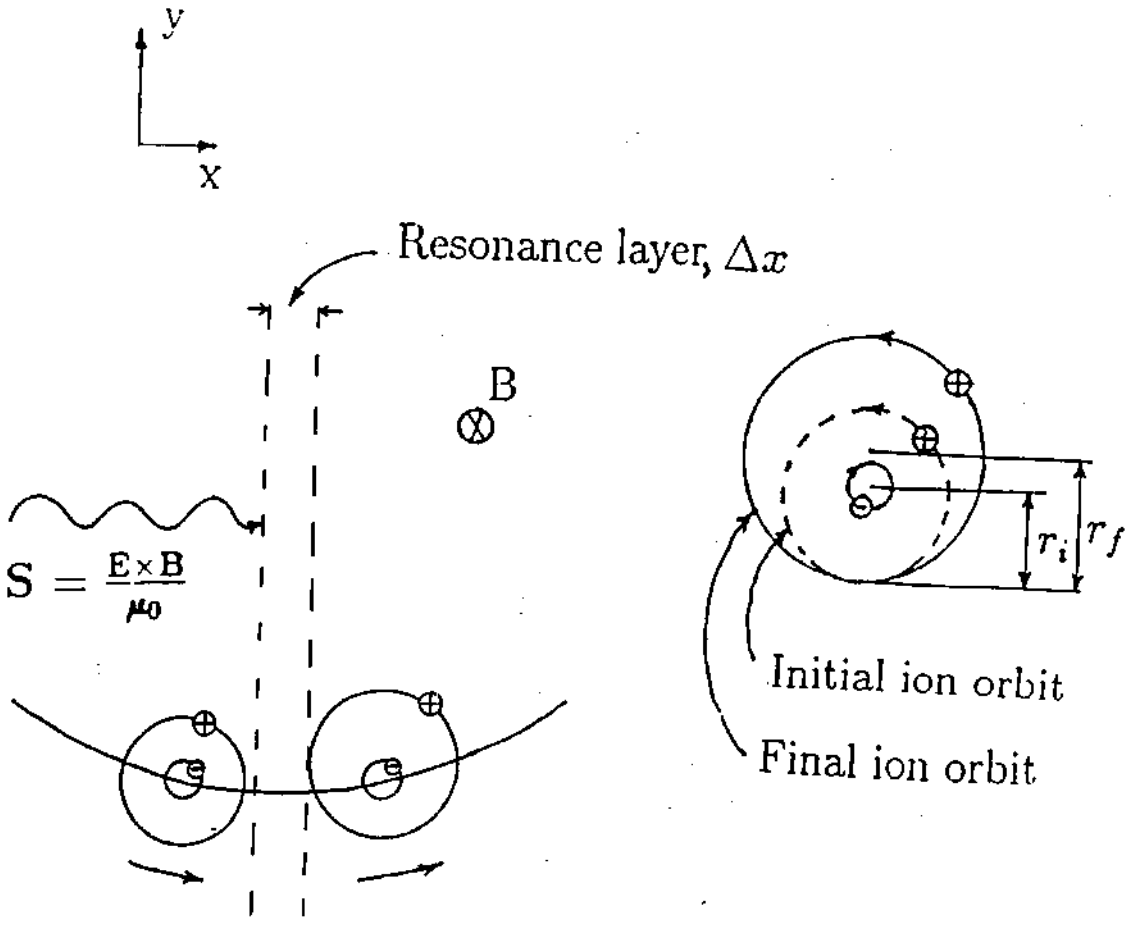

Figure 3.3: Creation of Dipoles during RF-Heating

Thus we have an electric dipole with a dipole moment $= Z_i e x_g = (P \cdot \Delta t)/(B v_{th,i} n_{res})$. With this, we have the electric field produced in time Δt due to n_{res} dipoles as

$$E_y(t + \Delta t) = \frac{P \cdot \Delta t}{\varepsilon_0 B v_{th,i}}$$

The electric field production rate is

$$\dot{E}_y = \frac{P}{\varepsilon_0 B v_{th,i}} \tag{3.23}$$

or, if one is willing to speculate on the lifetime of a dipole (say τ), then

$$E_y = \gamma \frac{P}{\varepsilon_0 B v_{th,i}} \tau \tag{3.24}$$

where γ is a factor which takes into account decreasing x_g during τ.

During wave heating, the increase in the magnetic moment $\overline{\mu}$ is

$$\Delta \overline{\mu} = \frac{m_i}{2B}(v_{\perp,f}^2 - v_{\perp,i}^2) \tag{3.25}$$

Using Eq. 3.20,

$$\Delta \overline{\mu} = \frac{P \cdot \Delta t}{B n_{res}} \tag{3.26}$$

Hence, diamagnetic depression of the field

$$\Delta B \simeq \mu_0 \Delta \overline{\mu} n_{res} \tau = \frac{\mu_0 P \tau}{B} \tag{3.27}$$

where μ_0 is the magnetic permeability.

Macroscopic Argument

The macroscopic argument relies on conservation of momentum [45]. As the wave energy is absorbed by the plasma, the wave momentum must appear as the field momentum.

If $\mathbf{S}$ and $\mathbf{v}_\phi$ are the Poynting flux and the wave phase velocity respectively, the momentum density, $\mathbf{g} = \mathbf{S}/v_\phi^2$.

Wave momentum absorbed per second = Wave momentum contained in a volume Av_ϕ (A is the RF-beam area) = $(\mathbf{S}/v_\phi^2).Av_\phi = (\mathbf{S}A)/v_\phi$.

This momentum must appear in the field, i.e.

$$\frac{d}{dt}\varepsilon_0(\mathbf{E}\times\mathbf{B}) = \frac{\mathbf{S}A}{v_\phi}.\frac{1}{V_{res}} \tag{3.28}$$

where V_{res} is the volume of the resonance region ($\sim A.\Delta x$, Δx being the resonance zone thickness).

Neglecting magnetic field depression and noting that close to the resonance zone $v_\phi \simeq v_{th,i}$,

$$\dot{E}_y \simeq \frac{1}{\varepsilon_0 B v_\phi}.\frac{SA}{V_{res}} = \frac{P}{\varepsilon_0 B v_{th,i}}$$

in agreement with Eq. 3.23.

Before we proceed to estimate the electric field in a tokamak, we briefly discuss below some factors which might cause a reduction in the electric field production rate and some consequences of the electric field.

(a) The actual electric field is expected to be smaller because the background plasma acts like a dielectric with a dielectric constant $\varepsilon = (1 + \frac{m_i n_i \mu_0 c^2}{B^2})\varepsilon_0$ ($\gg \varepsilon_0$). This reduces the electric field production rate to

$$\dot{E}_y \simeq \frac{P}{\varepsilon B v_{th,i}} \tag{3.29}$$

Also, the electric field causes the background particles to drift with a velocity [referring to Fig. 3.3]

$$\mathbf{v}_d = \frac{\mathbf{E}\times\mathbf{B}}{B^2} \sim \frac{E_y}{B}\hat{x} \tag{3.30}$$

(b) The dipoles move swiftly along the magnetic field lines to occupy a volume larger than V_{res}. For central heating, assuming that particles on all flux surfaces are resonating, the particles move quickly to occupy the entire plasma volume (this is a reasonable assumption for $\tau_\parallel = 2\pi R\bar{q}/v_\parallel \ll \tau_c$). Here $\bar{q}$ is the safety factor and $v_\parallel$ is the parallel velocity of the particle. The picture might then look like that depicted

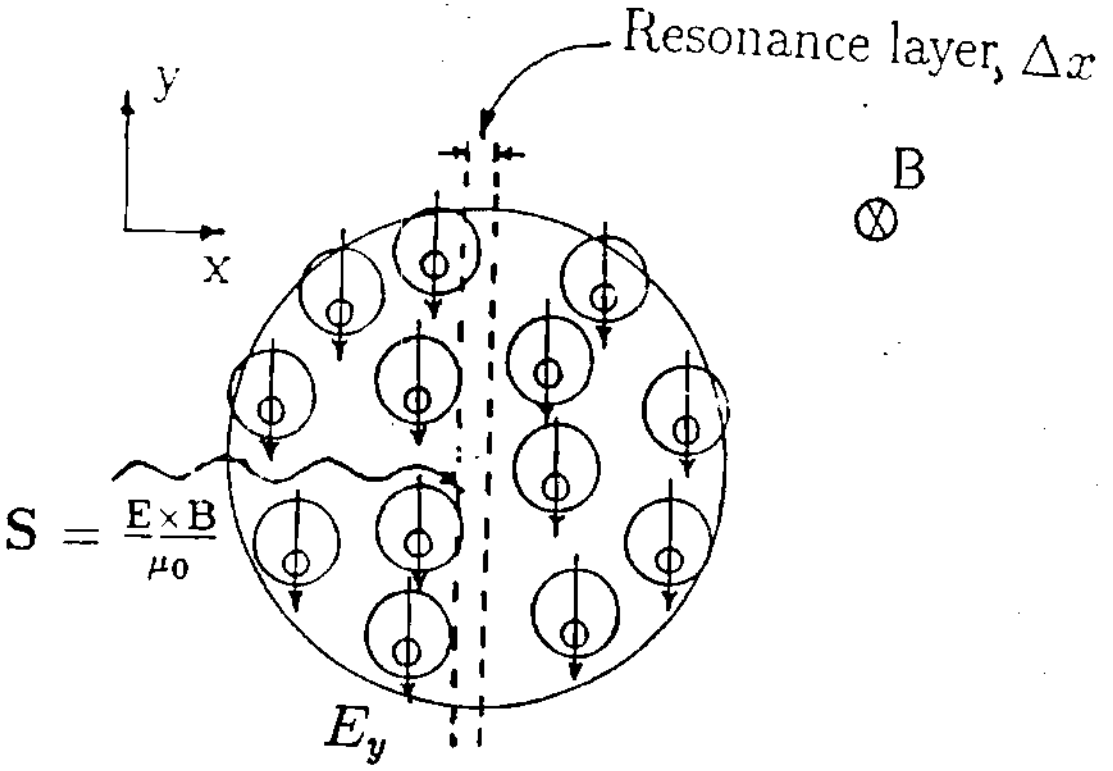

Figure 3.4: Polarization of the Plasma during Wave Heating

in Fig. 3.4. Hence, we should use the total plasma volume, V_{tot}, instead of V_{res} in estimating the power density. Fig. 3.4 also suggests the possibility of significant up-down potential variations.

(c) Implicit in the above arguments is the assumption of axisymmetry with regard to RF sources. In an actual tokamak with a finite number of RF sources, this clearly is not the case. Hence, the electric field is expected to be smaller than that estimated in the previous paragraphs.

Example

As an example, let us consider the data related to JET. Typical parameters during ICRH with D(H) minority heating scheme are [47, 48] :

R=3 m, a=1.25 m, b=1.7 m, B=3 T, P_{rf}=10 MW, T_i=5 keV, $n_i = 3 \cdot 10^{19}\ m^{-3}$, $k_{\|} \simeq 0$, $\Delta k_{\|} \simeq 9\ m^{-1}$. Here a and b are the minor and major axes of the elliptic cross section.

These parameters give us $v_{th,i} \simeq 10^6$ m/s, the ion cyclotron frequency $\Omega_i \simeq 3 \cdot 10^8$ rad/s, $\Delta x \simeq R\Delta k_{\|} v_{th,i}/\Omega_i = 0.09$ m. For central heating, assuming resonance across a vertical cylindrical shell passing through the center, $V_{res} \simeq A \cdot \Delta x = (2\pi R)(2b)(\Delta x) = 5.8\ m^3$

Using this to calculate the power density, $\dot{E}_y = 6.5 \times 10^{10}\ V m^{-1} s^{-1}$

In order to calculate the steady state electric field using Eq. 3.24, one needs to estimate the lifetime of a dipole. Here we give two estimates of the steady state electric field.

(a) We could get an estimate of the smallest steady state electric field by using the electron-ion collision time, τ_{ei}, as the lifetime of a dipole. (One could perhaps argue that τ_{ei} is the timescale over which the correlation between the electron-ion pair is destroyed.) Using

$$\tau_{ei} = 1.09 \times 10^{16} \cdot \frac{T_e^{3/2}(keV)}{n_i(m^{-3}) \cdot \ln \Lambda} \simeq 2 \cdot 10^{-4}\ s$$

and taking $\gamma = 0.5$, Eq. 3.24 gives $E_y = 7.6 \times 10^6\ \ V/m$.

The diamagnetic depression of the field is $\Delta B = 1.7 \times 10^{-4}\ T$.

Accounting for the background plasma response, if we use ε ($\varepsilon = 1260$ in this case) instead of ε_0, we get $E_y \simeq 6000\ V/m$.

In response to the field, the background particles drift with a velocity of $v_{dx} = 2000\ m/s$ close to the resonance zone.

If we use $V_{tot} \simeq 125\ m^3$ instead of V_{res}, we get an average electric field of $E_y = 280\ V/m$.

(b) A second estimate of the field can be made by arguing that the field due to the dipoles persists until the fast ion is slowed down by collisions. Using ion-ion collision time

$$\tau_i(s) = (6.60e17).\left(\frac{m_i}{m_p}\right)^{1/2}.\frac{(T_i(keV))^{3/2}}{n_i(m^{-3}).\ln\Lambda} = 0.012$$

and taking γ=0.5, $E_y = 3.9 \times 10^8$ V/m

The diamagnetic depression $\Delta B = 0.009$ T

If we use ε instead of ε_0, the electric field is reduced to $E_y = 3 \cdot 10^5$ V/m.

Electric fields of this magnitude give rise to large particle drifts, $v_{dx} \sim 1 \cdot 10^5$ m/s close to the resonance zone.

3.2 Effect of Poloidal Potential Variation on Particle Trapping

Before we consider the effect of poloidal electric field on transport, we wish to examine the effect of potential variation on particle trapping. For time scales greater than $1/\nu_{+f}$, the poloidal potential built up during wave heating acts on the background particles causing a redistribution of trapped particles. This phenomenon has been examined by Shurygin and Yushmanov [13] and Chang [12]. Following Chang [12], we examine particle trapping when (i) $e_j\Phi_{in} < e_j\Phi_{out}$ and (ii) $e_j\Phi_{in} > e_j\Phi_{out}$ where Φ_{in} and Φ_{out} are the potential on the high field and low field side of the tokamak

respectively. Here $e_j = Z_j e$ is the charge on the species j and $Z_j = -1, 1, Z$ for the electron, ion, and impurity species respectively and e is the unit charge.

3.2.1 $e\tilde{\Phi}(\theta)/T \sim \mathcal{O}(\epsilon)$ and $e_j\Phi_{in} < e_j\Phi_{out}$

This situation obtains for ions during ICRH or electrons during ECRH. In the present case, particle trapping can be separated into two categories. The first type, called B-trapping, is the usual magnetic trapping on the low field side modified by the electrostatic potential. The second type of trapping, called E-field trapping, occurs on the inside of the torus and is due to the potential well.

B-trapping

Referring to the tokamak geometry in Fig. 3.1, we have, by conservation of energy,

$$E = \frac{v_\perp^2(\theta)}{2} + \frac{v_\parallel^2(\theta)}{2} + \frac{e_j\Phi(\theta)}{m_j} = \frac{v_\perp^2(\theta')}{2} + \frac{v_\parallel^2(\theta')}{2} + \frac{e_j\Phi(\theta')}{m_j} \tag{3.31}$$

and

$$\mu = \frac{v_\perp^2(\theta)}{2B(\theta)} = \frac{v_\perp^2(\theta')}{2B(\theta')} \tag{3.32}$$

Here θ and θ' refer to different poloidal locations. For reflection at $\theta' = \pi$, $v_\parallel^2(\pi) \to 0$. Hence, the boundary of the trapped particle region is given by

$$\frac{v_\perp^2(\theta)}{2B(\theta)} \geq \frac{v_\perp^2(\theta)/2 + v_\parallel^2(\theta)/2 + e_j/m_j(\Phi(0) - \Phi(\pi))}{B(\pi)}$$

Taking $B = B_0/1 + \epsilon\cos\theta$ and $e_j\Phi(\theta) = e_j\Phi_c\cos\theta$ ($e_j\Phi_c > 0$), the above equation yields

$$S_\parallel^2 \leq \epsilon(1 + \cos\theta)(S_\perp^2 - |Z_j|X_0) \tag{3.33}$$

where $S = v/v_{th,j}$ and $\epsilon X_0 = (e\Phi_c/T)$. Here, we note that $X_0 \sim \mathcal{O}(1)$. At this stage, we will not distinguish between the electron, ion, and impurity temperatures. We assume that $T_e \simeq T_i \simeq T_Z = T$, where the subscripts e, i, Z refer to electron, main ion, and impurity ion respectively. Defining the pitch angle variable $\lambda = \mu B_0/E$,

Eqs. 3.31 and 3.32 can be used to determine the boundary of the trapped region on the $\lambda - E$ space. The result is

$$(1-\epsilon) \leq \lambda \leq (1+\epsilon)\left[1 - \frac{e_j\Phi(0)}{m_j E}\right] \tag{3.34}$$

In deriving Eq. 3.34, we have set $\Phi(\pi) = 0$.

E-trapping

For E-trapping, we expect particle reflection on the low field side of the tokamak. By considering reflection at $\theta' = 0$ and following similar steps as before, we obtain the boundary of the trapped region as

$$S_{\|}^2 \leq \epsilon(1-\cos\theta)(|Z_j|X_0 - S_{\perp}^2) \tag{3.35}$$

In the $\lambda - E$ space, the trapped region is

$$(1+\epsilon)\left[1 - \frac{e_j\Phi(0)}{m_j E}\right] \leq \lambda \leq 1-\epsilon \tag{3.36}$$

We note that the minimum energy a particle can have is $E_0 = e_j\Phi/m_j$. The trapped particle regions for B-trapping and E-trapping are shown in Fig. 3.5. The dotted lines show the trapped particle region for $\tilde{\Phi}(\theta) = 0$.

3.2.2 $e\tilde{\Phi}(\theta)/T \sim \mathcal{O}(\epsilon)$ and $e_j\Phi_{in} > e_j\Phi_{out}$

. This scenario holds good for ions during ECRH and electrons during ICRH. When $e_j\Phi_{in} > e_j\Phi_{out}$, only B-trapping is present. Letting $e_j\Phi(\theta) = -e_j\Phi_c\cos\theta$ $(e_j\Phi_c > 0)$ and proceeding as before, we determine the boundaries of the trapped particle region in the $S_{\|} - S_{\perp}$ space as

$$S_{\|}^2 \leq \epsilon(1+\cos\theta)(S_{\perp}^2 + |Z_j|X_0) \tag{3.37}$$

In the $\lambda - E$ space, setting $e_j\Phi(0) = 0$, the trapped particle region is bounded by

$$(1-\epsilon)\left[1 - \frac{e_j\Phi(\pi)}{m_j E}\right] \leq \lambda \leq (1+\epsilon) \tag{3.38}$$

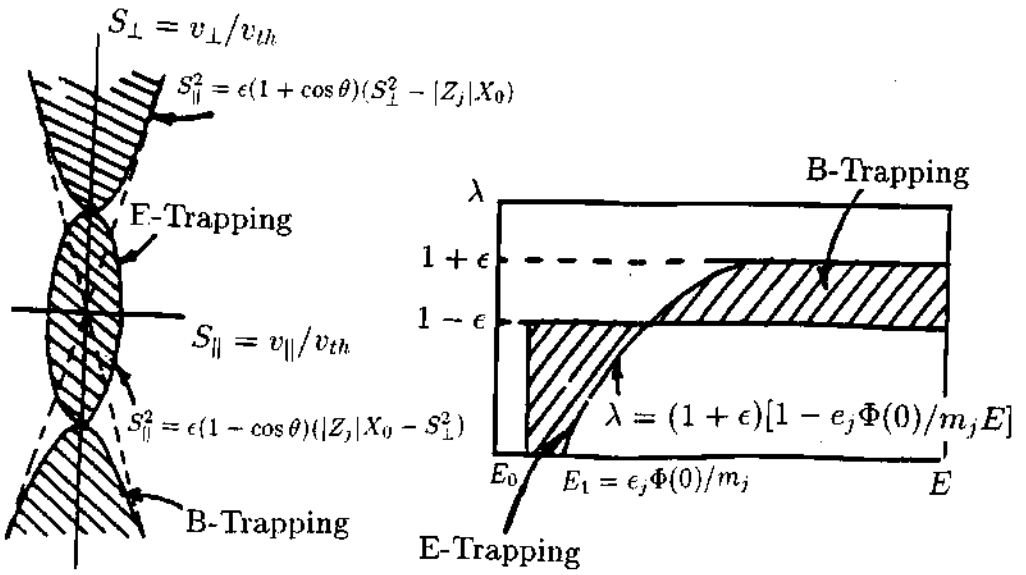

Figure 3.5: Particle Trapping when $e_j\Phi_{in} < e_j\Phi_{out}$

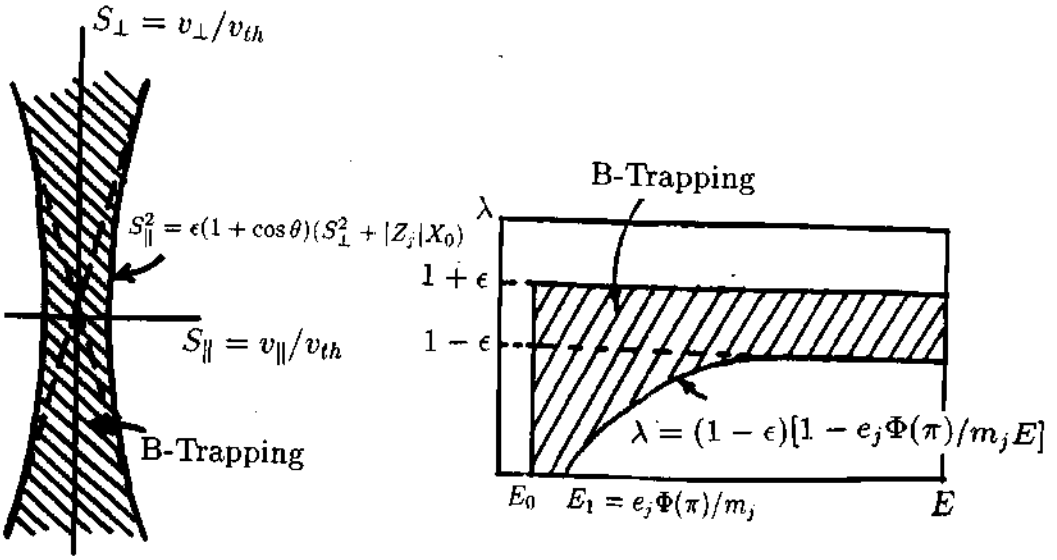

Figure 3.6: Particle Trapping when $e_j\Phi_{in} > e_j\Phi_{out}$

Fig. 3.6 shows the trapped particle region in the velocity $(S_{\parallel} - S_{\perp})$ space and $\lambda - E$ space.

From the previous arguments and from Figs. 3.5 and 3.6, we note that the presence of order ϵ poloidal potential variation leads to a redistribution of trapped particles. Such a redistribution could affect the way the problem of particle transport is handled. For instance, in a large aspect ratio tokamak, the collision operator is often taken as the pitch angle scattering operator [8] even among like species because of the smallness of the trapped particle region. As can be seen from Figs. 3.5 and 3.6, in the presence of a large poloidal potential variation, smallness of the trapped particle region is destroyed in the low energy region. In such cases, it may not be accurate to model the collision operator as pitch angle operator and the energy scattering may have to be included.

3.3 Particle Transport During Wave Heating

High power rf-heating could lead to significant changes in particle transport. This has been observed in many experiments (see Chapter IV) and several theoretical studies indicate a modification of transport of the resonant species and non-resonant particles during wave heating. A majority of theoretical studies have concentrated on ICRH, mainly because of its wide use in the current generation of fusion devices. For the purpose of the present review, we could put transport effects due to wave heating into two categories: (i) transport in the 'background' or non-resonant particles and (ii) transport due to wave particle interactions. An effect of the former type is the transport induced in the non-resonant species due to poloidal variation in the potential created during wave heating. Such a potential variation introduces an $\mathbf{E} \times \mathbf{B}$ drift in addition to the already existing ∇B and curvature drifts. Also, in the banana regime, there is a redistribution of trapped particles, as discussed in section 3.2,

causing additional change in transport. We discuss these effects in section 3.3.1. Rf-heating causes banana orbits of the resonant particles to become wider, which could eventually result in the loss of some particles due to interception by limiters or other protruding metallic structures. In addition, injection of waves with $k_{\parallel} \neq 0$ can add an inward or outward component to the tail ion (or electron) flow. We review some of these rf-driven transport mechanisms in section 3.3.2.

3.3.1 Effect of Poloidal Potential Variation on Transport

From now on, we will be particularly interested in a regime known as the "Banana Regime" [8]. In this regime, the time taken by a particle to complete the trapped orbit ($\tau_B = 1/\omega_B \sim \bar{q}R/\sqrt{\epsilon}v_{th}$ where $\bar{q}$ is the safety factor) is much smaller than the effective collision time for the particle to be scattered out of the trapped orbit ($\tau_{eff} = 1/\nu_{eff} \sim \epsilon\tau$ where τ is the 90^0 scattering time), i.e.,

$$\frac{\bar{q}R}{\sqrt{\epsilon}v_{th}} \cdot \frac{1}{\epsilon\tau} \ll 1$$

or

$$\frac{\bar{q}R\nu}{v_{th}} \ll \epsilon^{3/2}$$

where the collision frequency $\nu = 1/\tau$. Plasma ions and electrons in the core region of a majority of the present and most of the future tokamaks are expected to be in the banana regime. Also, light to moderately heavy impurities are expected to be in this regime. In addition, the mechanism for the production of a significant poloidal electric field described in Section 3.1 is valid in the banana regime. Hence, we shall restrict ourselves to the study of transport in the banana regime.

We note in passing that the effect of a poloidal potential variation of order ϵ on neoclassical transport in the collisional regime has been examined by Chang et al. [49,50]. Similar studies for the plateau regime have been conducted by Hazeltine et al. [51,52]. These studies indicate that a poloidal electric field of the order ϵ has a

significant effect upon neoclassical transport.

Banana Regime

The problem of transport in the collisionless banana regime in the presence of order ϵ poloidal potential variation has been studied by Chang [12]. He reconstructed the kinetic theory of Ref. [8] to include the contribution of zeroth order (in gyroradius) poloidal electric field. Electron flux is obtained [12] for a large aspect ratio tokamak. Ion flux could be obtained using ambipolarity which gives $\Gamma_i = \Gamma_e$. The problem consists in solving the first order version of the drift kinetic equation (Eq. 2.52). For electrons, Eq. 2.52 can be written as

$$\mathbf{v}_\parallel.\nabla f_{e1} - (C^l_{ee} + C^l_{ei}) f_{e1} = -\mathbf{v_{de}}.\nabla f_{e0} - (e/T_e) v_\parallel E_\parallel f_{e0} \tag{3.39}$$

where $\mathbf{v_{de}} = -\mathbf{v}_\parallel \times \nabla(v_\parallel/\Omega_e)$, C^l_e is the linearized collision operator. Here $\hat{n} = \mathbf{B}/B$ and the gradient is taken at constant $E = v^2/2 + e_j\Phi(r,\theta)/m$ and $\mu = v^2_\perp/2B$. $\mathbf{v}_{de}$ now includes the contribution of the poloidal electric field. The zeroth order distribution function, obtained from the zeroth order version of the drift kinetic equation, is a Maxwellian

$$f_{e0} = \hat{n}(m/2\pi T)^{3/2} \exp[-(v^2/2 + q\Phi(\theta)/m)]$$

Eq. 3.39 is transformed into an equivalent set of equations [12,8],

$$\mathbf{v}_\parallel.\nabla g_{ne} - C^l_e g_{ne} = -\alpha_n f_{e0}, \quad n = 1,2,3,4 \tag{3.40}$$

which are obtained by putting

$$\begin{aligned} f_{e1} \;=\; & \frac{2v_\parallel u_{i,\parallel}}{v^2_{th,e}} f_{e0} - (e/T_e) f_{e0} \int_0^{l_p} \frac{dl_p}{B_\theta} \left(BE_\parallel - \frac{B^2 < E_\parallel B >}{< B^2 >} \right) \\ & + v_\parallel f_{se}(B < E_\parallel B > / < B^2 >) + H_e \end{aligned}$$

where

$$H_e = \sum_{n=1}^{4} g_{ne} A_{ne}.$$

The four dynamical forces are

$$A_{1e} = \frac{\partial}{\partial r} p_e + \frac{T_i}{Z_i T_e} \frac{\partial}{\partial r} p_i$$

$$A_{2e} = \frac{\partial}{\partial r} \ln T_e \;\; ; \;\; A_{3e} = B_0 < E_{\|} B > / < B^2 >,$$

$$A_{4e} = -(T_i / Z_i T_e) \mu_i$$

Here, $u_{i,\|}$ is the ion parallel flow and f_{se} is the Spitzer function [12, 8], $\int_0^{l_r}$ is the integral along the poloidal projection of a field line. The parameter μ_i is related to the ion parallel flow by

$$u_{i,\|} = \left(\frac{v_{th,i}^2}{2\Omega_{i,\theta}} \right) \left[\frac{\mu_i}{h} - \left(\frac{\partial \ln p_i}{\partial r} - (Z_i e / T_i) \frac{\partial \Phi(r)}{\partial r} \right) h \right]$$

Further,

$$\alpha_n = \mathbf{v}_{\|} . \nabla (v_{\|} \gamma_n)$$

$$\gamma_1 = -h / \mid \Omega_{ep} \mid \;\; ; \;\; \gamma_2 = (E^* / T - 5/2) \gamma_1,$$

$$\gamma_3 = \hat{f}_{se} / h \;\; ; \;\; \gamma_4 = -1 / h \mid \Omega_{ep} \mid$$

where $E^* = v^2/2 + e\Phi(\theta), h = \mid \Omega_{ep} \mid / \Omega_{ep} = B_{\theta,0} / B_\theta$ and $\hat{f}_{se} = f_{se} / f_{e0}$. The particle flux is written as

$$\Gamma_e = \left\langle \int d^3 v \mathbf{v}_{\mathbf{de}} . \nabla r f_e \right\rangle = \sum_{n=1}^{4} (\alpha_1, g_{ne}) A_{ne}$$

where the variational solution to Eq. 3.40 is given by [12]

$$(\alpha_m, g_{ne}) = \left\langle \int d^3 v v_{\|} \gamma_m C_e^0 (g_{ne}^0) \right\rangle \tag{3.41}$$

Here $g_{ne}^0 = v_{\|} \gamma_n f_{e0} + G_{ne}^0$. The superscript 0 denotes a zeroth order quantity in $\epsilon = r/R$ expansion. G_{ne}^0 is obtained by the constraint equation [8],

$$\int \frac{d\theta}{v_{\|}} C_e^0 (v_{\|} \gamma_n f_{e0} + G_{ne}^0) = 0 \tag{3.42}$$

We note that the transport coefficients, (α_m, g_{ne}), can be written as

$$(\alpha_m, g_{ne}) = \left\langle \int d^3 v v_{\|}^2 \gamma_m (1/v_{\|}) C_e^0 (g_{ne}^0) \right\rangle \tag{3.43}$$

Substituting for $(1/v_\parallel)C_e^0(g_{ne}^0)$ from the first order version of Eq. 3.40,

$$\begin{aligned}(\alpha_m, g_{ne}) &= \left\langle \int d^3v v_\parallel^2 \gamma_m \hat{n}.\nabla g_{ne}^1 \right\rangle \\ &= \left\langle 2\int d^3v \gamma_m (E^* - \mu B - e\Phi(\theta)/m)\hat{n}.\nabla g_{ne}^1 \right\rangle\end{aligned}$$

After integrating by parts,

$$(\alpha_m, g_{ne}) = -\left\langle 2\int d^3v \hat{n}.\nabla[\gamma_m(E^* - \mu B)]g_{ne}^1 \right\rangle + \left\langle 2\int d^3v \hat{n}.\nabla(\gamma_m \frac{e\Phi(\theta)}{m})g_{ne}^1 \right\rangle$$

The first term gives the usual neoclassical contribution without a significant poloidal electric field, while the second term gives the contribution due to the potential variation on the flux surface. Chang has calculated [12] the transport coefficients $(\alpha_1, g_{1e}), (\alpha_1, g_{2e})$, and (α_1, g_{3e}). It is found that (α_1, g_{1e}) and (α_1, g_{2e}) experience almost a linear increase with increasing $\Phi(\theta)$ for both $\Phi_{in} < \Phi_{out}$ (ICRH) and $\Phi_{in} > \Phi_{out}$ (ECRH). The enhancement in (α_1, g_{1e}) over its value when $\Phi(\theta) \simeq 0$ is by a factor of ~ 2 for $\Phi_{in} < \Phi_{out}$ and ~ 1.3 for $\Phi_{in} > \Phi_{out}$ when $e\Phi(\theta) \sim \epsilon$. For (α_1, g_{2e}), the respective enhancement factors are about 2.5 and 1.8. For the Ware pinch coefficient, (α_1, g_{3e}), the enhancement factor is given by the fit [12],

$$\begin{aligned}\frac{(\alpha_1, g_{3e})_{e\Phi/T\sim\epsilon}}{(\alpha_1, g_{ne})_{e\Phi/T\sim 0}} &= (1 + 1.25X_0)^{1/2} \quad \Phi_{in} < \Phi_{out} \\ &= 1 - 0.59X_0 + 0.39X_0^2 - 0.048X_0^3 \quad \Phi_{in} > \Phi_{out}\end{aligned} \tag{3.44}$$

The value for Ware pinch coefficient

$$(\alpha_1, g_{3e})_{e\Phi/T\sim 0} = -1.46(1 + 0.67/Z_i)(r/R_0)^{1/2}(n_e/B_{\theta,0})$$

Qualitatively, the Ware pinch coefficient experiences a mild increase for $\Phi_{in} < \Phi_{out}$. For $\Phi_{in} > \Phi_{out}$, it decreases first up to $X_0 \sim 1$ and then experiences a steady increase for $X_0 > 1$. We note that the Ware pinch term can also change because of a decrease in $E_\parallel$ caused by a drop in the resistivity during wave heating.

Finally, the presence of an impurity species is found not to affect the transport coefficients calculated previously. This is because the inclusion of impurities results in

the replacement of ν_{ei} with $Z_{eff}\nu_{ei}$ in the pitch angle operator used in the calculations and this would result in a uniform change in the value of the electron transport coefficients independent of X_0 values. Chang, however, does not calculate the impurity or ion flux.

Shurygin and Yushmanov [13] have recently considered the effect of large poloidal electric fields on ion transport in the banana regime. Their analysis differs from that of Chang [12] in that they include the quasilinear operator in their calculations. They point out that random changes in $v_\perp$ could lead to diffusion of classical type, $D \sim \rho^2/\nu_{rf}$, where the 'quasilinear collision' rate $\nu_{rf} \simeq D_{\mathbf{v}}/v_{th}^2$ ($D_{\mathbf{v}}$ is defined in section 2.4). They, however, argue that quasilinear collisions do not lead to diffusion of the neoclassical type for $k_\parallel = 0$ (we will discuss this later in this section). They argue that the dominant effect on transport is due to the poloidal polarization of the plasma. To see qualitatively how such polarization could affect transport, we note that in the presence of a poloidal variation in the potential of the type $\Phi(\theta) = \Phi_c \cos\theta$, the effective magnetic well depth is $\epsilon_{eff} = \epsilon[1 - e_j\Phi_c/T]$. The neoclassical diffusion coefficient is $D \sim \sqrt{\epsilon_{eff}}\rho^2\nu \sim \sqrt{\epsilon[1 - \Phi_c/T]}\rho^2\nu$. Hence, the diffusion coefficient can be larger or smaller than the neoclassical value depending on the sign of e_j and Φ_c. This qualitative picture is not entirely accurate because any decrease in the B-well depth is somewhat compensated by the creation of an electrostatic potential well on the inside of the tokamak. It is the the combined effects of B as well as E-wells that lead to changes in transport. Calculations by Shurygin and Yushmanov [13] indicate a decrease in the radial flux of ions during ICRH and a slight increase in neoclassical transport of ions during ECRH. Also, an increase in trapped ion population during ECRH leads the authors [13] to speculate on enhanced transport due to rippling.

Fluid Theory

Finally, we discuss briefly a fluid theory due to Stacey [53] which qualitatively predicts an impurity flux component proportional to E_θ. The fluid theory by Stacey [53] is a modification of the theory originally developed by Stacey and Sigmar [54, 55] to compute the impurity transport in a strongly rotating plasma (toroidal velocity $v_\phi \simeq v_{th}$) resulting during strong NBI. The particle flux obtained in Refs. [54,55] can be written as

$$\begin{aligned}\Gamma_j = < n_j v_{rj} > \; &= \; < n_j v_{rj} >_{PS} + < n_j v_{rj} >_{NC} + < n_j v_{rj} >_M \\ &+ < n_j v_{rj} >_I + < n_j v_{rj} >_{\Phi'} + < n_j v_{rj} >_{\tilde{\Phi}} \end{aligned} \tag{3.45}$$

Here, j=i,Z for the main ions and impurity ions respectively. In the above equation, the first two terms are the usual Pfirsch-Schlüter (PS) and neoclassical (NC) components. The third, fourth, and fifth terms are the fluxes resulting from the beam-particle momentum exchange (M), inertial effects (I) and radial electric field (Φ'). These fluxes depend on the poloidal asymmetry in the particle density and, hence, indirectly on the poloidal potential variation. The last term is the flux resulting directly from the poloidal variation in the potential. In the limit of highly collisional impurities (i.e. the impurity parallel viscosity $\mu_Z \rightarrow 0$), this term for the impurities can be written as

$$\Gamma_{\tilde{\Phi}} = < n_Z v_{rZ} >_{\tilde{\Phi}} \simeq \frac{n_Z^0 m_Z \nu_{Zi}^0}{e_Z B_{\theta,0}^2} \epsilon^2 \beta_Z \left(\frac{\Phi^c}{\epsilon}\right) E_r^0 \tag{3.46}$$

where n_Z^0 is the flux surface averaged impurity density, E_r^0 is the leading order radial electric field and ν_{iZ}^0 is the impurity-ion collision frequency. The potential variation is assumed to be of the form

$$\Phi(r,\theta) = \Phi^0(r)[1 + \Phi^c \cos\theta + \Phi^s \sin\theta]$$

β_Z is the normalized gyroviscosity [53] given by

$$\beta_Z = \frac{\nu_{dZ}}{\nu_{Zi}} \quad with \quad \nu_{dZ} = \frac{T_Z \Theta}{2R^2 e_Z B}$$

Here, T_Z and e_Z are the impurity temperature and charge respectively and Θ is a quantity of the order unity for a strongly rotating ($v_\phi \simeq v_{th}$) plasma. From Eq. 3.46, it is clear that for $E_r^0 < 0$ (counter-injection), ICRH ($\Phi^c > 0$) produces inward flux ($\Gamma_{\tilde{\Phi}} < 0$), while ECRH ($\Phi^c < 0$) induces outward impurity flux ($\Gamma_{\tilde{\Phi}} > 0$). For strong co-injection, which could result in $E_r^0 > 0$, ICRH produces an outward impurity flux, while ECRH induces an inward impurity flux. In a non-rotating ($v_\phi << v_{th}$) plasma heated by ICRH or ECRH, the gyroviscosity is expected to be small. Nevertheless, Eq. 3.46 qualitatively predicts an inward impurity flux during ICRH and an outward flux during ECRH if E_r^0, which is negative during the ohmic phase, remains negative during cyclotron heating. (This seems to be the case on most devices. See the information on rotation velocities and potential variation during ECRH and ICRH in Chapter IV.)

3.3.2 Transport Due to Wave Particle Interactions

Wave particle interactions can affect the transport of the resonant species as well as the non-resonant species. We shall review a few important papers in this area. As mentioned before, much of the interest has centered on ICRH. However, some of the mechanisms described below apply to ECRH as well.

Whang and Morales [44] argue that during ion cyclotron wave heating, the toroidal canonical angular momentum, $P_\phi = mRv_\phi + eRA_\phi$, experiences negligible change in comparison with the magnetic moment, μ. Hence, when one allows for discrete changes in μ at each localized resonance, keeping P_ϕ constant, the minor radius of the drift orbit changes by [44]

$$\Delta r = S(\Delta\mu/\mu)\frac{\alpha\cos\theta}{2\sqrt{1+\alpha\cos\theta}}\frac{|\,v_{\|,0}\,|}{\Omega_\theta} \tag{3.47}$$

where $\alpha = (2\epsilon\mu B_0)/(mv_{\|,0}^2)$, $v_{\|,0}$ is the parallel velocity at resonance and $S = +1(-1)$ for co- (counter-) flowing ions. The change Δr is illustrated in Fig. 3.7. Discrete

changes in the minor radius by Δr leads Whang and Morales to conclude that rf-heating leads to a diffusion coefficient of the type $D \sim < (\Delta r)^2 > /2t$ where t is roughly the transit (or bounce) time for passing (or trapped) particles and $< >$ represents average over the phase between the particle velocity and the wave electric field. This diffusion mechanism has been contested by Shurygin and Yushmanov [13]. They argue that during cyclotron heating, only the perpendicular velocity increases and the parallel velocity does not change (this is true only for $k_{\parallel} = 0$). Hence, by conservation of toroidal canonical angular momentum, the particle has to pass through the same fixed resonance points (see Fig. 3.7). This would mean that only the type of the orbit changes, i.e., passing particles get trapped or trapped particles experience resonance localization (see Section 3.1.1) and an increase in the banana width, but there is no diffusion.

While the mechanism described above may not lead to diffusion, successive displacements Δr in the equatorial plane could result in a loss of the resonant particles if the collision frequency is low, i.e., $\nu_c > (\Delta r/(a - r_d))\omega_t$ where a and r_d are the minor radius and the initial drift orbit radius respectively. Chan et al. [56] point out that loss of trapped orbits in the above manner could result in significant changes in the impurity transport. It is well known that in a tokamak, counter-streaming (with respect to the plasma current) ions execute larger banana orbits as depicted in Fig. 3.8. During ICRH, the trapped particle orbits become wider, leading to the loss of some particles. From Fig. 3.8, it is clear that significantly more counter-streaming ions will be lost, resulting in an asymmetric confined ion distribution function which carries a net canonical angular momentum. Chan et al. [56] argue that the confined ions impart their momentum to the impurities via collisions causing them to drift inward. They solve the drift-kinetic equation with a driving term which includes collisions between impurities and heated minority ions to obtain an expression for the

impurity flux of the form

$$< \Gamma_Z >= -(m_Z Z_\alpha / m_\alpha Z) \int (d\theta/2\pi) h \frac{n_Z 3\sqrt{\pi}\bar{v}_Z \epsilon \cos\theta}{\tau_{Z\alpha}\Omega_{\theta,0}} G \qquad (3.48)$$

where the subscript (superscript) Z and α refer to impurities and heated ions respectively and $\bar{v}_j = v_{th,j}(j = \alpha, Z)$. The integral $G = \int d^3v' (v'_\parallel \bar{v}_\alpha^2 / v'^3) f_1^\alpha / n_\alpha$ is evaluated using the heated ion distribution function f_1^α obtained by Stix [22] and subtracting the particles in the loss region (see Fig. 3.8). It is found that $< \Gamma_Z >$ is always negative, independent of the direction of plasma current with respect to the toroidal magnetic field, B_ϕ. As can be seen from Eq. 3.48, the impurity flux is proportional to the impurity charge. The flux is found to decrease with increase in the plasma current and density. Calculations [56] for PLT parameters indicate that for moderate densities ($\sim 2 \times 10^{13} cm^{-3}$), the impurity pinch velocity $< V_Z >=< \Gamma_Z > / n_Z$ can be an order of magnitude larger than the neoclassical pinch.

Chen et al. [57] have examined the transport of energetic trapped ions during ICRH when $k_\parallel \neq 0$. They use quasilinear equations as well as a single particle model to derive the particle fluxes. For simplicity, we consider their single particle approach. The results obtained agree with those obtained using the quasilinear approach. During cyclotron wave heating, for small $k_\parallel v_\parallel / \omega$, wave damping primarily affects $v_\perp$, which changes the banana width but not the radial location of the banana tip. However, for $k_\parallel \neq 0$, there are small changes in $v_\parallel (\sim v_\phi)$ which cause the banana tip to move radially. Conservation of toroidal angular momentum could be used to relate the radial displacement, δr, of the banana tip to the change in parallel velocity, $\delta v_\parallel$, by

$$\delta r = -\delta v_\parallel / \Omega \qquad (3.49)$$

Change in $v_\parallel$ can be expressed in terms of change in the particle energy ΔW as it crosses the resonance zone. Following Kennel and Englemann [42], the change in the energy of a resonant particle, $\Delta W = m\delta(v^2)/2$. The gain in the parallel component of

energy, $\Delta W_{\|} = m\delta(v_{\|}^2)/2 = mv_{\|}\delta v_{\|}$. The energy lost by the wave is $\Delta W = nh\omega/2\pi$, where n is the number of quanta of energy lost to the particle and h is the Planck's constant. Similarly, $\Delta W_{\|} = (nh/2\pi)k_{\|}v_{\|}$. Hence $\Delta W_{\|}/\Delta W = k_{\|}v_{\|}/\omega$ or

$$\delta v_{\|} = \frac{k_{\|}\delta(v_{\|}^2)}{2\omega} = \frac{k_{\|}\Delta W}{m\omega} \tag{3.50}$$

Using this in Eq. 3.49

$$\delta r = -\frac{k_{\|}\Delta W}{m\omega\Omega_{\theta}} \tag{3.51}$$

Chen et al. [57] have obtained the result 3.50 using a calculation involving the rate of change of P_{ϕ}. If τ_B is the time required for a particle to move from one banana tip to another, then the banana tips move radially at a velocity

$$v_{r,Rf} = \frac{< \delta r >}{(\tau_B/2)} = -\frac{2k_{\phi} < \delta W >}{m\omega\Omega_{\theta}\tau_B} \tag{3.52}$$

The factor 2 appears because the particle passes through the resonance layer twice in time τ_B. For the fundamental resonance at $\omega = \Omega$ in the $k_{\|}v_{\|}/\omega << 1$ limit, using the result for $< \delta W > \simeq < \delta W_{\perp} >$ computed by Stix [22], Chen et al. [57] compute the convective particle flux

$$\Gamma_{r,c} = \frac{\dot{N} < \delta r >}{2\pi r 2\pi R_0} = -(B/B_{\theta})\left[\frac{R^2}{R_0 r \mid \sin\theta \mid}\sum_{\mathbf{k}}(\mid \frac{E^+}{B} \mid)^2 \frac{k_{\phi}}{\omega} N_{t.p.}\right]_{res} \tag{3.53}$$

where $\dot{N}$ is the number of particles crossing the resonance region per second $= 2 \times 2\pi R \mid B_{\theta}/B \mid \int d^3v f \mid v_{\|} \mid$ and $N_{t.p.}$ is the density of trapped particles in the resonance zone. We note that for symmetric $k_{\|} \simeq k_{\phi}$ spectrum, $\Gamma_{r,c} = 0$. Hence the convective flux is important only when $k_{\|}$ spectrum is highly asymmetric. Moreover, convective flux is inward or outward depending on whether k_{ϕ} is +ve or -ve with respect to the plasma current. In addition to the convective flux, the authors [57] also find a diffusive flux with a diffusion coefficient

$$D_{rf} = \frac{< (\delta r)^2 > - < \delta r >^2}{2(\tau_B/2)} = \frac{2k_{\phi}^2 W_{\perp}}{m^2\omega^2\Omega_{\theta}^2}\frac{< \delta W_{\perp} >}{\tau_B} \tag{3.54}$$

Comparing Eq. 3.52 with 3.54 and noting that $V_{diffusive} \sim D_{rf}/a$, the diffusive flux is smaller than the convective flux when $k_\phi \rho \ll 1$. Similarly, a comparison of $\Gamma_{r,c}$ with the neoclassical flux by Chen et.al. [57] indicates that for strong asymmetry in the wave spectrum, i.e. $k_\phi R \simeq 10 - 20$, the rf-driven transport could be comparable to or higher than the neoclassical flux depending on the energy of the ions. The authors [57], however, conclude that in most of the present experiments, the above mechanism does not play a significant role apparently because of a lack of strong asymmetry in the wave spectrum. It is, nevertheless, conceivable that antennas which launch waves preferentially may be used to improve the particle confinement or remove impurities and helium ash.

The formalism used in Ref. [57] does not contain the effect of collisions. Moreover, it concentrates mainly on the trapped particles while neglecting the contribution of the passing particles. In a recent paper, Chiu et al. [58] have generalized the above formalism to include collisions as well as passing particle contributions. They specialize for the case of ion heating using fast waves/ion Bernstein waves and take into account collisions between the main ions (self collision frequency ν_s) and between the main ions and the impurity ions (collision frequency ν_1). When collisions are momentum conserving, i.e. $\nu_s \gg \nu_1$, they obtain a result similar to Eq. 3.53. The result, however, includes the contribution of passing particles. It has the total particle density n_0 instead of the trapped particle density $N_{t,p}$. At the other limit, when $\nu_s \ll \nu_1$, they obtain a contribution to the total ion flux which could be an order of magnitude larger than the flux given by Eq. 3.53.

Chang et al. [59] have recently studied neoclassical transport of ICRH-heated high energy tail ions for the case when $k_\parallel = 0$. They have solved the drift-kinetic equation with a quasilinear term in addition to the collision term. The mechanism for tail ion transport as formulated by Chang et al. can be explained easily using a single particle model.

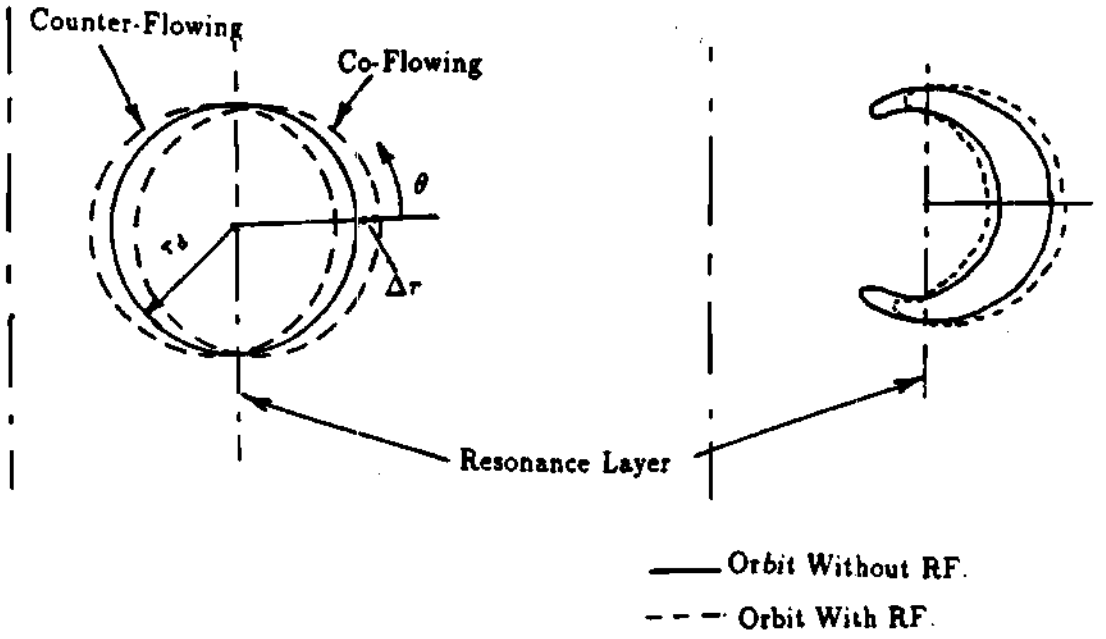

Figure 3.7: Drift Orbit Modification during RF Heating with $k_{\|} = 0$

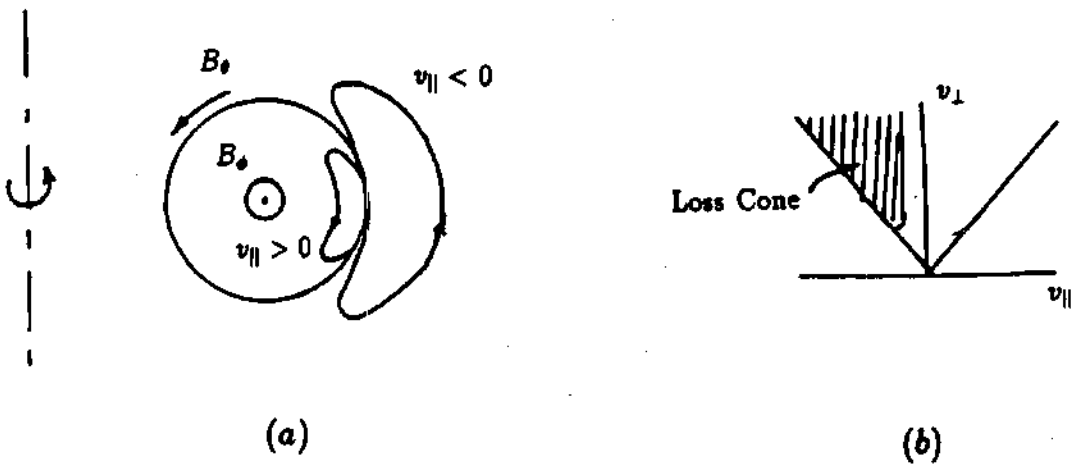

Figure 3.8: Drift Orbit Modification for Co- and Counter-Flowing ions

In the absence of a toroidal force, conservation of canonical angular momentum gives

$$eRA_\phi + mRv_\phi = const.$$

or

$$\psi - \frac{mRv_\phi}{e} = const. \tag{3.55}$$

where the poloidal flux function $\psi = -RA_\phi$. For the trapped particles, information about net radial motion can be obtained by taking the time derivative of Eq. 3.55.

$$\frac{d\psi}{dt} = \frac{\partial\psi}{\partial t} + \mathbf{v}.\nabla\psi = (m/e)\frac{d(v_\phi R)}{dt} \tag{3.56}$$

Integrating over trapped particle orbits and noting that $v_\phi = 0$ at the banana tips,

$$< \mathbf{v}.\nabla\psi >= -\left\langle\frac{\partial\psi}{\partial t}\right\rangle$$

where $< >$ denotes the average over a banana orbit. Using Maxwell's equations and $\nabla\psi = RB_\theta\hat{n}_\psi$, it can be shown that $\frac{\partial\psi}{\partial t} = RE_\phi$, and

$$< \mathbf{v}.\nabla\psi >= - < RE_\phi > \tag{3.57}$$

which is the usual Ware pinch effect. As the banana particles suffer Coulomb collisions and rf-scattering, the above result will be modified. For $k_\parallel = 0$, rf-scattering does not contribute to the toroidal momentum. Coulomb collisions, however, add a frictional force which modifies Eq. 3.56 to yield,

$$\frac{d\psi}{dt} = \frac{\partial\psi}{\partial t} + \mathbf{v}.\nabla\psi = (m/e)\frac{d(v_\phi R)}{dt} + \frac{F_\phi R}{e} \tag{3.58}$$

where F_ϕ is the toroidal friction. The above equation gives, after carrying out the same steps as before,

$$< \mathbf{v}.\nabla\psi >= -\left\langle\frac{\partial\psi}{\partial t}\right\rangle + \left\langle\frac{F_\phi R}{e}\right\rangle \tag{3.59}$$

If the $< F_\phi R >$ term does not vanish, we have a new pinch (or inverse pinch) term in addition to the Ware pinch. Physically, two mechanisms are responsible for $< F_\phi R > \neq 0$ [59],

(i) Difference in the path lengths between the banana tips due to the magnetic shear gives a contribution

$$< F_\phi > \simeq \frac{m \mid v_\parallel \mid}{\tau_s} \frac{\Delta_b}{\bar{q}R} \frac{\partial}{\partial r}(\bar{q}R) \tag{3.60}$$

where the friction force has been put in the form $F_\phi \simeq (m \mid v_\parallel \mid / \tau_s)$. Here, we assume that ion-electron slowing down collisions are responsible for friction. Also, Δ_b is the banana width and $\bar{q}$ is the safety factor.

(ii) As $\tau_s \propto T_e^{3/2}/n_e$, the gradients in T_e and n_e give rise to an imbalance in the friction force,

$$< F_\phi > \simeq \frac{m \mid v_\parallel \mid}{\tau_s} \left(\frac{1}{n_e} \frac{\partial n_e}{\partial r} - \frac{3}{2T_e} \frac{\partial T_e}{\partial r} \right) \tag{3.61}$$

The combined effect of the two phenomena would be to give us

$$< \mathbf{v}.\nabla\psi > \simeq \frac{m \mid v_\parallel \mid}{e\tau_s} R\Delta_b \left(\frac{1}{\bar{q}R} \frac{\partial}{\partial r}(\bar{q}R) + \frac{1}{n_e} \frac{\partial n_e}{\partial r} - \frac{3}{2T_e} \frac{\partial T_e}{\partial r} \right) \tag{3.62}$$

From a fluid perspective, the particle flux is

$$\Gamma_r = < n\mathbf{u}.\nabla\psi > = -\frac{1}{e} < R^2 \nabla\phi.(\mathbf{F} - \nabla.\mathbf{P} + en\mathbf{E}_\phi) > \tag{3.63}$$

In the standard neoclassical theory, the main contribution to the particle flux is due to the friction $\mathbf{F}$ and the toroidal electric field $\mathbf{E}_\phi$. Due to the fact that the lowest order distribution function is a Maxwellian, the off-diagonal elements in the stress tensor are of second order, making the second term in Eq. 3.63 small compared to other terms. During ICRH, the lowest order distribution function departs significantly from the Maxwellian, giving rise to a lower order contribution to the second term. It should be noted that from Eq. 3.62 the radial pinch velocity v_r is of the order $\sim (v_\parallel/\Omega_\theta r)\Delta_b/\tau_s$. Hence, particle transport due to the above mechanism is quite small, the maximum rate being of the order of one banana width in one slowing down time. Also, we note that the direction of the pinch term is inward due to the density gradient term and outward due to other terms.

Core [60] has studied the problem of resonant ion diffusion during ICRH with $k_{\|} \neq 0$ using a guiding center version of the Fokker-Planck equation which includes, in addition to the Coulomb and quasilinear collision operators, a term representing diffusion in the configuration space. He uses a diffusion coefficient very similar to the one given by Eq. 3.54. His analysis shows that for high power heating over long time scales, there is a pump-out of resonant ions from the region of resonant interaction into regions where damping is weak. Also, there is a degradation in the heating efficiency and thermonuclear reactivity.

3.4 Summary and Conclusion

In this chapter, we have surveyed the effects of cyclotron resonance wave heating on particle transport in tokamaks. We find that high power wave heating leads to the build up of an order ϵ poloidal potential variation, $\Phi(\theta)$, in the low collisionality regimes. It was found that such a variation in the potential could cause a redistribution of non-resonant trapped particles in the banana regime. A modification of trapped particle population along with the $\mathbf{E} \times \mathbf{B}$ drift due to the poloidal electric field produces significant changes in neoclassical transport. In a two species plasma (main ions and electrons), there is found to be an increase in the electron diffusion coefficient for both ICRH and ECRH, while, for ICRH, the Ware pinch coefficient shows a modest increase. For ECRH, it decreases first up to $e\Phi(\theta)/T \sim \epsilon$ and then increases for $e\Phi(\theta)/T > \epsilon$. The effect of the presence of an impurity species on ion or impurity transport has not been studied.

The problem of transport of high energy tail ions created during ICRH has received much attention. During wave heating, the trapped particle population increases and, in addition, the trapped particles experience a widening of their orbit. Loss of some of these high energy (significantly more counter-streaming) ions by interception with

limiters or other structures results in a confined ion population carrying a net canonical angular momentum. These ions impart their momentum to the impurity ions causing them to drift inward. The inward drift, however, decreases rapidly with increasing density and plasma current. Furthermore, the highly non-Maxwellian nature of the tail ions is found to give rise to a convective flux of tail ions. The magnitude of the flux is small compared with the neoclassical flux.

The above mechanisms operate even when $k_{\|} = 0$. For wave heating with $k_{\|} \neq 0$, trapped particles experience diffusive as well as convective motions. While the diffusive motion is present for symmetric as well as asymmetric $k_{\|}$ spectrum, the convective flux is present only for an asymmetric $k_{\|}$ spectrum. The convective flux is found to be larger than the diffusive flux, but smaller than the neoclassical flux for the conditions in the present experiments. The magnitude of the convective flux is found to increase when collisions between different species (for example, ions and impurities) dominate.

Thus, in conclusion, there is considerable theoretical evidence for significant changes in the particle transport during cyclotron (ICRH and ECRH) heating. ECRH and ICRH cause an order ϵ poloidal variation in the plasma potential. Such a variation in the potential is found to produce almost a linear increase in the neoclassical transport coefficients. Other mechanisms due to wave particle interactions induce changes in the non-resonant particle transport which are small in comparison with the neoclassical values. The present neoclassical formalisms, however, do not include the effect of impurities in calculating the particle transport in the presence of large poloidal electric fields. The presence of even a small amount of impurities can cause a significant increase in the main ion transport over the values for a plasma with only one ion species and electrons. As the present devices find a large impurity content during wave heating, it is imperative that the neoclassical theory should be reconsidered in the presence of impurities and large poloidal electric fields.

CHAPTER IV

WAVE HEATING AND TRANSPORT - EXPERIMENTS

The purpose of this chapter is to review some experimental observations related to particle transport during wave heating.

4.1 ECRH

4.1.1 Changes in Electron Density

In most small and medium sized tokamaks, ECRH is accompanied by a decrease in the electron density [31]. Results from ISX-B, TEXT and JFT-2 show this tendency [1,61,62]. Typical data from ISX-B during ECRH ($P_{rf} \sim 80\ kW$) is shown in Fig. 4.1. On T-10 ($P_{rf} \leq 2\ MW$), electron density profile broadening as well as a loss of particles has been observed [63]. The increase in T_e and consequent fall in the loop voltage results in reduced neoclassical pinch. This effect, however, is not sufficient to explain the magnitude of the drop in the electron density [31]. A recent study on TEXT [64], with ECRH power up to 200 kW, indicates an increase in the electron diffusion coefficient in the outer regions of the plasma, while it remains constant in the interior. On DOUBLET III, which is a large device, no change in the electron density has been observed for $P_{rf} \leq 0.7\ MW$ [65].

Finally, we briefly mention a study on electron transport during ECRH on the

IMS stellerator [66]. Central heating with ECRH ($P_{rf} \sim 2\ kW$) on the IMS stellerator produces electron density profiles which are hollow compared to the fairly flat profiles resulting during edge heating. Computer simulations using an 'anomalous' pinch velocity in addition to the diffusion term in the transport equation give good agreement with the measured density profiles. Furthermore, it is found that the poloidal electric fields are greater for the hollow profiles than for the flat profiles. The authors [66] indicate that the convective term is most likely a result of the increased poloidal electric field.

4.1.2 Impurity Transport

There have not been many studies of impurity transport during ECRH in tokamaks. This probably is due to the relatively low increase in the radiated power during ECRH. There are, however, two recent studies which deal with the problem of impurity transport during ECRH in considerable detail. These studies have been conducted on TFR and TEXT.

In TFR, the behavior of intrinsic impurities has been investigated in great detail [2]. Transport simulations have been carried out with a computer code using two transport parameters (a diffusion coefficient, D and an inward convective velocity, V) and using the experimentally determined n_e and T_e profiles.

For high density plasmas ($n_e(0) \sim 3.5 \times 10^{19}\ m^{-3}$) with a large iron concentration ($n_{Fe}(0) > 5 \times 10^{16}\ m^{-3}$), transport simulations with $D = 0.4\ m^2/s$ and $V = 6\ m/s$ give agreement with the experimentally determined impurity radiance for both the ohmic and ECRH ($P_{rf} \sim 520\ kW$) heated plasmas (see Figs. 4.2 and 4.3). Thus, there seems to be no change in the transport properties during the high density discharges. Also, during these experiments, electron density changes were relatively small.

For the low density discharges ($n_e(0) \sim 2 \times 10^{19}\ m^{-3}$) with an iron concentration similar to that mentioned above, the transport coefficients vary significantly. For

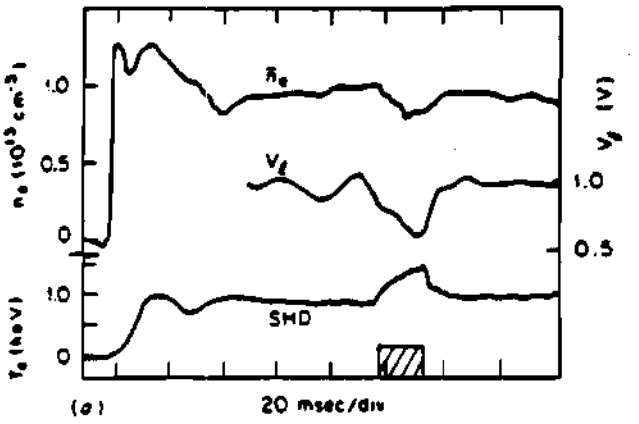

Figure 4.1: Central Electron Temperature, Loop Voltage, and Line-Averaged Electron Density vs Time for 80-kW microwave pulse of 16-ms duration. Data from ISX-B [1].

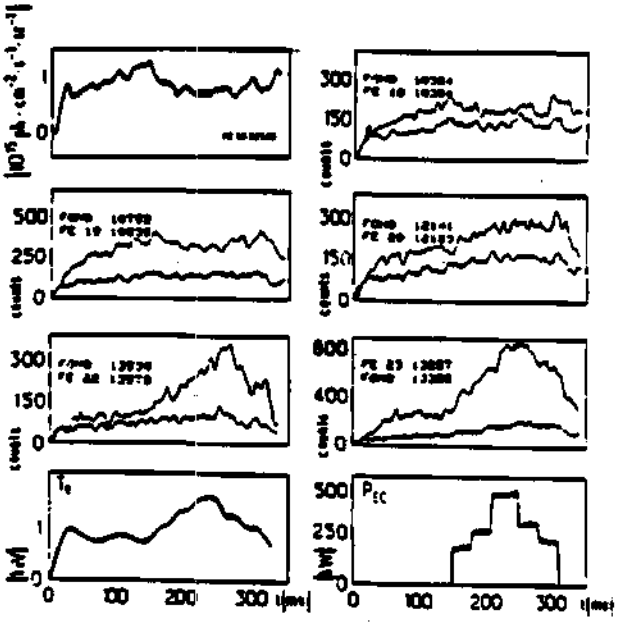

Figure 4.2: Experimental radiances of six iron lines for high density D-He iron dominated (ID) discharges ('fond' refers to background radiation). The central T_e and P_{EC} are also shown. Data from TFR [2].

$P_{rf} = 520\ kW$, the transport coefficients had to be increased from $D = 0.6\ m^2/s$ and $V = 6\ m/s$ during the ohmic phase to $D = 1.8\ m^2/s$ and $V = 18\ m/s$ during ECRH to give agreement with the experiments (see Fig. 4.4). The increase in the transport parameters is well above the uncertainty in their determination. The combined effect of increase in D and V is found to be a reduction in the impurity confinement time. Furthermore, during the low density discharges a strong pump-out in the electron density and an increase in the trapped electron population has been observed [2].

Transport simulations similar to the ones described above have been carried out for low density, low iron ($n_e(0) \sim 1.25 \times 10^{16}\ m^{-3}$) discharges. The results again show an increase by a factor of 3 of the impurity transport coefficients during ECRH.

In the TEXT tokamak, the transport of both intrinsic as well as injected impurities has been investigated [3]. Titanium was the major intrinsic impurity in TEXT. During ECRH ($P_{rf} \sim 200\ kW$), the titanium concentration in the plasma increases. There is also an increase in the titanium source by ~52% [3]. In order to better understand transport, scandium, an element similar to titanium, was injected by the laser ablation technique. This allowed a precise control over the impurity source. Transport studies with scandium reveal that the decay time for the scandium charge states that peak at $r/R > 0.7$ decreases during ECRH (Fig. 4.5). Furthermore, concentration of the central charge states of scandium decreases during ECRH. These results may indicate an outward impurity flux for $r/R > 0.7$ which could oppose the increase in the impurity source. However, the decay times for the charge states that peak at $r/R < 0.5$ remains relatively unchanged during ECRH, indicating insignificant transport changes at the core of the plasma. As in the case of TFR, numerical simulations have been carried out using two transport parameters (diffusion coefficient, D and convective velocity, V). Reasonable agreement with the data presented in Fig. 4.5 is obtained by increasing D from $1.0\ m^2/s$ during the ohmic phase to $1.5\ m^2/s$ during ECRH while keeping V fixed at $10\ m/s$. Thus, for power levels up to 200 kW,

there seems to be a significant change in the diffusion coefficient for radial locations $r/R > 0.7$.

4.1.3 Other Effects Related to Transport

In addition to the transport effects described above, ECRH induces changes in other plasma parameters which may directly or indirectly contribute to the observed transport effects.

One such effect is an increased trapping of the resonant species during ECRH. As described in Ref. [11] and in Chapter III, cyclotron heating increases the perpendicular energy of the resonant particles, leading to increased trapping. Such an effect has been observed on TOSCA, T-10 and TFR [67, 31, 2]. This effect is seen as a local peak (toward the outside of the torus) in the soft X-ray profile.

ECRH causes an increase in the plasma potential. Plasma potential measurements made on TEXT [68] using a heavy ion beam probe indicate that the potential increases (becomes less negative) during ECRH. The magnitude of the change is ~20%. At the center, the potential changes from ~-800 to -620 volts.

Another effect, which may be related to the potential changes, is the change in the plasma rotation velocity. Rotation measurement on DOUBLET III [69] indicates that the rotation velocity drops from 25200 m/s (co-rotation) during the ohmic phase to 10-15200 m/s during ECRH ($P_{rf} \leq 1\ MW$) for the effectively heated discharges with the electron temperature increasing from 0.8 keV to 1.2 keV during wave heating.

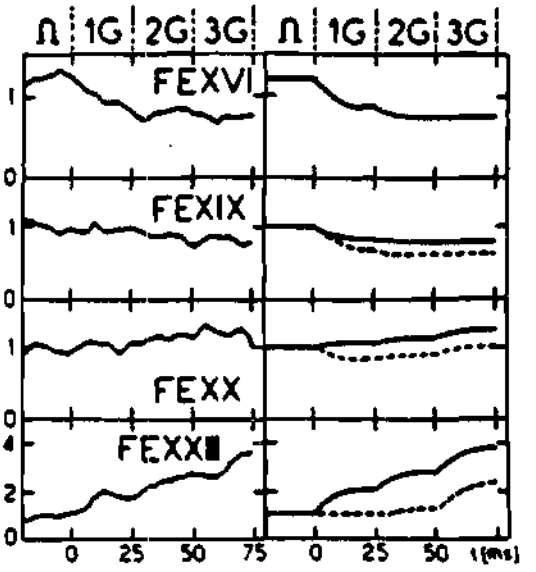

Figure 4.3: Experimental (left) and Simulated (right) Radiances of the High Density Discharges presented in Fig. 4.2. Simulated signals: the solid lines are for $D = 0.4\ m^2.s^{-1}$ and $V = 6.0\ m/s$; the dashed lines are for $D = 0.8\ m^2.s^{-1}$ and $V = 12.0\ m/s$. Data from TFR [2].

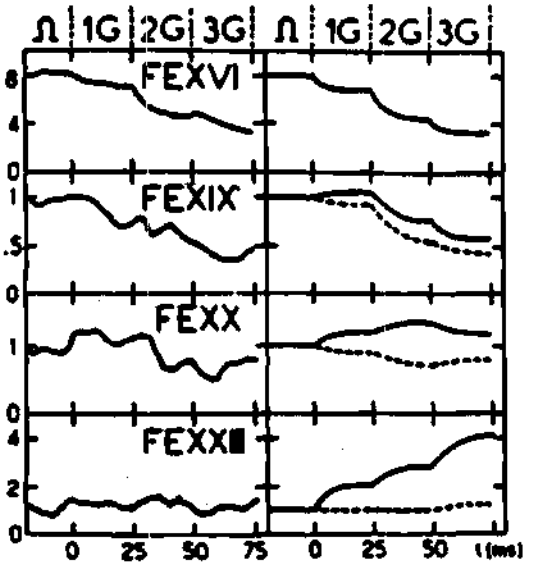

Figure 4.4: Experimental (left) and Simulated (right) Radiances of the Low Density ID Discharges. Simulated signals: the solid lines are for $D = 0.6\ m^2.s^{-1}$ and $V = 6.0\ m/s$; the dashed lines are for $D = 1.2\ m^2.s^{-1}$ and $V = 12.0\ m/s$ with 1 gyrotron and for $D = 1.8\ m^2.s^{-1}$ and $V = 18.0\ m/s$ with 2 and 3 gyrotrons. Data from TFR [2].

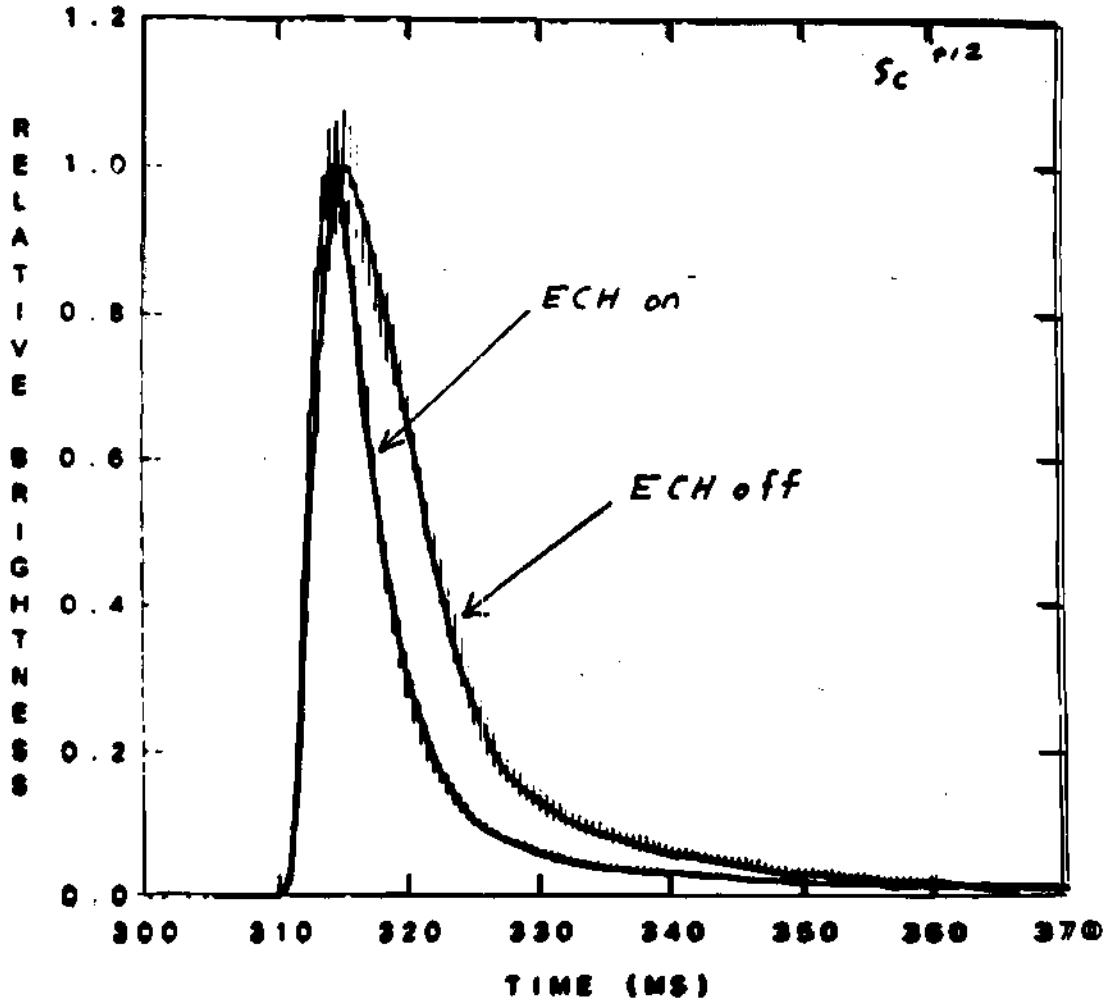

Figure 4.5: Typical Behavior of Intermediate Charge States of Injected Scandium. With ECRH, the Decay Time for Sc^{+12} decreases. Data from TEXT [3].

4.2 ICRH

4.2.1 Effect on Electron Density

In most tokamaks, the electron density rises with the application of ICRH. This has been observed on PLT, TFR, TEXTOR, JET and JIPP T-IIU [70–73, 4]. Fig. 4.6 shows the density evolution during ICRH on the JIPP T-IIU tokamak [4]. The density increase in Fig. 4.6 is mainly due to enhanced recycling due to ICRH and it scales almost linearly with the rf power. On TEXTOR ($P_{rf} \sim 1\ MW$), the increase in density is attributed partly to a profile broadening effect and partly to an increase in the central electron density during ICRH [72]. Studies on JET [74, 75] indicate that there is no change in the electron transport coefficients (i.e., diffusion coefficient, D and convective velocity, V) during ICRH. Thus, it appears that any change in the electron density during wave heating is due mainly to an increase in the electron source and not due to changes in the transport coefficients. In ASDEX, which is a tokamak with a divertor, no change in the electron density has been observed during ICRH [76].

4.2.2 Impurity Transport

In most devices, application of ICRH results in a higher impurity content. The change in the impurity content can be due to a change in the impurity source and/or due to a change in the impurity transport coefficients. It seems certain that ICRH always results in an increase in the impurity source. The mechanisms responsible for impurity generation are not completely understood. It is believed that erosion and sputtering of the wall (e.g. by the fast ions produced during ICRH) and a release of the antenna screening material (due probably to the impact of ions accelerated by the high rf fields) may be playing a major role. There seems to be a relation between the heating efficiency and the impurity release. Poorly heated plasmas have a higher

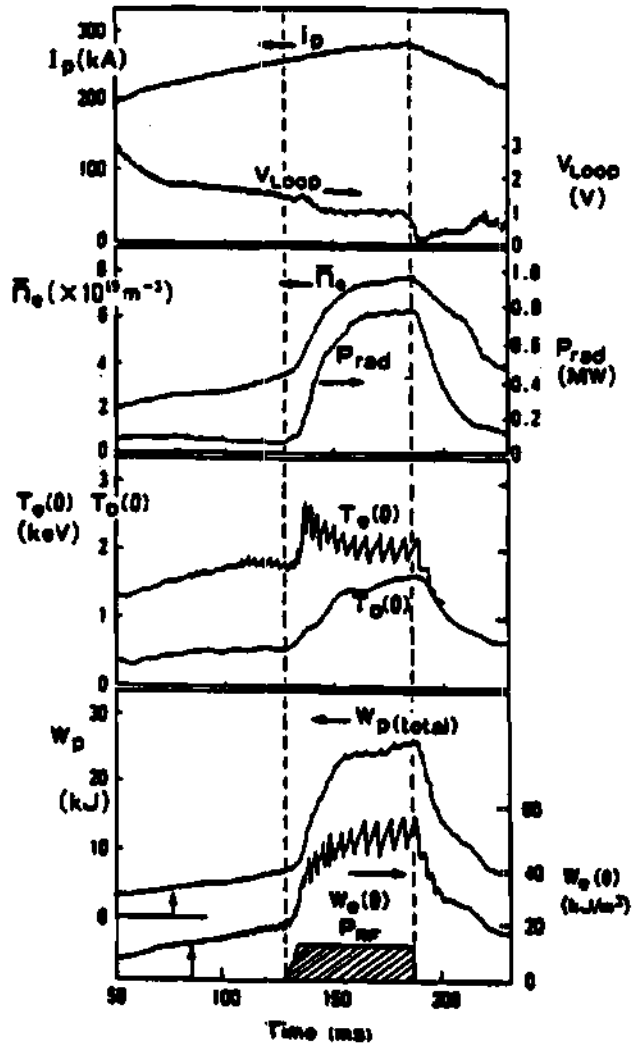

Figure 4.6: Typical Discharge on JIPP T-IIU with $P_{RF} = 2$ MW. W_p and $W_e(0)$ are the total stored energy and stored energy density of electrons respectively. Data from JIPP T-IIU [4].

impurity content.

Impact of high power ICRH on the impurity transport coefficients has been studied in a few tokamaks. In a study on JET, diffusion coefficients for nickel have been calculated [77] for ohmically heated plasmas. A diffusion coefficient, $D \sim 1\ m^2/s$, assumed to be constant across the plasma, and a convective velocity, $V = -2D\tau/a^2$, give good agreement between the experimentally determined nickel (Ni XXVI) intensity and the computer simulation. The authors [77] indicate that the diffusion coefficient (and hence the convective velocity) increases during ICRH. They, however, do not present any quantitative results.

An investigation of impurity transport from the vacuum vessel wall to the core of the plasma has been carried out on ASDEX [5]. In some experiments, titanium was injected into the plasma by the laser blow-off technique and the time evolution of the titanium line, Ti XX, in the core of the plasma was recorded for ohmic, neutral beam heated, and ICRH heated plasmas. Fig. 4.7 shows the result of such an experiment [5]. The decay time for titanium is of the order of the confinement time for titanium in the core of the plasma. From Fig. 4.7, it is clear that the confinement time for titanium is smaller for ICRH heated plasmas than for ohmic plasmas. However, for comparable powers, ICRH results in better titanium confinement than NBI (co-injection). Diffusion coefficients have been calculated for the above shots via computer simulation. For ohmic, NBI and ICRH heated plasmas, D is respectively 0.5, 1.0 and 0.9 m^2/s. Thus, there is a clear increase in the impurity diffusion coefficient during ICRH in comparison with the ohmic values. There seems to be a slight decrease in the diffusion coefficient for ICRH in comparison with NBI (co-injection) for comparable power levels ($P \sim 1.2\ MW$). In an earlier paper, Steinmetz et al. [76] have indicated that the improvement in the particle confinement time during ICRH with respect to NBI discharges may be due to an enhancement of the inward drift rather than due to a reduction in the diffusion coefficient. It appears that the computer simulations

mentioned above do not take this effect into consideration.

Impurity transport studies have also been conducted on TEXTOR [6]. For ICRH powers up to 1 MW, there is a noticeable increase in the concentration of light impurities such as oxygen and carbon. The impurity content scales linearly with the rf power. A typical example of light impurity behavior during ICRH is shown in Fig. 4.8 [6]. After ICRH is turned off, oxygen emission drops to a lower value. The time constant for the decay is of the order of the impurity confinement time ($\sim$ 75 milliseconds). As the increase in O VI brightness during ICRH is much more than could be explained by the changed plasma conditions (for e.g., increased T_e), the authors [6] conclude that there was an influx of impurity during ICRH. They, however, do not present any data on the transport coefficients.

4.2.3 Other Effects Related to Transport

As in the case of ECRH, ICRH induces changes in several plasma parameters that may be directly or indirectly related to transport.

ICRH produces significant changes in the plasma rotation. Central rotation velocity during ohmic heating has been measured on JET using MHD diagnostics [78,79]. The velocity is typically $2 - 2.5 \times 10^4\ m/s$ counter to the plasma current. When ICRH is turned on, the plasma velocity increases in the counter direction.

Rotation velocities during ohmic heating and ICRH have not been measured on TFTR. However, velocity measurements made during balanced NBI (total beam power ~4.7 MW; 1 beam co-; 1 beam ctr-injection) show that the plasma is rotating in the counter direction at $\sim 2.5 \times 10^4\ m/s$ [80]. With the application of 2 MW of ICRH, the central rotation velocity increases in the direction counter to the plasma current to $\sim 5 \times 10^4\ m/s$. This is in agreement with the measurement made on JET. Another point of interest is that the rotation velocity during NBI for co- and counter-injection decreases when ICRH is turned on [80]. Similar results have been

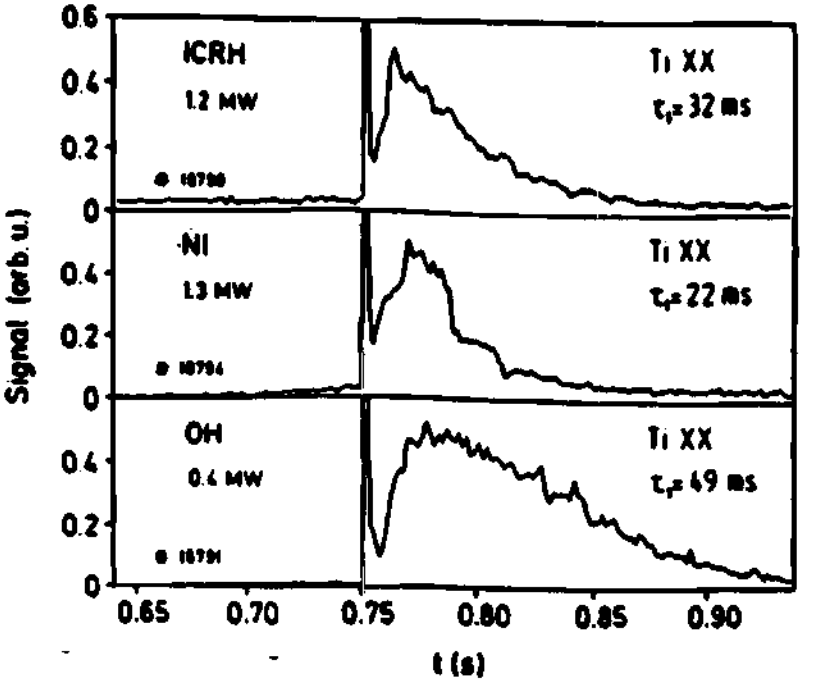

Figure 4.7: Time Dependence of the Ti XX signal after Laser Blow-off into Ohmic and Auxiliary Heated Discharges. Data from ASDEX [5].

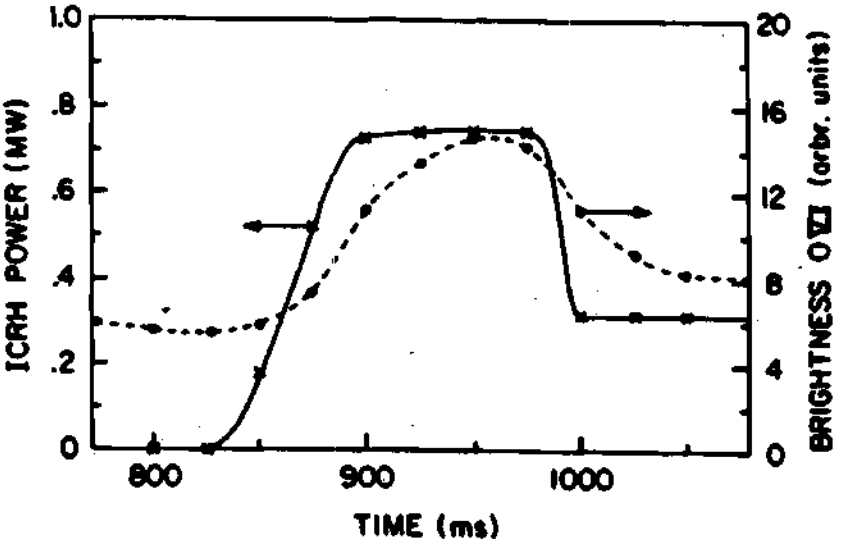

Figure 4.8: Brightness of O VI (1032 Å) emission during ICRH Shot. I_p=343 kA; $\bar{n}_e = 3.0 \times 10^{13}\ cm^{-3}$; $T_e(0) = 700\ \epsilon V$. Data from TEXTOR [6].

obtained on JET [78].

Finally, there is some evidence for resonance localization, discussed in Chapter 3, from PLT [81].

4.3 Summary and Conclusion

There is considerable evidence that cyclotron heating (ECRH and ICRH) induces significant changes in the particle source rates as well as the particle transport coefficients. These effects for ECRH and ICRH are briefly summarized below.

In most devices, ECRH leads to a decrease in the electron density. ECRH also increases the particle source rate, but the increase is apparently not serious at the present power levels. There is good evidence from TFR and TEXT [2, 3] that the impurity transport coefficients increase during ECRH. The increase in the transport coefficients sometimes (as in the iron dominated plasmas in TFR) leads to an outward flow of impurities. The changes in the impurity transport coefficients are substantial for low density discharges, while they appear to be small for high density discharges at the present ECRH power levels, which are quite small in most devices.

In plasmas heated by ICRH, the situation is more complicated. In most devices, ICRH causes a rise in the electron density and impurity concentration. In all cases, ICRH greatly enhances the particle source rate. In most devices, the rise in the electron and impurity densities has been attributed to a rise in the particle source rate. Evidence from JET [74, 75] indicates that the electron transport coefficients experience only small changes during ICRH. There is, however, evidence from JET and ASDEX [77, 5] that the impurity transport coefficients increase during ICRH. It seems likely that at least for the impurities, the increase in their concentration can be attributed to an increase in both the source rate and the transport coefficients.

In conclusion, it appears that cyclotron wave heating induces significant changes

in the particle transport coefficients as well as the particle sources. However, the mechanisms for these changes have not been clearly established. With improved diagnostics, it may be possible to identify the mechanisms causing changes in the transport coefficients. Also, development of better theoretical models which include the impurity effects should make it easier to interpret the experimental results.

CHAPTER V

TRANSPORT IN THE BANANA REGIME

In this chapter, we shall solve the drift kinetic equation derived in Section 2.2 in the banana regime for a large aspect ratio ($R/r = 1/\epsilon \gg 1$) tokamak. The solution will be obtained for a multispecies plasma in the presence of an order ϵ poloidal variation in the potential. We use an analytic procedure similar to that used by Connor [9] and Hirshman et al. [14]. We will reduce the drift kinetic equation to a set of algebraic equations for the so called "restoring coefficients" [14]. The restoring coefficients will be used in the subsequent chapters to obtain expressions for the particle transport and parallel current.

5.1 Low collisionality Ordering

The drift kinetic equation, derived in Section 2.2, forms the basis of our calculations. For a species j, the drift kinetic equation is written as

$$v_\parallel \hat{n} \cdot \nabla \bar{f}_{j1} + \mathbf{v}_{Dj} \cdot \nabla f_{j0} + \frac{e_j}{m_j} E_\parallel v_\parallel \frac{\partial f_{j0}}{\partial E} = C(\bar{f}_{j1}) \tag{5.1}$$

For the drift velocity, we use the small β result obtained in Appendix A.

$$\mathbf{v}_{Dj} = -v_\parallel \hat{n} \times \nabla \left(\frac{v_\parallel}{\Omega_j} \right)$$

Noting that ∇f_{j0} has only a radial component, we find

$$\mathbf{v}_{Dj} \cdot \nabla f_{j0} = \frac{m_j}{e_j} \frac{B_\phi}{B} \frac{v_\parallel}{r} \frac{\partial}{\partial \theta} \left(\frac{v_\parallel}{B} \right) \frac{\partial f_{j0}}{\partial r} \simeq \frac{m_j}{e_j} \frac{v_\parallel}{r} \frac{\partial}{\partial \theta} \left(\frac{v_\parallel}{B} \right) \frac{\partial f_{j0}}{\partial r}$$

where we have set $B_\phi \simeq B$ due to the fact that $B_\theta/B_\phi \ll 1$ in a small β device [8]. Hence, Eq. 5.1 can be written, after using the Maxwellian form for f_{j0}, as

$$\sigma q \frac{B_\theta}{B}\frac{1}{r}\frac{\partial \bar{f}_{j1}}{\partial \theta} + \frac{m_j}{e_j}\frac{q}{r}\frac{\partial}{\partial \theta}\left(\frac{q}{B}\right)\frac{\partial f_{j0}}{\partial r} - \frac{e_j}{T_j}(\sigma q)E_\parallel f_{j0} = C(\bar{f}_{j1})$$

where $\sigma q = v_\parallel$ with $\sigma = \pm$ and $q = |v_\parallel|$. Dropping the bar over $\bar{f}_{j1}$ and writing [9]

$$f_{j1} = -\frac{m_j}{e_j}\frac{\sigma q}{B_\theta}\frac{\partial f_{j0}}{\partial r} + g_j \tag{5.2}$$

we obtain

$$\sigma q \frac{B_\theta}{B}\frac{1}{r}\frac{\partial}{\partial \theta}\left(-\frac{m_j(\sigma q)}{e_j B_\theta}\frac{\partial f_{j0}}{\partial r}\right) + \frac{\sigma q}{r}\frac{B_\theta}{B}\frac{\partial g_j}{\partial \theta}$$
$$+\frac{m_j}{e_j}\frac{q}{r}\frac{\partial}{\partial \theta}\left(\frac{q}{B}\right)\frac{\partial f_{j0}}{\partial r} = C(f_{j1}) + \frac{e_j}{T_j}(\sigma q)E_\parallel f_{j0} \tag{5.3}$$

Using $B_\theta = B^0_\theta/(1+\epsilon\cos\theta)$ and $B_\phi = B^0_\phi/(1+\epsilon\cos\theta)$, $B_\theta/B = B^0_\theta/B^0 = \Theta$. Making use of this expression, the drift kinetic equation reduces to

$$\frac{\sigma q}{r}\Theta\frac{\partial g_j}{\partial \theta} = C(f_{j1}) + \frac{e_j}{T_j}(\sigma q)E_\parallel f_{j0} \tag{5.4}$$

We now make use of the fact that, in the banana regime, the typical time taken by a particle to complete the banana orbit ($\tau_B = 1/\omega_B$) is much less than the effective collision time for the particle to scatter out of the trapped orbit ($\tau_{eff} = 1/\nu_{eff}$), i.e.,

$$\frac{\nu_{eff}}{\omega_B} \ll 1$$

where ν_{eff} and ω_B are defined in Section 3.3.1. Expanding g_j in terms of the small parameter ν_{eff}/ω_B [9], i.e., $g_j = g^0_j + g^1_j + \cdots$ where $g^1_j/g^0_j = \mathcal{O}(\nu_{eff}/\omega_B)$, we obtain, after using our ordering assumptions for $C(f_{j1})$ and $E_\parallel$,

$$\frac{\partial g^0_j}{\partial \theta} = 0 \tag{5.5}$$

To the first order in ν_{eff}/ω_B,

$$\frac{\sigma q}{r}\Theta\frac{\partial g^1_j}{\partial \theta} = C(f_{j1}) + \frac{e_j}{T_j}(\sigma q)E_\parallel f_{j0} \tag{5.6}$$

Using the Hirshman-Sigmar collision operator, Eq. 2.63, we write

$$\frac{\sigma q\Theta}{\tau}\frac{\partial g_j^1}{\partial\theta} = \sum_k \nu_{jk}^D \frac{v_\parallel}{B}\frac{\partial}{\partial\mu}(\mu v_\parallel)\frac{\partial f_{j1}}{\partial\mu} + \sum_k \frac{2v_\parallel r_{kj}}{v_{th,j}^2}\nu_{jk}^S f_{j0} + \sum_k [\nu_{jk}^D - \nu_{jk}^S]\frac{v_\parallel u_{j1}(v)}{v^2} f_{j0} + \frac{e_j v_\parallel}{T_j} E_\parallel f_{j0}$$

Substituting for f_{j1} using Eq 5.2,

$$\frac{\sigma q\Theta}{\tau}\frac{\partial g_j^1}{\partial\theta} = \sum_k \frac{m_j}{e_j B_\theta}\frac{\partial f_{j0}}{\partial r}\nu_{jk}^D(\sigma q) + \sum_k \nu_{jk}^D \frac{\sigma q}{B}\frac{\partial}{\partial\mu}(\mu\sigma q)\frac{\partial g_j^0}{\partial\mu} + \sum_k \frac{2(\sigma q)r_{kj}}{v_{th,j}^2}\nu_{jk}^S f_{j0} + \sum_k [\nu_{jk}^D - \nu_{jk}^S]\frac{(\sigma q)u_{j1}(v)}{v^2} f_{j0} + \frac{e_j\sigma q}{T_j} E_\parallel f_{j0} \tag{5.7}$$

We now divide the velocity space into three regions: (i) the untrapped particle region, (ii) the trapped particle region, and (iii) a thin layer between regions (i) and (ii) in which the particles are marginally trapped (untrapped). Here, we will be chiefly concerned with the solution of Eq. 5.7 in the untrapped and trapped particle regions. We do not perform a detailed analysis of the boundary layer (see Appendix B for a discussion of the boundary layer). However, we use the behavior of the drift kinetic equation in the boundary layer to match the solution of Eq. 5.7 at the interface between the trapped and untrapped regions.

5.1.1 Untrapped Particle Region

For untrapped particles, we multiply Eq. 5.7 by $1/2\pi(\sigma q)$ and integrate between 0 and 2π.

$$\frac{\Theta}{\tau}\frac{1}{2\pi}\int_0^{2\pi} d\theta\frac{\partial g_j^1}{\partial\theta} = 0 = \frac{m_j}{e_j}\frac{\partial f_{j0}}{\partial r}\left(\frac{1}{2\pi}\int_0^{2\pi}\frac{\nu_j^D}{B_\theta}\,d\theta\right) + \frac{\partial}{\partial\mu}\mu\left(\frac{1}{2\pi}\int_0^{2\pi} d\theta\,\nu_j^D\frac{\sigma q}{B}\right)\frac{\partial g_j^0}{\partial\mu} + \frac{2f_{j0}}{v_{th,j}^2}\sum_k\left(\frac{1}{2\pi}\int_0^{2\pi} r_{kj}\nu_{jk}^S\,d\theta\right) + f_{j0}\left(\frac{1}{2\pi}\int_0^{2\pi}[\nu_j^D - \nu_j^S]\frac{u_{j1}(v)}{v^2}\,d\theta\right) + \frac{e_j}{T_j}E^0 f_{j0} \tag{5.8}$$

Here, $\nu_j^D = \sum_k \nu_{jk}^D$, $\nu_j^S = \sum_k \nu_{jk}^S$, and $E^0 = (1/2\pi)\int_0^{2\pi} E_\parallel\,d\theta$. We note that due to the presence of a significant poloidal variation in the potential, the collision frequencies and the velocity integrals $u_{j1}(v)$ and r_{kj} depend upon the poloidal angle.

This is due to the poloidal angle dependence of the velocity v, which is given by $v^2 = 2[E^* - e\Phi(\theta)/m]$. We can divide the untrapped particle region into (i) untrapped particles forming a part of the boundary layer (marginally untrapped particles) and (ii) well untrapped particles. In the present analysis, we will not carry out a detailed boundary layer analysis. We consider only the untrapped particles with a large kinetic energy in comparison with their potential energy. Hence, we treat the velocity to be independent of poloidal angle for these particles. It should be noted that Chang [12] also treats the kinetic energy as constant in his analysis. With this, Eq. 5.8 can be written as

$$\begin{aligned} \nu_j^D \frac{\partial}{\partial \mu} \mu \left(\frac{< v_\parallel >}{B^0} \right) \frac{\partial g_j^0}{\partial \mu} &= -\frac{m_j}{e_j B_\theta^0} \frac{\partial f_{j0}}{\partial r} \nu_j^D - \frac{2 f_{j0}}{v_{th,j}^2} \sum_k < r_{kj} > \nu_{jk}^S \\ &\quad - f_{j0} [\nu_j^D - \nu_j^S] \frac{< u_{j1}(v) >}{v^2} - \frac{e_j}{T_j} E^0 f_{j0} \end{aligned}$$

where

$$< x > = \frac{1}{2\pi} \int_0^{2\pi} hx \; d\theta \simeq \frac{1}{2\pi} \int_0^{2\pi} (1 + \epsilon \cos\theta) x \; d\theta$$

for a large aspect ratio tokamak. Integrating the above equation with respect to μ and insisting that $\partial g_j^0 / \partial \mu$ remain finite at $\mu = 0$, we obtain

$$\begin{aligned} \frac{\partial g_j^0}{\partial \mu} &= -\frac{B^0}{< v_\parallel >} \left[\frac{m_j}{e_j B_\theta^0} \frac{\partial f_{j0}}{\partial r} + \frac{m_j f_{j0}}{T_j \nu_j^D} \sum_k < r_{kj} > \nu_{jk}^S \right. \\ &\quad \left. + \left(1 - \frac{\nu_j^S}{\nu_j^D} \right) \frac{< u_{j1}(v) >}{v^2} f_{j0} + \frac{e_j}{T_j} E^0 \frac{f_{j0}}{\nu_j^D} \right] \end{aligned} \tag{5.9}$$

We note that for the passing (or untrapped) particles, the direction of the parallel velocity is the same when the particle traverses the flux surface. Hence, from Eq. 5.9,

$$\frac{\partial g_{j,+}^0}{\partial \mu} + \frac{\partial g_{j,-}^0}{\partial \mu} = 0 \tag{5.10}$$

where the subscripts + and − refer to the sign of the parallel velocity.

5.1.2 Trapped Particles

Turning our attention to trapped particles, we divide Eq. 5.7 by σq and integrate it with respect to θ between θ_1 and θ_2 (the turning points for the trapped orbit). This leads to

$$\begin{aligned}\frac{\Theta}{r}[g_j^1(\theta_2) - g_j^1(\theta_1)] &= \frac{m_j}{e_j}\frac{\partial f_{j0}}{\partial r}\left(\int_{\theta_1}^{\theta_2}\frac{\nu_j^D}{B_\theta}\,d\theta\right) + \frac{\partial}{\partial\mu}\mu\left(\int_{\theta_1}^{\theta_2} d\theta\,\nu_j^D\frac{\sigma q}{B}\right)\frac{\partial g_j^0}{\partial\mu} \\ &+ \frac{2f_{j0}}{v_{th,j}^2}\sum_k\left(\int_{\theta_1}^{\theta_2} r_{kj}\nu_{jk}^S\,d\theta\right) + f_{j0}\left(\int_{\theta_1}^{\theta_2}[\nu_j^D - \nu_j^S]\frac{u_{j1}(v)}{v^2}\,d\theta\right) \\ &+ \frac{e_j}{T_j}f_{j0}\int_{\theta_1}^{\theta_2} d\theta\,E_\parallel\end{aligned}$$

Writing the above equation for each value of σ, i.e., for $\sigma = +$ and $\sigma = -$, and subtracting the second equation from the first, we get

$$\begin{aligned}&\frac{\Theta}{r}[g_{j+}^1(\theta_2) - g_{j+}^1(\theta_1) - g_{j-}^1(\theta_2) + g_{j-}^1(\theta_1)] = \\ &\quad\frac{\partial}{\partial\mu}\mu\left(\int_{\theta_1}^{\theta_2} d\theta\,\nu_j^D\frac{q}{B}\right)\frac{\partial g_{j+}^0}{\partial\mu} + \frac{\partial}{\partial\mu}\mu\left(\int_{\theta_1}^{\theta_2} d\theta\,\nu_j^D\frac{q}{B}\right)\frac{\partial g_{j-}^0}{\partial\mu}\end{aligned} \tag{5.11}$$

where g_{j+}^0 and g_{j-}^0 are the solutions when the parallel velocity is $v_\parallel = +|v_\parallel|$ and $v_\parallel = -|v_\parallel|$ respectively. In obtaining the above equation, we have used the fact that the collision frequencies and the velocity integrals $u_{j1}(v)$ and r_{kj} do not depend on the sign of the parallel velocity.

We now note the important fact that the distribution function g_j must be continuous at the turning points of the trapped orbit, i.e.,

$$g_{j+}(\theta_2) = g_{j-}(\theta_2);\ g_{j+}(\theta_1) = g_{j-}(\theta_1)$$

Hence, $g_{j+}^0 = g_{j-}^0$ due to the fact that g_j^0 is independent of the poloidal angle (Eq. 5.5). Using this in Eq. 5.11, we get

$$\frac{\partial}{\partial\mu}\mu\left(\int_{\theta_1}^{\theta_2} d\theta\,\nu_j^D\frac{q}{B}\right)\frac{\partial g_j^0}{\partial\mu} = 0$$

or

$$\frac{\partial g_j^0}{\partial\mu} = \frac{K}{\mu\left(\int_{\theta_1}^{\theta_2} d\theta\,\nu_j^D\frac{q}{B}\right)} \tag{5.12}$$

where K is a constant to be determined by the boundary condition for the trapped region.

Boundary Condition for the Trapped Region

We determine the constant K by examining the behavior of the solution to the drift kinetic equation in the boundary layer [33,82]. In the boundary layer, the low collisionality expansion is invalid (see Appendix B). Hence, we consider the unexpanded version of the drift kinetic equation (Eq. 5.4) in the boundary layer. Dividing Eq 5.4 by σq, and integrating this equation across the boundary layer centered around μ_0 with thickness $\Delta\mu$, we have

$$\begin{aligned}
\frac{\Theta}{\tau}\int_{UT}^{T} d\mu \int_{\theta_1}^{\theta_2} d\theta \frac{\partial g_j}{\partial \theta} \;=\; & \frac{m_j}{e_j}\frac{\partial f_{j0}}{\partial \tau}\int_{UT}^{T} d\mu \left(\int_{\theta_1}^{\theta_2} \frac{\nu_j^D}{B_\theta}\, d\theta\right) \\
& + \int_{UT}^{T} d\mu \int_{\theta_1}^{\theta_2} d\theta \frac{\partial}{\partial \mu}\mu\left(\nu_j^D \frac{\sigma q}{B}\right)\frac{\partial g_j}{\partial \mu} \\
& + \frac{2 f_{j0}}{v_{th,j}^2}\int_{UT}^{T} d\mu \sum_k \left(\int_{\theta_1}^{\theta_2} r_{kj}\nu_{jk}^S\, d\theta\right) \\
& + f_{j0}\int_{UT}^{T} d\mu \left(\int_{\theta_1}^{\theta_2} [\nu_j^D - \nu_j^S]\frac{u_{j1}(v)}{v^2}\, d\theta\right) \\
& + \frac{e_j}{T_j} f_{j0}\int_{UT}^{T} d\mu \int_{\theta_1}^{\theta_2} d\theta\; E_\parallel
\end{aligned}$$

where θ_1 and θ_2 are defined in Fig. 5.1. The integration limits UT and T refer to the untrapped and trapped regions respectively. Writing the above equation for $\sigma = +$ and $\sigma = -$ separately, and subtracting the second equation (for $\sigma = -$) from the first, we obtain

$$\begin{aligned}
& \frac{\Theta}{\tau}\int_{UT}^{T}[g_{j+}(\theta_2) - g_{j+}(\theta_1) - g_{j-}(\theta_2) + g_{j-}(\theta_1)] = \\
& \quad \int_{UT}^{T} d\mu \int_{\theta_1}^{\theta_2} d\theta \frac{\partial}{\partial \mu}\mu\left(\nu_j^D \frac{q}{B}\right)\frac{\partial g_{j+}}{\partial \mu} + \int_{UT}^{T}\int_{\theta_1}^{\theta_2} \frac{\partial}{\partial \mu}\mu\left(\nu_j^D \frac{q}{B}\right)\frac{\partial g_{j-}^0}{\partial \mu}
\end{aligned} \tag{5.13}$$

where the subscripts $+$ and $-$ refer to the sign of the parallel velocity. Again, we have used the fact that the collision frequencies and the velocity integrals $u_{j1}(v)$ and r_{kj} do

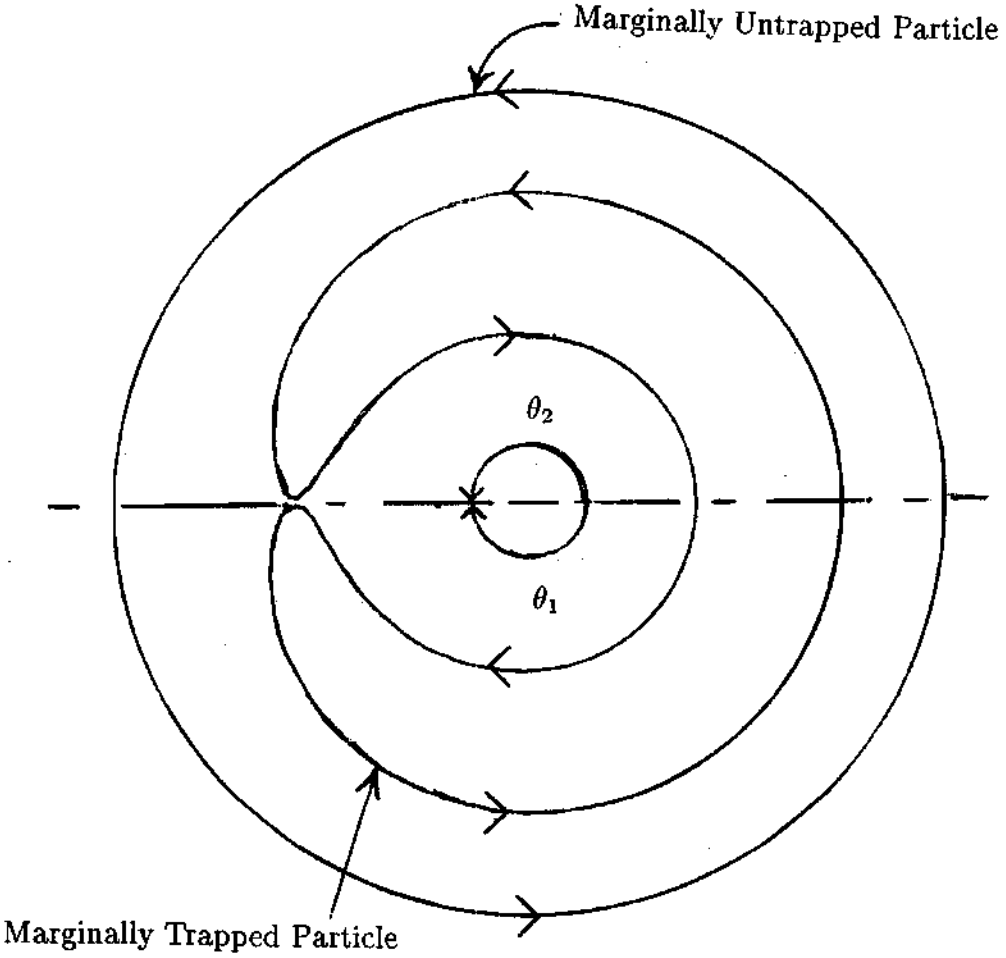

Figure 5.1: Marginally Trapped - Untrapped Orbits

not depend on the sign of the parallel velocity. For marginally untrapped particles,

$$g_{j+}(\theta_2) = g_{j+}(\theta_1); \quad g_{j-}(\theta_2) = g_{j-}(\theta_1)$$

For marginally trapped particles, continuity at the turning points implies,

$$g_{j+}(\theta_2) = g_{j-}(\theta_2); \quad g_{j+}(\theta_1) = g_{j-}(\theta_1)$$

Hence, the left hand side of Eq. 5.13 = 0 for all particles. This gives us

$$\mu_0 \int_{\theta_1}^{\theta_2} d\theta \left(\frac{q\nu_j^D}{B}\right)\left[\left(\frac{\partial g_{j+}}{\partial \mu}\right)_T - \left(\frac{\partial g_{j+}}{\partial \mu}\right)_{UT} + \left(\frac{\partial g_{j-}}{\partial \mu}\right)_T - \left(\frac{\partial g_{j-}}{\partial \mu}\right)_{UT}\right] = 0$$

Outside the boundary layer, using the expansion $g_j = g_j^0 + g_j^1 + \cdots$ and retaining only the lowest order terms, we have, for the untrapped region,

$$\left(\frac{\partial g_{j+}}{\partial \mu}\right)_{UT} + \left(\frac{\partial g_{j-}}{\partial \mu}\right)_{UT} = \left(\frac{\partial g_{j+}^0}{\partial \mu}\right)_{UT} - \left(\frac{\partial g_{j-}^0}{\partial \mu}\right)_{UT} = 0$$

Here, we have used Eq. 5.10 in the untrapped region. Expanding g_j in the trapped particle region, and noting that $g_{j+}^0(\theta_2) = g_{j-}^0(\theta_2) = g_j^0(\theta_2)$ and g_j^0 is independent of θ, we have

$$\mu_0 \left[\int_{\theta_1}^{\theta_2} d\theta \left(\frac{q\nu_j^D}{B}\right)\right] \frac{\partial g_j^0}{\partial \mu} = 0$$

or

$$\frac{\partial g_j^0}{\partial \mu} = 0$$

Hence, the constant $K = 0$, and we have

$$\frac{\partial g_j^0}{\partial \mu} = \begin{cases} -\frac{B^0}{<v_\parallel>}\left[\frac{m_j}{e_j B_\theta^0}\frac{\partial f_{j0}}{\partial r} + \frac{m_j f_{j0}}{T_j \nu_j^D}\sum_k < r_{kj} > \nu_{jk}^S \right. \\ \left. + \left(1 - \frac{\nu_j^S}{\nu_j^D}\right)\frac{<u_{j1}(v)>}{v^2} f_{j0} + \frac{e_j}{T_j} E^0 \frac{f_{j0}}{\nu_j^D}\right] & \text{for passing particles} \\ 0 & \text{for trapped particles} \end{cases} \tag{5.14}$$

5.2 Solution of Drift Kinetic Equation

Using Eq 5.1, we get

$$\frac{\partial f_{j1}}{\partial \mu} = -\frac{m_j}{e_j B_\theta}\frac{\partial f_{j0}}{\partial r}\frac{\partial v_\parallel}{\partial \mu} + \frac{\partial g_j}{\partial \mu}$$

Using $v_\parallel = \pm\sqrt{2}(E - \mu B - e\Phi)^{1/2}$ to obtain the derivative of $v_\parallel$, and retaining only the zeroth order term g_j^0, we get, after using Eq. 5.14

$$\begin{aligned}\frac{\partial f_{j1}}{\partial \mu} &= \frac{m_j}{e_j}\frac{B}{B_\theta}\frac{1}{v_\parallel}\frac{\partial f_{j0}}{\partial r} - \frac{B^0}{< v_\parallel >}\left[\frac{m_j}{e_j B_\theta^0}\frac{\partial f_{j0}}{\partial r} + \frac{m_j f_{j0}}{T_j \nu_j^D}\sum_k < r_{kj} > \nu_{jk}^S \right. \\ &\left. + \left(1 - \frac{\nu_j^S}{\nu_j^D}\right)\frac{< u_{j1}(v) >}{v^2} f_{j0} + \frac{e_j}{T_j}E^0\frac{f_{j0}}{\nu_j^D}\right] \\ &= \frac{m_j}{e_j}\left(\frac{B^0}{B_\theta^0}\right)\frac{\partial f_{j0}}{\partial r}\left[\frac{1}{v_\parallel} - \frac{1}{< v_\parallel >}\right] - \frac{\beta_1}{< v_\parallel >} \qquad (5.15)\end{aligned}$$

where

$$\beta_1 = B^0\left[\frac{m_j f_{j0}}{T_j \nu_j^D}\sum_k < r_{kj} > \nu_{jk}^S + \left(1 - \frac{\nu_j^S}{\nu_j^D}\right)\frac{< u_{j1}(v) >}{v^2} f_{j0} + \frac{e_j}{T_j}E^0\frac{f_{j0}}{\nu_j^D}\right]$$

5.2.1 Calculation of $< u_{j1}(v) >$ and r_{kj}

Calculation of $< u_{j1}(v) >$

Using the definition of $u_{j1}(v)$ from Eq. 2.69, we obtain, after integrating by parts in μ,

$$f_{j0}u_{j1}(v) = -\sum_\sigma \frac{3B}{4w} v\sigma \int d\mu\, \mu \frac{\partial f_{j1}}{\partial \mu}$$

where we have required that f_{j1} remain finite at $\mu = 0$ and $f_{j1} \to 0$ faster than $\mu \to \infty$. Using the expression for $\partial f_{j1}/\partial\mu$ derived in the previous section, we get

$$f_{j0}u_{j1}(v) = -\sum_\sigma \frac{3B}{4w} v\sigma \int d\mu\mu \left[\frac{m_j}{e_j}\left(\frac{B^0}{B_\theta^0}\right)\frac{\partial f_{j0}}{\partial r}\left[\frac{1}{v_\parallel} - \frac{1}{< v_\parallel >}\right] - \frac{\beta_1}{< v_\parallel >}\right]$$

Adding and subtracting $\beta_1/v_\parallel$ from the integrand, and defining $\beta = \beta_1 + \frac{m_j}{e_j}(\frac{B^0}{B_\theta^0})\frac{\partial f_{j0}}{\partial r}$, the above equation can be written as

$$f_{j0}u_{j1}(v) = -\sum_\sigma \frac{3B}{4w} v\sigma\beta \int d\mu\mu \left[\frac{1}{v_\parallel} - \frac{1}{< v_\parallel >}\right] + \sum_\sigma \frac{3B}{4w} v\sigma\beta_1 \int d\mu\mu \frac{1}{v_\parallel}$$

We note that β is not a function of μ. Multiplying the above equation by $v_{th,j}^2/v^2 = 1/x_j^2$ and flux surface averaging, we obtain

$$\frac{f_{j0} < u_{j1}(v) >}{x_j^2} = -\left\langle \sum_\sigma \frac{3B}{4w}\sigma\beta\frac{v_{th,j}^2}{v}\int d\mu\mu\left[\frac{1}{v_\parallel} - \frac{1}{< v_\parallel >}\right]\right\rangle$$

$$+\left\langle \sum_\sigma \frac{3B}{4w}\sigma\beta_1 \frac{v_{th,j}^2}{v}\int d\mu\mu\frac{1}{v_\parallel}\right\rangle$$
$$= I + II \tag{5.16}$$

The second term in the above equation can be integrated easily to obtain, after neglecting the dependence of the velocity v on θ (see Section 5.1.1),

$$II = \frac{2f_{j0}}{\nu_j^D}\sum_k < r_{kj} > \nu_{jk}^S + \left(1-\frac{\nu_j^S}{\nu_j^D}\right)\frac{< u_{j1}(v) >}{x_j^2} f_{j0} + \frac{2e_j}{m_j}E^0\frac{f_{j0}}{\nu_j^D}$$

Noting that β is independent of the poloidal angle, we can write the first term in Eq. 5.16 as

$$I = -\left\langle \sum_\sigma \frac{3B}{4w}\sigma\frac{v_{th,j}^2}{v}\int d\mu\mu\left[\frac{1}{v_\parallel}-\frac{1}{< v_\parallel >}\right]\right\rangle\beta$$
$$= -f_{t\Phi}\beta\left(\frac{v_{th,j}^2}{B^0}\right) \tag{5.17}$$

Evaluation of the coefficient $f_{t\Phi}$ depends upon a knowledge of the trapped-untrapped particle distribution. In the standard neoclassical theory, i.e., when $\bar{\Phi}(\theta) \simeq 0$, the trapped-untrapped boundary is independent of the particle energy, and for a large aspect ratio tokamak, $f_{t\Phi} = f_t \simeq 1.46\sqrt{\epsilon}$ [37,8,9,14,32]. In the presence of a poloidal potential variation of the order ϵ, as discussed in Section 3.2, particle trapping is a function of the particle energy. Hence, the coefficient $f_{t\Phi}$ is a function of the particle energy. We will evaluate the factor $f_{t\Phi}$ in the presence of poloidal potential variations for a large aspect ratio tokamak in Section 5.3. Using Eq. 5.17, Eq. 5.16 can be written as

$$\frac{< u_{j1}(v) >}{x_j^2}\left[\frac{\nu_j^S(1-f_{t\Phi})+\nu_j^D f_{t\Phi}}{\nu_j^D}\right] = -f_{t\Phi}\frac{m_j}{e_j B_\theta^0}\frac{v_{th,j}^2}{f_{j0}}\frac{\partial f_{j0}}{\partial r}$$
$$+2(1-f_{t\Phi})\left[\frac{e_j E^0}{m_j\nu_j^D}+\sum_k\frac{\nu_{jk}^S < r_{kj} >}{\nu_j^D}\right]$$

Using a notation similar to that used by Hirshman et al. [14], we write $1-f_{t\Phi} = f_{c\Phi}$ and $\nu_j^S f_{c\Phi} + \nu_j^D f_{t\Phi} = \nu_{j\Phi}$. Here, the subscript Φ denotes the presence of significant

poloidal electric fields. With this, the above equation can be written as

$$\frac{< u_{j1}(v) >}{x_j^2} = -f_{t\Phi}\frac{m_j}{e_j B_\theta^0} v_{th,j}^2 \frac{\partial \ln f_{j0}}{\partial r}\frac{\nu_j^D}{\nu_{j\Phi}} + 2(1-f_{t\Phi})\left[\frac{e_j E^0}{m_j \nu_{j\Phi}} + \sum_k \frac{\nu_{jk}^S < r_{kj} >}{\nu_{j\Phi}}\right] \quad (5.18)$$

This equation differs from a similar expression for $< u_{j1}(v) >$ derived by Hirshman et al. [14, Eq. 14] in that the quantities $f_{t\Phi}$, $f_{c\Phi}$ and $\nu_{j\Phi}$, which contain the effect of the poloidal electric field, are now energy dependent. In the absence of a significant poloidal electric field, the above expression reduces to Eq. 14 in Ref. [14].

Calculation of Restoring Coefficients

The momentum restoring coefficient is defined as [Eq. 2.70]

$$r_{kj} = \frac{\int m_k \nu_{kj}^S v_\parallel f_{k1} d^3v}{m_j n_j \{\nu_{jk}^S\}}$$

Calculation of r_{kj} is similar to the calculation of $u_{j1}(v)$. Transforming the velocity variables to w, μ, and integrating by parts with respect to μ, we obtain

$$r_{kj} = C \int dw d\mu \nu_{kj}^S \mu \frac{\partial f_{k1}}{\partial \mu} \quad (5.19)$$

where

$$C = -\frac{2\pi B}{n_j \{\nu_{jk}^S\}}\frac{m_k}{m_j}\sum_\sigma \sigma$$

In deriving Eq. 5.19, we have used the same boundary conditions used for deriving $u_{j1}(v)$. Using the expression 2.42 for f_{k0}, and noting that $v^2/2 = E - e < \Phi > /T - e\bar{\Phi}(\theta)/T$,

$$\frac{\partial f_{k0}}{\partial r} = f_{k0}\left[\frac{n_{k0}'}{n_{k0}} + \frac{e_k < \Phi >'}{T_k}\right] - f_{k0}\frac{T_k'}{T_k}\left[\frac{3}{2} - \frac{m_k E^*}{T_k}\right] \quad (5.20)$$

where the prime denotes derivative with respect to r. Using the same notation as Hirshman et. al. [14], we define the "driving forces" as

$$A_{1k} = \frac{n_{k0}'}{n_{k0}} - \frac{3}{2}\frac{T_k'}{T_k}; \quad A_{2k} = \frac{T_k'}{T_k}; \quad A_3 = E^0 \quad (5.21)$$

Using these definitions and Eq. 5.15 for $\partial f_{k1}/\partial\mu$, and making use of the result 5.18, we can write $< r_{kj} >$ as (see Appendix B for details)

$$
\begin{aligned}
< r_{kj} > \;=\; & -\frac{1}{\{\nu^S_{kj}\}}\left(\frac{T_k}{e_k B^0_\theta}\right)\left[\{\nu^S_{kj}\}\left(A_{1k}+\frac{e_k\Phi'}{T_k}\right)+\left\{\nu^S_{kj}\left(\frac{m_k E^*}{T_k}\right)\right\}A_{2k}\right] \\
& +\frac{1}{\{\nu^S_{kj}\}}\left(\frac{T_k}{e_k B^0_\theta}\right)\left[\left\{\frac{\nu^S_{kj}\nu^S_k}{\nu_{k\Phi}}f_{c\Phi}\right\}\left(A_{1k}+\frac{e_k\Phi'}{T_k}\right)\right. \\
& \left.+\left\{\frac{\nu^S_{kj}\nu^S_k}{\nu_{k\Phi}}\left(\frac{m_k E^*}{T_k}\right)f_{c\Phi}\right\}A_{2k}\right] \\
& +\frac{e_k}{m_k}A_3\frac{1}{\{\nu^S_{kj}\}}\left\{\frac{\nu^S_{kj}}{\nu_{k\Phi}}f_{c\Phi}\right\}+\sum_l\frac{1}{\{\nu^S_{kj}\}}\left\{\frac{\nu^S_{kj}\nu^S_{kl}}{\nu_{k\Phi}}f_{c\Phi}\right\}< r_{lk} > \qquad (5.22)
\end{aligned}
$$

In the above expression, the effect of the poloidal electric field is contained in $f_{c\Phi}$ $(= 1 - f_{t\Phi})$, $\nu_{k\Phi}$, and $E^*(= v^2/2 + e\Phi(\theta)/m)$. The most significant effect is contained in the neoclassical factor $f_{t\Phi}$ $(= 1 - f_{c\Phi})$. As we shall see in the next section, the factor $f_{t\Phi}$ contains the effect of modification of the boundary between the trapped and untrapped regions in the velocity space due to the poloidal electric field. When $\tilde{\Phi}(\theta) \simeq 0$, the above expression reduces to Eq. (26) in Ref. [14]. Noting that $\nu_{k\Phi} = f_{c\Phi}\nu^S_k + f_{t\Phi}\nu^D_k$,

$$\frac{f_{c\Phi}\nu^S_k}{\nu_{k\Phi}} = 1 - \frac{f_{t\Phi}\nu^D_k}{\nu_{k\Phi}}$$

Using this result and summing the Eq. 5.22 over j [9], we obtain, after changing the dummy index l to j, the following useful expression

$$
\begin{aligned}
\sum_j\{\nu^S_{kj}\}[< r_{kj} > - < r_{jk} >] \;=\; & \frac{e_k E^0}{m_k}-\frac{T_k}{e_k B^0_\theta}\left[\left\{\frac{\nu^S_k\nu^D_k}{\nu_{k\Phi}}f_{t\Phi}\right\}\left(A_{1k}+\frac{e_k\Phi'}{T_k}\right)\right. \\
& \left.+\left\{\frac{\nu^S_k\nu^D_k}{\nu_{k\Phi}}\left(\frac{m_k E^*}{T_k}\right)f_{t\Phi}\right\}A_{2k}\right]-\frac{e_k}{m_k}A_3\left\{\frac{\nu^D_k}{\nu_{k\Phi}}f_{t\Phi}\right\} \\
& -\sum_j\left\{\frac{\nu^S_{kj}\nu^D_k}{\nu_{k\Phi}}f_{t\Phi}\right\}< r_{jk} > \qquad (5.23)
\end{aligned}
$$

We will find this equation helpful in determining the particle fluxes.

5.3 Calculation of $f_{t\Phi}$

The factor $f_{t\Phi}$ defined by Eq. 5.17 plays an important role in the neoclassical theory. The factor $f_{t\Phi}$ is closely related to the fraction of trapped particles. In the absence of poloidal potential variation, the factor has been computed for a large aspect ratio tokamak by Rosenbluth et al. [37] and more recently by Balescu [32]. The value of $f_{t\Phi}$ in the absence of a poloidal electric field is approximately $1.46\sqrt{\epsilon}$ [37, 32]. In the presence of poloidal asymmetries in the potential, the trapped particle distribution changes and, as discussed in Section 3.2, the boundary between the trapped-untrapped regions is a function of the particle energy. We will calculate the value of $f_{t\Phi}$ for the case of a large aspect ratio tokamak using a method employed by Chang [12]. From Eq. 5.17,

$$f_{t\Phi} = \left\langle \sum_\sigma \frac{3B}{4w} \sigma \frac{v_{th,j}^2}{v} \int d\mu\mu \left[\frac{1}{v_\parallel} - \frac{1}{< v_\parallel >} \right] \right\rangle \left(\frac{B^0}{v_{th,j}^2} \right)$$

Defining $\xi = |v_\parallel|/v$ and $\lambda' = \mu B/w$, we obtain,

$$\begin{aligned} f_{t\Phi} &= \sum_\sigma \left(\frac{3}{8}\right) \sigma^2 \left\langle \int d\lambda' \lambda' \left[\frac{1}{\xi} - \frac{1}{< \xi >} \right] \right\rangle \\ &= \sum_\sigma \left(\frac{3}{8}\right) \sigma^2 \left\langle \int_T \frac{d\lambda' \lambda'}{\xi} \right\rangle + \sum_\sigma \left(\frac{3}{8}\right) \sigma^2 \left\langle \int_{UT} d\lambda' \lambda' \left[\frac{1}{\xi} - \frac{1}{< \xi >} \right] \right\rangle \end{aligned}$$

where the first integral is over the trapped particle region and the second integral is over the untrapped particle region. Here, due to the large aspect ratio assumption, we have used $B \simeq B^0$. We now observe that due to the large aspect ratio assumption, and due to our neglect of the boundary layer,

$$\frac{1}{\xi} - \frac{1}{< \xi >} \sim \mathcal{O}(\epsilon)$$

Furthermore, referring to Figs. 3.5 and 3.6, $\lambda'_{max} \simeq 1 - \epsilon$ over most of the velocity space. Hence the second integral makes a contribution of the order $(1-\epsilon)^2 \mathcal{O}(\epsilon) \sim \mathcal{O}(\epsilon)$. Hence, to the lowest order in ϵ, we write

$$f_{t\Phi} = \sum_\sigma \left(\frac{3}{8}\right) \sigma^2 \left\langle \int_{\lambda'_{min}}^{\lambda'_{max}} \frac{d\lambda' \lambda'}{\xi} \right\rangle + \mathcal{O}(\epsilon)$$

Expressing λ' in terms of ξ, we obtain

$$f_{tr} = \sum_{\sigma} \left(\frac{3}{8}\right) \sigma^2 \left\langle -2 \int_T (1-\xi^2) d\xi \right\rangle$$

We now examine the integration limits.

When $e_j\Phi_{in} < e_j\Phi_{out}$:

For B-trapping, using Eq. 3.33, we obtain,

$$\lambda'_{min} = (1-\epsilon)\left[1 + \frac{\epsilon|Z_j|X_0T}{m_j w}(1+\cos\theta)\right] \leq \lambda' \leq (1+\epsilon) = \lambda_{max}$$

or, in terms of the variable ξ,

$$\xi_{crit} = \sqrt{\epsilon}(1+\cos\theta)^{1/2}\left[1 - \frac{|Z_j|X_0T}{m_j w}\right]^{1/2} \geq \xi \geq 0 \qquad (5.24)$$

For E-trapping, using Eq. 3.35,

$$\lambda'_{min} = (1+\epsilon)\left[1 - \frac{\epsilon|Z_j|X_0T}{m_j w}(1-\cos\theta)\right] \leq \lambda' \leq (1+\epsilon) = \lambda_{max}$$

or

$$\xi_{crit} = \sqrt{\epsilon}(1-\cos\theta)^{1/2}\left[\frac{|Z_j|X_0T}{m_j w} - 1\right]^{1/2} \geq \xi \geq 0 \qquad (5.25)$$

When $e_j\Phi_{in} > e_j\Phi_{out}$:

In this case, we have only B-trapping. From Eq. 3.37, we get

$$\lambda'_{min} = (1-\epsilon)\left[1 - \frac{\epsilon|Z_j|X_0T}{m_j w}(1+\cos\theta)\right] \leq \lambda' \leq (1+\epsilon) = \lambda_{max}$$

or

$$\xi_{crit} = \sqrt{\epsilon}(1+\cos\theta)^{1/2}\left[1 + \frac{|Z_j|X_0T}{m_j w}\right]^{1/2} \geq \xi \geq 0 \qquad (5.26)$$

From Eqs. 5.25 and 5.26, we can determine the lower limit on $x_j^2 = m_j w/T$ by setting $\xi_{crit} = 1$. This gives,

For $e_j\Phi_{in} < e_j\Phi_{out}$,

$$x_j^2 \geq \frac{\epsilon(1-\cos\theta)|Z_j|X_0}{1+\epsilon(1-\cos\theta)} = x_{j,crit}^2 \tag{5.27}$$

For $e_j\Phi_{in} > e_j\Phi_{out}$,

$$x_j^2 \geq \frac{\epsilon(1+\cos\theta)|Z_j|X_0}{1-\epsilon(1+\cos\theta)} = x_{j,crit}^2 \tag{5.28}$$

Using Eqs. 5.24, 5.25, and 5.26, we obtain

$$f_{t\Phi} = \sum_\sigma \left(\frac{3}{4}\right)\sigma^2 \left\langle \int_0^{\xi_{crit}} (1-\xi^2)d\xi \right\rangle = \frac{3}{2}\left\langle \xi_{crit} - \frac{\xi_{crit}^3}{3} \right\rangle$$

Using Eqs. 5.27 and 5.28, the maximum value of $f_{t\Phi}$ is found to be 1. Hence, $f_{t\Phi} \leq 1$. For $x_j > x_{j,crit}$, we can simplify the above equation by retaining only the first term. In this case,

$$f_{t\Phi} \simeq \frac{3}{2} < \xi_{crit} > + \mathcal{O}(\epsilon^{3/2})$$

Here, we have used $\sum_\sigma \sigma^2 = 2$. In the present work, the factor $f_{t\Phi}$ appears in the velocity integrals of the type {} (Eq. 2.71). As will be shown in the next chapter (see Section 6.3), the contribution to the integral from the low velocity region is negligible for a large aspect ratio tokamak. Hence, the above expression for $f_{t\Phi}$ is adequate for our purposes. Using the results 5.24, 5.25, and 5.26, we have for $e_j\Phi_{in} < e_j\Phi_{out}$,

$$\begin{aligned} f_{t\Phi} &\simeq \frac{3}{2}\sqrt{\epsilon}\left\langle (1-\cos\theta)^{1/2} \right\rangle \left| 1 - \frac{|Z_j|X_0T}{m_j w} \right|^{1/2} \\ &= f_t \left| 1 - \frac{|Z_j|X_0T}{m_j w} \right|^{1/2} \end{aligned} \tag{5.29}$$

Similarly, for $e_j\Phi_{in} > e_j\Phi_{out}$,

$$\begin{aligned} f_{t\Phi} &\simeq \frac{3}{2}\sqrt{\epsilon}\left\langle (1+\cos\theta)^{1/2} \right\rangle \left| 1 + \frac{|Z_j|X_0T}{m_j w} \right|^{1/2} \\ &= f_t \left| 1 + \frac{|Z_j|X_0T}{m_j w} \right|^{1/2} \end{aligned} \tag{5.30}$$

Here, we have used the fact that $< (1-\cos\theta)^{1/2} > = < (1+\cos\theta)^{1/2} >$. In either case, we note that $f_{t\Phi} > \sqrt{\epsilon}$. This justifies our neglect of the the untrapped particle

contribution, which is of the order ϵ. We observe that when $\tilde{\Phi}(\theta) \simeq 0$, i.e. $X_0 \simeq 0$, we have $f_{t\Phi} = f_t = 3/2 < (1 \pm \cos\theta)^{1/2} > \sqrt{\epsilon} = 1.35\sqrt{\epsilon}$. This value is somewhat smaller than the value $(1.46\sqrt{\epsilon})$ quoted before. The main effect of the poloidal electric field is contained in the term $|1 \pm |Z_j|X_0 T/m_j w|^{1/2}$, and hence, for the present work, the above expressions for $f_{t\Phi}$ are adequate.

CHAPTER VI

PARTICLE TRANSPORT

In the previous chapter, we derived a linear system of equations for the momentum restoring coefficients r_{jk}. In this chapter, we will derive expressions for the particle fluxes in terms of the restoring coefficients for a large aspect ratio tokamak. The results of calculations for a three species plasma (electron, ion, and an impurity species) will be presented at the end of the chapter.

6.1 Expression for Particle Flux

The radial particle flux is defined as

$$\Gamma_j = \left\langle \int d^3v \; f_j v_{dr,j} \right\rangle \tag{6.1}$$

where $v_{dr,j}$ is the radial component of the drift for the species j. Using the definition of the flux surface average and the radial component of the drift velocity (see Appendix A), we can write

$$\Gamma_j = \frac{1}{2\pi} \int_0^{2\pi} h d\theta \int \sum_\sigma \frac{2\pi B dw d\mu}{|v_\parallel|} \frac{m_j}{e_j} \frac{v_\parallel}{r} \frac{\partial}{\partial \theta} \left(\frac{v_\parallel}{B} \right) f_j$$

where we have expressed the velocity integral in terms of the variables w and μ. Integrating by parts in θ and using the drift kinetic equation (Eq. 5.1) to express $\partial f_j / \partial \theta$ in terms of the collision term and the parallel electric field, we obtain

$$\Gamma_{j\Phi} = -\left\langle \sum_k \frac{R_{jk}}{e_j B_\theta} \right\rangle - \frac{n_{j0} E^0}{B_\theta^0} \tag{6.2}$$

where

$$R_{jk} = \int d^3v\ m_j v_\parallel C(f_{j1}, f_{k1})$$

Here, we have used the large aspect ratio assumption in flux surface averaging over the second integral. Using momentum conservation and quasineutrality in Eq. 6.2, we find that the particle fluxes are ambipolar, i.e.

$$\sum_j e_j \Gamma_{j\Phi} = 0 \tag{6.3}$$

Making use of the Hirshman-Sigmar collision operator (Eq. 2.63),

$$\begin{aligned} R_{jk} &= \int d^3v\ m_j v_\parallel \left[\nu_{jk}^D \mathcal{L} f_{j1} + \frac{2 v_\parallel \tau_{kj}}{v_{th,j}^2} \nu_{jk}^S f_{j0} \right. \\ &\left. + [\nu_{jk}^D - \nu_{jk}^S] \frac{v_\parallel u_{j1}(v)}{v^2} f_{j0} \right] \end{aligned}$$

Using the definitions of $\tau_{kj}, u_{j1}(v)$, and changing the integration variables to w and μ, the integrations can be carried out to yield

$$R_{jk} = -m_k n_k \{\nu_{kj}^S\} \tau_{jk} + m_j n_j \{\nu_{jk}^S\} \tau_{kj}$$

Using the momentum conservation relation, $m_j n_j \{\nu_{jk}^S\} = m_k n_k \{\nu_{kj}^S\}$, we get

$$R_{jk} = -m_j n_j \{\nu_{jk}^S\} [\tau_{jk} - \tau_{kj}] \tag{6.4}$$

Hence,

$$\Gamma_{j\Phi} = \left\langle \sum_k \frac{m_j n_j \{\nu_{jk}^S\} [\tau_{jk} - \tau_{kj}]}{e_j B_\theta} \right\rangle - \frac{n_{j0} E^0}{B_\theta^0}$$

Again, using the large aspect ratio approximation, and retaining only the lowest order terms in ϵ, the first term can be simplified to yield

$$\Gamma_{j\Phi} = \sum_k \frac{m_j n_{j0} \{\nu_{jk}^S\}}{e_j B_\theta^0} [< \tau_{jk} > - < \tau_{kj} >] - \frac{n_{j0} E^0}{B_\theta^0} \tag{6.5}$$

Interchanging j and k in Eq. 5.23, and using the resulting expression for the restoring coefficients in the above equation, we obtain

$$\begin{aligned} \Gamma_{j\Phi} &= -\frac{m_j n_{j0} T_j}{e_j^2 B_\theta^{02}} \left[\left(A_{1j} + \frac{e_j \Phi'}{T_j} \right) \left\{ f_{t\Phi} \frac{\nu_j^S \nu_j^D}{\nu_{j\Phi}} \right\} + A_{2j} \left\{ f_{t\Phi} \frac{\nu_j^D \nu_j^S}{\nu_{j\Phi}} \left(\frac{m_j E^*}{T_j} \right) \right\} \right] \\ &- \frac{m_j n_{j0}}{e_j B_\theta^0} \sum_k \left\{ \frac{f_{t\Phi} \nu_j^D \nu_{jk}^S}{\nu_{j\Phi}} \right\} < \tau_{kj} > - \frac{n_{j0} A_3}{B_\theta^0} \left\{ \frac{f_{t\Phi} \nu_j^D}{\nu_{j\Phi}} \right\} \end{aligned} \tag{6.6}$$

where the restoring coefficients are given by Eq. 5.22. We note here that the procedure used for obtaining the above expression for the particle flux in the presence of a poloidal electric field is similar to that used by Connor [9] and Hirshman et al. [14]. The above expression for the particle flux differs from the corresponding expression [Eq. (30a)] in Ref. [14] in that $f_{t\Phi}$ is energy dependent and $E^* = v^2/2 + e\Phi(\theta)/m$. When $\tilde{\Phi}(\theta) = 0$, the above expression reduces to Eq. (30a) in Ref. [14].

6.2 Calculation of Transport Coefficients

Equation 6.6 reveals that the particle fluxes depend upon the known "driving forces" A_{1j}, A_{2j}, A_3, the radial electric field Φ', and the momentum restoring coefficients $< r_{kj} >$. We shall shortly show that the radial electric field does not contribute to the particle fluxes. Hence, our task is to solve for the restoring coefficients in terms of the driving forces A_{1j}, A_{2j} and A_3. The restoring coefficients are given by (Eq. 5.22)

$$\begin{aligned} < r_{kj} > \; = \; & -\frac{1}{\{\nu_{kj}^S\}}\left(\frac{T_k}{e_k B_\theta^0}\right)\left[\{\nu_{kj}^S\}\left(A_{1k} + \frac{e_k\Phi'}{T_k}\right) + \left\{\nu_{kj}^S\left(\frac{m_k E^*}{T_k}\right)\right\} A_{2k}\right] \\ & + \frac{1}{\{\nu_{kj}^S\}}\left(\frac{T_k}{e_k B_\theta^0}\right)\left[\left\{\frac{\nu_{kj}^S \nu_k^S}{\nu_{k\Phi}} f_{c\Phi}\right\}\left(A_{1k} + \frac{e_k\Phi'}{T_k}\right) + \left\{\frac{\nu_{kj}^S \nu_k^S}{\nu_{k\Phi}}\left(\frac{m_k E^*}{T_k}\right) f_{c\Phi}\right\} A_{2k}\right] \\ & + \frac{e_k}{m_k} A_3 \frac{1}{\{\nu_{kj}^S\}}\left\{\frac{\nu_{kj}^S}{\nu_{k\Phi}} f_{c\Phi}\right\} + \sum_l \frac{1}{\{\nu_{kj}^S\}}\left\{\frac{\nu_{kj}^S \nu_{kl}^S}{\nu_{k\Phi}} f_{c\Phi}\right\} < r_{lk} > \end{aligned} \tag{6.7}$$

Eqs. 6.7 constitute a linear system of equations for the restoring coefficients with A_{1k}, A_{2k}, A_3, and Φ' as the driving terms. Hence, we can determine the restoring coefficients by considering the driving terms individually [14].

6.2.1 Response to the Radial Electric Field

Setting $A_{1k} = A_{2k} = A_3 = 0$ in Eq. 6.7, we obtain

$$< r_{kj} > + \frac{\Phi'}{B_\theta^0} = \frac{1}{\{\nu_{kj}^S\}} \sum_l \left\{\frac{\nu_{kj}^S \nu_{kl}^S}{\nu_{k\Phi}} f_{c\Phi}\right\}\left[< r_{lk} > + \frac{\Phi'}{B_\theta^0}\right]$$

As the restoring coefficients $< r_{kj} >, < r_{lk} >$ are all determined by the driving force $\Phi^{'}/B_{\theta}^{0}$, which is independent of any particular species, the only solution to the above system of equations is

$$< r_{kj} >=< r_{lk} >= -\frac{\Phi^{'}}{B_{\theta}^{0}}$$

Using this in the expression for the particle fluxes, Eq. 6.5, we immediately see that the radial electric field does not contribute to the particle flux, i.e.,

$$\Gamma_j(\Phi^{'}) = 0$$

6.2.2 Particle Flux due to the Gradient Terms

We now set $\Phi^{'} = A_3 = 0$ in Eq. 6.7 and calculate the response to A_{1k} and A_{2k}. Using the expression

$$\left\{\nu_{kj}^{S} - \frac{\nu_{kj}^{S}\nu_{k}^{S}}{\nu_{k\Phi}} + \frac{\nu_{kj}^{S}\nu_{k}^{S}}{\nu_{k\Phi}} f_{t\Phi}\right\} = \left\{\frac{\nu_{k}^{D}\nu_{kj}^{S}}{\nu_{k\Phi}} f_{t\Phi}\right\}$$

Eq. 6.7 can be written as

$$\begin{aligned}\sum_{l}\left\{f_{c\Phi}\frac{\nu_{kl}^{S}\nu_{kj}^{S}}{\nu_{k\Phi}}\right\}\frac{1}{\{\nu_{kj}^{S}\}}[< r_{kj} > - < r_{lk} >] \;=\; & -\frac{1}{\{\nu_{kj}^{S}\}}\left(\frac{T_k}{e_k B_{\theta}^{0}}\right)\left[A_{1k}\left\{f_{t\Phi}\frac{\nu_{k}^{D}\nu_{kj}^{S}}{\nu_{k\Phi}}\right\}\right. \\ & \left. + A_{2k}\left\{f_{t\Phi}\frac{\nu_{k}^{D}\nu_{kj}^{S}}{\nu_{k\Phi}}\left(\frac{m_k E^{*}}{T_k}\right)\right\}\right] \\ & -\frac{1}{\{\nu_{kj}^{S}\}}\left\{f_{t\Phi}\frac{\nu_{k}^{D}\nu_{kj}^{S}}{\nu_{k\Phi}}\right\} < r_{kj} > \end{aligned} \quad (6.8)$$

Here, we note that for a large aspect ratio tokamak, $f_{c\Phi} = 1 - f_{t\Phi} \gg f_{t\Phi}$ over most of the velocity space. This fact and the form of the Eq. 6.8 suggest that the restoring coefficients can be expanded in $f_{t\Phi}$ as

$$< r_{kj} >= V_{\Phi} + f_{t\Phi} < r_{kj} >_1 + \cdots \quad (6.9)$$

where, to the zeroth order in $f_{t\Phi}$, the restoring coefficients of all the species equal a common rotation velocity V_{Φ}. Such an expansion has been used by Hirshman et al. [14] to solve for the particle fluxes. As discussed in Ref. [14], the validity of such an expansion depends upon two conditions.

1) Collisional coupling among passing particles of the various species should be sufficiently strong to establish a common flow. This condition is usually met in a device even with a small impurity concentration.

2) The trapped particle fraction is sufficiently small. As observed in Section 5.3, the quantity $f_{t\Phi}$ is proportional to the fraction of trapped particles. In a large aspect ratio tokamak ($\epsilon \ll 1$), when $\bar{\Phi}(\theta) \simeq 0$, this condition is satisfied. In this case, $f_{t\Phi} = f_t \sim \mathcal{O}(\sqrt{\epsilon})$. In the presence of a poloidal electric field, we may obtain one of the two scenarios outlined below.

1. When $X_0 \simeq 1$, for electrons, ions, and lighter impurities the following discussion is valid.

   In the presence of a significant poloidal electric field, we have found that the boundary between the trapped-untrapped particle regions is a function of the particle energy (see Section 3.2). Referring to Figs. 3.5 and 3.6, we find that for the low energy particles, the extent of the trapped particle region in the λ direction is not small. Analytically, this difficulty manifests in the velocity dependence of the quantity $f_{t\Phi}$, which is velocity independent when $\bar{\Phi}(\theta) = 0$. As a result, velocity integrals of the type $\{f_{t\Phi}F(v)\} \neq f_t\{F(v)\}$ where $F(v)$ is an arbitrary function of velocity. Actually $\{f_{t\Phi}F(v)\} > f_t\{F(v)\}$, especially for large values of the poloidal electric field (i.e. $X_0 > 1$). However, we note from Figs. 3.5 and 3.6 that the extent of the region with increased trapping is small in the E direction for a large aspect ratio tokamak. Furthermore, the contribution of the low velocity region with enhanced trapping to the velocity integrals of the type $\{f_{t\Phi}F(v)\}$ is small (see Section 6.3). We, therefore, assume that $\{f_{t\Phi}F(v)\} \sim \mathcal{O}(f_t)$. Specifically, we assume that the enhancement of velocity integrals of the type $\{f_{t\Phi}F(v)\}$ over similar integrals when $\bar{\Phi}(\theta) = 0$ is only by a factor less than an order of magnitude.

2. When $X_0 \simeq 1$, for a heavy impurity ($Z_j = Z \gg 1$), the quantity $|1 \pm ZX_0T/m_Zw|^{1/2}$ can be quite large and $f_{t\Phi}$ can approach unity for moderate values of $\sqrt{\epsilon}$. Physically, this means that most of the impurity particles are trapped in the electrostatic potential well. If this situation obtains, the expansion 6.9 is not valid.

From now on, we concentrate on those situations where $f_{t\Phi} < 1$. With this, we use the expansion 6.9 in the expression for particle fluxes to obtain

$$\begin{aligned}\Gamma_{j\Phi} &= -\frac{m_j n_{j0} T_j}{e_j^2 B_\theta^{0^2}} \left[A_{1j} \left\{ f_{t\Phi} \frac{\nu_j^S \nu_j^D}{\nu_{j\Phi}} \right\} + A_{2j} \left\{ f_{t\Phi} \frac{\nu_j^D \nu_j^S}{\nu_{j\Phi}} \left(\frac{m_j E^*}{T_j} \right) \right\} \right] \\ &\quad -\frac{m_j n_{j0}}{e_j B_\theta^0} \left\{ \frac{f_{t\Phi} \nu_j^D \nu_j^S}{\nu_{j\Phi}} \right\} V \end{aligned} \tag{6.10}$$

Here, we have retained only the lowest order (in $f_{t\Phi}$) restoring coefficient V_Φ to obtain the particle fluxes to the order $f_{t\Phi}$. Using the ambipolarity condition to obtain the common toroidal rotation velocity V_Φ, we get

$$V_\Phi = -\frac{\sum_j \frac{m_j n_j T_j}{e_j B_\theta^0} \left[A_{1j} \left\{ \frac{f_{t\Phi} \nu_j^S \nu_j^D}{\nu_{j\Phi}} \right\} + A_{2j} \left\{ \frac{f_{t\Phi} \nu_j^S \nu_j^D}{\nu_{j\Phi}} \left(\frac{m_j E^*}{T_j} \right) \right\} \right]}{\sum_j m_j n_j \left\{ f_{t\Phi} \frac{\nu_j^D \nu_j^S}{\nu_{j\Phi}} \right\}} \tag{6.11}$$

Using this expression in Eq. 6.10, we obtain the following expression for the diffusive particle fluxes.

$$\Gamma_{j\Phi}(A_1, A_2) = \sum_{k;n=1,2} L_{1n,\Phi}^{jk} A_{nk} \tag{6.12}$$

where

$$\begin{aligned} L_{11,\Phi}^{jj} &= -\left(\frac{\sum_{l \neq j} m_l n_l \left\{ f_{t\Phi} \frac{\nu_l^D \nu_l^S}{\nu_{l\Phi}} \right\}}{\sum_l m_l n_l \left\{ f_{t\Phi} \frac{\nu_l^D \nu_l^S}{\nu_{l\Phi}} \right\}} \right) L_{j\Phi} \\ L_{12,\Phi}^{jj} &= \frac{\left\{ f_{t\Phi} \frac{\nu_j^D \nu_j^S}{\nu_{j\Phi}} \left(\frac{m_j E^*}{T_j} \right) \right\}}{\left\{ f_{t\Phi} \frac{\nu_j^D \nu_j^S}{\nu_{j\Phi}} \right\}} L_{11,\Phi}^{jj} \\ L_{11,\Phi}^{jk} &= \frac{Z_j}{Z_k} \frac{T_k}{T_j} \left(\frac{m_k n_k \left\{ f_{t\Phi} \frac{\nu_l^D \nu_l^S}{\nu_{l\Phi}} \right\}}{\sum_l m_l n_l \left\{ f_{t\Phi} \frac{\nu_l^D \nu_l^S}{\nu_{l\Phi}} \right\}} \right) L_{j\Phi} \end{aligned}$$

$$L^{jk}_{12,\Phi} = \frac{\left\{ f_{t\Phi} \frac{\nu^D_t \nu^S_t}{\nu_{t\Phi}} \left(\frac{m_t E^*}{T_t} \right) \right\}}{\left\{ f_{t\Phi} \frac{\nu^D_t \nu^S_t}{\nu_{t\Phi}} \right\}} L^{jk}_{11,\Phi}$$

and

$$L_{j\Phi} = \frac{m_j n_j T_j}{e_j^2 B_\theta^{02}} \left\{ f_{t\Phi} \frac{\nu^S_j \nu^D_j}{\nu_{j\Phi}} \right\}$$

From the above equations, it is easy to see that

$$\frac{\Gamma_i}{\Gamma_e} \sim \mathcal{O}\left(\sqrt{\frac{m_i}{m_e}} \right)$$

Hence, in order to satisfy ambipolarity, $\Gamma_Z \simeq -(e_i)/(e_Z)\Gamma_i$. Thus ion and impurity diffusion occur at a comparable rate at the beginning of the discharge. Over a longer time scale, the ion and impurity density and temperature profiles adjust to make the ion and impurity fluxes comparable to the electron flux. When this condition (known as the "stationary state" [9]) obtains, ambipolarity gives

$$\Gamma_{e\Phi} = Z_i \Gamma_{i\Phi} + Z \Gamma_{Z\Phi}$$

Using the expression for the particle flux [Eq. 6.12] in the above expression, we find that the stationary state is reached when

$$\frac{T_i}{Z_i} \left[\frac{n_i'}{n_i} + \left(y_{i\Phi} - \frac{3}{2} \right) \frac{T_i'}{T_i} \right] = \frac{T_Z}{Z} \left[\frac{n_Z'}{n_Z} + \left(y_{Z\Phi} - \frac{3}{2} \right) \frac{T_Z'}{T_Z} \right] \tag{6.13}$$

where

$$y_{j\Phi} = \frac{\left\{ f_{t\Phi} \frac{\nu^D_j \nu^S_j}{\nu_{j\Phi}} \left(\frac{m_j E^*}{T_j} \right) \right\}}{\left\{ f_{t\Phi} \frac{\nu^D_j \nu^S_j}{\nu_{j\Phi}} \right\}} \tag{6.14}$$

6.2.3 Particle Flux due to the Parallel Electric Field

The effect of the parallel electric field is expected to be significant only for the electrons due to their smaller mass. We shall, therefore, calculate only the electron flux due to the parallel electric field. Perpendicular transport of electrons due to the parallel electric field is also known as the Ware pinch effect [83]. We have discussed this

effect in Section 3.3.2. The solution method used here is similar to the one used by Connor [9]. Setting $A_{1k} = A_{2k} = \Phi' = 0$ in Eq. 6.7, we obtain

$$< r_{kj} >= \frac{e_k}{m_k} A_3 \frac{1}{\{\nu^S_{kj}\}} \left\{ \frac{\nu^S_{kj}}{\nu_{k\Phi}} f_{c\Phi} \right\} + \sum_l \frac{1}{\{\nu^S_{kj}\}} \left\{ \frac{\nu^S_{kj}\nu^S_{kl}}{\nu_{k\Phi}} f_{c\Phi} \right\} < r_{lk} >$$

Noting that $f_{c\Phi} = 1 - f_{t\Phi}$, to the lowest order in $f_{t\Phi}$, we have

$$< r_{kj} >= \frac{e_k}{m_k} A_3 \frac{1}{\{\nu^S_{kj}\}} \left\{ \frac{\nu^S_{kj}}{\nu_{k\Phi}} \right\} + \sum_l \frac{1}{\{\nu^S_{kj}\}} \left\{ \frac{\nu^S_{kj}\nu^S_{kl}}{\nu_{k\Phi}} \right\} < r_{lk} > \qquad (6.15)$$

Again, as discussed before, we have used the assumption $\{f_{t\Phi}F(v)\} \sim \mathcal{O}(f_t)$ in obtaining the above equation. An examination of the order of magnitude of the first term on the right hand side of Eq. 6.15 indicates that

$$\frac{< r_{ej} >}{< r_{ij} >} \sim \mathcal{O}\left[\frac{m_i \nu_{i\Phi}}{m_e \nu_{e\Phi}}\right] \sim \mathcal{O}\left(\sqrt{\frac{m_i}{m_e}}\right) \gg 1$$

Similarly

$$\frac{< r_{ej} >}{< r_{Ij} >} \sim \mathcal{O}\left[\frac{m_I \nu_{I\Phi}}{m_e \nu_{e\Phi}}\right] \gg 1$$

Hence

$$< r_{ej} > \gg < r_{ij} >, < r_{Ij} > \qquad (6.16)$$

Retaining only the driving term A_3 in Eq. 6.6, the expression for the particle flux can be written as

$$\Gamma_{j\Phi}(A_3) = -\frac{m_j n_{j0}}{e_j B^0_\theta} \sum_k \left\{ \frac{f_{t\Phi}\nu^D_j \nu^S_{jk}}{\nu_{j\Phi}} \right\} < r_{kj} > -\frac{n_{j0}A_3}{B^0_\theta} \left\{ \frac{f_{t\Phi}\nu^D_j}{\nu_{j\Phi}} \right\}$$

For electrons, using Eq. 6.16, we write

$$\Gamma_{e\Phi}(A_3) = \frac{m_e n_{e0}}{B^0_\theta} \left\{ \frac{f_{t\Phi}\nu^D_e \nu^S_{ee}}{\nu_{e\Phi}} \right\} < r_{ee} > -\frac{n_{e0}A_3}{B^0_\theta} \left\{ \frac{f_{t\Phi}\nu^D_e}{\nu_{e\Phi}} \right\}$$

Using Eq. 6.15, we obtain $< r_{ee} >$ as

$$< r_{ee} >= -\frac{\frac{eA_3}{m_c} \left\{ \frac{\nu^S_{cc}}{\nu_{c\Phi}} \right\}}{\left\{ \frac{\nu^S_{cc}}{\nu_{c\Phi}} (\nu_{e\Phi} - \nu^S_{ee}) \right\}} \qquad (6.17)$$

Using this, the electron flux can be written as

$$\Gamma_{e\Phi}(A_3) = -\frac{n_{e0}A_3}{B^0_\theta} \left[\left\{ \frac{f_{t\Phi}\nu^D_e}{\nu_{e\Phi}} \right\} + \frac{\left\{ \frac{f_{t\Phi}\nu^D_c \nu^S_{cc}}{\nu_{c\Phi}} \right\} \left\{ \frac{\nu^S_{cc}}{\nu_{c\Phi}} \right\}}{\left\{ \frac{\nu^S_{cc}}{\nu_{c\Phi}} (\nu_{e\Phi} - \nu^S_{ee}) \right\}} \right] \qquad (6.18)$$

6.3 Results and Discussion

Before we present the results on transport coefficients, we wish to make an additional simplification which greatly facilitates the calculations. In the absence of a poloidal electric field, $\nu_j = \nu_j^S + f_t(\nu_j^D - \nu_j^S)$. For a large aspect ratio tokamak ($f_t \ll 1$), we can set $\nu_j = \nu_j^S$ to the lowest order in f_t [14]. In the presence of a poloidal electric field, $\nu_{j\Phi} = \nu_j^S + f_{t\Phi}(\nu_j^D - \nu_j^S)$. Noting that $f_{t\Phi} = f_t|1 \pm |Z_j|X_0/x_j^2|^{1/2}$, we observe that in the low energy region where $x = v/v_{th} \ll 1$, $f_{t\Phi}$ can be quite large, approaching 1 (see Section 5.3). Hence, we have to examine the consequences of $f_{t\Phi} \simeq 1$ in the low energy region on the velocity integrals appearing in the transport coefficients.

We begin by observing that most of the velocity integrals appearing in the transport coefficients are of the type $\{f_{t\Phi}F(v)/\nu_{j\Phi}\}$ where $F(v)$ is an arbitrary function of velocity. We specifically consider $F(v) = \nu_j^D\nu_j^S$. The conclusions drawn below are expected to be valid for other forms of $F(v)$ appearing in the transport coefficients. We have

$$\left\{\frac{f_{t\Phi}F(v)}{\nu_{j\Phi}}\right\} = \left\{\frac{\nu_j^S\nu_j^D f_{t\Phi}}{\nu_j^S\left[1 + f_{t\Phi}\left(\frac{\nu_j^D}{\nu_j^S} - 1\right)\right]}\right\}$$

$$= \frac{8}{3\sqrt{\pi}}\int_{x_{j,crit}}^{\infty} x_j^4 \exp(-x_j^2)\left[\frac{\nu_j^D f_{t\Phi}}{1 + f_{t\Phi}\left(\frac{\nu_j^D}{\nu_j^S} - 1\right)}\right] dx_j \qquad (6.19)$$

In the absence of a poloidal electric field, $x_{j,crit} = 0$, and the lower limit in the above integral is zero. In the presence of a poloidal electric field, for large values of x_j, i.e. $x_j \gg 1$, $f_{t\Phi} \to f_t$ and we can set $\nu_{j\Phi} = \nu_j^S$. We, therefore, examine only the region of the velocity space where $f_{t\Phi} \simeq 1$. We have, in this region, $x_j \sim \mathcal{O}(f_t\sqrt{X_0|Z_j|}) < 1$ for $f_t \to 0$. Setting $f_{t\Phi} = 1$, the integrand in the above equation reduces to

$$Integrand \simeq x_j^4 \exp(-x_j^2)\nu_j^S$$

In this region, $x_j \sim \mathcal{O}(x_{j,crit}) \ll 1$, and ν_j^S scales as $\sim 1/x_j^3$ for electrons and $\sim 1/x_j$ for ions as well as impurities. Hence, the value of the integrand is $\leq x_j \exp(-x_j^2) \ll 1$,

leading to negligible contribution from this region of the velocity space. Hence, the contribution to the velocity integral from the region where $f_{t\Phi} \simeq 1$ is small for a large aspect ratio tokamak. We, therefore, set $\nu_{j\Phi} \simeq \nu_j^S$ in the transport coefficients. With this, the expressions for the rotation velocity, diffusion coefficients, and the Ware pinch effect can be written as

$$V_\Phi = -\frac{\sum_j \frac{m_j n_j T_j}{e_j B_\theta^0}\left[A_{1j}\left\{f_{t\Phi}\nu_j^D\right\} + A_{2j}\left\{f_{t\Phi}\nu_j^D\left(\frac{m_j E^*}{T_j}\right)\right\}\right]}{\sum_j m_j n_j \left\{f_{t\Phi}\nu_j^D\right\}} \tag{6.20}$$

$$\Gamma_{j\Phi}(A_1, A_2) = \sum_{k;n=1,2} L^{jk}_{1n,\Phi} A_{nk} \tag{6.21}$$

where

$$\begin{aligned}
L^{jj}_{11,\Phi} &= -\left(\frac{\sum_{l\neq j} m_l n_l \left\{f_{t\Phi}\nu_l^D\right\}}{\sum_l m_l n_l \left\{f_{t\Phi}\nu_l^D\right\}}\right) L_{j\Phi} \\
L^{jj}_{12,\Phi} &= \frac{\left\{f_{t\Phi}\nu_j^D\left(\frac{m_j E^*}{T_j}\right)\right\}}{\left\{f_{t\Phi}\nu_j^D\right\}} L^{jj}_{11,\Phi} \\
L^{jk}_{11,\Phi} &= \frac{Z_j}{Z_k}\frac{T_k}{T_j}\left(\frac{m_k n_k \left\{f_{t\Phi}\nu_k^D\right\}}{\sum_l m_l n_l \left\{f_{t\Phi}\nu_l^D\right\}}\right) L_{j\Phi} \\
L^{jk}_{12,\Phi} &= \frac{\left\{f_{t\Phi}\nu_k^D\left(\frac{m_k E^*}{T_k}\right)\right\}}{\left\{f_{t\Phi}\nu_k^D\right\}} L^{jk}_{11,\Phi}
\end{aligned}$$

and

$$L_{j\Phi} = \frac{m_j n_j T_j}{e_j^2 B_\theta^{0\,2}}\left\{f_{t\Phi}\nu_j^D\right\} \tag{6.22}$$

$$\Gamma_{e\Phi}(A_3) = -\frac{n_{e0}A_3}{B_\theta^0}\left[\left\{\frac{f_{t\Phi}\nu_e^D}{\nu_e^S}\right\} + \frac{\left\{\frac{f_{t\Phi}\nu_e^D\nu_{ee}^S}{\nu_e^S}\right\}\left\{\frac{\nu_{ei}^S}{\nu_e^S}\right\}}{\left\{\frac{\nu_{ei}^S}{\nu_e^S}(\nu_e^S - \nu_{ee}^S)\right\}}\right] = L^e_{13,\Phi} A_3 \tag{6.23}$$

For $\tilde{\Phi}(\theta) = 0$, $f_{t\Phi} = f_t$ and the diffusion coefficients L^{jk}_{1n} reduce to the form given by Hirshman et al. [14, Eq. 36]. For $\tilde{\Phi}(\theta) = 0$ and $\nu_{jk}^S = \nu_{jk}^D$, the Ware pinch coefficient reduces to the expression for Ware pinch derived by Connor [9, Eq. 38].

We note that some of the velocity integrals in the above expressions involve $E^* = w + e\Phi(\theta)/m$. As the effect of a poloidal electric field is significant only in the low

velocity region, and as the contribution of the low velocity region to the velocity integrals of the form $\{F(v)\}$ is small, we use $E^* \simeq w$ in evaluating the velocity integrals.

In the following sections, we discuss the electron and ion diffusion coefficients, electron Ware pinch, and the plasma rotation velocity in the presence of a poloidal electric field. Impurity transport can be obtained using the ambipolarity condition

$$\Gamma_{Z\Phi} \simeq -\frac{Z_i}{Z}\Gamma_{i\Phi}$$

The velocity integrals appearing in the transport coefficients (see Eqs. 6.20, 6.21, and 6.23) are analytically intractable. Hence, consistent with the approach used by Chang [12], we present numerical results for the transport coefficients.

6.3.1 Electron Transport

In the presence of significant impurity concentration, electron transport is much smaller than ion transport until the "stationary state" [9] is reached when the ion and impurity profiles adjust to make the ion and impurity fluxes comparable to the electron flux [Eq. 6.13].

To facilitate comparison of our results with previous results, we write the diffusive electron flux as

$$\begin{aligned}
\Gamma_{e\Phi} \;=\; & L^{ee}_{11,\Phi}\left(1+\frac{T_i}{T_eZ_i}\right)\frac{n_e'}{n_e} + \left[L^{ee}_{11,\Phi} + L^{ee}_{11,\Phi}\left(y_{e\Phi}-\frac{5}{2}\right)\right]\frac{T_e'}{T_e} \\
& + L^{ee}_{11,\Phi}\left(\frac{T_i}{Z_iT_e}\right)\left(y_{i\Phi}-\frac{3}{2}\right)\frac{T_i'}{T_i} + L^{ee}_{11,\Phi}\left(\frac{T_i}{Z_iT_e}\right)\left(\frac{n_i'}{n_i}-\frac{n_e'}{n_e}\right) \\
& - \frac{Z}{T_Z}L^{eZ}_{11,\Phi}\left[\frac{T_i}{Z_i}\left[\frac{n_i'}{n_i}+\left(y_{i\Phi}-\frac{3}{2}\right)\frac{T_i'}{T_i}\right]\right. \\
& \left. - \frac{T_Z}{Z}\left[\frac{n_Z'}{n_Z}+\left(y_{Z\Phi}-\frac{3}{2}\right)\frac{T_Z'}{T_Z}\right]\right] \qquad (6.24)
\end{aligned}$$

This equation is obtained by rearranging the terms in Eq. 6.21 and by neglecting some terms of the order $\sim \sqrt{m_e/m_i}$. Setting $\nu_{j\Phi} \simeq \nu_j^S$, we obtain $y_{j\Phi}$ from Eq. 6.14

A brief list of symbols relevant for the results in Chapter VI

Φ_{in}, Φ_{out}	Potential on the inside (at $\theta = \pi$) and outside (at $\theta = 0$) of the tokamak respectively
Φ_c	Amplitude of the poloidal asymmetry in the potential
X_0	$e\Phi_c/\epsilon T$, is the magnitude of the poloidal potential variation. $X_0 \simeq 0$ in the standard neoclassical theory
Z_{eff}	$\sum_{j\neq e} n_j z_j^2/n_e$
$L^{jk}_{1n,\Phi}$, L^{jk}_{1n}	Diffusive transport coefficients in the presence (subscript Φ) and absence of a significant poloidal potential variation respectively ($n = 1, 2;\ j, k = e, i, Z$)
F^{jk}_{1n}	$L^{jk}_{1n,\Phi}/L^{jk}_{1n}$ is the transport enhancement factor
$f_{t\Phi}$	Neoclassical factor (Eqs. 5.29-5.30)
$y_{j\Phi}$	$\{f_{t\Phi}\nu_j^D(m_jE^*/T_j)\}/\{f_{t\Phi}\nu_j^D\}$ where E^* is the total energy of the particle
F^e_{13}	$L^e_{13,\Phi}/L^e_{13}$ is the Ware pinch enhancement factor. $L^e_{13,\Phi}$ and L^e_{13} are the Ware pinch coefficients in the presence and absence of the poloidal electric field respectively
$F^k_{R,n}$	$R^k_{n,\Phi}/R^k_n$ is the enhancement of the rotation coefficients. Here, $R^k_{n,\Phi}$ and R^k_n are the rotation coefficients in the presence and absence of a significant poloidal electric field respectively (see Eq. 6.30)

as

$$y_{j\Phi} = \frac{\left\{ f_{t\Phi} \nu_j^D \left(\frac{m_j E^*}{T_j} \right) \right\}}{\left\{ f_{t\Phi} \nu_j^D \right\}} \tag{6.25}$$

We now define the transport enhancement factors as

$$F_{1n}^{jk} = \frac{L_{1n,\Phi}^{jk}}{L_{1n}^{jk}} \tag{6.26}$$

where $n = 1, 2$ (refer to Eq. 6.21). Here, $L_{1n,\Phi}^{jk}$ and L_{1n}^{jk} are the transport coefficients with and without a poloidal electric field respectively. L_{1n}^{jk} is obtained by using $f_{t\Phi} = f_t$ in Eqs. 6.21.

The electron transport enhancement factors F_{11}^{ek} $(k = e, Z)$ and the quantities $y_{j\Phi}$ $(j = e, i, Z)$ as functions of the magnitude of the poloidal potential variation X_0 are shown in Fig. 6.1. Deuterium is the main ion and the impurity species considered is carbon. We also set $T_e \simeq T_i \simeq T_Z$. We note that the topology of the curves seems to be related to the nature of the factor $f_{t\Phi}$, which is proportional to the trapped particle fraction (see Section 5.3). As discussed in Section 3.2, when $q\Phi_{in} > q\Phi_{out}$, B-trapping is enhanced by the potential variation. Behavior of the enhancement factors F_{11}^{ek} seems to reflect this. For $q\Phi_{in} < q\Phi_{out}$, the situation is somewhat complicated. For the low energy particles, there is a reduction in B-trapping, which, however, is somewhat compensated by the presence of E-trapped particles. It is not clear whether the total trapped particle fraction increases or decreases, especially when X_0 is small. It appears that for small values of X_0, there can be a decrease in the trapped particle fraction which is reflected in the behavior of enhancement factors for small X_0. It also appears that for large values of X_0, there can be an increase in the trapped particle fraction. The quantity $y_{j\Phi}$ is related to plasma rotation. We discuss plasma rotation in Section 6.3.4.

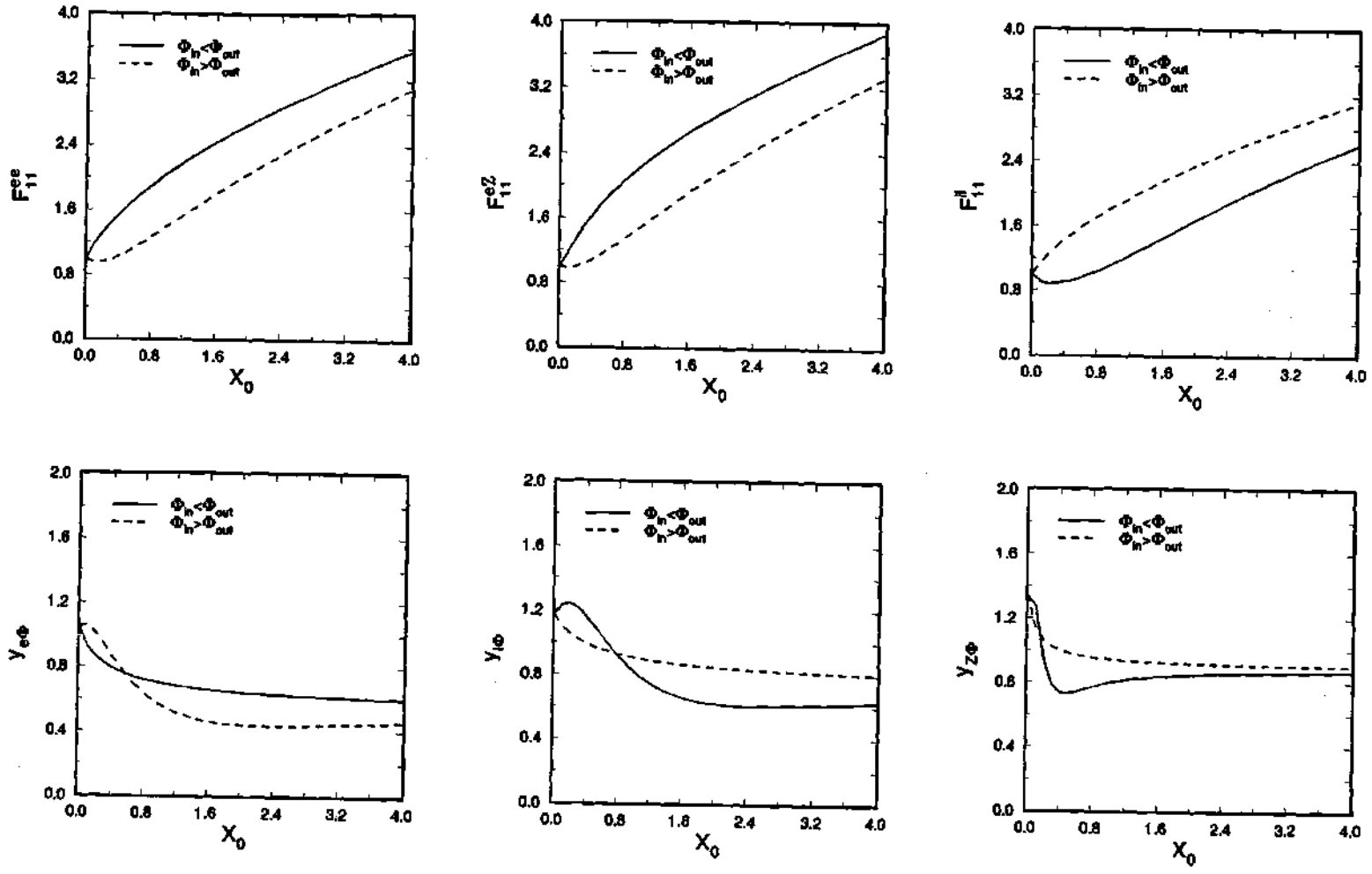

Fig. 6.1 Particle Transport Coefficients as a Function of X_0
(Impurity: Carbon, Z_{eff}=3.0)

Effect of Impurity Content on Transport Enhancement

Fig. 6.2 shows the variation of electron enhancement factors F_{11}^{ee}, F_{11}^{eZ} and the quantities $y_{e\Phi}$, $y_{i\Phi}$ with Z_{eff} in the presence of carbon impurity. Variation of F_{11}^{ee} and $y_{i\Phi}$ with Z_{eff} is generally weak, with the increase in F_{11}^{ee} being $\leq 10\%$ when Z_{eff} varies from 1.2 to 3.8. These results seem to confirm the conclusion reached by Chang [12] that the presence of an impurity does not affect the electron enhancement factors. However, as we shall see later in connection with Ware pinch enhancement and neoclassical conductivity reduction, the presence of an impurity species can have a significant effect upon some of the enhancement factors.

Contrary to the behavior of F_{11}^{ee}, the factor F_{11}^{eZ} decreases as Z_{eff} increases. However, due to the smallness of the transport coefficient L_{11}^{eZ} in comparison with L_{11}^{ee}, the impact of the transport enhancement factor F_{11}^{eZ} upon electron transport is small. The behavior of F_{11}^{eZ} is similar to that of the ion enhancement factor F_{11}^{ii}, which we will discuss later in Section 6.3.2.

Comparison with Previous Results

Our main purpose here is to compare our results on electron flux in the absence of impurities with the results obtained by Chang [12] for a two species plasma in the presence of a poloidal electric field. We will also comment on the nature of our results in relation to those obtained by Connor [9] for a three species plasma in the absence of a poloidal electric field.

1. **Comparison with Chang's Results**: Referring to Eq. 6.24, we note that in the absence of impurities, $L_{11,\Phi}^{eZ} = 0$, $n_e'/n_e = n_i'/n_i$, and the last two terms in Eq. 6.24 vanish. The resulting expression is similar to the expression for the diffusive electron flux in a two species plasma obtained by Chang [12] using a variational approach. The expression for the electron flux in Ref. [12] can be

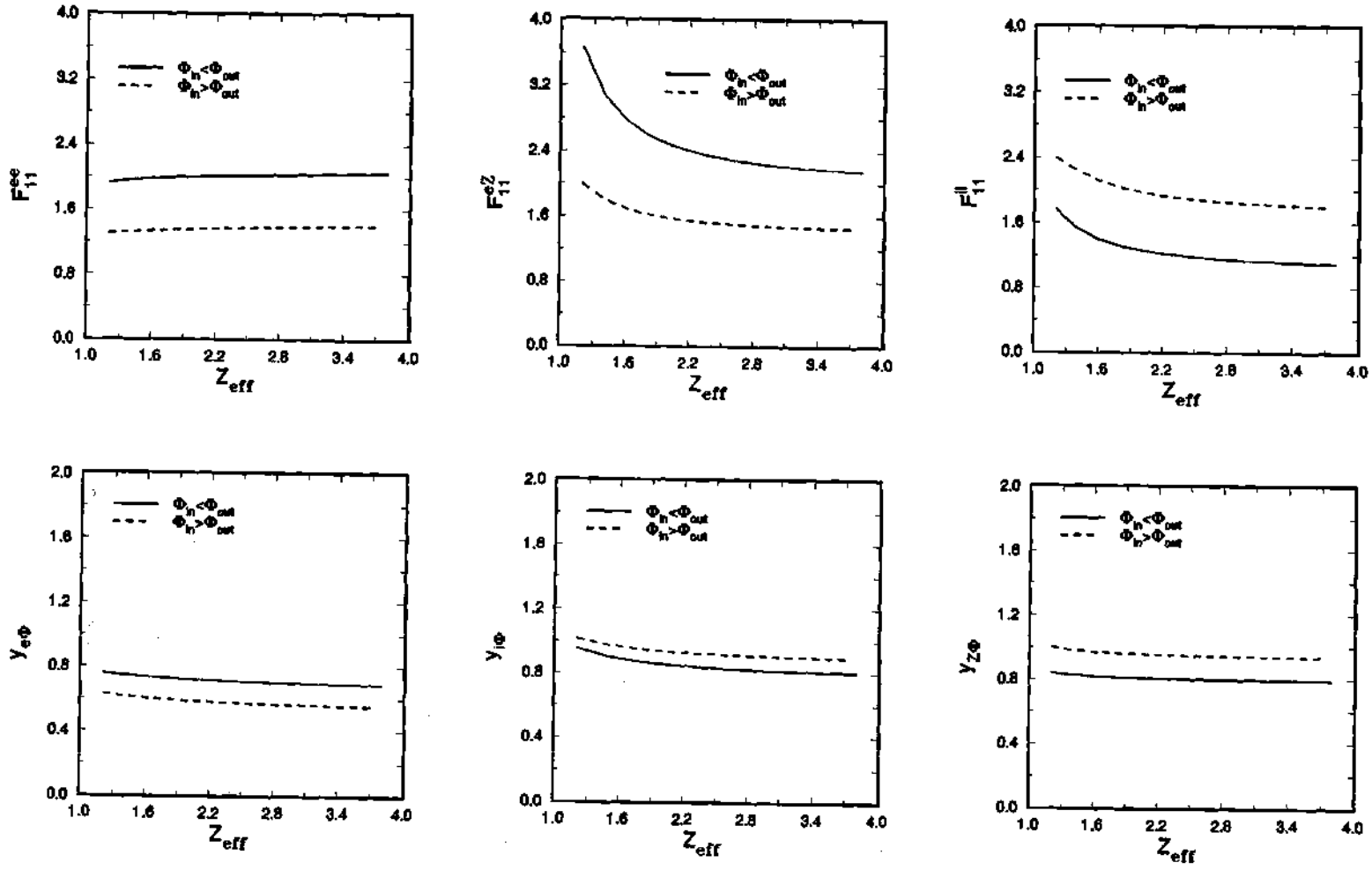

Fig. 6.2 Effect of Impurity content on Transport Enhancement
(Impurity: Carbon, X_0=1.0)

written as

$$\Gamma_e = (\alpha_1, g_{1e}) F_{11}^{(e)} \left(1 + \frac{T_i}{T_e Z_i}\right) \frac{n_e'}{n_e} + \left[(\alpha_1, g_{1e}) F_{11}^{(e)} + (\alpha_1, g_{2e}) F_{12}^{(e)}\right] \frac{T_e'}{T_e}$$
$$+ (\alpha_1, g_{1e}) F_{11}^{(e)} \left(\frac{T_i}{Z_i T_e}\right) \left(y - \frac{3}{2}\right) \frac{T_i'}{T_i} \tag{6.27}$$

Here (α_1, g_{1e}) and (α_1, g_{2e}) are the transport coefficients in the absence of a poloidal electric field [8]. $F_{11}^{(e)}$ and $F_{12}^{(e)}$ are the transport enhancement factors in the presence of a poloidal electric field and y is the variational parameter [12]. To facilitate comparison with the results obtained by Chang [12], we define a transport coefficient $L_{12m,\Phi}^{ee}$ as

$$L_{12m,\Phi}^{ee} = L_{11,\Phi}^{ee} \left(y_{e\Phi} - \frac{5}{2}\right)$$

and the corresponding enhancement factor as

$$F_{12m}^{ee} = \frac{L_{12m,\Phi}^{ee}}{L_{12m}^{ee}} \tag{6.28}$$

A comparison of the transport enhancement factors $F_{11}^{(e)}$ and $F_{12}^{(e)}$ reported in Ref. [12] with the corresponding quantities F_{11}^{ee} and F_{12m}^{ee} calculated in this thesis (Eqs. 6.26 and 6.28) indicates a significant discrepancy. The discrepancy is about 15% at $X_0 = 4$ and F_{11}^{ee}, F_{12m}^{ee} are smaller than $F_{11}^{(e)}$, $F_{12}^{(e)}$. The difference is smaller for lower values of X_0, being about 5% at $X_0 = 1$. Our calculation of the enhancement factors $F_{11}^{(e)}$ and $F_{12}^{(e)}$ using the expressions in Ref. [12] yields a much closer agreement between F_{11}^{ee}, F_{12m}^{ee} and $F_{11}^{(e)}$, $F_{12}^{(e)}$, the difference being less than $\sim 2\%$ at $X_0 = 4$. Furthermore, a comparison of the variational parameter y with the corresponding quantity $y_{i\Phi}$ in Eq. 6.24 indicates very good agreement between the quantities.

2. **Relation to Connor's Results**: While our principal interest in this work is the calculation of transport coefficients in the presence of a poloidal electric field, it is of some interest to compare our results when $\tilde{\Phi}(\theta) \simeq 0$ with those

obtained by Connor [9] using the heavy impurity assumption ($m_Z \gg m_i$). We note that our results are obtained in the presence of an impurity species of arbitrary mass.

Connor's results [9] on electron transport are valid after the stationary state is reached. When this condition obtains, as a consequence of Eq. 6.13, the last term in Eq. 6.24 vanishes and we obtain an expression for the diffusive electron flux which is similar in form to that obtained by Connor [9, Eq. (51)]. Agreement between L_{11}^{ee} and y_e (L_{11}^{ee} and $y_{e\Phi}$ when $\tilde{\Phi}(\theta) = 0$) calculated in this work and those obtained by Connor [9] is exact. However, due to the large impurity mass assumption, Connor's results for y_i differ from those calculated in this work significantly as the impurity mass decreases. For example, when $\alpha = n_Z Z^2/n_i Z_i^2 = 1$, the discrepancy between our results and Connor's results for y_i increases from 5% to 30% as the impurity is varied from tungsten ($m_Z \gg m_i$) to carbon. We discuss this point further in connection with ion transport. Finally, we note that our expression [Eq. 6.24] for the electron flux is valid even before the stationary state is reached.

6.3.2 Ion Transport

We now consider ion diffusion coefficients. Again, to facilitate comparison with previous results, we express the main ion flux as

$$\begin{aligned}\Gamma_{i\Phi} \;=\; & \frac{Z_i T_e}{T_i} L_{11,\Phi}^{ii} \left[\left[\frac{T_i}{Z_i T_e} \left[\frac{n_i'}{n_i} - \left(\frac{3}{2} - y_{i\Phi} \right) \frac{T_i'}{T_i} \right] - \frac{T_Z}{Z T_e} \left[\frac{n_Z'}{n_Z} - \left(\frac{3}{2} - y_{Z\Phi} \right) \frac{T_Z'}{T_Z} \right] \right] \right. \\ & - \frac{m_e n_e \{ f_{t\Phi} \nu_e^D \}}{\sum_{k \neq i} m_k n_k \{ f_{t\Phi} \nu_k^D \}} \left[\frac{1}{Z_e} \left[\frac{n_e'}{n_e} - \left(\frac{3}{2} - y_{e\Phi} \right) \frac{T_e'}{T_e} \right] \right. \\ & \left. \left. - \frac{T_Z}{Z T_e} \left[\frac{n_Z'}{n_Z} - \left(\frac{3}{2} - y_{Z\Phi} \right) \frac{T_Z'}{T_Z} \right] \right] \right] \end{aligned} \tag{6.29}$$

As expected, in the absence of impurities, the above equation reduces to Eq. 6.24 with $(Z_i T_e/T_i) L_{11,\Phi}^{ii} = (1/Z_i) L_{11,\Phi}^{ee}$ to satisfy ambipolarity. In the presence of impurities

the second term is negligible, and we recover an expression which has the same form as the one obtained by Connor [9, Eq. (48)]. The transport enhancement factor F_{11}^{ii} and the quantities $y_{i\Phi}$, $y_{Z\Phi}$ as a function of X_0 are shown in Fig. 6.1. The behavior of ion enhancement factors is qualitatively similar to that of electron enhancement factors. However, the ion enhancement factors depend upon the impurity content as well as the type of the impurity species.

Effect of Impurity Content on Ion Transport Enhancement

The dependence of the ion transport enhancement factor F_{11}^{ii} upon impurity concentration as shown in Fig. 6.2. In the presence of a poloidal electric field of the order ϵ, i.e. $e\tilde{\Phi}(\theta)/T \sim \mathcal{O}(\epsilon)$, due to their larger charge, the fraction of impurity ions trapped in the electrostatic potential well is greater than that of the main ions. This causes a reduction in the collisional coupling between the main ions and the impurity ions, resulting in a drop in the ion transport coefficients. This effect is more pronounced for smaller values of Z_{eff} due to the increasingly important role being played by the impurity species in determining the ion transport. We note that the electron enhancement factor F_{11}^{e2} also exhibits a behavior similar to that of F_{11}^{ii}.

Effect of Impurity Species on Ion Transport

In considering the effect of impurity species on ion transport, we are primarily interested in the effect of impurity charge and mass upon ion transport at constant $\alpha = n_Z Z^2/n_i Z_i^2$. As discussed in Section 6.2.2, the fraction of impurity ions trapped in the electrostatic potential well increases with Z. This causes a reduction in the collisional coupling between the impurity ions and main ions, resulting in a reduction in the ion transport. This effect, which is due to the impurity charge, is somewhat offset by the impurity mass. An increase in the impurity mass leads to an increase in ion transport and it appears that, at least for small to moderate Z impurities,

Table 6.1: Effect of Impurity Species on Ion Transport ($X_0 = 1$)

Impurity	Z	m_Z/m_i	F_{11}^{ii}	
			$\Phi_{in} < \Phi_{out}$	$\Phi_{in} > \Phi_{out}$
Helium	2	2	1.098	1.777
Carbon	6	6	1.342	2.065
Iron	26	28	1.454	2.249
Tungsten	60	92	1.427	2.201

the transport enhancement due to the impurity mass is more important than the transport reduction due to the impurity charge.

Table. 6.1 shows the transport enhancement factor F_{11}^{ii} in the presence of different impurity species for $\alpha = 1$ and $X_0 = 1$. F_{11}^{ii} increases as the impurity mass increases, reaching a maximum for iron. For tungsten, the enhancement factor is smaller than that for iron, apparently indicating the transport reducing effect of impurity charge. We note that the charge state indicated in Table 6.1 corresponds to an electron temperature of $\sim$ 10 keV. We also note that a heavy impurity like tungsten may not be in the banana regime under conditions that prevail in most tokamaks. The comparison presented in Table 6.1 is intended to demonstrate the opposing effects of impurity charge and mass on ion transport enhancement.

Finally, we note that in the absence of a poloidal electric field the quantities $L_{11,\Phi}$, $y_{i\Phi}$, and $y_{Z,\Phi}$ depend upon the impurity mass. Our calculations indicate that the discrepancy between our results and those obtained by Connor [9], using the heavy impurity assumption, can be quite large when the impurity mass is small. For example, when the impurity strength parameter $\alpha = 1$, the discrepancy in L_{11}^{ii}, y_i, and y_Z can be $\sim$ 90%, 30%, and 20% respectively for carbon impurity. The differences decrease as the impurity mass increases. However, even for tungsten, the discrepancy in L_{11}^{ii} is $\sim$ 30% when $\alpha = 1$.

6.3.3 Ware Pinch Effect

We define the Ware pinch enhancement factor as

$$F_{13}^{e} = \frac{L_{13.\Phi}^{e}}{L_{13}^{e}}$$

Fig. 6.3 shows the variation of the Ware pinch enhancement factor as a function of X_0. The Ware pinch enhancement factor is topologically similar to the diffusion enhancement factors. However, the enhancement is much weaker than that of the diffusion coefficients.

Variation of F_{13}^{e} with Z_{eff} is shown in Fig. 6.4. The Ware pinch enhancement factor generally decreases with increasing Z_{eff}. However, when $\Phi_{in} > \Phi_{out}$ and for $X_0 \leq 1$, it remains constant or might even increase slightly. Referring to Eq. 6.23, the effect of electron-electron collisions is contained primarily in the second term. It appears that the presence of impurities generally leads to a reduction in the contribution of the electron-electron collisions relative to the first term, leading to a decrease in the Ware Pinch enhancement factor. The behavior of the Ware pinch enhancement factor with increasing Z_{eff} is similar to the behavior of the neoclassical conductivity reduction factor. We discuss this in Section 7.4.1.

Comparison with Previous Results

We now compare our result for the Ware pinch enhancement factor (F_{13}^{e}) with the result ($F_{13}^{(e)}$) obtained by Chang [12] in the absence of impurities. Fig. 6.5 compares the result of the present work with the result obtained by Chang. We have used the analytical fit in Ref. [12] to reproduce Chang's results. The analytical fit for the Ware Pinch enhancement factor is

$$F_{13}^{(e)} = 1 - 0.59X_0 + 0.39X_0^2 - 0.048X_0^3$$

As with the electron diffusion coefficients, we find that our results differ from those obtained by Chang by $\sim 20\%$ for $X_0 = 4$ and the enhancement factors calculated

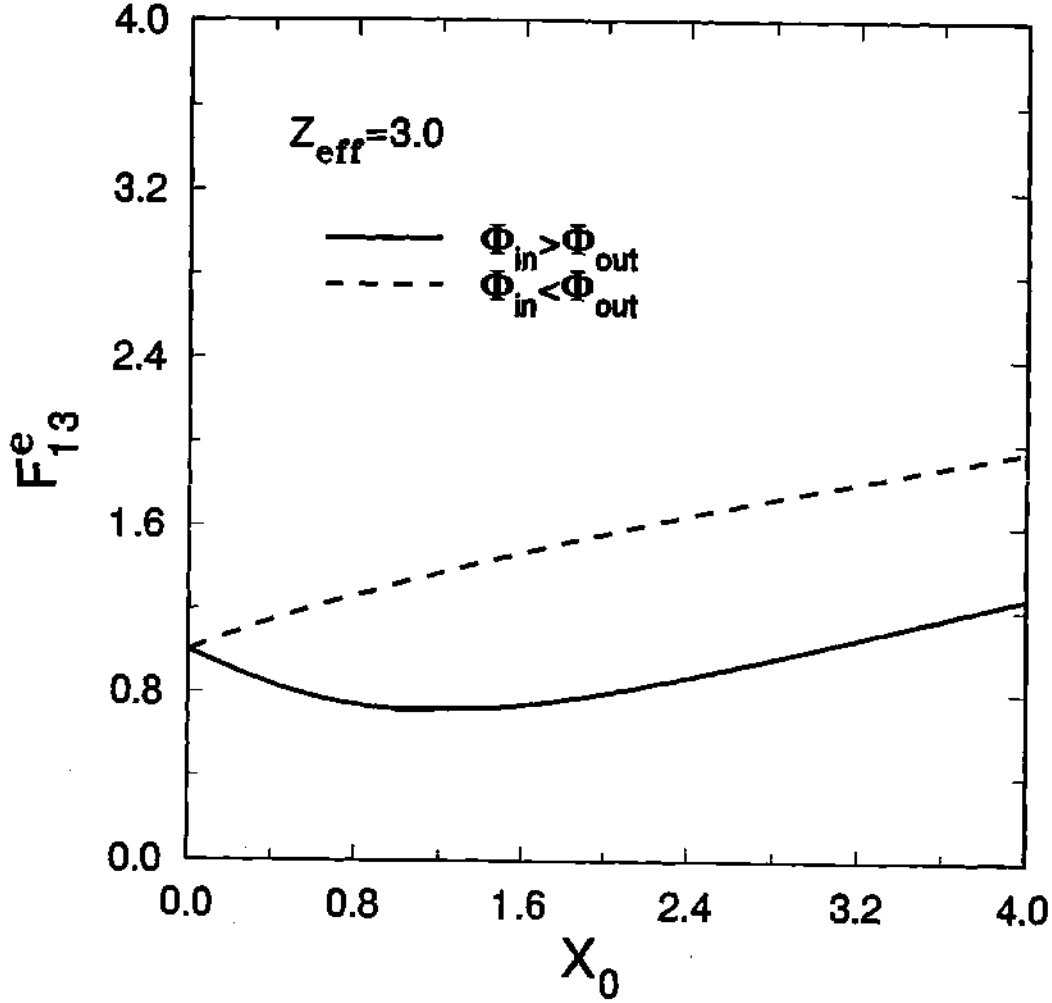

Fig. 6.3 Ware Pinch Enhancement as a Function of X_0

here are smaller than those in Ref. [12].

Finally, when $\tilde{\Phi}(\theta) = 0$, our results for the Ware pinch are identical to those obtained by Hirshman et al. [14]. Also, if we set $\nu_{jk}^S = \nu_{jk}^D$ and $\nu_{e\Phi} = \nu_e^D$ in Eq. 6.18, we obtain results identical to those obtained by Connor [9].

6.3.4 Plasma Rotation Velocity

While deriving the expressions for the diffusive fluxes, we obtained an expression for the common plasma toroidal rotation velocity, V_Φ (Eq. 6.20). Neglecting the contribution of electrons, we write the rotation velocity for a three species plasma as

$$V_\Phi = \sum_{k;n=1,2} R_{n,\Phi}^k A_{nk} \tag{6.30}$$

where

$$\begin{aligned} R_{1,\Phi}^k &= -\left(\frac{m_k n_k T_k}{e_k B_\theta^0}\right) \frac{\{f_{t\Phi}\nu_k^D\}}{\sum_j m_j n_j \{f_{t\Phi}\nu_j^D\}} \\ R_{2,\Phi}^k &= -\left(\frac{m_k n_k T_k}{e_k B_\theta^0}\right) \frac{\left\{f_{t\Phi}\nu_k^D \left(\frac{m_k E^*}{T_k}\right)\right\}}{\sum_j m_j n_j \{f_{t\Phi}\nu_j^D\}} \end{aligned}$$

As in the case of transport coefficients, we define the rotation enhancement factors as

$$F_{R,n}^k = \frac{R_{n,\Phi}^k}{R_n^k} \tag{6.31}$$

Fig. 6.6 shows the variation of rotation enhancement factors with X_0. We observe that for constant gradients, the rotation velocity decreases for most values of X_0. With increasing X_0, most of the rotation enhancement factors asymptotically approach a constant value. It appears that the drop in the rotation enhancement factors is a result of reduction in the collisional coupling between the main ions and impurity ions caused by enhanced trapping due to the poloidal electric field.

Fig. 6.7 shows the variation of rotation enhancement factors with Z_{eff}. The behavior of the enhancement factors is analogous to the behavior of the ion transport enhancement factor F_{11}^{ii}. As with ion transport, the drop in the rotation velocity is

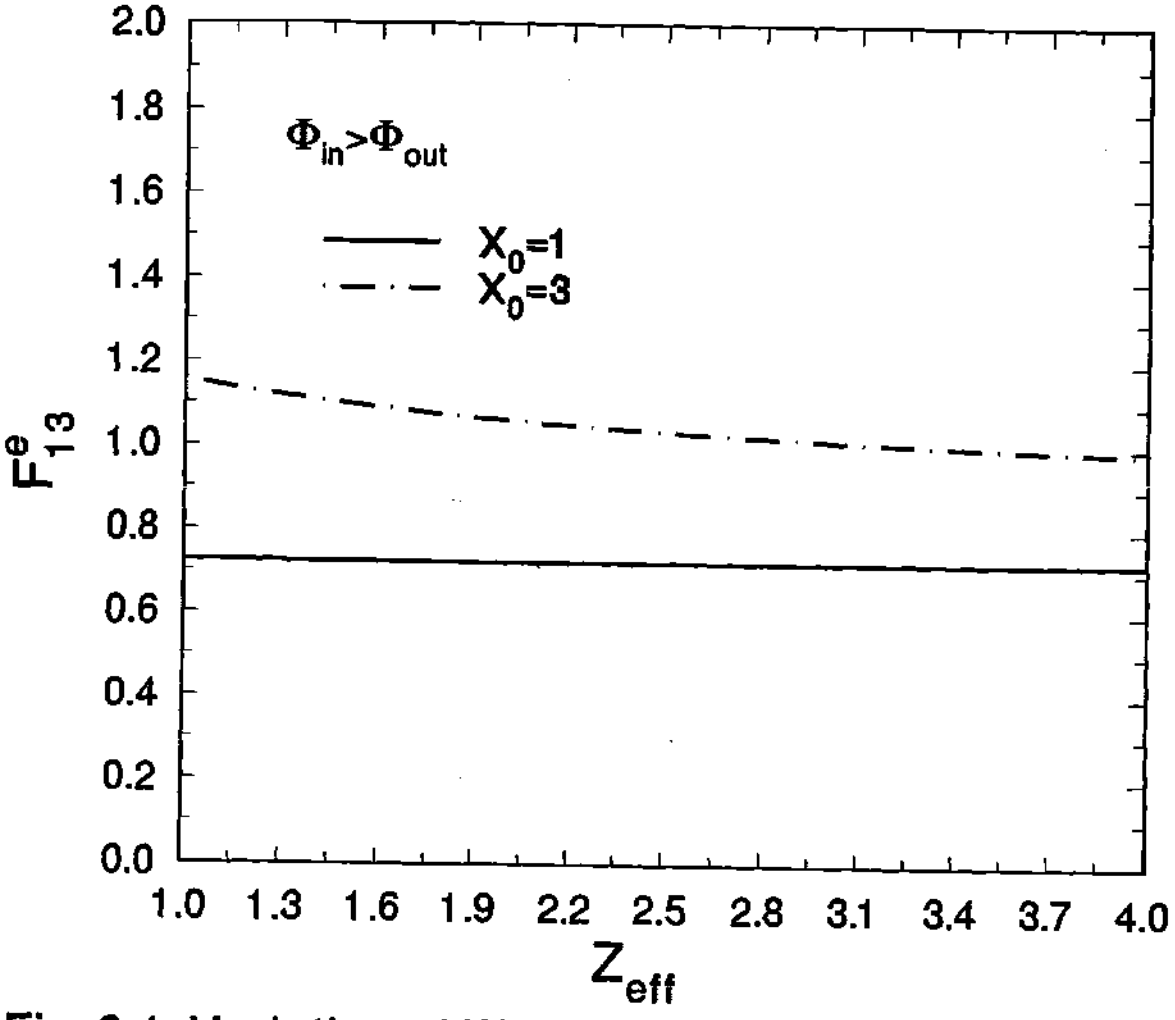

Fig. 6.4 Variation of Ware Pinch Enhancement with Z_{eff}

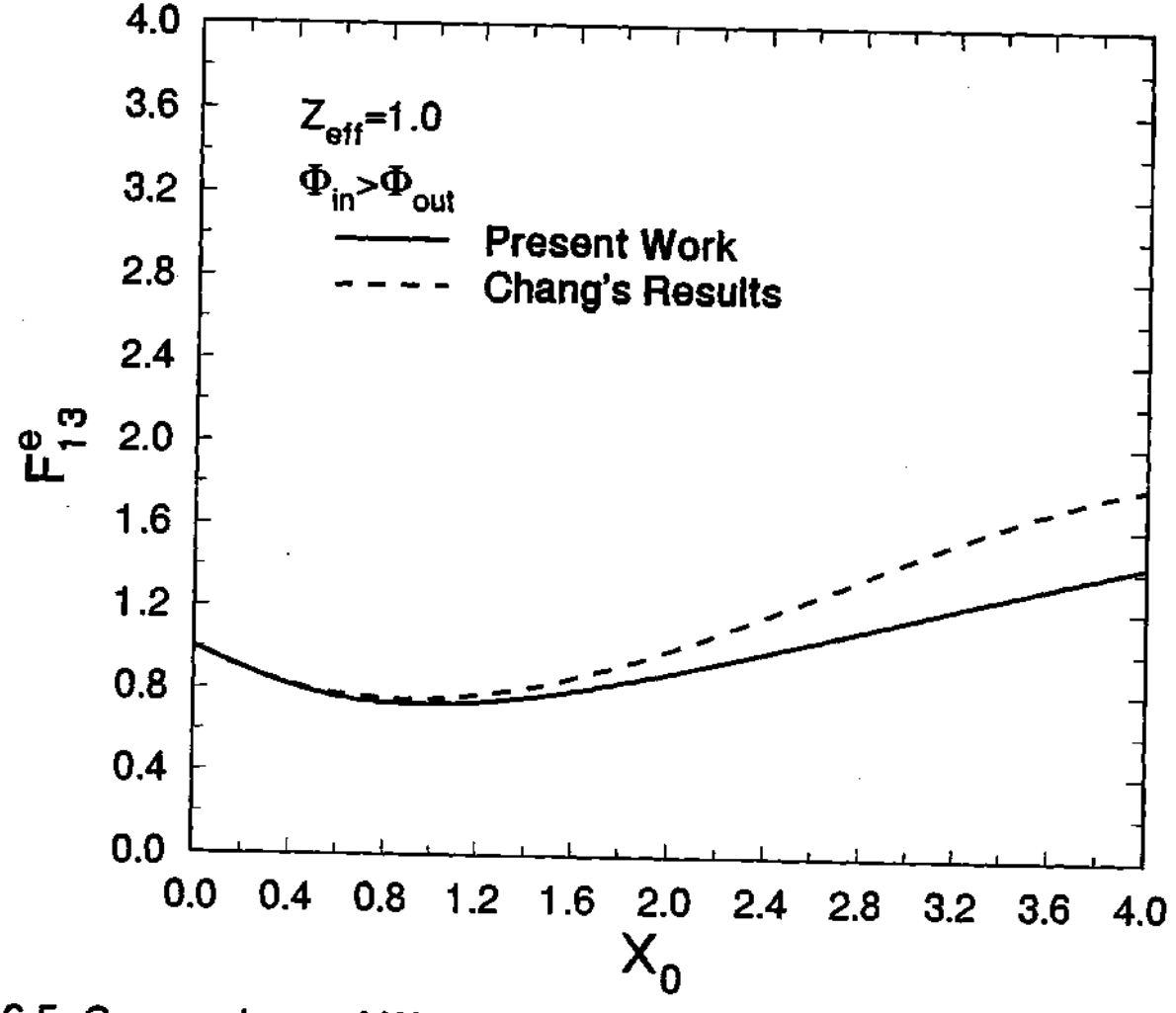

Fig. 6.5 Comparison of Ware Pinch Enhancement with Chang's Results.

caused by increased trapping of the impurity ions due to their larger Z. This results in reduced collisional coupling between the main ions and impurity ions, leading to a reduction in the common flow velocity. The presence of an impurity species of larger Z has a similar effect upon the rotation velocity.

For an electron-ion plasma, Shurygin and Yushmanov [13] have calculated the radial electric field enhancement factor in the presence of a poloidal electric field. Their calculations indicate that the radial electric field, which is proportional to the rotation velocity, shows a behavior similar to that displayed by the enhancement factors $F^i_{R,n}$. Furthermore, the variational parameter y, calculated by Chang [12], and the quantity $y_{j\Phi}$ [Eq. 6.25] show a behavior similar to that of $R^i_{2,\Phi}$.

6.3.5 Summary and Conclusion

In this section, we summarize the important results, discuss their significance, and comment upon some of the experimental observations related to transport during wave heating.

Summary of Theoretical Results:

1. The results presented in this chapter indicate that the electron and ion diffusion coefficients, and the electron Ware pinch exhibit qualitatively similar behavior in the presence of a significant poloidal potential variation. The transport coefficients increase monotonically for $e_j\Phi_{in} > e_j\Phi_{out}$. For $e_j\Phi_{in} < e_j\Phi_{out}$, the transport coefficients decrease slightly for smaller values of X_0 ($X_0 \sim 1$) and increase when X_0 becomes larger ($X_0 > 1$).

2. The presence of an impurity species does not seem to cause a significant change in the enhancement of the electron diffusive fluxes. The change is typically $<$ 8%. The change in the electron Ware pinch enhancement can be more significant ($\sim$ 16%) at larger values of the poloidal electric field ($X_0 \sim 3$).

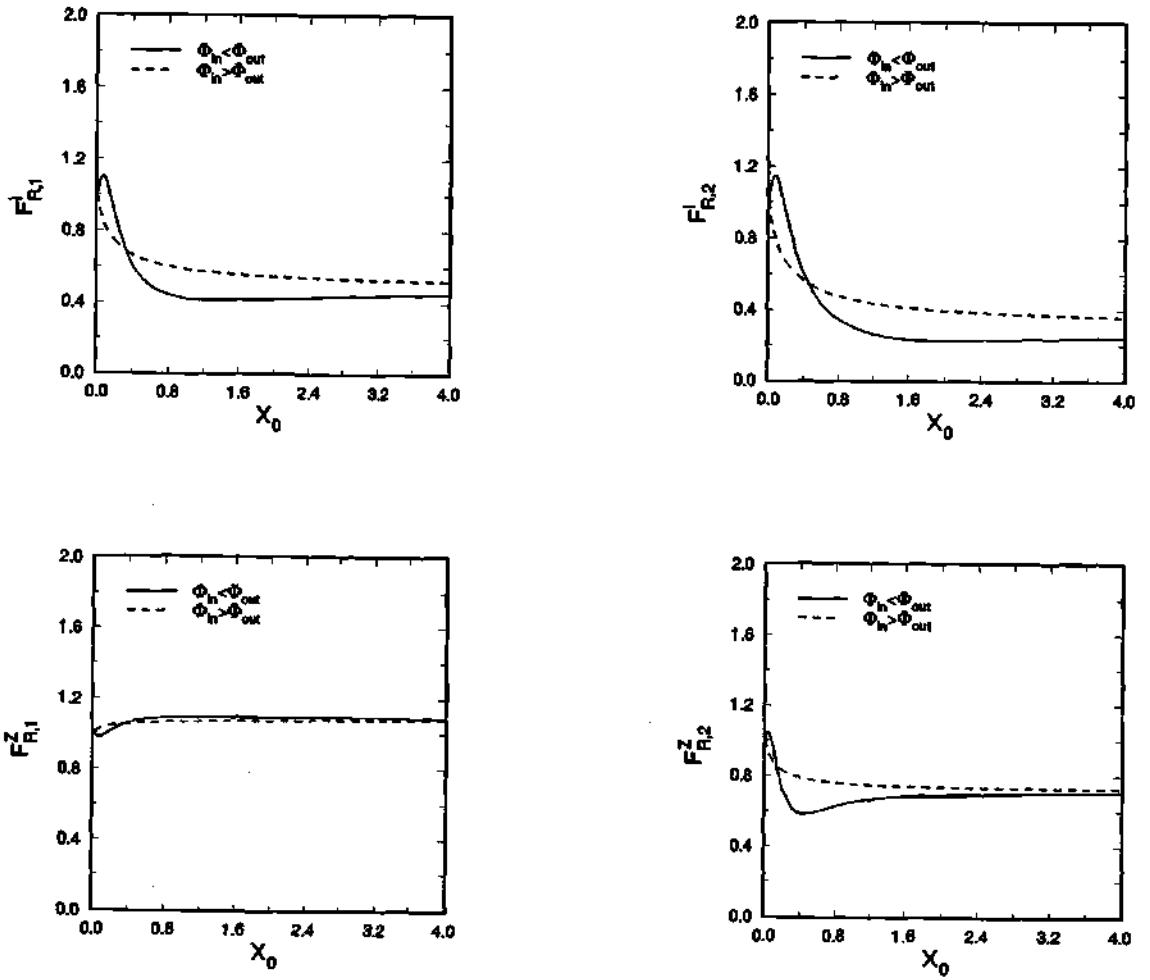

Fig. 6.6 Rotation Enhancement Factors as a Function X_0
(Impurity: Carbon, Z_{eff}=3.0)

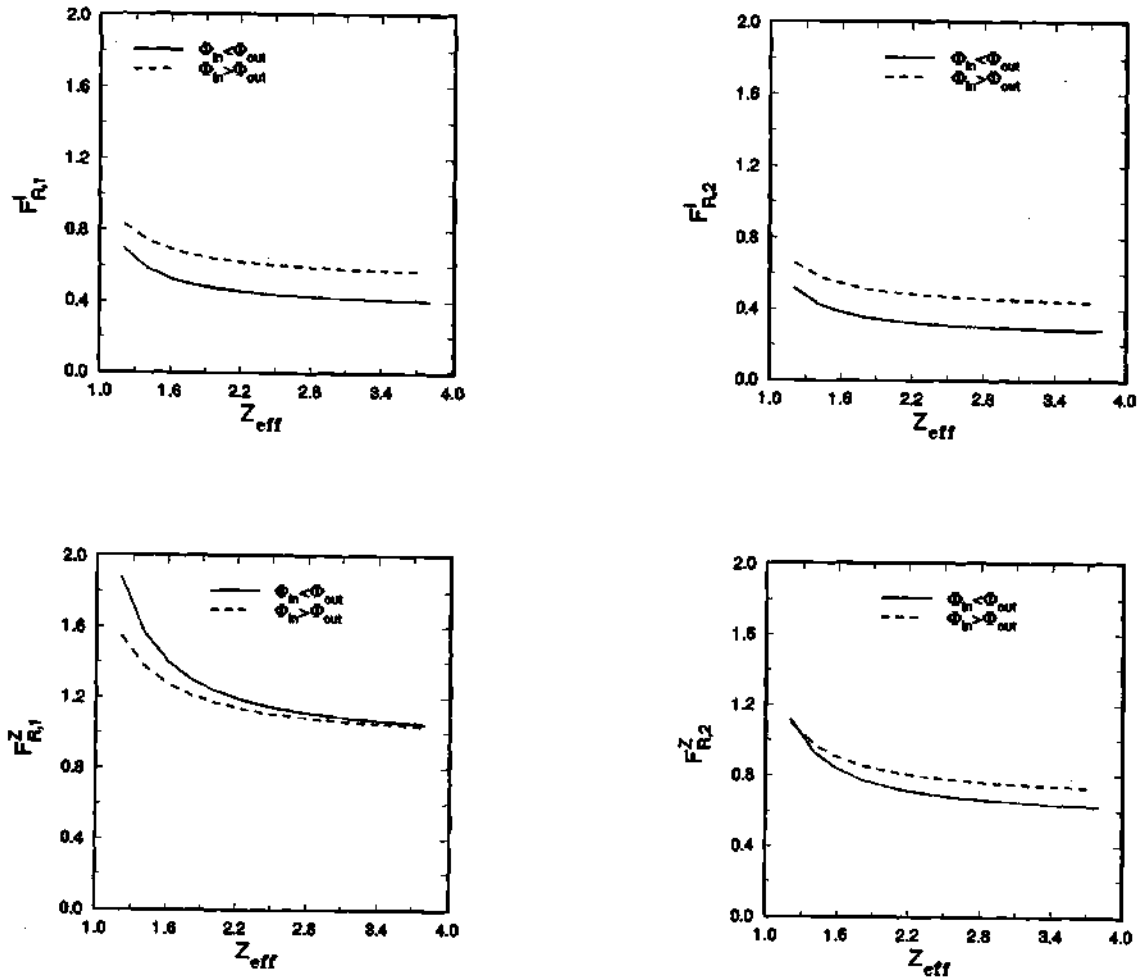

Fig. 6.7 Rotation Enhancement Factors as a Function of Z_{eff}
(Impurity: Carbon, X_0=1.0)

3. We find that the main ion diffusion coefficients increase by a factor up to 2 during both ECRH ($\Phi_{in} > \Phi_{out}$) and ICRH ($\Phi_{in} < \Phi_{out}$) for most values of the potential variation ($X_0 = e\tilde{\Phi}(\theta)/T\epsilon$), implying an increase in both the outward diffusion of main ions and the inward diffusion of impurities. Only when the poloidal potential variation is small, i.e. $X_0 \leq 1$, do the main ion diffusion coefficients decrease slightly ($\sim 10\%$) during ICRH, which implies only a small reduction in the inward impurity diffusion ($\Gamma_Z \simeq -Z_i/Z\ \Gamma_i$). It seems unlikely that any significant reduction in the inward impurity diffusion can be achieved with either ECRH or ICRH.

4. Enhancement of the ion diffusive flux is affected by both the impurity content and impurity species. An increase in the impurity content generally leads to a decrease in the ion enhancement factors. In addition, ion enhancement factors seem to depend on the impurity mass as well as charge. For low to moderate Z impurities, the mass effect seems to dominate, causing an increase in the transport enhancement factors.

5. The presence of a poloidal electric field seems to cause a significant ($> 50\%$) reduction in the common rotation velocity for an impure plasma, if the density and temperature profiles do not change with the application of poloidal electric field.

Relation to Experimental Results

We now make a few remarks about the experimental results related to particle transport and examine the significance of the present results to experiments.

1. As discussed in Chapter IV, the experimental results on transport processes do not present a very clear picture. There seems to be some evidence for inward impurity flow during ICRH. ECRH could cause a slight reduction in the inward

impurity diffusion. However, the evidence is much weaker for ECRH. The results obtained in this chapter indicate otherwise. As discussed above, ECRH can lead to enhanced outward ion flux and inward impurity flux. For ICRH, depending on the value of X_0, there can be a small reduction or an increase in the ion (impurity) flow. We, however, note that most of the experimental evidence for particle transport is indirect and subject to various interpretations. Furthermore, it is likely that any change in the impurity concentration during both ECRH and ICRH is due to changes in the particle source rates as well as transport. A direct comparison of the results presented here with experimental data will only be meaningful when well defined experiments dedicated to the study of the effects of ECRH/ICRH on transport are available.

2. It is generally thought that neoclassical transport is small in comparison with other anomalous processes causing transport in a tokamak. However, recent analysis of JET results by Giannella et al. [84], Pasini et al. [85] indicates that the impurity and electron diffusion coefficients are close to the neoclassical levels in the core region of the plasma ($r/a \leq 0.4$). Fussmann et al. [86] have analyzed the ASDEX data. They report good agreement for impurity transport between experimental measurements and simulations based on neoclassical predictions for pellet fueled and counter NBI shots.

   Transport enhancements of the type discussed in this work are likely to be important in such regimes where the transport coefficients are of the same order of magnitude as those predicted by the neoclassical theory.

3. Our calculations indicate that the rotation velocity drops during both ECRH and ICRH for most values of X_0. As discussed in Chapter IV, on JET during the ohmic phase and on TFTR during balanced neutral beam injection, the central rotation velocity increases in the counter direction when ICRH is turned on.

This seems to contradict the results obtained in this chapter. We, however, note that in these experiments, the presence of ICRH also leads to a steep temperature gradient close to the center. Hence, even with reduced rotation coefficients, increased rotation could be predicted if the temperature gradient sharply increases. A dedicated analysis would be required to draw conclusions about the predicted net effect.

There have been few experimental measurements of rotation velocity during ECRH. The results from D-III tokamak seem to indicate that for some shots the rotation velocity decreases even with increased temperature gradients. This seems to agree with the results obtained in this work. However, the data on rotation are limited and, therefore, any comparison with experimental measurements is only tentative.

CHAPTER VII

PLASMA CURRENT

In this chapter, we discuss the effect of a poloidal potential variation of order ϵ upon the plasma current. First, we derive the expressions for the neoclassical conductivity and bootstrap current for a large aspect ratio tokamak. We then evaluate the neoclassical conductivity for a plasma with an arbitrary number of species. Finally, the bootstrap current coefficients are evaluated for a three species (electron, ion, and an impurity species) plasma.

7.1 Expression for Plasma Current

The general expression for the flux surface averaged plasma current is

$$J = \sum_j e_j n_j < u_j > \tag{7.1}$$

where the parallel velocity of the species j is given by

$$u_j = \frac{1}{n_j} \int d^3v \sigma q f_{j1}$$

Here, σ is the sign of the parallel velocity and q is the magnitude of the parallel velocity. The procedure for calculating $< u_j >$ is similar to that used for calculating $< u_{j1}(v) >$ and r_{kj} [Section 5.2.1]. Expressing the velocity integral in terms of w and μ, we obtain, after integrating by parts in μ,

$$u_j = -\frac{1}{n_j} \sum_\sigma 2\pi B \sigma \int dw \int d\mu \mu \frac{\partial f_{j1}}{\partial \mu}$$

Using Eq. 5.15 to express $\partial f_{j1}/\partial\mu$ and carrying out the steps similar to those in Section 5.2.1, we obtain

$$< u_j >= -\frac{T_j}{m_j}\left\{\frac{f_{t\Phi}\beta}{f_{j0}B^0}\right\} + \frac{T_j}{m_j}\left\{\frac{\beta_1}{f_{j0}B^0}\right\}$$

where β and β_1 have been defined in Section 5.2 and the operator $\{\}$ is defined by Eq. 2.71. Using the expression 5.18 for $< u_{j1}(v) >$ in β and β_1, we can write

$$\begin{aligned} < u_j > \;=\; & -\left[\left\{\frac{f_{t\Phi}\nu_j^S}{\nu_{j\Phi}}\left(\frac{T_j}{e_jB_\theta^0}\right)\frac{f_{j0}'}{f_{j0}}\right\} + \sum_l\left\{\frac{f_{t\Phi}\nu_{jl}^S}{\nu_{j\Phi}}\right\} < r_{lj} > + \frac{e_jA_3}{m_j}\left\{\frac{f_{t\Phi}}{\nu_{j\Phi}}\right\}\right] \\ & + \left\{\left(\frac{\nu_j^S}{\nu_{j\Phi}} - 1\right)\left(\frac{T_j}{e_jB_\theta^0}\right)\frac{f_{j0}'}{f_{j0}}\right\} + \sum_l\left\{\frac{\nu_{jl}^S}{\nu_{j\Phi}}\right\} < r_{lj} > + \frac{e_jA_3}{m_j}\left\{\frac{1}{\nu_{j\Phi}}\right\} \end{aligned} \quad (7.2)$$

where

$$\frac{f_{j0}'}{f_{j0}} = \left[A_{1j} + \frac{e_j < \Phi >'}{T_j} + \left(\frac{m_jE^*}{T_j}\right)A_{2j}\right]$$

By setting $A_{1j} = A_{2j} = A_3 = 0$, we find that $< u_j >= - < \Phi >' /B_\theta^0$, which is the common plasma rotation velocity and, hence, does not contribute to the parallel current.

7.2 Parallel Conductivity

We now compute the component of the parallel current due to the parallel ohmic electric field. Setting $A_{1j} = A_{2j} =< \Phi >'= 0$ in Eq. 7.2, we note that the electron parallel velocity is much larger than the ion and impurity parallel velocities. In fact, $< u_e > / < u_i >\sim \mathcal{O}(\sqrt{m_i/m_e})$. Hence, we consider only the electron contribution. Furthermore, as discussed in Section 6.2.3, $< r_{ee} >\gg< r_{ie} >, < r_{Ie} >$ (see Eq. 6.16). Hence, we can write

$$< u_e >= -\left[\left\{\frac{f_{t\Phi}\nu_{ee}^S}{\nu_{e\Phi}}\right\} < r_{ee} > -\frac{eA_3}{m_e}\left\{\frac{f_{t\Phi}}{\nu_{e\Phi}}\right\}\right] + \left\{\frac{\nu_{ee}^S}{\nu_{e\Phi}}\right\} < r_{ee} > -\frac{eA_3}{m_e}\left\{\frac{1}{\nu_{e\Phi}}\right\} \quad (7.3)$$

To the order $f_{t\Phi}$, $< r_{ee} >$ is determined from Eq. 6.7 as

$$< r_{ee} >= \frac{-\frac{eA_3}{m_e}\left\{\frac{f_{c\Phi}\nu_{ec}^S}{\nu_{c\Phi}}\right\}}{\left[\left\{\nu_{ee}^S\right\} - \left\{f_{c\Phi}\frac{\nu_{ec}^S\nu_{ec}^S}{\nu_{c\Phi}}\right\}\right]} \quad (7.4)$$

Using Eq. 7.4 in 7.3, the parallel ohmic current can be written as

$$J = \frac{n_e e^2 A_3}{m_e}\left[\left\{\frac{f_{c\Phi}}{\nu_{e\Phi}}\right\} + \frac{\left\{f_{c\Phi}\frac{\nu^S_{ec}}{\nu_{c\Phi}}\right\}^2}{\left[\{\nu^S_{ee} - \left\{f_{c\Phi}\frac{\nu^S_{ec}\nu^S_{ec}}{\nu_{c\Phi}}\right\}\right]}\right] \tag{7.5}$$

In the absence of a significant poloidal electric field, the above expression reduces to the expression (38a) in Ref. [40]. The above equation is valid for an arbitrary number of species.

7.3 Bootstrap Current

We now compute the parallel currents due to the perpendicular gradients A_{1j} and A_{2j}. We begin by expressing Eq. 7.1 for the current in terms of the velocity differences. Rewriting 7.1 as

$$J = -\sum_k n_k e_k(< u_e > - < u_k >) + \sum_k n_k e_k < u_e >$$

and using quasineutrality, $\sum_k n_k e_k \simeq 0$, we obtain

$$J = -\sum_k n_k e_k(< u_e > - < u_k >) \tag{7.6}$$

Thus, to calculate the bootstrap current in a n-species plasma, we have to calculate the n-1 parallel velocity differences in the presence of the driving terms A_{1j} and A_{2j}. We will follow the procedure used by Hirshman et al. [14] for calculating the velocity differences. Using the expressions for the restoring coefficients [Eq. 6.7], the parallel velocity [Eq. 7.2], and the particle flux in the absence of A_3 [Eq. 6.6], we obtain, correct to first order in $f_{t\Phi}$, the following expression for the parallel friction [see Appendix C for details]

$$\begin{aligned} < R_{jk} > \;=\; & -m_j n_j \{\nu^S_{jk}\}\Big[\,(< u_j > - < u_k >) + (u^0_{jk,\Phi} - u^0_{kj,\Phi}) \\ & + \sum_l \Big[\Delta^{jk}_l[(< u_l > - < u_j >) + u^0_{lj,\Phi}] \\ & - \Delta^{kj}_l[(< u_l > - < u_k >) + u^0_{lk,\Phi}]\Big]\Big] \end{aligned} \tag{7.7}$$

where

$$u^0_{pq,\Phi} = \left(\frac{e_p B^0_\theta}{m_p n_p}\right) \frac{f_t \Gamma_{p\Phi}}{\{f_{t\Phi}\nu^D_p\}} \gamma^{pq}_{n\Phi} + \left(\frac{T_p}{e_p B^0_\theta}\right) f_t \gamma^{pq}_{T\Phi} A_{2p} \tag{7.8}$$

and

$$\gamma^{pq}_{n\Phi} = \frac{1}{f_t}\left[\left\{f_{t\Phi}\frac{\nu^S_{pq}\nu^D_p}{\nu^S_p}\right\}\frac{1}{\{\nu^S_{pq}\}} - \left\{f_{t\Phi}\frac{\nu^D_p}{\nu^S_p}\right\}\right] \tag{7.9}$$

$$\gamma^{pq}_{T\Phi} = \frac{\left\{f_{t\Phi}\nu^D_p\left(\frac{m_p E^*}{T_p}\right)\right\}}{\{f_{t\Phi}\nu^D_p\}}\gamma^{pq}_{n\Phi} - \frac{1}{f_t}\left[\left\{f_{t\Phi}\left(\frac{m_p E^*}{T_p}\right)\frac{\nu^S_{pq}\nu^D_p}{\nu^S_p}\right\}\frac{1}{\{\nu^S_{pq}\}} - \left\{f_{t\Phi}\left(\frac{m_p E^*}{T_p}\right)\frac{\nu^D_p}{\nu^S_p}\right\}\right] \tag{7.10}$$

$$\Delta^{pq}_l = \left[\left\{\frac{\nu^S_{pq}\nu^S_{pl}}{\nu^S_p}\right\}\frac{1}{\{\nu^S_{pq}\}} - \left\{\frac{\nu^S_{pl}}{\nu^S_p}\right\}\right] \tag{7.11}$$

The above expression for $< R_{jk} >$ is accurate to the order Δ^{pq}_l ($\Delta^{pq}_l < 1$). Consistent with our approach in Section 6.3, we have used $\nu_{p\Phi} \simeq \nu^S_p$ in deriving the above expressions. We note that the quantities $u^0_{pq,\Phi}$, $\gamma^{pq}_{n\Phi}$, and $\gamma^{pq}_{T\Phi}$ have a form similar to those of u^0_{pq}, γ^{pq}_n, and γ^{pq}_T defined by Eqs. (51a), (51c), and (51d) in Ref. [14]. The expression for Δ^{pq}_l is identical to that given by Eq. (51b) in Ref. [14]. The difference between $u^0_{pq,\Phi}$, $\gamma^{pq}_{n\Phi}$, and $\gamma^{pq}_{T\Phi}$ and the corresponding quantities in Ref. [14] is due to the energy dependence of the quantity $f_{t\Phi}$ when $\tilde{\Phi}(\theta) \neq 0$. Setting $\tilde{\Phi}(\theta) = 0$ causes the differences to vanish.

An important point concerns the quantity $\gamma^{pq}_{n\Phi}$. As pointed out by Hirshman et al. [14], in the absence of a poloidal potential variation, $\gamma^{pq}_{n\Phi} = \gamma^{pq}_n \neq 0$ when $\nu^S_{pq} \neq \nu^D_{pq}$. In other words, the component of the parallel friction proportional to γ^{pq}_n is driven by the difference in the slowing down and pitch angle diffusion frequencies. Setting $\nu^S_{pq} = \nu^D_{pq}$ causes this component of the friction to vanish. In the presence of a poloidal potential variation, setting $\nu^S_{pq} = \nu^D_{pq}$ does not cause $\gamma^{pq}_{n\Phi}$ to vanish. In this case, the component of the parallel friction proportional to $\gamma^{pq}_{n\Phi}$ is driven by the difference between ν^S_{pq} and ν^D_{pq} as well as the energy dependence of the neoclassical factor $f_{t\Phi}$.

Using the expression 7.7 for the parallel friction in Eq. 6.2 for the particle flux and retaining only the gradient terms, we obtain the following equation for the parallel

velocity differences [see Appendix C for details]

$$\sum_k m_j n_j \bar{\nu}^S_{jk}(< u_j > - < u_k >) = \Gamma_{j\Phi}(e_j B^0_\theta) + < R_{j0,\Phi} > \tag{7.12}$$

where

$$\bar{\nu}^S_{jk} = \{\nu^S_j\}\left\{\frac{\nu^S_{jk}}{\nu^S_j}\right\} + \sum_l \{\nu^S_{jl}\}\Delta^{lj}_k \tag{7.13}$$

and

$$< R_{j0,\Phi} >= m_j n_j \sum_k \left[\{\nu^S_j\}\left\{\frac{\nu^S_{jk}}{\nu^S_j}\right\} u^0_{kj,\Phi} - [\{\nu^S_{jk}\}u^0_{jk,\Phi} - \sum_l \{\nu^S_{jk}\}\Delta^{kj}_l u^0_{lk,\Phi}]\right] \tag{7.14}$$

Here, $\bar{\nu}^S_{jk}$ is identical to the quantity $\bar{\nu}^{ab}_S$ and $< R_{j0,\Phi} >$ is similar in its form to $\bar{R}_{a0}$ in Ref. [14]. Eq. 7.12 provides an expression for the (n-1) parallel velocity differences that can be used in the equation 7.6 to obtain the bootstrap current. We will explicitly evaluate the bootstrap current coefficients for a 3-species plasma in Section 7.4.2.

7.4 Results and Discussion

We now present the results on parallel conductivity and bootstrap current in a multi-species tokamak. For simplicity, we consider a large aspect ratio tokamak and make use of the approximation $\nu_{j\Phi} \simeq \nu^S_j$ in our calculations [see the discussion in Section 6.3]. The results on parallel conductivity are valid for a plasma with an arbitrary number of ion species. Due to algebraic complexity, we limit our consideration of bootstrap current to a two-ion species plasma.

7.4.1 Neoclassical Conductivity

Writing the expression 7.5 for the parallel ohmic current as

$$J = \sigma_\Phi E^0_\parallel \tag{7.15}$$

where

$$\sigma_\Phi = \frac{n_e e^2}{m_e}\left[\left\{\frac{f_{c\Phi}}{\nu_{e\Phi}}\right\} + \frac{\left\{f_{c\Phi}\frac{\nu^S_{ec}}{\nu_{c\Phi}}\right\}^2}{\left[\{\nu^S_{ee} - \left\{f_{c\Phi}\frac{\nu^S_{ec}\nu^S_{ec}}{\nu_{c\Phi}}\right\}\right]}\right] \tag{7.16}$$

A brief list of symbols relevant for the results in Chapter VII. (See page 116 in Chapter VI for additional symbols.)

X_0	$e\Phi_c/\epsilon T$, is the magnitude of the poloidal potential variation. Φ_c is the amplitude of the poloidal potential variation. $X_0 \simeq 0$ in the standard neoclassical theory
Z_{eff}	$\sum_{j\neq e} n_j z_j^2/n_e$
$L^k_{3n,\Phi}$, L^k_{3n}	Bootstrap current coefficients in the presence (subscript Φ) and absence of a significant poloidal potential variation respectively
F^k_{3n}	$L^k_{3n,\Phi}/L^k_{3n}$ is the transport enhancement factor
$\sigma_{NC,\Phi}$, σ_{NC}	Neoclassical conductivity reduction factor in the presence (subscript Φ) and absence of a poloidal electric field respectively
F^e_{33}	$\sigma_{NC,\Phi}/\sigma_{NC}$ is the enhancement (or reduction) of the neoclassical conductivity reduction factor
$J_{nc,\Phi}$, J_{nc}	Bootstrap (neoclassical) current in the presence (subscript Φ) and absence of a poloidal electric field respectively
α_n, α_T	Density and temperature profile exponents defined by $$n_j(r) = n_{j0}(1-\rho^2)^{\alpha_n};\ T_j(r) = T_{j0}(1-\rho^2)^{\alpha_T}$$ where $\rho = r/R$.

For a large aspect ratio tokamak, we can write σ_Φ as

$$\sigma_\Phi = \sigma_{CL} - f_t \sigma_{NC,\Phi} \tag{7.17}$$

where σ_{CL}, the conductivity in a plasma with a uniform magnetic field, is given by

$$\sigma_{CL} = \frac{n_e e^2}{m_e}\left[\frac{1}{\{\nu_e^S\}} + \frac{\left\{\frac{\nu_{ec}^S}{\nu_e^S}\right\}^2}{\left\{\frac{\nu_{ec}^S(\nu_e^S-\nu_{ec}^S)}{\nu_e^S}\right\}}\right] \tag{7.18}$$

and $\sigma_{NC,\Phi}$, the neoclassical conductivity reduction factor, is given by

$$\sigma_{NC,\Phi} = \frac{n_e e^2}{f_t m_e}\left[\left\{\frac{f_{t\Phi}\nu_e^D}{(\nu_e^S)^2}\right\} + \frac{2\left\{\frac{\nu_{ec}^S}{\nu_e^S}\right\}\left\{\frac{f_{t\Phi}\nu_{ec}^S\nu_e^D}{(\nu_e^S)^2}\right\}}{\left\{\frac{\nu_{ec}^S(\nu_e^S-\nu_{ec}^S)}{\nu_e^S}\right\}} + \frac{\left\{\frac{\nu_{ec}^S}{\nu_e^S}\right\}^2\left\{\frac{f_{t\Phi}(\nu_{ec}^S)^2\nu_e^D}{(\nu_e^S)^2}\right\}}{\left\{\frac{\nu_{ec}^S(\nu_e^S-\nu_{ec}^S)}{\nu_e^S}\right\}^2}\right] \tag{7.19}$$

Here the expression for $\sigma_{NC,\Phi}$ is accurate to the order $f_{t,\Phi}$. When $\tilde{\Phi}(\theta) \simeq 0$, the expression 7.15 for the parallel current reduces to Eq. 49 in Ref. [14]. Also, when $\nu_{jk}^S = \nu_{jk}^D$ and $\tilde{\Phi}(\theta) = 0$, the expression 7.15 reduces to Eq. (46) in Ref. [9].

In the standard neoclassical theory [$\tilde{\Phi}(\theta) \simeq 0$], σ_{NC} is only a function of Z_{eff}. In the present case, due to the energy dependence of the boundary between the trapped-untrapped regions [see Section 3.2], $\sigma_{NC,\Phi}$ is a function of the poloidal electric field. Consistent with our approach in the previous chapter, we define the enhancement factor for the neoclassical conductivity reduction as

$$F_{33} = \frac{\sigma_{NC,\Phi}}{\sigma_{NC}} \tag{7.20}$$

F_{33} is a function of Z_{eff} and, hence, is independent of the number of ion species. Fig. 7.1 shows the variation of F_{33} with the magnitude of the poloidal potential variation, X_0. The behavior of F_{33} is similar to that of the Ware pinch enhancement factor F_{13}. When $\Phi_{in} < \Phi_{out}$ (as during ICRH or NBI), B-trapping of the electrons is enhanced by the potential variation. The monotonic increase in F_{33} seems to reflect the increase in trapping. As discussed in Section 6.3.1, the situation is somewhat complicated when $\Phi_{in} > \Phi_{out}$. For the low energy particles there is a reduction in B-trapping, which is to some extent compensated by the presence of E-trapped particles. It appears

that for smaller values of X_0, the decrease in B-trapping is the dominant effect, while for larger values of X_0, increased E-trapping more than compensates for the decrease B-trapping. The behavior of F_{33} for $\Phi_{in} > \Phi_{out}$ seems to reflect this change in the trapped electron contribution.

Effect of Impurity Concentration

Fig. 7.2 shows the variation of the enhancement factor F_{33} with Z_{eff}. For $\Phi_{in} > \Phi_{out}$ with $X_0 > 1$ and for $\Phi_{in} < \Phi_{out}$, the enhancement factor F_{33} decreases, signifying a decrease in the neoclassical conductivity reduction factor. However, for $\Phi_{in} > \Phi_{out}$ and $X_0 \sim 1$, F_{33} increases with Z_{eff}.

Before we attempt an explanation of the behavior of F_{33} with an increase in the impurity content, we note that the neoclassical conductivity reduction factor $\sigma_{NC,\Phi}$ has three terms (see Eq. 7.19). The first term in Eq. 7.19 contains primarily the effect of electron collisions with main ions and impurity ions, while the other two terms depend mainly on electron-electron collisions. As pointed out by Hirshman et al. [10], an increase in the impurity content causes a decrease in the neoclassical conductivity reduction by increasing the electron-ion collisions as well as by decreasing the effect of electron-electron collisions. The former effect results in a decrease in the first term in Eq. 7.19, while the latter effect causes a reduction in the last two terms in Eq. 7.19.

The presence of a poloidal electric field affects $\sigma_{NC,\Phi}$ primarily by affecting the fraction of trapped particles. When $\Phi_{in} > \Phi_{out}$ and $X_0 \sim 1$, the trapped electron fraction decreases in the region of the velocity space where $v \sim v_{th}$. [We note that the major contribution to velocity integrals of the type $\{F(v)\}$ comes from the region where $v \sim \mathcal{O}(v_{th})$.] Hence, the conductivity reducing effect of impurity ions is weaker, giving rise to a slight increase in F_{33} with Z_{eff}. In all other cases, the fraction of trapped electrons in the region of the velocity space where $v \sim v_{th}$ increases, and

hence the conductivity reducing effect of impurity ions is stronger. This results in a decrease in F_{33} with Z_{eff}. We note that the behavior of Ware pinch enhancement factor F_{13}^{ϵ} as a function of Z_{eff} is similar to that of F_{33}. Hence, the present discussion applies to the behavior of F_{13}^{ϵ} as well.

Comparison With Previous Results

Comparison of the results obtained in this work with those obtained by Chang [12] in the absence of impurities indicates a $\sim 20\%$ discrepancy between the two results at $X_0 \simeq 4$. As with the Ware pinch enhancement factor, the values obtained in the present work are smaller than those obtained by Chang. It appears that the discrepancy decreases as X_0 becomes smaller. We note in passing that in Ref. [12] the analytical fit for the neoclassical conductivity reduction factor (α_3, g_{3e}) for the case $\Phi_{in} > \Phi_{out}$ does not seem to reproduce the curve shown in Fig. 12 [12]. Our comparison here is with the curve in Fig. 12 in Ref. [12].

Finally, we note that Chang [12] concludes that the presence of an impurity species in modest amounts $(n_Z Z << n_e)$ does not alter the transport enhancement factors calculated for an electron-ion plasma. As can be seen from Fig. 7.2, this clearly is not the case. While the effect of impurities on electron diffusion is insignificant, the effect is significant for the Ware pinch and conductivity reduction factor, especially at $X_0 > 1$. As can be seen from Fig. 7.2, even for Z_{eff} close to 1, the change in the enhancement factor F_{33} seems to be significant. It appears that the cause of the discrepancy can be found in the way Chang treats the electron collision term. The electron collision term C_e can be written as $C_e = C_{ee} + C_{ei} + C_{eI}$. If one neglects electron-electron collisions, as Chang seems to do, then $C_e = C_{ei} + C_{eI} \simeq (\nu_{ei}^D + \nu_{eI}^D)\mathcal{L} \simeq Z_{eff}\nu_{ei}^D\mathcal{L}$, where $\mathcal{L}$ is the Lorentz operator and $Z_{eff} = \sum_{j\neq e} n_j Z_j^2/n_e$. In this case, the effect of including an impurity species is equivalent to replacing ν_{ei}^D by $Z_{eff}\nu_{ei}^D$ in the expressions for enhancement factors for a pristine plasma. Z_{eff} cancels leaving the

enhancement factors unaltered. In the present work, the results on diffusion as well as Ware pinch and conductivity were obtained in the presence of electron-electron collision terms. In this case, $C_e \simeq (\nu_{ee} + Z_{eff}\nu_{ei}^D)\mathcal{L}$ and Z_{eff} does not cancel when we compute the enhancement factors.

7.4.2 Bootstrap Current

The bootstrap current is obtained using Eq. 7.6 and the expression for the parallel velocity difference, Eq. 7.12. As the solution of the simultaneous equations [Eqs. 7.12] is complicated for a general multispecies plasma, we illustrate the bootstrap current calculations for a two ion species plasma. Unlike Ref. [14], our calculations are valid for a plasma with an impurity species of arbitrary mass.

Using Eq. 7.12, we obtain the following expressions for the velocity differences for a two ion species plasma

$$< u_e > - < u_i >= \frac{< R_{e\Phi} >}{m_e n_e \bar{\nu}_{ei}^S}\left[1 - \frac{1}{\bar{\nu}}\right] - \frac{< R_{I\Phi} >}{m_I n_I \bar{\nu}_{Ii}^S}\frac{1}{\bar{\nu}}\frac{\bar{\nu}_{iI}^S}{\bar{\nu}_{ie}^S} - \frac{< R_{i\Phi} >}{m_i n_i \bar{\nu}_{ie}^S}\frac{1}{\bar{\nu}} \tag{7.21}$$

$$< u_e > - < u_I >= \frac{< R_{e\Phi} >}{m_e n_e \bar{\nu}_{eI}^S}\frac{1}{\bar{\nu}} + \frac{< R_{I\Phi} >}{m_I n_I \bar{\nu}_{Ii}^S}\frac{1}{\bar{\nu}}\frac{\bar{\nu}_{iI}^S}{\bar{\nu}_{ie}^S}\frac{\bar{\nu}_{ei}^S}{\bar{\nu}_{eI}^S} + \frac{< R_{i\Phi} >}{m_i n_i \bar{\nu}_{ie}^S}\frac{1}{\bar{\nu}}\frac{\bar{\nu}_{ei}^S}{\bar{\nu}_{eI}^S} \tag{7.22}$$

where

$$< R_{j\Phi} >= \Gamma_{j\Phi}(Z_j e B_\theta^0) + < R_{j0,\Phi} >$$

and

$$\bar{\nu} = 1 - \frac{\bar{\nu}_{ei}^S \bar{\nu}_{iI}^S \bar{\nu}_{Ie}^S}{\bar{\nu}_{eI}^S \bar{\nu}_{ie}^S \bar{\nu}_{Ii}^S}$$

Using the above expressions for the velocity differences and the expression 7.12 for the current, we can write the gradient driven current as [14]

$$J_{nc,\Phi} = \sum_{k;m=1,2} T_k L_{3m,\Phi}^k A_{mk} \tag{7.23}$$

where the expressions for the bootstrap current coefficients are of the form

$$L_{31,\Phi}^k = L_0 \frac{C_{ei}}{T_k}\left[\hat{C}_{eI,\Phi} L_{11,\Phi}^{ek} + \hat{C}_{iI,\Phi} L_{11,\phi}^{ik}\right] \tag{7.24}$$

$$L_{32,\Phi}^k = L_0 \frac{C_{ei}}{T_k}\left[\hat{C}_{eI,\Phi} L_{12,\Phi}^{ek} + \hat{C}_{iI,\Phi} L_{12,\phi}^{ik} + \hat{D}_{k\Phi}\right] \tag{7.25}$$

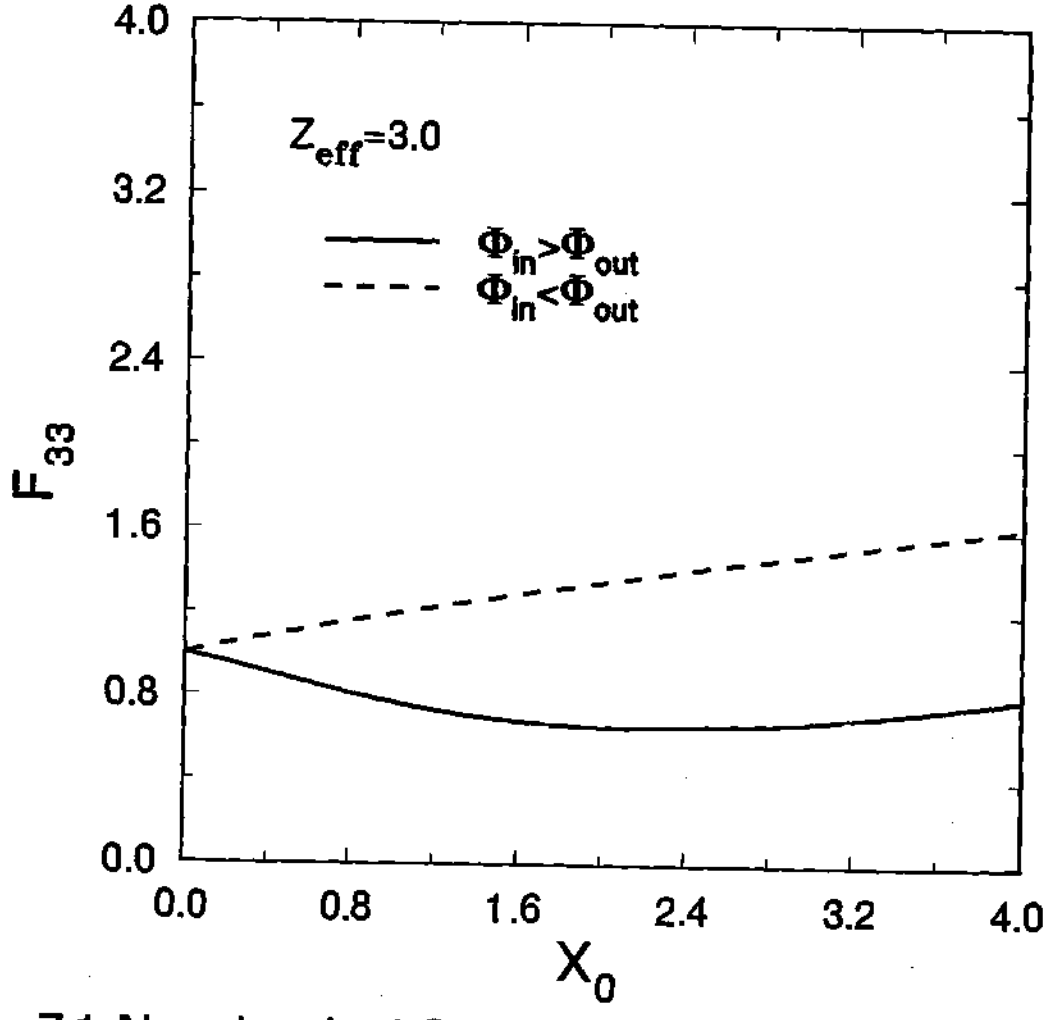

Fig. 7.1 Neoclassical Conductivity Reduction As a Function of X_0

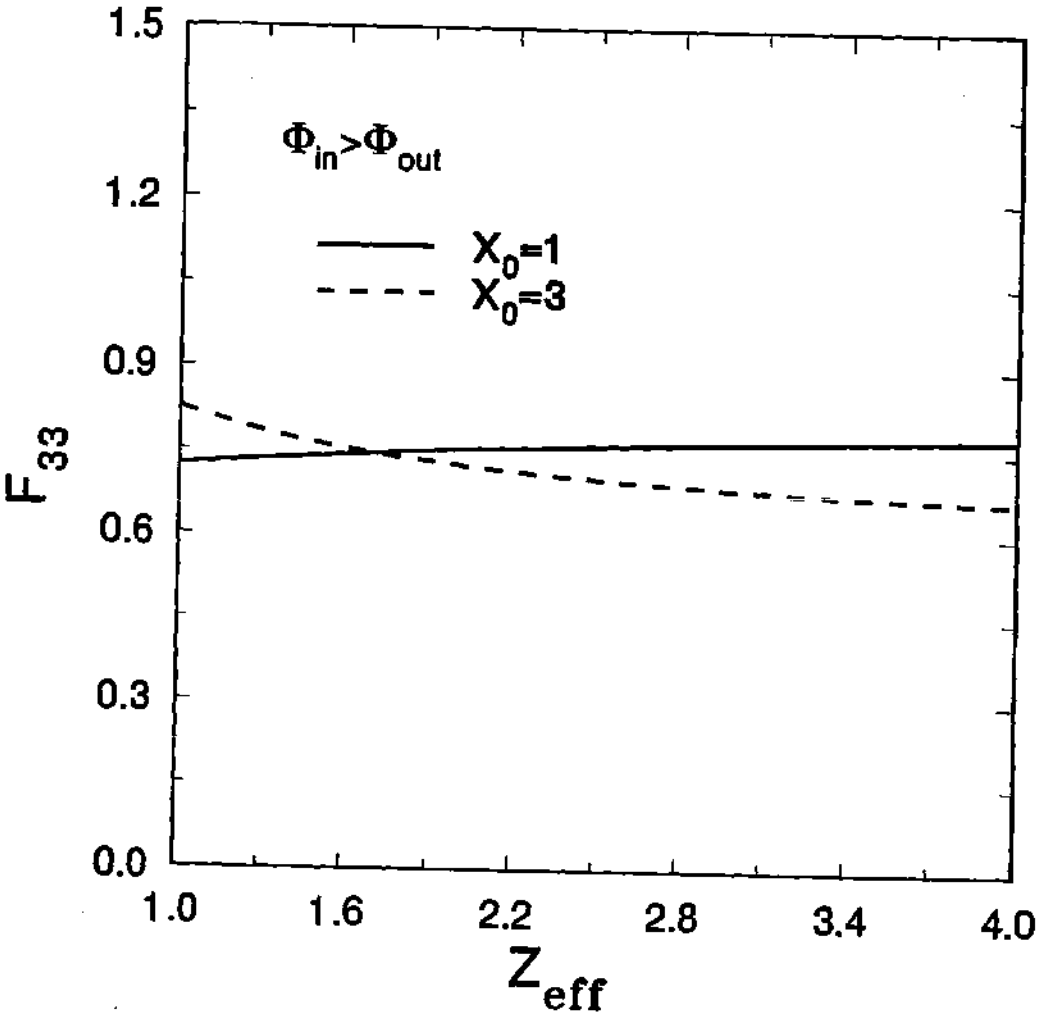

Fig. 7.2 Neoclassical Conductivity Reduction as a Function of Z_{eff}

where $L^{jk}_{1n,\Phi}$ are the diffusion coefficients [see Eq. 6.12] and

$$L_0 = -f_t \frac{n_e}{B^0_\theta}$$

$$C_{ei} = \frac{n_i}{n_e} \frac{eZ_i}{f_t} \frac{B^0_\theta}{\bar{\nu}^S_{ei} \bar{\nu}}$$

The quantities $\hat{C}_{eI,\Phi}$, $\hat{C}_{iI,\Phi}$, and $\hat{D}_{k,\Phi}$ are complicated functions of the collision frequencies and they are given in Appendix C. Our calculations indicate that

$$\frac{\hat{C}_{eI,\Phi}}{\hat{C}_{iI,\Phi}} \sim \mathcal{O}\left(\sqrt{\frac{m_i}{m_e}}\right) \tag{7.26}$$

From the expressions 7.24 and 7.25 for bootstrap current coefficients and the expressions for the diffusion coefficients $L^{jk}_{11,\Phi}$ in Eq. 6.12, it is easy to see that

$$L^e_{31,\Phi} - Z_i L^i_{31,\Phi} = Z L^Z_{31,\Phi} \tag{7.27}$$

As mentioned in Ref. [14], this is a consequence of ambipolarity of the particle fluxes.

Before proceeding with a discussion of the results, we wish to illustrate the relationship between the bootstrap current and the cross field diffusive particle fluxes. Using the expressions for the particle flux [Eq. 6.12] in Eq. 7.23, we can write the bootstrap current as

$$J_{nc,\Phi} = L_0 C_{ei} \left[\hat{C}_{eI,\Phi} \Gamma_{e\Phi} + \hat{C}_{iI,\Phi} \Gamma_{i\Phi} + \sum_k \hat{D}_{k\Phi} A_{2k} \right] \tag{7.28}$$

For simplicity, we consider the case of zero temperature gradients, i.e., $A_{2k} = 0$. In this case, the last term in Eq. 7.28 vanishes. In the absence of a significant impurity concentration, $\Gamma_{e\Phi} \sim \Gamma_{i\Phi}$ and, as a consequence of Eq. 7.26, the second term in Eq. 7.28 negligible. In the presence of a significant impurity concentration, a similar situation obtains after the stationary state ($\Gamma_{e\Phi} \sim \Gamma_{i\Phi}$) is reached. Before the stationary state is reached,

$$\frac{\Gamma_{e\Phi}}{\Gamma_{i\Phi}} \sim \mathcal{O}\left(\sqrt{\frac{m_i}{m_e}}\right)$$

and the second term in Eq. 7.28 is comparable to the first term. Thus, in the presence of impurities enhancement of the ion flux due to a poloidal electric field will have a significant effect on the bootstrap current. We note here that an analysis of the relation between the particle fluxes and the bootstrap current similar to the one given here has been carried out by Connor [9] in the absence of a poloidal electric field.

Finally, we write the expression for the bootstrap current in a form which facilitates comparison with Chang's [12] results in the absence of impurities.

$$\begin{aligned} J_{nc,\Phi} &= T_e L^e_{31,\Phi}\left(1+\frac{T_i}{T_e Z_i}\right)\frac{n_e'}{n_e} + T_e\left[L^e_{31,\Phi} + (L^e_{32,\Phi} - \frac{5}{2}L^e_{31,\Phi})\right]\frac{T_e'}{T_e} \\ &+ T_e L^e_{31,\Phi}\left(\frac{T_i}{Z_i T_e}\right)\left(\frac{Z_i L^i_{32,\Phi}}{L^e_{31,\Phi}} - \frac{3}{2}\right)\frac{T_i'}{T_i} + T_i L^i_{31,\Phi}\left(\frac{n_i'}{n_i} - \frac{n_e'}{n_e}\right) \\ &- \left(\frac{ZT_i}{Z_i}\right)L^Z_{31,\Phi}\left(\frac{n_e'}{n_e}\right) + \frac{3}{2}\left(\frac{ZT_i}{Z_i}\right)L^Z_{31,\Phi}\left(\frac{T_i'}{T_i}\right) + T_Z L^Z_{31,\Phi}\left(\frac{n_Z'}{n_Z}\right) \\ &+ T_Z(L^Z_{32,\Phi} - \frac{3}{2}L^Z_{31,\Phi})\left(\frac{T_Z'}{T_Z}\right) \end{aligned} \tag{7.29}$$

We note that, of the six transport coefficients L^k_{3n} $(n = 1,2; k = e,i,Z)$, only five are independent. The coefficient L^Z_{31} is dependent on the transport coefficients L^e_{31} and L^i_{31} (see Eq. 7.27). Furthermore, the coefficient L^Z_{32} is generally small. Hence, we will primarily concentrate on the behavior of four transport coefficients, L^k_{3n} $(n = 1,2; k = e,i)$.

We now present the results of our calculations of the effect of a poloidal electric field upon the bootstrap current coefficients. We consider a two ion species plasma in which the impurity is carbon. We will later comment on the effect of impurity species on the bootstrap current coefficients.

Effect of Poloidal Electric Field

We define the bootstrap current enhancement factor as

$$F^k_{3m} = \frac{L^k_{3m,\Phi}}{L^k_{3m}} \tag{7.30}$$

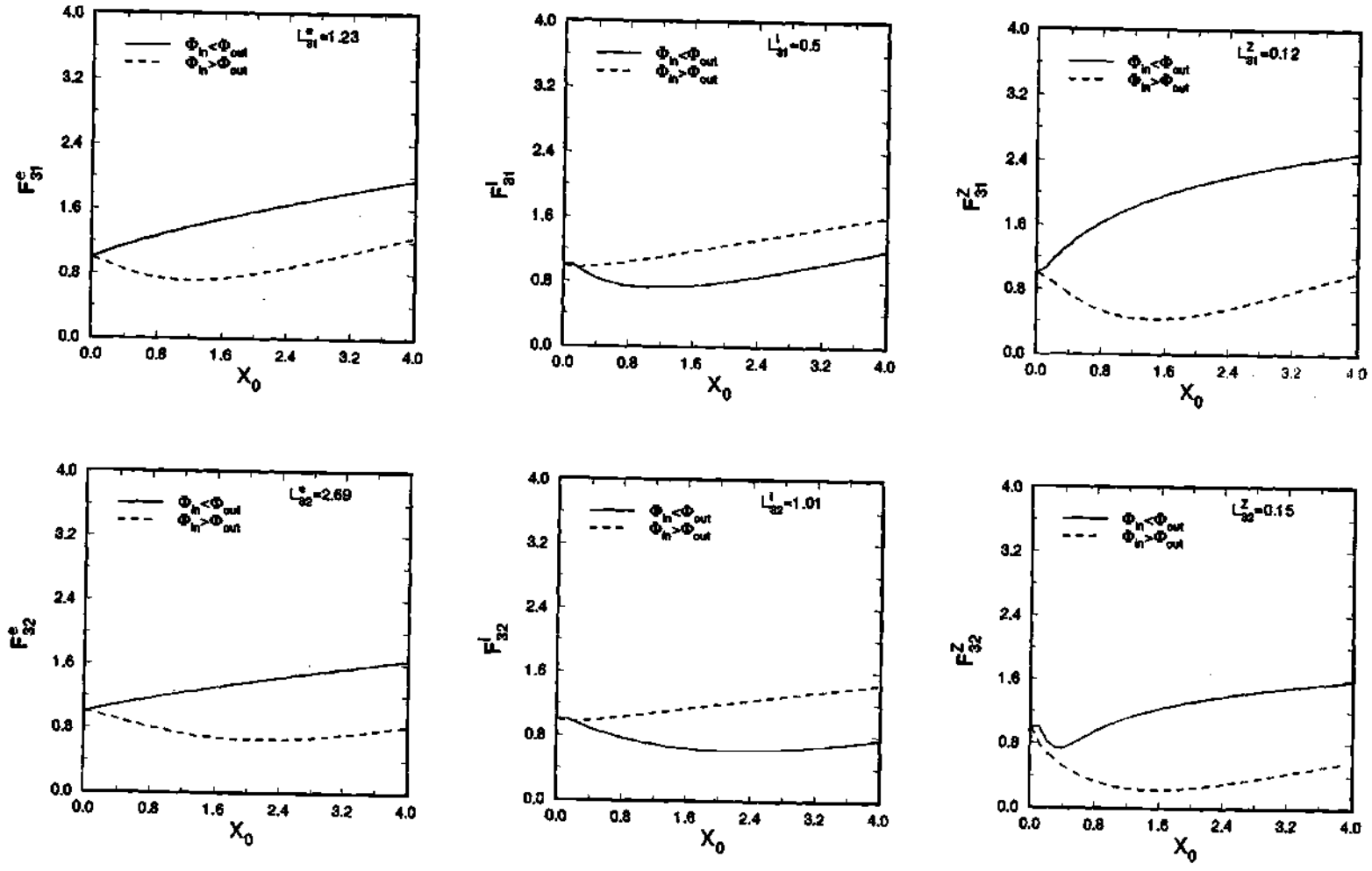

Fig. 7.3 Bootstrap Current Enhancement Factors
(Impurity: Carbon, Z_{eff}=3.0)

where L^k_{3m} are the transport coefficients in the absence of a poloidal electric field. Variation of the bootstrap current enhancement factors F^k_{3m} as a function of the poloidal electric field is shown in Fig. 7.3. The magnitude of the transport coefficients when $\bar{\Phi}(\theta) = 0$ are also shown on Fig. 7.3. Due to Onsager symmetry [14], $L^e_{31} = L^e_{13}$, and hence, the variation of F^e_{31} with X_0 is identical to that of the Ware pinch enhancement factor, F^e_{13}. As can be seen from Fig. 7.3, enhancement of the bootstrap current coefficients over their magnitude for $\bar{\Phi}(\theta) = 0$ is at the most by a factor of 2. Furthermore, it is clear from Fig. 7.3 that electron and ion enhancement factors (F^e_{3n} and F^i_{3n}) behave differently for for $\Phi_{in} \lesssim \Phi_{out}$. Hence, the effect of a poloidal electric field upon the bootstrap current cannot be deduced easily from the behavior of the individual enhancement factors. We will evaluate the effect of the enhancement of bootstrap current coefficients and temperature/density profiles upon the magnitude of the bootstrap current later in this chapter.

Effect of Impurity concentration

Fig. 7.4 shows the variation of the bootstrap current enhancement factors F^e_{31}, F^e_{32}, F^i_{31}, and F^i_{32} as a function of the impurity concentration (Z_{eff}) for $X_0 = 1$. Due to Onsager symmetry, the variation of F^e_{31} is identical to that of F^e_{13}. As with the diffusion coefficients, the variation of the bootstrap enhancement factors with Z_{eff} is more pronounced for smaller values of Z_{eff} due to the increasingly important role being played by the impurity species in this range of Z_{eff}. As Z_{eff} increases, the transport enhancement factors asymptotically reach a constant value. The presence of an impurity species increases collisional coupling among the species, resulting in a decrease in L^e_{31} as well as L^i_{31}. The presence of a poloidal electric field in an impure plasma affects the bootstrap current primarily by increasing (or decreasing) the trapped ion and impurity fraction, and hence the collisional coupling between them. We recall here that the bootstrap current is primarily a trapped particle effect. When $\Phi_{in} < \Phi_{out}$, for

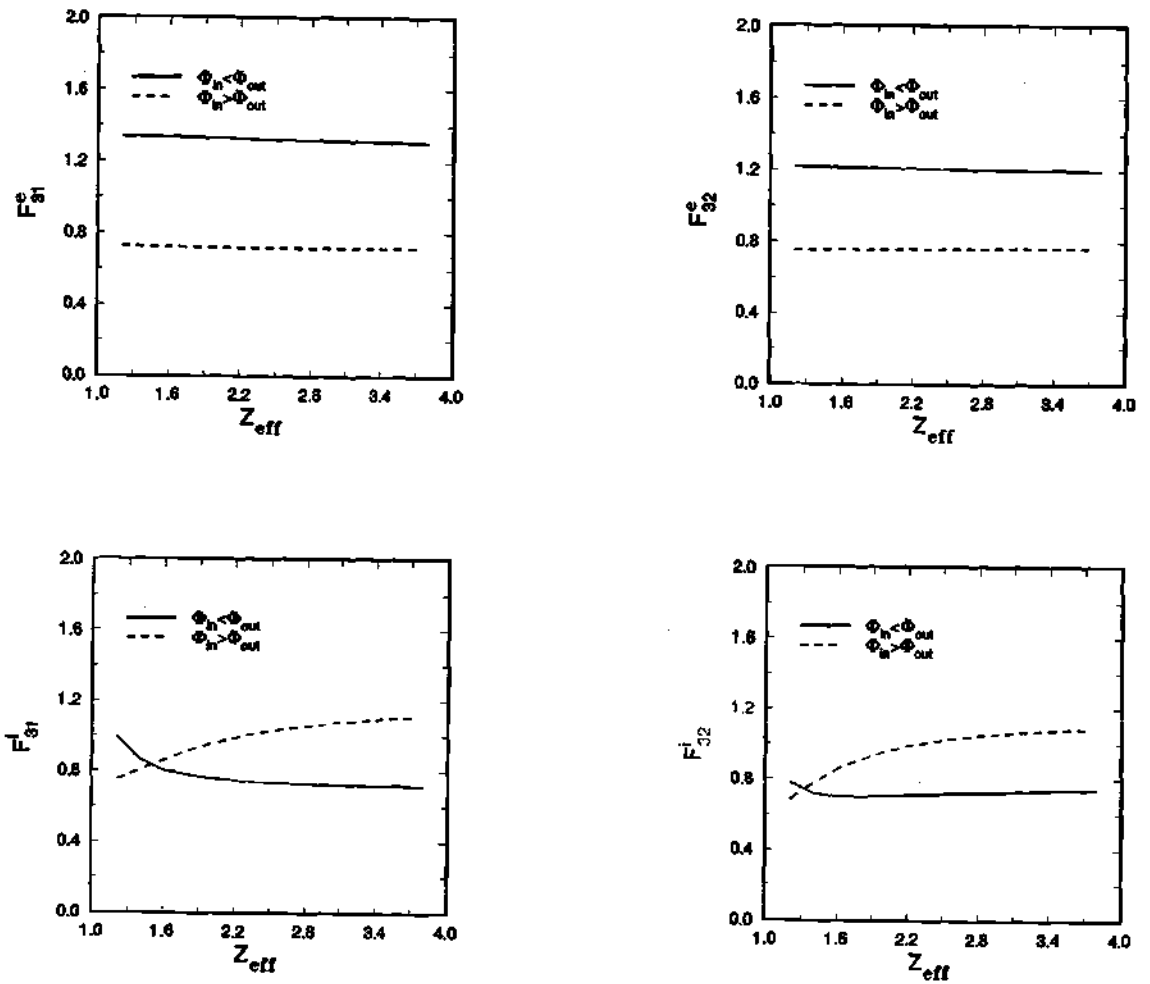

Fig. 7.4 Variation of Bootstrap Current Enhancement with Z_{eff}
(Impurity: Carbon, X_0=1.0)

moderate values of X_0 ($X_0 < 4$), the trapped ion population decreases, resulting in a decrease in F_{31}^i. For $\Phi_{in} > \Phi_{out}$, the opposite effect occurs, i.e., the trapped ion fraction increases, causing an increase in F_{31}^i.

Effect of Impurity Species

Comparison of the bootstrap current enhancement factors in the presence of different impurity species is meaningful for smaller impurity concentrations as the tolerable level of impurity content drops sharply for heavier impurities. The behavior of the electron enhancement factors F_{3n}^e is not significantly affected by the impurity species. As the impurity enhancement factors F_{3n}^Z are small in comparison with other enhancement factors, we will consider only the behavior of ion enhancement factors F_{3n}^i.

Table 7.1 shows the variation in F_{31}^i for $\alpha = 1$ at $X_0 = 1$. The behavior of F_{32}^i is similar to that of F_{31}^i. An explanation of the behavior of F_{31}^i in the presence of different impurity species is complicated by the fact that F_{31}^i is a function of Z_{eff}, Z, and m_Z in this case. Even when α is held constant, Z_{eff} varies from 1.33 for helium to 1.97 for tungsten. From Table 7.1, it appears that F_{31}^i generally decreases for $\Phi_{in} < \Phi_{out}$ and increases for $\Phi_{in} > \Phi_{out}$ when we change the impurity species from helium to tungsten (equivalent to changing Z_{eff}, Z, and m_Z). This behavior is similar to that of F_{31}^i when Z_{eff} is changed with a fixed impurity species (see the previous discussion on the effect of Z_{eff} on F_{31}^i). However, in the present case, the impurity charge and mass also change. An increase in Z leads to enhanced trapping of the impurity ions in the electrostatic potential well. This causes a reduction in the ion-impurity collisional coupling, which can enhance F_{31}^i. This seems to be the case for $\Phi_{in} < \Phi_{out}$ when the impurity species changes from iron to tungsten. Here, it appears that the transport reducing effect of Z_{eff} is being offset by the transport enhancing effect of increased Z.

Table 7.1: Effect of Impurity Species on Bootstrap Current Enhancement Factor ($X_0 = 1.0$)

Impurity	Z	m_Z/m_i	Z_{eff}	F^i_{31}	
				$\Phi_{in} < \Phi_{out}$	$\Phi_{in} > \Phi_{out}$
Helium	2	2	1.33	1.08	0.77
Carbon	6	6	1.71	0.79	0.89
Iron	26	28	1.92	0.67	1.09
Tungsten	60	92	1.97	0.67	1.18

Comparison with Previous Results

We now compare our results on the bootstrap current with the results obtained by Chang [12] in the absence of impurities and with those of Hirshman et al. [14] obtained in the presence of impurities for the case of negligible poloidal electric field.

1. **Comparison with Chang's Results**: Referring to Eq. 7.29, in the absence of impurities, $L^Z_{31,\Phi} = L^Z_{32,\Phi} = 0$, $n_i'/n_i = n_e'/n_e$, and the last five terms vanish. The resulting equation has the following form

$$J_{nc,\Phi} = T_e L^e_{31,\Phi}\left(1+\frac{T_i}{T_e Z_i}\right)\frac{n_e'}{n_e} + T_e\left[L^e_{31,\Phi} + (L^e_{32,\Phi} - \frac{5}{2}L^e_{31,\Phi})\right]\frac{T_e'}{T_e} + T_e L^e_{31,\Phi}\left(\frac{T_i}{Z_i T_e}\right)\left(\frac{Z_i L^i_{32,\Phi}}{L^e_{31,\Phi}} - \frac{3}{2}\right)\frac{T_i'}{T_i} \quad (7.31)$$

Using the expressions 7.24, 7.25 for the bootstrap current coefficients, and noting that in the absence of impurities the second term in 7.24 is negligible, we obtain

$$\frac{Z_i L^i_{32,\Phi}}{L^i_{31,\Phi}} = \frac{Z_i T_e}{Z_e T_i}\left[\frac{L^{ei}_{12,\Phi}}{L^{ee}_{11,\Phi}} + \frac{\hat{D}_{i\Phi}}{\hat{C}_{eI,\Phi} L^{ee}_{11,\Phi}}\right]$$

Numerical calculations yield $\hat{D}_{i\Phi} \simeq 0$ in the absence of impurities. Using the expressions for the diffusion coefficients $L^{ei}_{12,\Phi}$ and $L^{ee}_{11,\Phi}$ from Eq. 6.12, we obtain

$$\frac{Z_i L^i_{32,\Phi}}{L^i_{31,\Phi}} = \frac{\left\{f_{t\Phi}\nu^D_i\left(\frac{m_i E^*}{T_i}\right)\right\}}{\left\{f_{t\Phi}\nu^D_i\right\}} = y_{i\Phi}$$

With this result, the Eq. 7.31 has the same form as the expression for the bootstrap current obtained by Chang [12]

$$J_{nc,\Phi} = T_e(\alpha_3, g_{1e})_\Phi \left(1 + \frac{T_i}{T_e Z_i}\right) \frac{n_e'}{n_e} + T_e\left[\alpha_3, g_{1e})_\Phi + (\alpha_3, g_{2e})_\Phi\right] \frac{T_e'}{T_e}$$
$$+T_e(\alpha_3, g_{1e}) \left(\frac{T_i}{Z_i T_e}\right) \left[y - \frac{3}{2}\right] \frac{T_i'}{T_i} \qquad (7.32)$$

where the subscript Φ is used to indicate the value of the transport coefficient in the presence of a poloidal electric field.

We now compare the transport coefficients $(\alpha_3, g_{1e})_\Phi$ and y with the corresponding quantities $L^e_{31,\Phi}$ and $y_{i\Phi}$ in Eq. 7.31. (Apparently, Chang has not calculated $(\alpha_3, g_{2e})_\Phi$ in Ref. [12]). Onsager symmetry yields $(\alpha_3, g_{1e})_\Phi = (\alpha_1, g_{3e})_\Phi$ [8] and $L^e_{31,\Phi} = L^e_{13,\Phi}$ [14]. Hence, a comparison of (α_3, g_{1e}) and $L^e_{31,\Phi}$ is equivalent to the comparison of the Ware pinch coefficients (α_1, g_{3e}) and $L^e_{13,\Phi}$. Our previous comparison of the Ware pinch enhancement factors in Section 6.3.3 yields a significant discrepancy ($\sim 20\%$ at $X_0 = 4$) between the two results. However, a comparison of the variational parameter y with the quantity $y_{i\Phi}$ (see Section 6.3.1) yields very good agreement between the two quantities.

2. **Comparison with calculations by Hirshman et al.**: Finally, we point out that for $\bar{\Phi}(\theta) = 0$, our calculations agree with the transport coefficients calculated using the analytical expressions obtained by Hirshman et al. [14, 40] for a heavy impurity such as iron or tungsten. For lighter impurities, such as carbon or helium, the ion enhancement factors F^i_{3n} differ from those calculated using the expressions in Refs. [14,40] by less than 3% when the impurity content is low ($Z_{eff} < 1.5$). For a lighter impurity like carbon the difference in F^i_{3n} calculated using the two approaches can be as high as 20% for higher impurity concentrations ($Z_{eff} \simeq 3.0$). This is to be expected as the expressions in Refs. [14, 40] were obtained in the limit $m_Z/m_i \gg 1$. Nevertheless, the analytic expressions in Refs. [14, 40] provide a convenient means for calculating the bootstrap current

coefficients for most impurities and concentration if one could tolerate a discrepancy of the order $\sim 20\%$ for low Z impurities at higher concentrations. We have reproduced the analytical expressions for the bootstrap current coefficients from Refs. [14,40] in Appendix C.

Transport Enhancement of Bootstrap Current and Profile Effects

The bootstrap current depends upon the transport coefficients L_{3n}^{k} as well as the "driving forces" A_{1k} and A_{2k}. As the driving forces depend upon the density and temperature profiles, enhancement (or reduction) of bootstrap current is dependent on the enhancement (or reduction) of the transport coefficients as well as the electron and ion temperature/density profiles. In this section, we consider the profile effects as well as the enhancement of transport coefficients upon the magnitude of the bootstrap current.

We begin by considering a situation where the temperature and density profiles can be approximated by

$$T_j(r) = T_{j0}(1-\rho^2)^{\alpha_{Tj}}$$

and

$$n_j(r) = n_{j0}(1-\rho^2)^{\alpha_{nj}}$$

Here $\rho = r/a$ where a is the minor radius. For simplicity, we assume $T_e \simeq T_i \simeq T_Z$. With this,

$$\frac{T_j'}{T_j} = \frac{T'}{T} = -\frac{2\alpha_T}{a}\left(\frac{\rho}{1-\rho^2}\right)$$

and

$$\frac{n_j'}{n_j} = -\frac{2\alpha_{nj}}{a}\left(\frac{\rho}{1-\rho^2}\right)$$

Here, the prime denotes derivative with respect to the radial coordinate r. We shall further assume that Z_{eff} is constant in the core region of the plasma where the present

formalism is expected to be valid. This leads to

$$\frac{n_j^{'}}{n_j} = \frac{n^{'}}{n} = -\frac{2\alpha_n}{a}\left(\frac{\rho}{1-\rho^2}\right)$$

Hence,

$$A_{1k} = \frac{n_k^{'}}{n_k} - \frac{3}{2}\frac{T_k^{'}}{T_k} = \frac{2}{a}\left(\frac{\rho}{1-\rho^2}\right)\left[\frac{3}{2}\alpha_T - \alpha_n\right]$$

and

$$A_{2k} = \frac{T_k^{'}}{T_k} = -\frac{2}{a}\left(\frac{\rho}{1-\rho^2}\right)[\alpha_T]$$

With this, Eq. 7.23 for the bootstrap current can be written as

$$J_{nc,\Phi} = \frac{2T}{a}\frac{\rho}{1-\rho^2}\left[\alpha_T \sum_k \left(1.5L_{31,\Phi}^k - L_{32,\Phi}^k\right) - \alpha_n \sum_k L_{31,\Phi}^k\right] \tag{7.33}$$

We recall that the subscript Φ indicates the presence of a significant poloidal electric field. In the absence of poloidal electric field, we have

$$J_{nc} = \frac{2T}{a}\frac{\rho}{1-\rho^2}\left[\alpha_T \sum_k \left(1.5L_{31}^k - L_{32}^k\right) - \alpha_n \sum_k L_{31}^k\right] \tag{7.34}$$

Subtracting Eq. 7.34 from Eq. 7.33, we obtain the change in the bootstrap current due to inclusion of the effects of a poloidal electric field as

$$\begin{aligned} J_{nc,\Phi} - J_{nc} \;=\; & \frac{2T}{a}\frac{\rho}{1-\rho^2}\left[\alpha_T \sum_k \left[1.5\left(L_{31,\Phi}^k - L_{31}^k\right) - \left(L_{32,\Phi}^k - L_{32}^k\right)\right]\right. \\ & \left. -\alpha_n \sum_k \left(L_{31,\Phi}^k - L_{31}^k\right)\right] \end{aligned} \tag{7.35}$$

From the above equation, we can determine the relation between α_n and α_T for the change in the bootstrap current to be positive. Setting $J_{nc,\Phi} - J_{nc} \geq 0$, we obtain the following condition for the change in the bootstrap current due to inclusion of a poloidal electric field to be positive (i.e. for the poloidal electric field to enhance, rather than reduce, the bootstrap current)

$$\alpha_n > \frac{\sum_k \left(L_{32,\Phi}^k - L_{32}^k\right) - 1.5\sum_k \left(L_{31,\Phi}^k - L_{31}^k\right)}{\sum_k \left(L_{31}^k - L_{31,\Phi}^k\right)}\alpha_T \tag{7.36}$$

We note that the relationship between α_n and α_T depends upon the impurity species, concentration, and the sign and magnitude of the potential variation. As an example, we consider the case of carbon impurity with $Z_{eff} = 3.0$. When $\tilde{\Phi}(\theta) = 0$, we obtain

$$L_{31}^e = 1.23 \quad L_{31}^i = 0.5 \quad L_{31}^Z = 0.12 \quad \sum_k L_{31}^k = 1.85$$

$$L_{32}^e = 2.68 \quad L_{32}^i = 1.0 \quad L_{32}^Z = 0.15 \quad \sum_k L_{32}^k = 3.83$$

Here, note that L_{3n}^k is actually L_{3n}^k/L_0. For simplicity, we have suppressed the factor L_0. When $\tilde{\Phi}(\theta) \neq 0$ and $\Phi_{in} < \Phi_{out}$ (as during ICRH or NBI), we obtain the following enhancement factors.

When $X_0 = 1$

$$F_{31}^e = 1.3 \quad F_{31}^i = 0.72 \quad F_{31}^Z = 1.73 \quad \sum_k L_{31,\Phi}^k = 2.20$$

$$F_{32}^e = 1.2 \quad F_{32}^i = 0.73 \quad F_{32}^Z = 1.04 \quad \sum_k L_{32,\Phi}^k = 4.13$$

When $X_0 = 3$

$$F_{31}^e = 1.77 \quad F_{31}^i = 0.98 \quad F_{31}^Z = 2.31 \quad \sum_k L_{31,\Phi}^k = 2.96$$

$$F_{32}^e = 1.51 \quad F_{32}^i = 0.65 \quad F_{32}^Z = 1.47 \quad \sum_k L_{32,\Phi}^k = 4.95$$

When $\tilde{\Phi}(\theta) \neq 0$ and $\Phi_{in} > \Phi_{out}$ (as during ECRH), we obtain the following enhancement factors.

When $X_0 = 1$

$$F_{31}^e = 0.72 \quad F_{31}^i = 1.07 \quad F_{31}^Z = 0.47 \quad \sum_k L_{31,\Phi}^k = 1.49$$

$$F_{32}^e = 0.76 \quad F_{32}^i = 1.06 \quad F_{32}^Z = 0.27 \quad \sum_k L_{32,\Phi}^k = 3.16$$

When $X_0 = 3$

$$F_{31}^e = 1.01 \quad F_{31}^i = 1.44 \quad F_{31}^Z = 0.71 \quad \sum_k L_{31,\Phi}^k = 2.06$$

$$F_{32}^{e} = 0.70 \quad F_{32}^{i} = 1.32 \quad F_{32}^{Z} = 0.39 \quad \sum_{k} L_{32,\Phi}^{k} = 3.28$$

Using these values, we find that the following requirements must be satisfied in order to obtain an enhancement ($J_{nc,\Phi} - J_{nc} > 0$) in the bootstrap current due to a poloidal electric field.

(a)When $\Phi_{in} < \Phi_{out}$:

For $X_0 = 1$, $\alpha_n > 0.64\alpha_T$.

For $X_0 = 3$, $\alpha_n > 0.49\alpha_T$.

(b)When $\Phi_{in} > \Phi_{out}$:

For $X_0 = 1$, $\alpha_n < -0.36\alpha_T$.

For $X_0 = 3$, $\alpha_n > 4.12\alpha_T$.

Figures 7.5 and 7.6 show the relation between α_n and α_T, as a function of X_0, that is needed for an enhancement of the bootstrap current. Under conditions that prevail in most tokamaks, the presence of a poloidal electric field such that $\Phi_{in} > \Phi_{out}$ (as during ECRH) results in a reduction in the bootstrap current (Fig. 7.5). On the other hand, when $\Phi_{in} < \Phi_{out}$ (as during ICRH of NBI), the bootstrap current increases if the density profile is more peaked than roughly the square root of the temperature profile, i.e., $\alpha_n > 0.5\alpha_T$ (see Fig. 7.6). The behavior of α_n/α_T depicted in Figs. 7.5 and 7.6 follows from the behavior of the enhancement factors F_{3n}^{k} as a function of X_0. We further note that varying Z_{eff} from 2 to 4 has only a minor effect on the behavior of α_n/α_T shown in Figs. 7.5 and 7.6.

Finally, in the present study we have used the same profile exponents for electrons, ions, and impurities (i.e. $\alpha_{nj} = \alpha_n$ and $\alpha_{Tj} = \alpha_T$). It turns out that the conclusions drawn here are valid even when $\alpha_{nj} \neq \alpha_n$ and $\alpha_{Tj} \neq \alpha_T$, as the next example demonstrates. It appears that the relation between the temperature and density profiles is more significant than minor differences in the temperature/density profiles of different species.

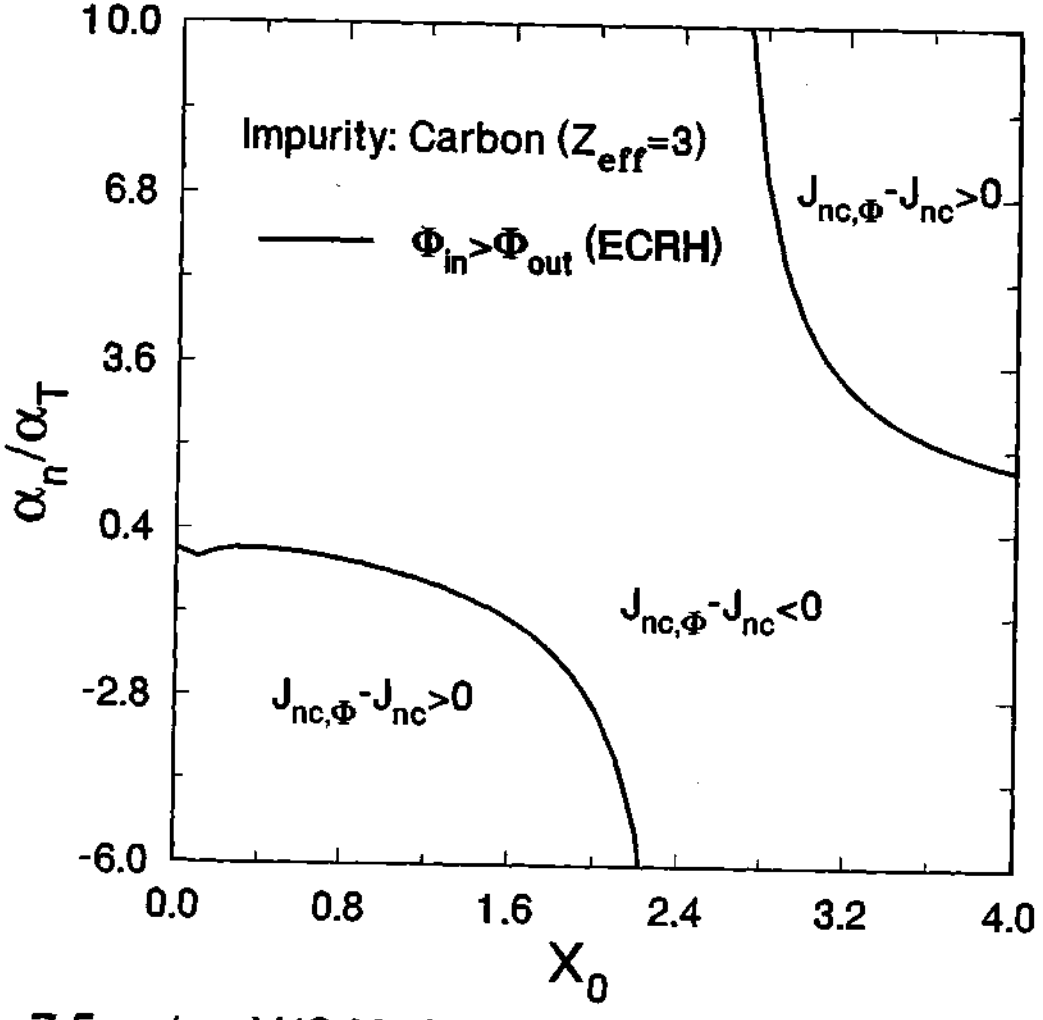

Fig. 7.5 α_n/α_T V/S X_0 for Bootstrap Current Enhancement ($\Phi_{in}>\Phi_{out}$)

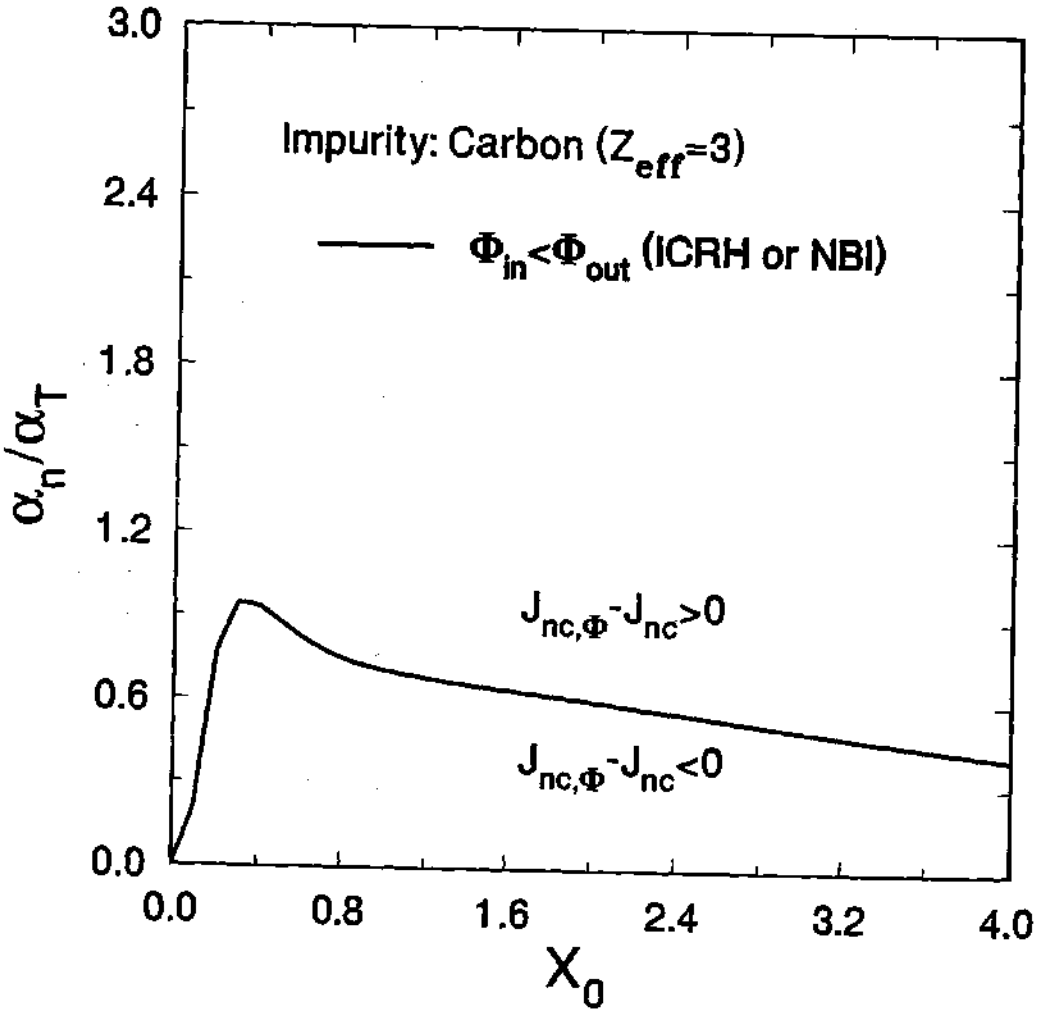

Fig. 7.6 α_n/α_T V/S X_0 for Bootstrap Current Enhancement ($\Phi_{in}<\Phi_{out}$)

Example

Finally, we consider the example of a JET discharge with combined ICRH and NBI. The density and temperature profiles for a pellet fueled shot are shown in Fig. 7.7. The profiles in Fig. 7.7 and the following parameters are taken from Ref. [7]. In the present case, clearly $\alpha_T > \alpha_n$.

Minor radius a=1.16 m, $P_{ICRH} \simeq 12.5\ MW$, $P_{NBI} \simeq 5.2\ MW$, $R = 3\ m$, $n_{e0} = 6.47 \times 10^{19}\ m^{-3}$, $T_{e0} = 11.8\ keV$, $T_{i0} = 8.9\ keV$.

Consistent with the large aspect ratio approximation, we consider a point close to the center. Specifically, we take $\epsilon = 0.04$. This gives $r = 0.12\ m$ and $\rho = 0.1$. At this radius, all the relevant quantities can be estimated from Fig. 7.7. Assuming $T_i = T_Z$,

$$\frac{T_i'}{T_i} = \frac{T_Z'}{T_Z} \simeq -1.2\ m^{-1}$$

$$\frac{T_e'}{T_e} \simeq -2.1\ m^{-1}$$

$$\frac{n_e'}{n_e} \simeq -0.27\ m^{-1}$$

Assuming a constant Z_{eff} in the core region of the plasma,

$$\frac{n_i'}{n_i} = \frac{n_Z'}{n_Z} = \frac{n_e'}{n_e} \simeq -0.27\ m^{-1}$$

Furthermore, at this radius, $T_e \simeq 10.5\ keV$, $T_i \simeq 8.4\ keV$, $n_e \simeq 5.8 \times 10^{19}\ m^{-3}$. Taking the effective charge to be $Z_{eff} = 3.0$ in the presence of carbon impurity, we obtain

$$n_i = 3.5 \times 10^{19}\ m^{-3};\quad n_Z = 3.9 \times 10^{18}\ m^{-3}$$

With these values, and with the transport coefficients for $X_0 = 0$ and the transport enhancement factors for $X_0 \neq 0$, we obtain

When $\tilde{\Phi}(\theta) = 0$,

$$J_{nc} = -26.25 L_0$$

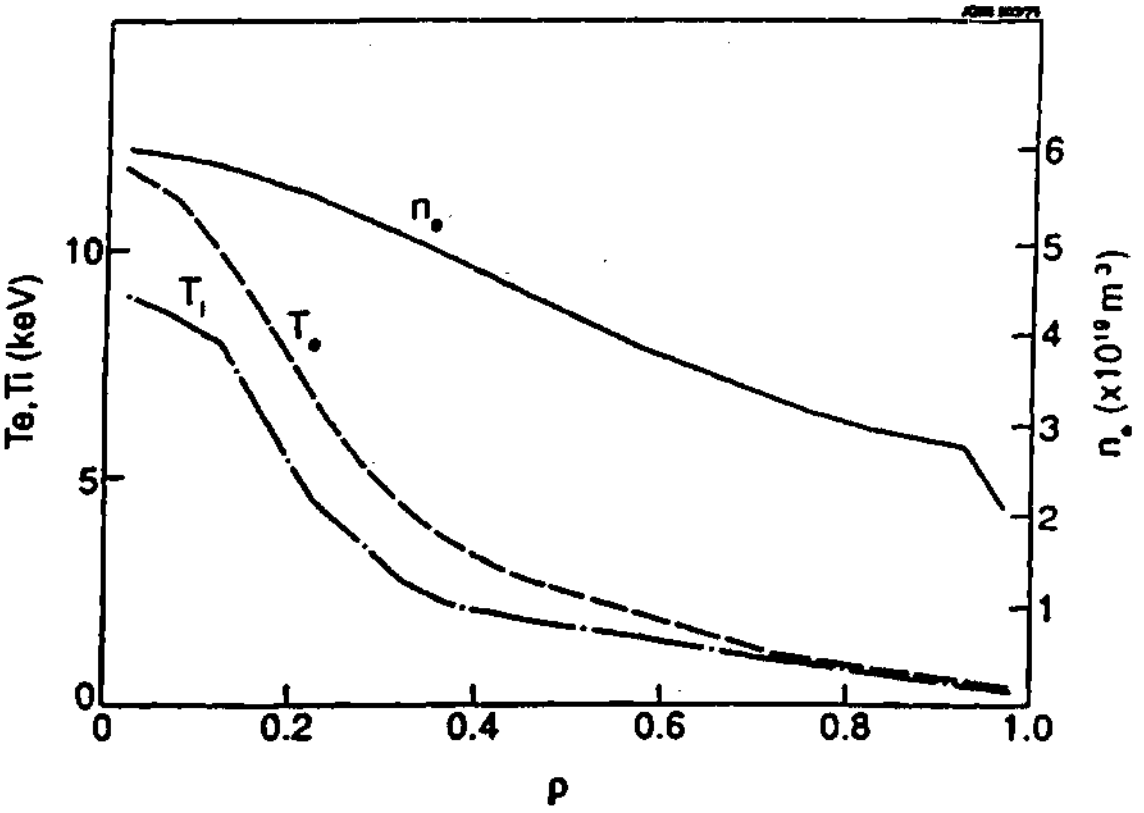

Figure 7.7: Temperature and Density Profiles for a Pellet Injected JET Shot [7]

The bootstrap current for $X_0 = 1$ is

$$J_{nc,\Phi} = -24.8 L_0$$

and the bootstrap current for $X_0 = 3$ is

$$J_{nc,\Phi} = -22.8 L_0$$

Hence, in the present case, the bootstrap current decreases by a small amount. This is not surprising as in the present case $\alpha_n \ll \alpha_T$, and our previous analysis indicates a decrease in the bootstrap current for $\alpha_n < 0.49\alpha_T$.

7.4.3 Summary and Conclusion

In this section, we summarize some of the important results on neoclassical conductivity and bootstrap current and discuss their significance.

1. The results presented in this work on plasma conductivity indicate that depending on the magnitude and sign of the poloidal potential variation, the neoclassical conductivity reduction factor can increase by as much as $\sim 70\%$ or decrease by $\sim 35\%$. Also, in most cases, an increase in the impurity content results in a decrease in the magnitude of the neoclassical conductivity reduction.

   While the above conclusions are based on calculations performed in the large aspect ratio limit, we expect similar results in smaller aspect ratio devices. In a small aspect ratio device ($\sqrt{\epsilon} \sim \mathcal{O}(1)$), the neoclassical conductivity reduction, which is of the order $\sqrt{\epsilon}$, is expected to be more significant. Hence, changes in the neoclassical conductivity reduction due to altered trapped particle fraction are also expected to be significant.

   We further note that plasma conductivity measurements play an important role in estimating the impurity content (Z_{eff}) in tokamaks. Hence, it is imperative

that the plasma conductivity predictions be as accurate as possible during various heating scenarios such as ICRH, ECRH or NBI as well as with varying levels of impurities. We feel that calculation of conductivity in a multi-species plasma in the presence of a significant poloidal electric field is a significant step in that direction.

2. In this work we have calculated the bootstrap current coefficients for a two ion species plasma in the presence of a significant poloidal electric field. The variation of the bootstrap current enhancement factors with the magnitude of the poloidal potential variation is qualitatively similar to that of the electron and ion diffusion enhancement factors. Our calculations indicate that depending on the magnitude and sign of the potential variation relative to the species under consideration, the transport coefficients may increase by a factor of ~ 2 or decrease by as much as $\sim 40\%$.

3. Enhancement of the bootstrap current coefficients depends upon the impurity content as well as the impurity species. It appears that the effect of varying the impurity content is more significant for the ion enhancement factors (F^i_{3n}). For $\Phi_{in} < \Phi_{out}$, the ion enhancement factors decrease with an increase in the impurity content while for $\Phi_{in} > \Phi_{out}$, the enhancement factors increase with the impurity content.

4. The nature of the impurity species seems to affect the bootstrap enhancement factors F^i_{3n}. At constant $\alpha = n_Z Z^2/n_i Z_i^2$, heavier impurities seem to cause a reduction in F^i_{3n} for $\Phi_{in} < \Phi_{out}$ and an increase in F^i_{3n} for $\Phi_{in} > \Phi_{out}$.

5. The magnitude of the bootstrap current is influenced as much by the enhancement of the transport coefficients as by the nature of the density profile relative to the temperature profile. We have calculated an increase in the bootstrap current when $\Phi_{in} < \Phi_{out}$ (e.g. ICRH or NBI) if the density profiles are more

peaked than roughly the square root of the temperature profiles in a deuterium plasma with carbon impurity. It is found that the bootstrap current generally decreases when $\Phi_{in} > \Phi_{out}$ (e.g. ECRH).

6. Finally, we note that in many of the present devices as well as future devices increasing importance is being given to bootstrap current. In designing many of the future devices a significant fraction of the current is assumed to be gradient driven. In these situations, an accurate prediction of the bootstrap current in auxiliary heated, multispecies plasma is of great importance. It is felt that the present formalism is a significant step in this direction.

CHAPTER VIII

SUMMARY AND RECOMMENDATIONS

8.1 Summary

In this thesis, we have extended the investigation of the effect of a poloidal electrostatic potential variation of order ϵ on the neoclassical particle transport and current in a tokamak plasma to the realistic case of a multiple ion species plasma. The final result of the present work is the calculation of the effect of the poloidal electric field on the ion diffusion coefficients, neoclassical conductivity, and bootstrap current.

We have solved the drift kinetic equation using the low collisionality ordering for a large aspect ratio ($\epsilon \ll 1$) tokamak. Both of these assumptions imply that the present theory is applicable to the core region of the plasma. The low collisionality assumption somewhat restricts the present theory to low to moderate Z impurities. Perhaps the more restrictive assumption is that the fraction of trapped particles is assumed to be small, i.e. $f_t \ll 1$. While this assumption is not too restrictive in treating low Z impurities or small values of potential variation ($X_0 \simeq 1-2$), it breaks down for larger Z impurities or for large values of the potential variation. In these scenarios, most of the impurity ions are trapped in the electrostatic potential well and $f_t \simeq 1$. Hence, the present formalism is appropriate for treating the case of low Z impurities such as carbon, berrylium, or helium.

We find that the main ion diffusion coefficients increase during both ECRH ($\Phi_{in} > \Phi_{out}$) and ICRH ($\Phi_{in} < \Phi_{out}$) for most values of the potential variation ($X_0 =$

$e\tilde{\Phi}(\theta)/T\epsilon$), implying an increase in the inward diffusion of impurities. Only when the poloidal potential variation is small, i.e. $X_0 \leq 1$, do the main ion diffusion coefficients decrease slightly ($\sim 10\%$) during ICRH, implying a small reduction in the inward impurity diffusion ($\Gamma_Z \simeq -Z_i/Z\ \Gamma_i$). It seems unlikely that any significant reduction in the inward impurity diffusion can be achieved with either ECRH or ICRH.

This result is important in interpreting the experimental results on impurity transport. Although it is generally believed that the neoclassical particle transport is small in comparison with anomalous transport processes, recent results from JET [84,85] seem to indicate that the particle transport in the core region of the plasma is close to the values predicted by the neoclassical theory. Furthermore, one can expect the neoclassical effects to be significant in such improved confinement regimes as H-mode and VH-mode [87]. It is expected that modifications of the neoclassical particle transport coefficients of the type examined in this work are significant in such regimes or regions of the plasma where the particle transport is close to the neoclassical levels.

It is found that in the presence of a poloidal potential variation of order ϵ, the neoclassical conductivity reduction factor (σ_{NC}) decreases by $\sim$ 35% or increases by $\sim$ 70% depending on the magnitude and sign of the potential variation. It also appears that the presence of impurities results in a decrease in the neoclassical conductivity reduction factor for most values of the poloidal potential variation. Such variations in the ohmic conductivity can have significant implications to any simulation of experimental results using a neoclassical conductivity model.

We further find that the presence of a poloidal electric field causes a significant change in the bootstrap current coefficients. The bootstrap current coefficients can increase by a factor of $\sim$ 2 or decrease by $\sim$ 40% depending on the magnitude and sign of the potential variation. The change in the bootstrap current, however, seems to depend on the enhancement (reduction) of the bootstrap current coefficients as

well as the nature of the temperature and density profiles relative to each other. We have calculated the change in the bootstrap current due to inclusion of the effects of a poloidal electric field in the presence of carbon impurity. The results indicate an increase in the bootstrap current during ICRH or NBI ($\Phi_{in} < \Phi_{out}$) if the density profiles are more peaked than roughly the square root of the temperature profiles and a decrease in the bootstrap current, generally, during ECRH ($\Phi_{in} > \Phi_{out}$). Increasing importance is being given to bootstrap current in the present as well as future devices. In designing many of the future devices, a significant fraction of the current is assumed to be gradient driven. It is important to include the effect of a poloidal electric field in estimating the contribution of the bootstrap current to total current during strong wave heating or NBI.

8.2 Suggestions for Future Work

Finally, to complete the picture of the effects of a poloidal electric field on neoclassical transport in a large aspect ratio tokamak, a few additional calculations need to be carried out.

- In the present work, we have calculated the particle transport and bootstrap current coefficients for a specific impurity (carbon). In order to facilitate the use of the results of this work, it is desirable to provide analytical fits which enable calculation of the transport coefficients as a function of the magnitude and sign of the poloidal potential variation, impurity concentration, impurity charge and mass.

- As pointed out in the previous section, the present formalism is valid when the fraction of trapped particles is small. Extension of this formalism to include the case when most impurity ions are trapped greatly extends the limits of this theory.

- Calculation of energy transport in the presence of a poloidal electric field in a multispecies plasma.

APPENDIX A

A.1 Expressions for $d\mu/dt$, dE/dt, and $d\xi/dt$

We have the equation of motion given by

$$\frac{d\mathbf{v}_\perp}{dt} + \frac{d\mathbf{v}_\parallel}{dt} = \frac{e}{m}\mathbf{E} - \Omega v_\perp \hat{\rho} \tag{A.1}$$

Taking the dot product of Eq. A.1 with $\mathbf{v}_\perp$, we have

$$\mathbf{v}_\perp \cdot \frac{d\mathbf{v}_\perp}{dt} + \mathbf{v}_\perp \cdot \frac{d\mathbf{v}_\parallel}{dt} = \frac{e}{m}\mathbf{v}_\perp \cdot \mathbf{E} - \Omega v_\perp \mathbf{v}_\perp \cdot \hat{\rho}$$

Noting that $\mathbf{v}_\perp \cdot \hat{\rho} = 0$, dividing throughout by B, and adding and subtracting $(v_\perp^2/2)d/dt(1/B)$, we obtain

$$\frac{d\mu}{dt} = -\frac{\mu}{B}\frac{dB}{dt} - \frac{v_\parallel}{B}\mathbf{v}_\perp \cdot \frac{d\hat{n}}{dt} + \frac{e}{mB}\mathbf{E} \cdot \mathbf{v}_\perp$$

Taking the dot product of Eq. A.1 with $\mathbf{v}$, we get

$$\mathbf{v} \cdot \frac{d\mathbf{v}}{dt} = \frac{e}{m}\mathbf{E} \cdot \mathbf{v} - \Omega v_\perp \hat{\rho} \cdot \mathbf{v}$$

Noting that $\hat{\rho} \cdot \mathbf{v} = 0$ and $(v^2/2) = E - (e\Phi/m)$, we write the above equation as

$$\begin{aligned} \frac{dE}{dt} &= \frac{e}{m}\left(\frac{d\Phi}{dt} + \mathbf{E} \cdot \mathbf{v}\right) \\ &= \frac{e}{m}\left(\frac{\partial\Phi}{\partial t} + \mathbf{v} \cdot \nabla\Phi - \mathbf{v} \cdot \nabla\Phi - \mathbf{v} \cdot \frac{\partial \mathbf{A}}{\partial t}\right) \end{aligned}$$

or

$$\frac{dE}{dt} = \frac{e}{m}\left(\frac{\partial\Phi}{\partial t} - \mathbf{v} \cdot \frac{\partial \mathbf{A}}{\partial t}\right) \tag{A.2}$$

Finally, taking the dot product of Eq. A.1 with $\hat{\rho}$, we have

$$\hat{\rho} \cdot \frac{d\mathbf{v}_\perp}{dt} + \hat{\rho} \cdot \frac{d\mathbf{v}_\parallel}{dt} = \frac{e}{m}\hat{\rho} \cdot \mathbf{E} - \Omega v_\perp \hat{\rho} \cdot \hat{\rho}$$

Observing that $\hat{\rho} \cdot \hat{n} = 0$ and $\hat{\rho} \cdot \hat{n}_\perp = 0$,

$$\hat{\rho} \cdot \frac{d\hat{n}_\perp}{dt} = \frac{e}{mv_\perp} \hat{\rho} \cdot \mathbf{E} - \Omega - \frac{v_\parallel}{v_\perp} \hat{\rho} \cdot \frac{d\hat{n}}{dt}$$

We evaluate the left hand side of the above equation as follows.

$$\begin{aligned} \hat{\rho} \cdot \frac{d\hat{n}_\perp}{dt} &= (\hat{e}_3 \cos\xi + \hat{e}_2 \sin\xi) \cdot \frac{d}{dt}(\hat{e}_2 \cos\xi - \hat{e}_3 \sin\xi) \\ &= -\frac{d\xi}{dt} + \hat{e}_3 \cdot \frac{d\hat{e}_2}{dt} \cos^2\xi - \hat{e}_2 \cdot \frac{d\hat{e}_3}{dt} \sin^2\xi \\ &\quad + \sin\xi \cos\xi \hat{e}_2 \cdot \frac{d\hat{e}_2}{dt} - \sin\xi \cos\xi \hat{e}_3 \cdot \frac{d\hat{e}_3}{dt} \end{aligned}$$

Noting that

$$\hat{e}_2 \cdot \frac{d\hat{e}_2}{dt} = \frac{d}{dt}\left(\frac{\hat{e}_2 \cdot \hat{e}_2}{2}\right) = 0 = \hat{e}_3 \cdot \frac{d\hat{e}_3}{dt}$$

and

$$\hat{e}_2 \cdot \frac{d\hat{e}_3}{dt} = \frac{d}{dt}(\hat{e}_2 \cdot \hat{e}_3) - \hat{e}_3 \cdot \frac{d\hat{e}_2}{dt} = -\hat{e}_3 \cdot \frac{d\hat{e}_2}{dt}$$

we have

$$\hat{\rho} \cdot \frac{d\hat{n}_\perp}{dt} = -\frac{d\xi}{dt} + \hat{e}_3 \cdot \frac{d\hat{e}_2}{dt}$$

Hence,

$$\frac{d\xi}{dt} = \Omega + \hat{e}_3 \cdot \frac{d\hat{e}_2}{dt} + \frac{v_\parallel}{v_\perp} \hat{\rho} \cdot \frac{d\hat{n}}{dt} - \frac{e}{mv_\perp} \hat{\rho} \cdot \mathbf{E} \tag{A.3}$$

A.2 Gyro-averaging Procedure

A.2.1 Calculation of $\overline{d\mu/dt}$

In Section 2.2.2, we encountered the gyro-averaging procedure. Here we explicitly evaluate the gyroaverage of $d\mu/dt$. We will make use of the assumption that quantities that do not explicitly depend upon the gyrophase are constant. With this

$$\overline{\frac{d\mu}{dt}} = -\overline{\frac{\mu}{B}\frac{dB}{dt}} - \overline{\frac{v_\parallel}{B}\mathbf{v}_\perp \cdot \frac{d\hat{n}}{dt}} + \overline{\frac{e}{mB}\mathbf{E} \cdot \mathbf{v}_\perp} \tag{A.4}$$

As mentioned in Section 2.2.2, retaining only the convective part of the substantial derivatives, we get

$$\overline{\frac{d\mu}{dt}} = \overline{-\frac{\mu}{B}v_\parallel \hat{n}\cdot\nabla B} - \overline{\frac{\mu}{B}v_\perp \hat{n}_\perp\cdot\nabla B} - \overline{\frac{v_\parallel}{B}\mathbf{v}_\perp\cdot(\mathbf{v}\cdot\nabla)\hat{n}} + \overline{\frac{e}{mB}\mathbf{E}\cdot\mathbf{v}_\perp} \qquad (A.5)$$

where

$$\overline{-\frac{\mu}{B}v_\parallel \hat{n}\cdot\nabla B} = -\frac{\mu}{B}v_\parallel \hat{n}\cdot\nabla B$$

Due to the presence of $\cos\xi$ and $\sin\xi$ in $\hat{n}_\perp$,

$$\overline{-\frac{\mu}{B}v_\perp \hat{n}_\perp\cdot\nabla B} = 0$$

Writing $\mathbf{v} = v_\parallel\hat{n} + v_\perp\hat{n}_\perp$, and noting that $\overline{\hat{n}_\perp} = 0$,

$$\overline{-\frac{v_\parallel}{B}\mathbf{v}_\perp\cdot(\mathbf{v}\cdot\nabla)\hat{n}} = \overline{-\frac{v_\parallel v_\perp^2}{B}\hat{n}_\perp\cdot(\hat{n}_\perp\cdot\nabla)\hat{n}} = -\frac{v_\parallel v_\perp^2}{B}\overline{\hat{n}_\perp\hat{n}_\perp} : \nabla\hat{n}$$

Using $\hat{n}_\perp = \hat{e}_2\cos\xi - \hat{e}_3\sin\xi$,

$$\overline{-\frac{v_\parallel}{B}\mathbf{v}_\perp\cdot(\mathbf{v}\cdot\nabla)\hat{n}} = -\frac{v_\parallel v_\perp^2}{2B}(\hat{e}_2\hat{e}_2 + \hat{e}_3\hat{e}_3) : \nabla\hat{n} = -\frac{v_\parallel v_\perp^2}{2B}(\mathbf{I} - \hat{n}\hat{n}) : \nabla\hat{n}$$

where we have used the identity $\mathbf{I} = \hat{n}\hat{n} + \hat{e}_2\hat{e}_2 + \hat{e}_3\hat{e}_3$. Carrying out the vector operations on the right hand side, the above equation can be written as

$$\overline{-\frac{v_\parallel}{B}\mathbf{v}_\perp\cdot(\mathbf{v}\cdot\nabla)\hat{n}} = -\frac{v_\parallel v_\perp^2}{2B}[\nabla\cdot\hat{n} - \hat{n}\cdot(\hat{n}\cdot\nabla)\hat{n}] \qquad (A.6)$$

We know that

$$\hat{n}\times\nabla\times\hat{n} = \frac{1}{2}\nabla(\hat{n}\cdot\hat{n}) - (\hat{n}\cdot\nabla)\hat{n} = -(\hat{n}\cdot\nabla)\hat{n}$$

and

$$\hat{n}\cdot(\hat{n}\cdot\nabla)\hat{n} = -\hat{n}\cdot\hat{n}\times\nabla\times\hat{n} = 0$$

Using these, Eq. A.6 reduces to

$$\overline{-\frac{v_\parallel}{B}\mathbf{v}_\perp\cdot(\mathbf{v}\cdot\nabla)\hat{n}} = -\frac{v_\parallel v_\perp^2}{2B}\nabla\cdot\hat{n} \qquad (A.7)$$

We have

$$\nabla \cdot \mathbf{B} = \nabla \cdot (B\hat{n}) = B\nabla \cdot \hat{n} + \hat{n} \cdot \nabla B = 0$$

Using this identity in Eq. A.7, we obtain

$$-\overline{\frac{v_\parallel}{B}\mathbf{v}_\perp \cdot (\mathbf{v} \cdot \nabla)\hat{n}} = \frac{v_\parallel v_\perp^2}{2B^2}\hat{n} \cdot \nabla B = \frac{v_\parallel \mu}{B}\hat{n} \cdot \nabla B \tag{A.8}$$

Also

$$\overline{\frac{e}{mB}\mathbf{E} \cdot \mathbf{v}_\perp} = \frac{e}{mB}\mathbf{E} \cdot \overline{\mathbf{v}_\perp} = 0 \tag{A.9}$$

Hence,

$$\overline{\frac{d\mu}{dt}} = -\frac{v_\parallel \mu}{B}\hat{n} \cdot \nabla B + \frac{v_\parallel \mu}{B}\hat{n} \cdot \nabla B = 0 \tag{A.10}$$

A.2.2 Calculation of $\overline{d\tilde{f}_1/dt}$

In Section 2.2.2, we found the gyrophase dependent part of the first order distribution function to be

$$\tilde{f}_1 = -\frac{v_\perp}{\Omega}\hat{\rho} \cdot \nabla f_0 = -\vec{\rho} \cdot \mathbf{h}$$

Using this expression, we explicitly evaluate the gyrophase average of $d\tilde{f}_1/dt$.

$$\overline{\frac{d\tilde{f}_1}{dt}} = -\overline{\frac{d}{dt}(\vec{\rho} \cdot \mathbf{h})} = -\overline{\frac{d\vec{\rho}}{dt} \cdot \mathbf{h}} - \overline{\frac{d\mathbf{h}}{dt} \cdot \vec{\rho}} \tag{A.11}$$

Noting that $\mathbf{h}$ is independent of the gyrophase, and expanding $d\mathbf{h}/dt$, we obtain

$$\begin{aligned}\overline{\frac{d\tilde{f}_1}{dt}} \;=\; & -\overline{\frac{d\vec{\rho}}{dt}} \cdot \mathbf{h} - \overline{\vec{\rho} \cdot \frac{\partial \mathbf{h}}{\partial t}} - \overline{\vec{\rho} \cdot (\mathbf{v}_\parallel \cdot \nabla)\mathbf{h}} - \overline{\vec{\rho} \cdot (\mathbf{v}_\perp \cdot \nabla)\mathbf{h}} \\ & - \overline{\vec{\rho} \cdot \frac{\partial \mathbf{h}}{\partial \mu}\left(\frac{d\mu}{dt}\right)} - \overline{\vec{\rho} \cdot \frac{\partial \mathbf{h}}{\partial E}\left(\frac{dE}{dt}\right)} - \overline{\vec{\rho} \cdot \frac{\partial \mathbf{h}}{\partial \xi}\left(\frac{d\xi}{dt}\right)}\end{aligned}$$

Using the fact that $\mathbf{h}$ is independent of the gyrophase and the magnetic moment, and $\overline{\vec{\rho}} = 0$, we have

$$\overline{\vec{\rho} \cdot \frac{\partial \mathbf{h}}{\partial t}} = \overline{\vec{\rho} \cdot (\mathbf{v}_\parallel \cdot \nabla)\mathbf{h}} = \overline{\vec{\rho} \cdot \frac{\partial \mathbf{h}}{\partial \mu}\left(\frac{d\mu}{dt}\right)} = \overline{\vec{\rho} \cdot \frac{\partial \mathbf{h}}{\partial \xi}\left(\frac{d\xi}{dt}\right)} = 0 \tag{A.12}$$

And

$$\begin{aligned}\overline{\vec{\rho}\cdot(\mathbf{v}_\perp\cdot\nabla)\mathbf{h}} &= \frac{v_\perp^2}{\Omega}\overline{\hat{\rho}\cdot(\hat{n}_\perp\cdot\nabla)\mathbf{h}} \\ &= \frac{v_\perp^2}{\Omega}\overline{\hat{\rho}\hat{n}_\perp}:\nabla\mathbf{h} \qquad \text{(A.13)} \\ &= \frac{v_\perp^2}{2\Omega}(\hat{e}_2\times\hat{e}_3)\cdot\nabla\times\mathbf{h} \\ &= \frac{v_\perp^2}{2\Omega}\hat{n}\cdot\nabla\times\nabla f_0 = 0 \qquad \text{(A.14)}\end{aligned}$$

Noting that

$$\frac{\partial}{\partial E}\left(\frac{e}{m}\mathbf{v}\cdot\frac{\partial\mathbf{A}}{\partial t}\right)\sim\mathcal{O}(\delta\omega) \qquad \text{(A.15)}$$

we have

$$\overline{\vec{\rho}\cdot\frac{d\mathbf{h}}{dE}\left(\frac{dE}{dt}\right)}\sim\mathcal{O}(\delta^2\omega)\sim\mathcal{O}(\delta^3) \qquad \text{(A.16)}$$

Dropping this term, we obtain the following equation

$$\overline{\frac{d\tilde{f}_1}{dt}} = -\overline{\frac{d\vec{\rho}}{dt}}\cdot\mathbf{h} + \text{terms of order } \delta^3 \qquad \text{(A.17)}$$

$$\begin{aligned}\overline{\frac{d\vec{\rho}}{dt}} &= \overline{\frac{d}{dt}\left(\frac{\hat{n}\times\mathbf{v}_\perp}{\Omega}\right)} \\ &= \overline{\hat{n}\times\mathbf{v}_\perp\frac{d}{dt}\left(\frac{1}{\Omega}\right)} + \overline{\frac{1}{\Omega}\hat{n}\times\frac{d\mathbf{v}_\perp}{dt}} + \overline{\frac{1}{\Omega}\frac{d\hat{n}}{dt}\times\mathbf{v}_\perp} \qquad \text{(A.18)}\end{aligned}$$

The first term in the above equation is

$$A = \overline{\hat{n}\times\mathbf{v}_\perp\frac{d}{dt}\left(\frac{1}{\Omega}\right)} = -\overline{\frac{\hat{n}\times\mathbf{v}_\perp}{\Omega}\frac{1}{B}\frac{dB}{dt}} \qquad \text{(A.19)}$$

Dropping the term $\partial B/\partial t$ and writing $\mathbf{v} = \mathbf{v}_\perp + \mathbf{v}_\parallel$, we get

$$A = -\frac{v_\perp^2}{\Omega B}\overline{\hat{n}\times\hat{n}_\perp(\hat{n}_\perp\cdot\nabla)B} = -\frac{v_\perp^2}{\Omega B}\overline{\hat{\rho}(\hat{n}_\perp\cdot\nabla)B} \qquad \text{(A.20)}$$

Expanding $\hat{n}_\perp$ and $\hat{\rho}$ in terms of guiding center coordinates, and gyro-averaging,

$$A = \frac{\mu}{\Omega}(\hat{e}_3\times\hat{e}_2)\times\nabla B == -\frac{\mu}{\Omega}\hat{n}\times\nabla B \qquad \text{(A.21)}$$

The second term in Eq. A.18, upon using the equation of motion, becomes

$$B = \overline{\frac{1}{\Omega}\hat{n} \times \frac{d\mathbf{v}_\perp}{dt}} = \overline{\frac{1}{\Omega}\hat{n} \times \left(\frac{e}{m}\mathbf{E} - \Omega v_\perp \hat{\rho} - \frac{d\mathbf{v}_\parallel}{dt}\right)} \tag{A.22}$$

Noting that $\hat{n} \times \hat{\rho} = \hat{n} \times \hat{n} = 0$, we obtain

$$B = \overline{\frac{\hat{n} \times \mathbf{E}}{B}} - \frac{v_\parallel}{\Omega}\overline{\hat{n} \times \frac{d\hat{n}}{dt}} \tag{A.23}$$

Expanding $d\hat{n}/dt$ and dropping terms of order $\geq \delta^2$, we obtain, after gyro-averaging

$$B = \frac{\hat{n} \times \mathbf{E}}{B} - \frac{1}{\Omega}\hat{n} \times [v_\parallel^2(\hat{n} \cdot \nabla)\hat{n}] \tag{A.24}$$

The third term in Eq. A.18 is

$$C = \overline{\frac{1}{\Omega}\frac{d\hat{n}}{dt} \times \mathbf{v}_\perp} = -\frac{v_\perp}{\Omega}\overline{\hat{n}_\perp \times \frac{d\hat{n}}{dt}} \tag{A.25}$$

Writing $\hat{n}_\perp = \hat{\rho} \times \hat{n}$, we write the above equation as

$$C = -\frac{v_\perp}{\Omega}\overline{\hat{n}(\hat{\rho} \cdot \frac{d\hat{n}}{dt})} - \overline{\frac{d\hat{n}}{dt}(\hat{\rho} \cdot \hat{n})} = -\frac{v_\perp}{\Omega}\overline{\hat{n}(\hat{\rho} \cdot \frac{d\hat{n}}{dt})} \tag{A.26}$$

Expanding the substantial derivative of $\hat{n}$ and carrying out steps similar to those leading to Eq. A.13,

$$C = -\frac{v_\perp^2}{2\Omega}\hat{n}[\hat{e}_3 \cdot (\hat{e}_2 \cdot \nabla)\hat{n} - \hat{e}_2 \cdot (\hat{e}_3 \cdot \nabla)\hat{n}] = -\frac{v_\perp^2}{2\Omega}\hat{n}[\hat{n} \cdot (\nabla \times \hat{n})] \tag{A.27}$$

Combining Eqs. A.21, A.24, and A.27, Eq. A.18 can be written as

$$\overline{\frac{d\vec{\rho}}{dt}} = -\frac{\mathbf{E} \times \hat{n}}{B} - \frac{\hat{n}}{\Omega} \times [\mu \nabla B + v_\parallel^2(\hat{n} \cdot \nabla)\hat{n}] - \frac{v_\perp^2}{2\Omega}\hat{n}[\hat{n} \cdot (\nabla \times \hat{n})] \tag{A.28}$$

Using a notation similar to that used by Hinton and Hazeltine [8],

$$-\overline{\frac{d\vec{\rho}}{dt}} = \mathbf{v}_D + \breve{v}_\parallel \hat{n} \tag{A.29}$$

where

$$\mathbf{v}_D = \frac{\mathbf{E} \times \hat{n}}{B} + \frac{\hat{n}}{\Omega} \times [\mu \nabla B + v_\parallel^2(\hat{n} \cdot \nabla)\hat{n}] \tag{A.30}$$

and

$$\breve{v}_\parallel = \frac{v_\perp^2}{2\Omega}[\hat{n} \cdot (\nabla \times \hat{n})] \tag{A.31}$$

Drift for a small β tokamak

We have for equilibrium,

$$\mathbf{J} \times \mathbf{B} = \nabla p$$

Using the Ampere's law,

$$(\nabla \times \mathbf{B}) \times \mathbf{B} = \mu_0 \nabla p$$

Expanding the left hand side using $\mathbf{B} = B\hat{n}$, and dividing throughout by B^2, we get

$$(\hat{n} \cdot \nabla) - \frac{\nabla B}{B} + \frac{\hat{n}(\hat{n} \cdot \nabla B)}{B} = \frac{\mu_0 \nabla p}{B^2}$$

where we have used $\nabla(\hat{n} \cdot \hat{n}) = 0$. Taking the cross product of the above equation with $\hat{n}$,

$$\hat{n} \times (\hat{n} \cdot \nabla)\hat{n} = \frac{\hat{n} \times \nabla B}{B} + \frac{\hat{n} \times \nabla p}{(\frac{B^2}{\mu_0})}$$

We note that the terms on the right hand side are of the order $1/l$ and β/l respectively. If we assume, as done by Hinton and Hazeltine [8], that $\beta = 2\mu_0 p/B^2 \sim \mathcal{O}(\delta) \ll 1$, then the second term is much less than the first term. Hence,

$$\hat{n} \times (\hat{n} \cdot \nabla)\hat{n} = \frac{\hat{n} \times \nabla B}{B} + \mathcal{O}(\delta) \simeq \frac{\hat{n} \times \nabla B}{B}$$

Using this, the drift $\mathbf{v}_D$ can be written as

$$\mathbf{v}_D = \frac{\hat{n} \times \nabla \Phi}{B} + \frac{\hat{n}}{\Omega} \times \mu \nabla B + \frac{v_\parallel^2}{\Omega} \frac{\hat{n} \times \nabla B}{B}$$

or

$$\mathbf{v}_D = -v_\parallel \hat{n} \times \nabla \left(\frac{v_\parallel}{\Omega} \right) \tag{A.32}$$

where the gradient is taken at constant $E = v^2/2 + e\Phi/m = v_\parallel^2/2 + \mu B + e\Phi/m$.

APPENDIX B

B.1 Boundary Layer Formalism

In Chapter V, we used the low collisionality, or the banana regime, ordering in solving the drift kinetic equation. In the banana regime, $\nu_{eff}\tau_B \ll 1$. We expect this ordering to hold in the far trapped and far untrapped regions. We should, however, note that in the narrow layer between the trapped and untrapped particles ("boundary layer") comprising marginally trapped and marginally untrapped particles, $\nu_{eff}\tau_B \not\ll 1$ because $\tau_B \to \infty$. Particles in this layer are highly susceptible to collisions. The break down in the banana regime ordering manifests in the discontinuity in $\partial g_j^0/\partial\mu$ at the interface between the trapped-untrapped regions [Eq. 5.14].

Hinton and Rosenbluth Analysis

Hinton and Rosenbluth [88] have solved the drift kinetic equation for the electron-ion problem in the absence of poloidal electric fields. Without going through the details of their calculations, we may write the resulting distribution function as

$$G_1 = G_0 + G_l + G_c$$

where $G_0 = g_j^0$ is the conventional banana regime solution, G_l is the solution confined to the boundary layer, and G_c is the correction to the conventional solution due to proper matching of the solution at the boundary layer.

Hinton et al. [88] have calculated the transport coefficients using a variational approach. Here, we consider the diffusion coefficient to study the effect of the boundary layer on the conventional solutions obtained without using the boundary layer

analysis. The diffusion coefficient in the presence of the boundary layer is given by [88]

$$L_{11} \simeq L_{11}^{0}(1-\beta) \tag{B.1}$$

where the boundary layer correction β is given by

$$\beta = 0.9\nu_{*e}^{1/2} \ln\left[\frac{0.62}{\nu_{*e}^{1/2}}\right]$$

Here, $\nu_{*e} = \nu_e/(\omega_{te}\epsilon^{3/2}) \ll 1$, where ν_e, ω_{te} are the electron collision frequency and electron transit frequency respectively.

Conclusion

We may draw two conclusions from Eq. B.1.

1. The boundary layer seems to result in a decrease in the transport coefficients.
2. The magnitude of the correction decreases with decreasing collisionality. For example, for $\nu_{*e} = 0.1$, $\beta \simeq 0.19$ and for $\nu_{*e} = 0.01$, $\beta \simeq 0.16$.

Hence, it appears that the boundary layer correction is significant for plasmas with higher collisionality. As most of the current major devices and future devices are expected to be in the low collisionality regime, we can expect the boundary layer correction to the transport coefficients to be small.

We also note that the analysis of Hinton et al. [88] is quite complex and makes use of many simplifying assumptions. In addition, the analysis uses a simple Lorentz gas model. Balescu [32] has pointed out that, in view of the uncertainties in modeling, it seems unlikely that a detailed analysis of the boundary layer yields results significantly better than the results obtained using simple interpolation formulas between the banana and plateau limits. Hence, we shall ignore the corrections due to the presence of the boundary layer.

B.2 Calculation of Restoring Coefficients

The momentum restoring coefficients are given by Eq. 5.19,

$$r_{kj} = C \int dw d\mu \nu_{kj}^{S} \mu \frac{\partial f_{k1}}{\partial \mu} \tag{B.2}$$

where

$$C = -\frac{2\pi B}{n_j \{\nu_{jk}^{S}\}} \frac{m_k}{m_j} \sum_{\sigma} \sigma$$

Using Eq. 5.15 for $\partial f_{k1}/\partial \mu$ and making use of the result 5.18, we can write r_{kj} as

$$\begin{aligned} r_{kj} &= C \int dw d\mu \, \nu_{kj}^{S} \mu \frac{m_k}{e_k} \left(\frac{B}{B_\theta}\right) \frac{\partial f_{k0}}{\partial \tau} \left(\frac{1}{v_\parallel} - \frac{\nu_k^S}{\nu_{k\Phi}} \frac{1}{< v_\parallel >}\right) \\ &\quad -C \int dw d\mu \, \nu_{kj}^{S} \frac{\mu B}{< v_\parallel >} \left[\frac{m_k f_{k0}}{T_k} \sum_l \frac{\nu_{kl}^{S} < r_{lk} >}{\nu_{k\Phi}} + \frac{e_k E^0}{T_k} \frac{f_{k0}}{\nu_{k\Phi}}\right] \\ &= r_{kj}^1 + r_{kj}^2 \end{aligned}$$

Using

$$\frac{\partial f_{k0}}{\partial \tau} = f_{k0} \left(\frac{N_k'}{N_k} - \frac{3}{2} \frac{T_k'}{T_k}\right) + \frac{T_k'}{T_k} \left(\frac{m_k E^*}{T_k}\right) f_{k0} \tag{B.3}$$

where

$$\frac{N_k'}{N_k} = \frac{n_{k0}'}{n_{k0}} + \frac{e_k < \Phi >'}{T_k}$$

we have

$$\begin{aligned} r_{kj}^1 &= C \int dw d\mu \, \nu_{kj}^{S} \mu f_{k0} \frac{m_k}{e_k} \left(\frac{B}{B_\theta}\right) \left[\frac{N_k'}{N_k} - \frac{3}{2} \frac{T_k'}{T_k}\right] \left(\frac{1}{v_\parallel} - \frac{\nu_k^S}{\nu_{k\Phi}} \frac{1}{< v_\parallel >}\right) \\ &\quad +C \int dw d\mu \, \nu_{kj}^{S} \mu f_{k0} \frac{m_k}{e_k} \left(\frac{B}{B_\theta}\right) \left[\frac{m_k}{T_k} E^* \frac{T_k'}{T_k}\right] \left(\frac{1}{v_\parallel} - \frac{\nu_k^S}{\nu_{k\Phi}} \frac{1}{< v_\parallel >}\right) \\ &= r_{kj}^{1,1} + r_{kj}^{1,2} \end{aligned}$$

We can write $r_{kj}^{1,1}$ as

$$\begin{aligned} r_{kj}^{1,1} &= C \left[\frac{N_k'}{N_k} - \frac{3}{2} \frac{T_k'}{T_k}\right] \frac{m_k}{e_k} \left(\frac{B}{B_\theta}\right) \int \frac{dw \mu d\mu f_{k0} \nu_{kj}^{S}}{v_\parallel} \left(1 - \frac{\nu_{kj}^{S}}{\nu_{k\Phi}}\right) \\ &\quad +C \left[\frac{N_k'}{N_k} - \frac{3}{2} \frac{T_k'}{T_k}\right] \frac{m_k}{e_k} \left(\frac{B}{B_\theta}\right) \int \left(\frac{\nu_{kj}^{S} \nu_k^S}{\nu_{k\Phi}}\right) f_{k0} dw \\ &\quad \int \mu \, d\mu \left(\frac{1}{v_\parallel} - \frac{1}{< v_\parallel >}\right) \end{aligned}$$

Using the definition of C and carrying out the integration, we get, after flux surface averaging,

$$\begin{aligned}\left\langle \tau_{kj}^{1,1} \right\rangle &= -\frac{m_k n_k}{m_j n_j}\frac{1}{\{\nu_{jk}^S\}}\left(\frac{T_k}{e_k B_\theta^0}\right)\left[\frac{N_k'}{N_k}-\frac{3}{2}\frac{T_k'}{T_k}\right]\left\{\nu_{kj}^S-\frac{\nu_{kj}^S\nu_k^S}{\nu_{k\Phi}}\right\} \\ &\quad -\frac{m_k n_k}{m_j n_j}\frac{1}{\{\nu_{jk}^S\}}\left(\frac{T_k}{e_k B_\theta^0}\right)\left[\frac{N_k'}{N_k}-\frac{3}{2}\frac{T_k'}{T_k}\right]\left\{f_{t\Phi}\frac{\nu_{kj}^S\nu_k^S}{\nu_{k\Phi}}\right\}\end{aligned}$$

In obtaining the above equation, we have made use of the definition of $f_{t\Phi}$ given by Eq. 5.17. Also, we have used the fact that in the large aspect ratio limit,

$$\exp\left[-\frac{e_k\Phi(\theta)}{T_k}\right] \simeq \left[1-\frac{e_k\Phi(\theta)}{T_k}+\cdots\right]$$

and we have retained only $\mathcal{O}(\epsilon^0)$ terms in carrying out the velocity integrals. A similar analysis gives

$$\begin{aligned}\left\langle \tau_{kj}^{1,2} \right\rangle &= -\frac{m_k n_k}{m_j n_j}\frac{1}{\{\nu_{jk}^S\}}\left(\frac{T_k}{e_k B_\theta^0}\right)\frac{T_k'}{T_k} \\ &\quad \left[\left\{\left(\nu_{kj}^S-\frac{\nu_{kj}^S\nu_k^S}{\nu_{k\Phi}}\right)\left(\frac{m_k E^*}{T_k}\right)\right\}+\left\{f_{t\Phi}\left(\frac{\nu_{kj}^S\nu_k^S}{\nu_{k\Phi}}\right)\left(\frac{m_k E^*}{T_k}\right)\right\}\right]\end{aligned}$$

and

$$\left\langle \tau_{kj}^{2} \right\rangle = \frac{m_k n_k}{m_j n_j}\frac{1}{\{\nu_{jk}^S\}}\left[\sum_l\left\{\frac{\nu_{kj}^S\nu_{kl}^S}{\nu_{k\Phi}}f_{c\Phi}\right\}<\tau_{lk}>+\frac{e_k E^0}{m_k}\left\{\frac{\nu_{kj}^S}{\nu_{k\Phi}}f_{c\Phi}\right\}\right]$$

Adding the results $< \tau_{kj}^{1,1} >$, $< \tau_{kj}^{1,2} >$, and $< \tau_{kj}^{2} >$, and using the momentum conservation relation $m_j n_j\{\nu_{jk}^S\} = m_k n_k\{\nu_{kj}^S\}$, we get the desired result

$$\begin{aligned}<\tau_{kj}> &= -\frac{1}{\{\nu_{kj}^S\}}\left(\frac{T_k}{e_k B_\theta^0}\right)\left[\{\nu_{kj}^S\}\left(A_{1k}+\frac{e_k\Phi'}{T_k}\right)+\left\{\nu_{kj}^S\left(\frac{m_k E^*}{T_k}\right)\right\}A_{2k}\right] \\ &\quad +\frac{1}{\{\nu_{kj}^S\}}\left(\frac{T_k}{e_k B_\theta^0}\right)\left[\left\{\frac{\nu_{kj}^S\nu_k^S}{\nu_{k\Phi}}f_{c\Phi}\right\}\left(A_{1k}+\frac{e_k\Phi'}{T_k}\right)+\left\{\frac{\nu_{kj}^S\nu_k^S}{\nu_{k\Phi}}\left(\frac{m_k E^*}{T_k}\right)f_{c\Phi}\right\}A_{2k}\right] \\ &\quad +\frac{1}{\{\nu_{kj}^S\}}\frac{e_k}{m_k}A_3\left\{\frac{\nu_{kj}^S}{\nu_{k\Phi}}f_{c\Phi}\right\}+\frac{1}{\{\nu_{kj}^S\}}\sum_l\left\{\frac{\nu_{kj}^S\nu_{kl}^S}{\nu_{k\Phi}}f_{c\Phi}\right\}<\tau_{lk}>\end{aligned}$$

APPENDIX C

C.1 Expression for Parallel Velocity Difference

In Chapter VII, we used n-1 parallel velocity differences to calculate the bootstrap current. Here, we derive the equation for the velocity difference [Eq. 7.12] used in Chapter VII to calculate the bootstrap current. Using Eq. 7.2 for the parallel velocity difference, we easily obtain,

$$\begin{aligned} < u_j > - < u_k > \;=\; & -\left(\frac{T_j}{e_j B_\theta^0}\right)\left\{\left[A_{1j} + \frac{e_j < \Phi >'}{T_j} + \left(\frac{m_j E^*}{T_j}\right) A_{2j}\right]\frac{f_{t\Phi}\nu_j^D}{\nu_{j\Phi}}\right\} \\ & + \sum_l \left\{\frac{f_{c\Phi}\nu_{jl}^S}{\nu_{j\Phi}}\right\} < r_{lj} > \\ & + \left(\frac{T_k}{e_k B_\theta^0}\right)\left\{\left[A_{1k} + \frac{e_k < \Phi >'}{T_k} + \left(\frac{m_k E^*}{T_k}\right) A_{2k}\right]\frac{f_{t\Phi}\nu_k^D}{\nu_{k\Phi}}\right\} \\ & - \sum_l \left\{\frac{f_{c\Phi}\nu_{kl}^S}{\nu_{k\Phi}}\right\} < r_{lk} > \end{aligned} \tag{C.1}$$

From Eq. 6.4, we have

$$< R_{jk} >= -m_j n_j \{\nu_{jk}^S\}[< r_{jk} > - < r_{kj} >] \tag{C.2}$$

Adding and subtracting $(< u_j > - < u_k >)$ from the right hand side of the above equation, and using the definition of the restoring coefficients $< r_{jk} >$, $< r_{kj} >$ from Eq. 6.7, we can write, after a few steps of algebra,

$$\begin{aligned} < R_{jk} > \;=\; & -m_j n_j \{\nu_{jk}^S\}\Big[(< u_j > - < u_k >) + (DF)_j \gamma_{n\Phi}^{jk} - (DF)_k \gamma_{n\Phi}^{kj} \\ & + \gamma_{T\Phi}^{jk}\left(\frac{T_j}{e_j B_\theta^0}\right) f_t A_{2j} - \gamma_{T\Phi}^{kj}\left(\frac{T_k}{e_k B_\theta^0}\right) f_t A_{2k} \\ & + \sum_l \left[\Delta_{l\Phi}^{jk} < r_{lj} > - \Delta_{l\Phi}^{kj} < r_{lk} >\right] \\ & - f_t \sum_l \left[\Delta_{l\Phi,1}^{jk} < r_{lj} > - \Delta_{l\Phi,1}^{kj} < r_{lk} >\right]\Big] \end{aligned} \tag{C.3}$$

where $(DF)_p$ is a combination of the "driving forces" A_{1p}, A_{2p}, and $< \Phi >'$, given by

$$(DF)_p = -\left(\frac{T_p}{e_p B_\theta^0}\right) f_t \left[A_{1p} + \frac{e_p < \Phi >'}{T_p} + \frac{\left\{ f_{t\Phi} \frac{\nu_p^D \nu_p^S}{\nu_{p\Phi}} \left(\frac{m_p E^*}{T_p} \right) \right\}}{\left\{ f_{t\Phi} \frac{\nu_p^S \nu_p^D}{\nu_{p\Phi}} \right\}} A_{2p} \right]$$

and

$$\gamma_{n\Phi}^{pq} = \frac{1}{f_t} \left[\left\{ f_{t\Phi} \frac{\nu_{pq}^S \nu_p^D}{\nu_{p\Phi}} \right\} \frac{1}{\{\nu_{pq}^S\}} - \left\{ f_{t\Phi} \frac{\nu_p^D}{\nu_{p\Phi}} \right\} \right] \tag{C.4}$$

$$\gamma_{T\Phi}^{pq} = \frac{\left\{ f_{t\Phi} \frac{\nu_p^S \nu_p^D}{\nu_{p\Phi}} \left(\frac{m_p E^*}{T_p} \right) \right\}}{\left\{ f_{t\Phi} \frac{\nu_p^D \nu_p^S}{\nu_{p\Phi}} \right\}} \gamma_{n\Phi}^{pq} - \frac{1}{f_t} \left[\left\{ f_{t\Phi} \left(\frac{m_p E^*}{T_p} \right) \frac{\nu_{pq}^S \nu_p^D}{\nu_{p\Phi}} \right\} \frac{1}{\{\nu_{pq}^S\}} - \left\{ f_{t\Phi} \left(\frac{m_p E^*}{T_p} \right) \frac{\nu_p^D}{\nu_{p\Phi}} \right\} \right] \tag{C.5}$$

$$\Delta_{l\Phi}^{pq} = \left[\left\{ \frac{\nu_{pq}^S \nu_{pl}^S}{\nu_{p\Phi}} \right\} \frac{1}{\{\nu_{pq}^S\}} - \left\{ \frac{\nu_{pl}^S}{\nu_{p\Phi}} \right\} \right] \tag{C.6}$$

$$\Delta_{l\Phi,1}^{pq} = \frac{1}{f_t} \left[\left\{ f_{t\Phi} \frac{\nu_{pq}^S \nu_{pl}^S}{\nu_{p\Phi}} \right\} \frac{1}{\{\nu_{pq}^S\}} - \left\{ f_{t\Phi} \frac{\nu_{pl}^S}{\nu_{p\Phi}} \right\} \right] \tag{C.7}$$

Using the relations 7.2 and 5.22 for the parallel velocity and restoring coefficients, we can relate the restoring coefficients to the parallel velocity with the following expression

$$< \tau_{lm} > = < u_l > + (DF)_l \gamma_{n\Phi}^{lm} + f_t \left(\frac{T_l}{e_l B_\theta^0} \right) A_{2l} \gamma_{T\Phi}^{lm} + \sum_n \Delta_{n\Phi}^{lm} < \tau_{nl} > - f_t \sum_n \Delta_{n\Phi,1}^{lm} < \tau_{nl} > \tag{C.8}$$

Using Eq. 6.6 for the particle fluxes (with $A_3 = 0$), we can express $(DF)_l$ as

$$(DF)_l = \left(\frac{e_l B_\theta^0}{m_l n_l} \right) \frac{\Gamma_{l\Phi}}{\left\{ \frac{f_{t\Phi} \nu_l^S \nu_l^D}{f_t \nu_{l\Phi}} \right\}} + f_t \sum_k \frac{\left\{ f_{t\Phi} \frac{\nu_l^D \nu_{lk}^S}{\nu_{l\Phi}} \right\} < \tau_{kl} >}{\left\{ f_{t\Phi} \frac{\nu_l^S \nu_l^D}{\nu_{l\Phi}} \right\}}$$

Specializing for a large aspect ratio tokamak ($f_t \ll 1$), we note that the first term on the right hand side is of the order f_t in the driving forces A_{1l} and A_{2l}, while the second term is of the order f_t^2. Retaining only the term of the order f_t,

$$(DF)_l \simeq \left(\frac{e_l B_\theta^0}{m_l n_l} \right) \frac{\Gamma_{l\Phi}}{\left\{ \frac{f_{t\Phi} \nu_l^S \nu_l^D}{f_t \nu_{l\Phi}} \right\}} \tag{C.9}$$

Here, we treat $f_{t\Phi} \sim \mathcal{O}(f_t)$ as discussed in Section 6.2.2. Using Eq. C.8 in Eq. C.3, we can write the parallel friction as

$$\begin{aligned}
< R_{jk} > \;=\; & -m_j n_j \{\nu_{jk}^S\} \Big[(< u_j > - < u_k >) + (u^0_{jk,\Phi} - u^0_{kj,\Phi}) \\
& + \sum_l \Big[\Delta^{jk}_{l\Phi}[< u_l > + u^0_{lj,\Phi}] - \Delta^{kj}_{l\Phi}[< u_l > + u^0_{lk,\Phi}]\Big] \\
& + \sum_l \sum_n \Big[\Delta^{jk}_{l\Phi}\Delta^{lj}_{n\Phi} - \Delta^{kj}_{l\Phi}\Delta^{lk}_{n\Phi,1}\Big] < r_{nl} > \\
& - f_t \sum_l \Big[\Delta^{jk}_{l\Phi,1}[< u_l > + u^0_{lj,\Phi}] - \Delta^{kj}_{l\Phi,1}[< u_l > + u^0_{lk,\Phi}]\Big] \\
& - f_t \sum_l \sum_n \Big[\Delta^{jk}_{l\Phi}\Delta^{lj}_{n\Phi,1} - \Delta^{kj}_{l\Phi}\Delta^{lk}_{n\Phi,1} + \Delta^{jk}_{l\Phi,1}\Delta^{lj}_{n\Phi} - \Delta^{kj}_{l\Phi,1}\Delta^{lk}_{n\Phi,1}\Big] < r_{nl} > \\
& + (f_t)^2 \sum_l \sum_n \Big[\Delta^{jk}_{l\Phi,1}\Delta^{lj}_{n\Phi,1} - \Delta^{kj}_{l\Phi,1}\Delta^{lk}_{n\Phi,1}\Big] < r_{nl} > \Big] \qquad \text{(C.10)}
\end{aligned}$$

where

$$u^0_{pq,\Phi} = \left(\frac{e_p B^0_\theta}{m_p n_p}\right) \frac{f_t \Gamma_{p\Phi}}{\left\{\frac{f_{t\Phi}\nu_T^S \nu_p^D}{\nu_{p\Phi}}\right\}} \gamma^{pq}_{n\Phi} + \left(\frac{T_p}{e_p B^0_\theta}\right) f_t \gamma^{pq}_{T\Phi} A_{2p} \qquad \text{(C.11)}$$

Using $\nu_{p\Phi} \simeq \nu_p^S$ (see Section 6.3) in the above equation, and noting that $\Delta^{pq}_{r\Phi} = \Delta^{pq}_r < 1$, the above equation can be written, by retaining only terms of the order f_t and $f_t \Delta^{pq}_r$, as

$$\begin{aligned}
< R_{jk} > \;=\; & -m_j n_j \{\nu_{jk}^S\} \Big[(< u_j > - < u_k >) + (u^0_{jk,\Phi} - u^0_{kj,\Phi}) \\
& + \sum_l \Big[\Delta^{jk}_l[(< u_l > - < u_j >) + u^0_{lj,\Phi}] \\
& - \Delta^{kj}_l[(< u_l > - < u_k >) + u^0_{lk,\Phi}]\Big]\Big] \qquad \text{(C.12)}
\end{aligned}$$

As $\sum_r \Delta^{pq}_r = 0$, we have subtracted terms of the form $\sum_l \Delta^{jk}_l < u_j >$ and $\sum_l \Delta^{kj}_l < u_k >$ from the right hand side of Eq. C.10 to obtain the above equation.

From Eq. 6.2, we note that the the diffusive particle fluxes are related to the parallel friction by the relation

$$(e_j B^0_\theta)\Gamma_{j\Phi} = -\sum_k < R_{jk} >$$

Using Eq. C.12 for $< R_{jk} >$ in the above equation, and using the definition of Δ^{pq}_r,

we obtain the expression for the parallel velocity difference as

$$\sum_k m_j n_j \bar{\nu}_{jk}^S (< u_j > - < u_k >) = \Gamma_{j\Phi}(e_j B_\theta^0) + < R_{j0,\Phi} > \qquad \text{(C.13)}$$

where $\bar{\nu}_{jk}^S$ and $< R_{j0,\Phi} >$ are given by Eqs. 7.13 and 7.14 respectively.

C.2 Bootstrap Current Coefficients

Using Eqs. 7.21 and 7.22 for the parallel velocity differences in Eq. 7.12 for the current, the expression for bootstrap current can be written as [14]

$$J_{bs,\Phi} = \sum_{k;m=1,2} T_k L_{3m,\Phi}^k A_{mk} \qquad \text{(C.14)}$$

where

$$L_{31,\Phi}^k = L_0 \frac{C_{ei}}{T_k} \left[\hat{C}_{eI,\Phi} L_{11,\Phi}^{ek} + \hat{C}_{iI,\Phi} L_{11,\phi}^{ik} \right] \qquad \text{(C.15)}$$

$$L_{32,\Phi}^k = L_0 \frac{C_{ei}}{T_k} \left[\hat{C}_{eI,\Phi} L_{12,\Phi}^{ek} + \hat{C}_{iI,\Phi} L_{12,\phi}^{ik} + \hat{D}_{k\Phi} \right] \qquad \text{(C.16)}$$

Here, $L_{1n,\Phi}^{jk}$ are the diffusion coefficients [see Section 6.3] and

$$L_0 = -f_t \frac{n_e}{B_\theta^0}$$

$$C_{ei} = \frac{n_i}{n_e} \frac{eZ_i}{f_t} \frac{B_\theta^0}{\bar{\nu}_{ei}^S \bar{\nu}}$$

Before we give the expressions for $\hat{C}_{eI,\Phi}$, $\hat{C}_{iI,\Phi}$, and $\hat{D}_{j\Phi}$, we define the following useful quantities

$$G_\Phi^{pq} = \left(\frac{Z_p e B_\theta^0}{m_p n_p} \right) \frac{f_t \gamma_{n\Phi}^{pq}}{\{ f_{t\Phi} \nu_p^D \}}$$

$$H_\Phi^{pq} = \gamma_{T\Phi}^{pq} \left(\frac{T_p}{Z_p e B_\theta^0} \right) f_t$$

$$N^{jk} = \{ \nu_j^S \} \left\{ \frac{\nu_{jk}^S}{\nu_j^S} \right\}$$

$$K = \left(\frac{n_I Z}{n_i Z_i} \right) \frac{\bar{\nu}_{ei}^S}{\bar{\nu}_{eI}^S} - 1$$

$$
\begin{aligned}
C_e &= K + \bar{\nu} \\
C_i &= \frac{\hat{\nu}^S_{ei}}{\hat{\nu}^S_{ie}} K \\
C_I &= \frac{\hat{\nu}^S_{iI}}{\hat{\nu}^S_{Ii}} C_i
\end{aligned}
$$

Using these quantities, we define the following expressions

$$
\begin{aligned}
C^j_{1\Phi} &= \left(\frac{Z_j e B^0_\theta}{m_j n_j}\right) - \sum_k \{\nu^S_{jk}\} G^{jk}_\Phi \\
C^j_{2\Phi} &= \sum_k \{\nu^S_{jk}\} H^{jk}_\Phi \\
M^{jk}_{kj,\Phi} &= N^{jk} G^{kj}_\Phi \\
P^{jk}_{kj,\Phi} &= N^{jk} H^{kj}_\Phi \\
\bar{C}_{j\Phi} &= C_j (C^j_{1\Phi} + M^{jj}_{jj,\Phi}) \\
\bar{D}_{j\Phi} &= C_j (P^{jj}_{jj,\Phi} - C^j_{2\Phi}) \\
E^{jk}_{kj,\Phi} &= C_j M^{jk}_{kj,\Phi} \\
F^{jk}_{kj,\Phi} &= C_j P^{jk}_{kj,\Phi} \\
\hat{C}_{j\Phi} &= \bar{C}_{j\Phi} + \sum_{k \neq j} E^{kj}_{jk,\Phi}
\end{aligned}
$$

With these definitions, we can express the coefficients in Eqs. C.15 and C.16 as

$$
\begin{aligned}
\hat{D}_{j\Phi} &= \bar{D}_{j\Phi} + \sum_{k \neq j} F^{kj}_{jk,\Phi} \\
\hat{C}_{eI,\Phi} &= (\hat{C}_{e\Phi} + \frac{\hat{C}_{I\Phi}}{Z}) \\
\hat{C}_{iI,\Phi} &= (\hat{C}_{i\Phi} - \frac{Z_i \hat{C}_{I\Phi}}{Z})
\end{aligned}
$$

Finally, we present below the bootstrap current coefficients for a three species plasma as given by Hirshman et al. [14, 40] for a large aspect ratio tokamak.

$$
L^e_{31} = L_0 [1 + K_1 (Z_{eff})] \tag{C.17}
$$

$$Z_i L_{31}^i = L_0 \left[[1 + K_1(Z_{eff})]\xi_i + \left(\frac{\alpha}{1+\alpha} - \frac{n_Z Z}{n_e} \right) [1 + K_1(\alpha)]\xi_z \right] \quad \text{(C.18)}$$

$$Z L_{31}^Z = L_{31}^e - Z_i L_{31}^i \quad \text{(C.19)}$$

$$L_{32}^e = L_0 [2.5 + K_2(Z_{eff})] \quad \text{(C.20)}$$

$$Z_i L_{32}^i = L_0 \left[\left(\frac{\alpha}{1+\alpha} - \frac{n_z Z}{n_e} \right) [2.5 + K_2(\alpha)] + \frac{\{x^2 \nu_i^D\}}{\{\nu_i^D\}} \xi_i \left[[1 + K_1(Z_{eff})] - \left(\frac{\alpha}{1+\alpha} - \frac{n_z Z}{n_e} \right) [1 + K_1(\alpha)] \right] \right] \quad \text{(C.21)}$$

$$Z L_{32}^Z = 1.33 L_0 \xi_z \left[[1 + K_1(Z_{eff})] - \left(\frac{\alpha}{1+\alpha} - \frac{n_z Z}{n_e} \right) [1 + K_1(\alpha)] \right] \quad \text{(C.22)}$$

where

$$\xi_i = \frac{m_i n_i \{\nu_i^D\}}{\sum_k m_k n_k \{\nu_k^D\}}$$

$$\xi_z = 1 - \xi_i$$

$$K_1(x) = \frac{0.68}{x} \left(\frac{1 + 0.1x^{-1}}{1 + 0.13x^{-1}} \right)$$

$$K_2(x) = \frac{0.71}{x} \left(\frac{1 + 0.025x}{1 + 0.059x} \right)$$

and $\alpha = n_Z Z / n_i z_i^2$.

BIBLIOGRAPHY

[1] R. M. Gilgenbach, M. E. Read, K. E. Hackett, F. Lucey, B.Hui, et al., Phys. Rev. Lett. **44**, 647 (1980).

[2] TFR Group/FOM ECRH Team, Nucl. Fusion **28**, 1995 (1988).

[3] W. L. Rowan, M. E. Austin, J. Y. Chen, P. E. Phillips, B. Richards., et al., 30th Annual DPP-APS Meeting (Hollywood, Florida 1988). Paper 6T11.

[4] Y. Ogama, K. Masai, T. Watari, R. Akiyama, R. Ando et al., Nucl. Fusion **29**, 1873 (1989).

[5] J. Roth and G. Janeschitz, Nucl. Fusion **29**, 915 (1989).

[6] J. Castracane, Y. Demers, and H. H. Mai, Plasma Phys. and Contr.Fus. **29**, 759 (1987).

[7] B. Balet, J. G. Cordey, and P. M. Stubberfield, Plasma Phys. Contr. Fusion **34**, 3 (1992).

[8] F. L. Hinton and R. D. Hazeltine, Rev. Mod. Phys. **48**, 239 (1976).

[9] J. W. Connor, Plasma Phys. **15**, 765 (1973).

[10] S. P. Hirshman and D. J. Sigmar, Nucl. Fusion **21**, 1079 (1981).

[11] J. Y. Hsu, V. S. Chan, R. W. Harvey, R. Prater, and S. K. Wong, Phys. Rev. Lett. **53**, 564 (1984).

[12] C. S. Chang, Phys. Fluids **26**, 2140 (1983).

[13] R. V. Shurygin and P. N. Yushmanov, Sov. J. Plasma. Phys. **12**,306(1986).

[14] S. P. Hirshman, D. J. Sigmar, and J. F. Clarke, Phys. Fluids **19**, 656 (1976).

[15] M. Porkolab, in "Fusion" (Ed. E.Teller). Vol. 1, Part B, 151 (1981).

[16] T. H. Stix, "Theory of Plasma Waves", McGrawhill, New York, 1962.

[17] W. M. Manheimer, in "Infrared and Millimeter Waves",Vol. 2 (Ed. K. J. Button). Academic Press, New York (1979). pages 299-352.

[18] J. Wesson, "Tokamaks", Clarendon Press, Oxford (1987); Chapter 5, Sections 5.6-5.10.

[19] J. Adam, Plasma Phys. and Contr. Fus. **29**, 443 (1987).

[20] W. M. Stacey, Jr.," Fusion", John Wiley and Sons, New York (1984); Also "Fusion Plasma Analysis", John Wiley and Sons, New York (1981).

[21] N. A. Krall and A. W. Trivelpiece, "Principles of Plasma Physics", San Francisco Press, Inc., San Francisco (1986).

[22] T. H. Stix, Nucl. Fusion **15**, 737 (1975).

[23] K. Miyamoto, "Plasma Physics for Nuclear Fusion", The MIT Press, Cambridge, Massachusetts (1976).

[24] D. G. Swanson,"Plasma Waves", Academic Press, Inc., San Diego (1989).

[25] T. M. Antonsen, Jr. and W. M. Mannheimer, Phys. Fluids **21**, 2295 (1978).

[26] M. Bambilla, Max-Planck Institute Report, IPP 5/20 (1988).

[27] K. Steinmetz, in Applications of Radio-Frequency Power to Plasmas (Proc. 7th Topical Conf., Kissimmee, Florida). AIP (1987). Page 211.

[28] F. F. Chen,"Plasma Physics and Controlled Fusion", Plenum Press, New York (1984).

[29] I. Fidone, G. Granata, G. Ramponi, and R. L. Meyer, Phys. Fluids **21**, 645 (1978).

[30] O. Eldridge, W. Namkung, and A. C. England, "Electron Cyclotron Heating in Tokamaks", Oak Ridge National Lab. Report, ORNL/TM-6052 (1978).

[31] A. C. Riviere, in Applications of Radio-Frequency Power to Plasmas (Proc. 7th Topical Conf.,Kissimmee, Florida). AIP (1987), Page 1.

[32] R. Balescu, *Transport Processes in Plasmas*, (Elsevier Science Publishers. B. V., Amsterdam, 1988).

[33] E. A. Frieman, Phys. Fluids **13**, 490 (1970).

[34] R. D. Hazeltine, Plasma Phys. **15**, 77 (1973).

[35] A. Baños, Jr., Plasma Phys. **1**, 305 (1967).

[36] S. Chapman and T. G. Cowling, *The Mathematical Theory of Non-Uniform Gases*, 2nd ed. (Cambridge University Press, London, 1952).

[37] M. N. Rosenbluth, R. D. Hazeltine, and F. L. Hinton, Phys. Fluids **15**, 116 (1972).

[38] P. H. Rutherford, Phys. Fluids **13**, 482 (1970).

[39] S. P. Hirshman and D. J. Sigmar, Phys. Fluids **19**, 1532 (1976).

[40] S. P. Hirshman and D. J. Sigmar, Phys. Fluids **20**, 418 (1977).

[41] Lyman Spitzer, Jr., *Phys of Fully Ionized Gases*, 2nd ed. (Interscience, New York, 1962).

[42] C. F. Kennel and F. Englemann, Phys. Fluids **9**, 2377 (1966).

[43] V. S. Chan and S. K. Wong, Phys. Fluids **30**, 830 (1987).

[44] K. W. Whang and G. J. Morales, Nucl. Fusion **23**, 481 (1983).

[45] D. F. Düchs, Z. Naturforsch **42 a**, 1193 (1987).

[46] K. Indireshkumar and W. M. Stacey, Jr., Bull. Am. Phys. Soc. **35**, 1987 (1990). Paper 3S17.

[47] V. P. Bhatnagar, J. G. Cordey, J. Jacquinot, and D. F. H. Start, Plasma Phys. Contr. Fusion **31**, 333 (1989).

[48] JET Team, Plasma Phys. Contr. Fusion **30**, 1467 (1988).

[49] C. S. Chang and R. D. Hazeltine, Nucl. Fusion **20**, 1397 (1976).

[50] C. S. Chang and R. D. Hazeltine, Phys. Fluids **25**, 536 (1982).

[51] R. D. Hazeltine and A. A. Ware, Phys. Fluids **19**, 1163 (1976).

[52] R. D. Hazeltine, A. A. Ware, D. J. Sigmar, S. P. Hirshman, J. E. McCune, et al., in *Plasma Physics and Controlled Nuclear Fusion Research* (International Atomic Energy Agency, Vienna, 1975), Vol. I, p589.

[53] W. M. Stacey, Jr., "The Effect of Poloidal Electric Fields on Impurity Asymmetries and Transport in Tokamaks", Georgia Tech Report, GTFR-63 (1986).

[54] W. M. Stacey, Jr. and D.J.Sigmar, Phys. Fluids **27**, 2078 (1984).

[55] W. M. Stacey, Jr., A. W. Bailey, D. J. Sigmar, and K. C. Shaing, Nucl. Fusion **25**, 463 (1985).

[56] V. S. Chan, S. C. Chiu, and S. K. Wong, Nucl. Fusion **25**, 697 (1985).

[57] L. Chen, J. Vaclavik, and G. W. Hammett, Nucl. Fusion **28**, 389 (1988).

[58] S. C. Chiu and V. S. Chan, Nucl. Fusion **29**, 1907 (1989).

[59] C. S. Chang, G. W. Hammett, and R. J. Goldston, "Neoclassical Transport of Energetic Minority Tail Ions generated by Ion-Cyclotron Resonance Heating in Tokamak Geometry", Princeton Plasma Physics Lab. Report, PPPL-2662 (1990).

[60] W. G. F. Core, Nucl. Fusion **29**, 1101 (1989).

[61] B. Richards, G. Cima, R. L. Hickok, K. W. Gentle, W. L. Rowan et al., 30th Annual DPP-APS Meeting (Hollywood, Florida, 1988). Paper 6T10.

[62] R. J. LaHaye, C. P. Moeller, A. Funahashi, T. Yamamoto, K. Hoshino et al., Nucl. Fusion **21**, 1425 (1981).

[63] V. V. Alikaev, A. A. Bagdasarov, E. L. Berezovskij, A. B. Berlizov, G. A. Bobrovskij, et al., Plasma Phys. and Contr .Nuclear Fus. Res.(IAEA Kyoto). A-II-4 (1986).

[64] K. W. Gentle, B. Richards, D. L. Brower, M. E. Austin, G. Cima et al., in Contr. Fusion and Plasma Heating (Proc. 16th Euro. Conf., Venice, 1989). Vol. 13 B, Part 1, European Physical Society (1989).

[65] R. Prater, S. Ejima, R. W. Harvey, R. J. James, K. Matsuda et al., 14th Euro. Conf. on Contr. Fus. and Plasma Phys., Madrid (1987). Europhys. Conf. Abstracts 11D, III-885.

[66] J. N. Talmadge, C. A. Storlie, D. T. Anderson, F. S. B. Anderson, R. P. Doerner et al., Nucl. Fusion **29**, 1806 (1989).

[67] D. C. Robinson, M. W. Alcock, N. R. Ainsworth, B. Lloyd, and A. W. Morris, Proc. 3rd Joint Int. Symp. on Heating in Toroidal Plasmas, Grenoble, **2** 647 (1982).

[68] R. L. Hickok, P. M. Schoch, X. Z. Yong, D. C. Singh, B. Richards et al., 30th Annual DPP-APS Meeting (Hollywood, Florida, 1988). Paper 6T13.

[69] Project Staff, "DOUBLET III Annual Report", GA Technologies Report, GA-A18468,UC-20(1986).

[70] D. Q. Hwang, G. Grotz, and J. C. Hosea, J. Vac. Sci. Technol. **20**, 1273 (1983).

[71] TFR Group, Proc. 1st Joint Int.Symp.on Heating in Toroidal Plasmas, Grenoble, **2**, 207 (1978).

[72] R. R. Weynants, V. P. Bhatnagar, T. Delvigne, P. Descomps, F.Durodié et al., AIP Conference Proc., No. 129, p 40-43 (1985).

[73] P. Nielsen, A. Gadd, C. Gowers, K. Hirsch, H. Salzman et al., 29th Annual DPP-APS Meeting (San Diego, California, 1987). Paper 5V14.

[74] A. Gondhalekar, A. Cheetham, S. A. Cohen, W. Houlberg, T. T. C. Jones et.al., 29th Annual DPP-APS Meeting (San Diego, California, 1987). Paper 5V9.

[75] A. Cheetham, J. P. Christiansen, S. Conti, A. Gondhalekar, F. Hendriks et al., in Contr. Fus. and Plasma Heating, (Proc. 13th Euro. Conf., Schliersee, 1986). Vol. 10 C, Part I, European Physical Society (1986).

[76] K. Steinmetz, H. Niedermeyer, J. M. Noterdaeme, F. Wesner, and F. Wagner, "Heating and Confinement in the Ion Cyclotron Range of Frequencies on the Divertor Tokamak ASDEX", Max Planck Institute Report, IPP III/130 (1988).

[77] K. Behringer, A. Boileau, F. Bombarda, W. B. Denn, W. Engelhardt et al., in Plasma Phys. and Contr. Nuclear Fusion Res. (IAEA, Kyoto). A-IV-1 (1986).

[78] D. Stork, A. Boileau, F. Bombarda, D. J. Campbell, C. Challis et al., 14th Euro. Conf. on Contr. Fus. and Plasma Phys., Madrid (1987). Europhysics Conf. Abstracts 11D, I-306.

[79] N. C. Hawkes, M. Van Hellermann, A. Boileau, L. Horton, E. Kallne et al., 15th Euro. Conf. on Contr. Fus. and Plasma Phys., Dubrovnik (1988), Europhysics Conf. Abstracts 12B, III-1061.

[80] K. P. Jaehnig, R. J. Fonck, R. B. Howell, and R.J.Knize, 30th Annual DPP-APS Meeting (Hollywood, Florida, 1988). Paper 8T1.

[81] R. Kaita, R. J. Goldston, P. Beiersdorfer, D. L. Herndon, J. Hosea et al., Nucl. Fusion **23**, 1089 (1983).

[82] P. H. Rutherford, Phys. Fluids **13**, 482 (1970).

[83] A. A. Ware, Phys. Rev. Lett. **25**, 916 (1970).

[84] R. Giannella, N. C. Hawkes, L. Lauro Taroni, M. Mattioli, J. O'Rourke, and D. Pasini, Plasma Phys. Contr. Fusion **34**, 687 (1992).

[85] D. Pasini, R. Giannella, L. Lauro Taroni, M. Mattioli, B. Denne-Hinnov, et al., Plasma Phys. Contr. Fusion **34**, 677 (1992).

[86] G. Fussmann, A. R. Field, A. Kallenbach, K. Krieger, K. -H. Steuer, and the ASDEX -Team, Max Planck Institute Report, IPP III/180 (1991).

[87] C. M. Greenfield, K. H. Burrell, J. C. Deboo, R. J. Groebner, G. L. Jackson, et al., Bull. Am. Phys. Soc. **36**, 2475 (1991).

[88] F. L. Hinton and M. N. Rosenbluth, Phys. Fluids **16**, 836 (1973).

VITA

K. Indireshkumar was born in Hassan, India on January 12, 1960. After obtaining his bachelor's and master's degrees in mechanical engineering from the Bangalore University and the Indian Institute of Science, India respectively, he entered the Georgia Institute of Technology to pursue his doctoral studies. After spending a year in the Mechanical Engineering Program at Georgia Tech, he joined the Fusion Research Center and began working with Prof. W. M. Stacey, Jr. as his thesis advisor. In 1987, he spent two months as a summer student trainee at the Princeton Plasma Physics Laboratory and he obtained another master's degree in mechanical engineering from Georgia Tech in 1991.